EPFL

Thèse n°8619

Advanced Frameworks to Aggregate and Unlock the Power Flexibility of Distributed Energy Resources Located in Active Distribution Networks

Présentée le 14 janvier 2022

Faculté des sciences et techniques de l'ingénieur
Groupe SCI STI RC
Programme doctoral en énergie

pour l'obtention du grade de Docteur ès Sciences

par

Mohsen KALANTAR NEYESTANAKI

Acceptée sur proposition du jury

Prof. D. Dujic, président du jury
Dr S.-R. Cherkaoui, directeur de thèse
Prof. P. Pinson, rapporteur
Prof. F. Capitanescu, rapporteur
Dr W. Sattinger, rapporteur
Prof. M.Paolone, rapporteur

École polytechnique fédérale de Lausanne

2022

Beautiful is what we see,
more beautiful is what we know,
most beautiful, by far, is what we don't.
— Nicolas Steno

To my parents & my wife...

Acknowledgements

I would like to thank my thesis director Prof. Rachid Cherkaoui for his constant and unconditional support along the years. I believe that his dedication, enthusiasm and passion for each new project are the best example of how to approach research in order to make it move forward.

The collaboration with brilliant colleagues from Swissgrid has been a great honor for me. I would like to express my deep and sincere gratitude to all my colleagues from Swissgrid namely Dr. Walter Sattinger, Dr. Marek Zima, Dr. Evangelos Vrettos, and Dr. Jonas Muehlethaler. Their valuable and insightful discussions, comments and advice helped me to a very great extent to accomplish my PhD.

My sincere thanks go to Prof. Farhad Rachidi for his generosity and friendship. I am also profoundly grateful to Prof. Mokhtar Bozorg for all his scientific advice. Moreover, I would like to extend my appreciation to my former and new colleagues and friends in ELL building who provided an excellent and delightful atmosphere for me during my doctoral study.

Finally, from the bottom of my heart, I would like to thank my mother, my father, my wife and my brothers for their continuous support, confidence and for constantly believing in me: you are my source of happiness.

Mohsen Kalantar Neyestanaki

Abstract

> We will make electricity so cheap that only the rich will burn candles.
>
> — Thomas A. Edison

Environmental concerns as well as recent developments in renewable energy technologies are leading to a fast transition in electric power systems towards replacing fossil fuel and nuclear generation with renewable generation. This transition has two significant implications for electric power systems:

- The capacity of conventional dispatchable electric power plants, which are the main providers of power flexibility[1], is sharply falling. It is notable that the security of electric power systems can be preserved if and only if there is an adequate amount of power flexibility to guarantee the frequency stability, voltage regulation, power quality, and congestion management.
- The share of renewable energy sources (RESs) in the electric power generation portfolio is steeply soaring. It raises a significant stress on electric power systems due to the fact that the generated electricity from RESs is intrinsically intermittent and accompanied with uncertainties, to put it simply, is non-dispatchable.

The simultaneous realization of these two issues puts electric power systems in a turning point. This thesis devotes a deep attention to the power flexibility provision issue with the purpose of empowering transmission system operators (TSOs) and distribution system operators (DSOs) to steer electric power systems optimally and securely in this emerging architecture. To this end, it sets out to unlock the potential power flexibility of distributed energy resources (DERs) located in distribution networks. In this way, it modernizes traditional top-to-down (from transmission system to distribution systems) power flexibility provision mechanism to a bi-directional power flexibility provision structure between TSO and DSOs.

The first part of the thesis deals with the problem from TSO's perspective. It develops

[1] Ancillary services

two decision making tools for TSOs to help them optimally quantify their required power flexibility from flexibility providers (including flexible distribution networks) in a sequential energy and flexibility market structure. The first tool concentrates solely on active power flexibility and accordingly offers a framework to model aggregated active power flexibility of distribution networks from TSO's point of view. In contrast, the second tool introduces a holistic TSO-DSO coordination framework to enable TSO and DSO to exchange both active and reactive power flexibility. Both developed tools employ mathematical techniques to cast the TSO's decision making process as a two-stage linear stochastic optimization problem while accounting for risk associated to the uncertainties. The frameworks, offered in these tools, lay a ground for TSO and DSOs to exchange bi-directional power flexibility without having to reveal their confidential grids data.

The second part of the thesis deals with the problem from DSO's perspective. It first concentrates on an active distribution network (ADN) and constructs a set of linear scenario-based robust optimization problems to characterize the maximum active/reactive power flexibility that the ADN can provide upon request at its point of common coupling (PCC) to the upper-layer grid. Second, it constructs a linear grid&uncertainties-cognizant ADN management method to determine the amount of active/reactive power flexibility that should be provided by each DER during the real-time operation in such a way that the ADN can provide, with minimum deviation, the active/reactive power flexibility requested by the upper-layer grid at the PCC.

In addition to dealing with the problem from both TSO's and DSO's perspectives, a privileged feature of the thesis is that it offers linear tractable algorithms to deal with all above-mentioned tasks while considering grid's constraints and uncertainties stemming from the forecast errors of demand and renewable generation.

Keywords: Active/reactive power flexibility, ancillary services, active distribution network (ADN) management, battery management system (BMS), decision making under uncertainties, distributed energy resources (DERs), energy storage system (ESS), linearized power flow model, optimal power flow (OPF), real-time optimization-based control, robust/stochastic optimization, TSO-DSO interface, TSO-DSO coordination, two-stage optimization.

Résumé

Les préoccupations environnementales ainsi que les développements récents dans les technologies des énergies renouvelables conduisent les systèmes d'alimentation électrique à une transition rapide vers le remplacement de la production d'énergie fossile et nucléaire par une production d'énergie renouvelable. Cette transition a deux implications importantes pour les systèmes d'alimentation électrique :

- La capacité des centrales électriques conventionnelles dispatchables, qui sont les principaux fournisseurs de flexibilité, est en forte baisse. Il est à noter que la sécurité des systèmes d'alimentation électrique peut être préservée si et seulement si il existe une quantité adéquate de flexibilité de puissance pour garantir la stabilité de fréquence et dc tension la qualité de l'énergie et la gestion des congestions.
- Le pourcentage des sources d'énergie renouvelables (SER) dans le portefeuille de production d'électricité est en forte hausse. Il soulève un stress majeur sur les systèmes d'alimentation électrique, parce que l'électricité produite par des SER est intrinsèquement intermittente et accompagnée d'incertitudes, ce sont généralement des sources non-dispatchable.

L'avènement simultanée de ces deux enjeux place les systèmes d'alimentation à un tournant majeur. Cette thèse traite en profondeur de la question de la provision de flexibilité de l'énergie dans le but de renforcer la capacité des opérateurs de systèmes de transmission (TSO) et des opérateurs de systèmes de distribution (DSO) à piloter les systèmes d'alimentation de manière optimale et en toute sécurité dans cette architecture émergente. À cette fin, les méthode proposées dans cette thèse visent à libérer la flexibilité potentielle de puissance des ressources énergétiques distribuées (RED) situées dans les réseaux de distribution. De cette manière, elles modernisent et transforment le mécanisme traditionnel de provision de flexibilité de puissance du haut vers le bas (du système de transport aux systèmes de distribution) en une structure de provision de flexibilité de puissance bidirectionnelle entre les TSOs et les DSOs.

Abstract

La première partie de la thèse traite du problème vu du TSO. Elle développe d'abord un cadre pour modéliser les flexibilités de puissance agrégées des réseaux de distribution vue du TSO, en essayant de faciliter une collaboration étroite entre TSO et DSOs. Ensuite, elle propose deux modèles d'optimisation linéaires tenant compte des risques pour quantifier les besoins nécessaires du TSO en terme de flexibilité soit de la puissance active seule soit des puissances active et réactive (y compris les flexibilités agrégées des réseaux de distribution) dans une structure de marché décentralisée énergie et flexibilité.

La deuxième partie de la thèse traite du problème vu de DSO. Elle se concentre d'abord sur un réseau de distribution actif (ADN) et construit un ensemble de problèmes d'optimisation robuste linéaires et basés sur des scénarios pour caractériser la flexibilité maximum des puissances actives/réactives quún ADN peut offrir à son point de couplage avec le réseau en amout (ex :TSO). Deuxièmement, elle construit une méthode linéaire de gestion de l'ADN, qui tient compte des incertitudes, pour déterminer la quantité de flexibilité de puissance active/réactive qui doit être fournie par chaque DER pendant l'exploitation en temps réel de manière que l'ADN puisse fournir, avec un écart minimum, la flexibilité de puissance active/réactive requise par le réseau en amout.

En plus de traiter le problème vu du TSO et du DSO, la particularité de cette thèse est qu'elle propose des algorithmes linéaires tractables pour traiter toutes les tâches mentionnées ci-dessus tout en considérant les contraintes du réseau et les incertitudes résultant des erreurs de prédiction de la demande et de la génération renouvelable.

Keywords : Active/reactive power flexibility, ancillary services, active distribution network (ADN) management, battery management system (BMS), decision making under uncertainties, distributed energy resources (DERs), energy storage system (ESS), linearized power flow model, optimal power flow (OPF), real-time optimization-based control, robust/stochastic optimization, TSO-DSO interface, TSO-DSO coordination, two-stage optimization.

Contents

List of Figures

List of Tables

1 Introduction

> If you want to find the secrets of the universe, think in terms of energy, frequency and vibration.
>
> — Nikola Tesla

1.1 Motivations

Grid operators constantly leverage active & reactive power flexibility so-called ancillary services to securely steer the electric power system and supply the electricity demand of end-users. More specifically, they deploy ancillary services to counteract the impact of either unforeseeable grid contingencies like lines/power plants outages or uncertainties stemming from the forecast errors of renewable generation and demand, thereby, preserving the security of supply and respecting the grid's constraints. Continuous, economical and adequate provision of ancillary services is therefore of paramount importance and inadequate level of ancillary services might result in limited load shedding or widespread blackout.

The electric power system as the most complex energy infrastructure has been recently evolving to satisfy the novel economical, technical and environmental requirements as well as new policies. As schematically shown in Fig. 1.1, in this evolution:

- At both transmission and distribution levels, the electric power system is embracing more and more renewable energy sources (RESs) to follow the planed environmental policies and targets [2–12].
- At the distribution level, the electric power system is embracing proliferating number of distributed energy resources (DERs) [13–16].

Traditionally, the required ancillary services of the electric power system were mainly

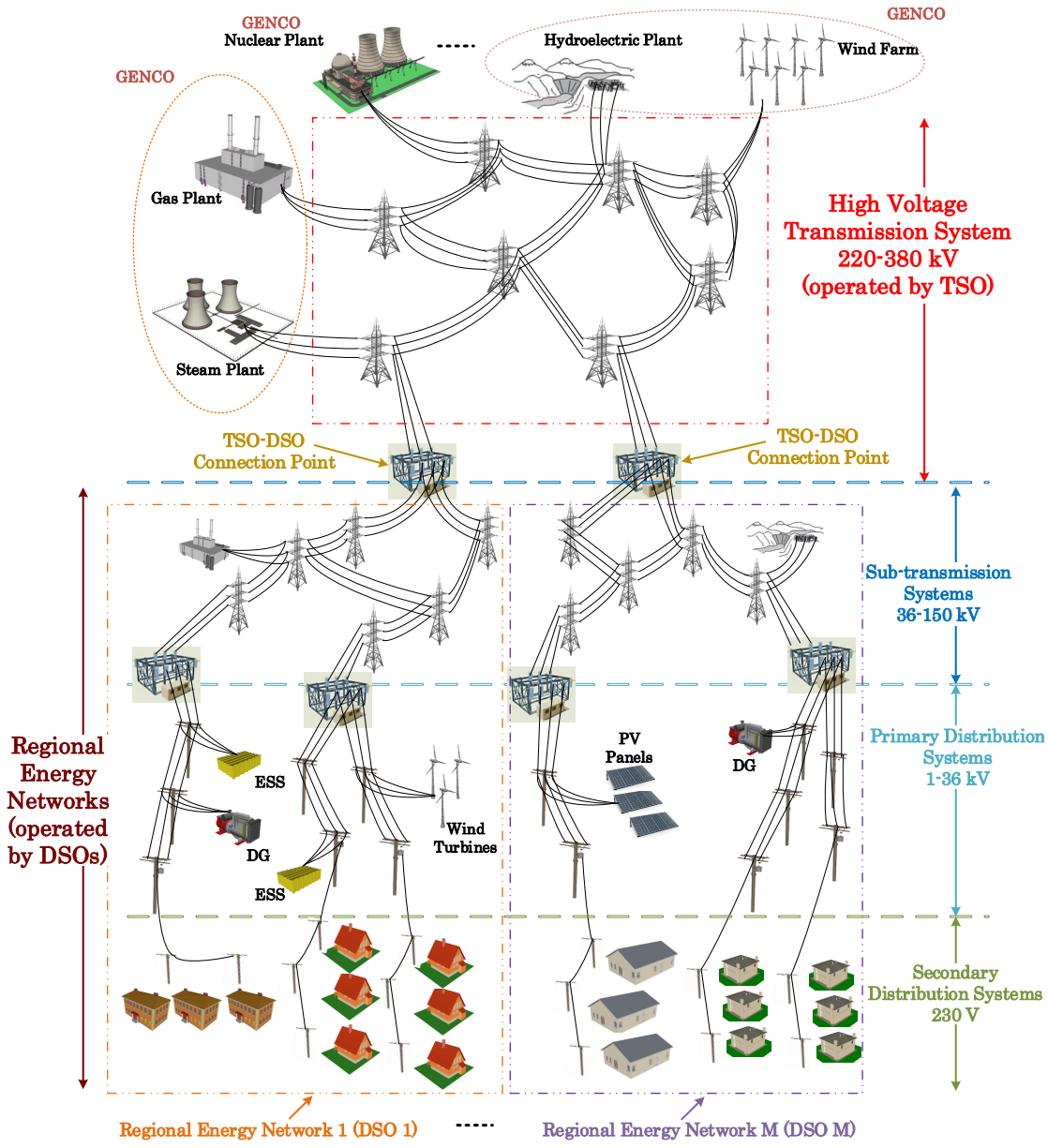

Figure 1.1: The general structure of the electric power system.

provided by conventional dispatchable power plants (DPPs). However, the recent evolution is giving rise to not only a surge in uncertainties stemming from forecast errors of renewable generation, but also a significant fall in the size of DPPs. In other words, the recent evolution is putting the electric power system in the situation where the size of ancillary services providers pales in comparison with the size of uncertainties. Consequently, the traditional mechanisms for power flexibility provision are no longer able to efficiently accomplish their tasks.

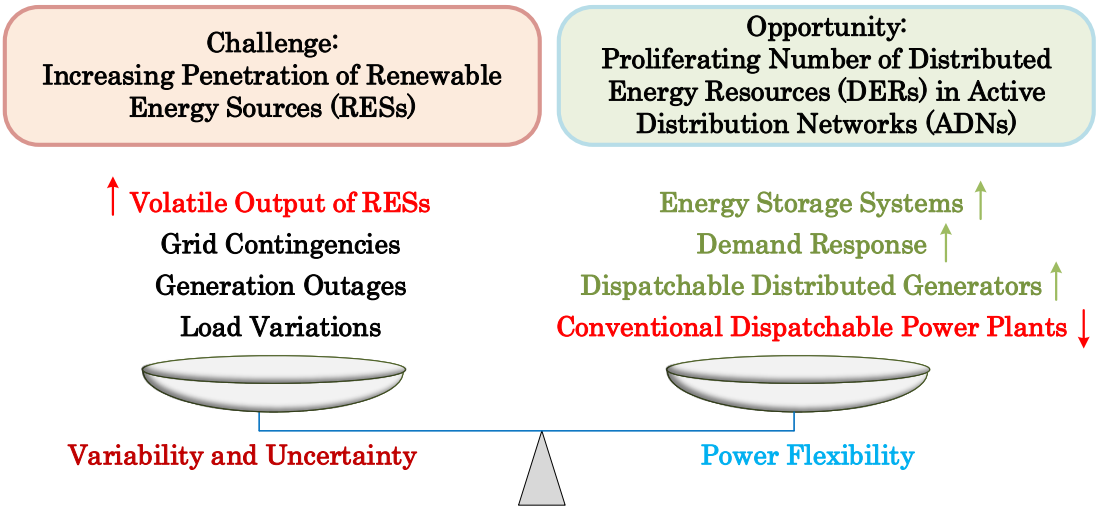

Figure 1.2: Power flexibility versus variability and uncertainty.

In this context, this thesis pays a particular attention to the second aspect of the evolution, i.e. proliferating number of DERs at distribution level, and takes it as an opportunity to deal with the power flexibility provision issue in the emerging architecture of the electric power system. More specifically, it tries to unlock the potential power flexibility of the DERs located in distribution networks and maintain a balance between uncertainties and flexibility as shown in Fig. 1.2. It consequently modernizes the traditional top-to-down (from transmission system to distribution systems) power flexibility provision mechanism to a bi-directional power flexibility provision structure between transmission system operator (TSO) and distribution system operators (DSOs). In this respect, the thesis dedicates two separate parts to address the problem of power flexibility exchange between TSO and DSOs from both TSO's perspective and DSO's perspective.

1.2 Thesis outline

This thesis is organized as follows.

Chapter 2 first establishes a framework to model aggregated flexibility of distribution networks (AFENs) as seen from transmission system operator's (TSO's) perspective. Then, thanks to the established AFEN modeling framework, it constructs a two-stage linear stochastic optimization model to optimally book the TSO's required size of active power flexibility from AFENs and dispatchable power plants (DPPs). The model relies on the value of lost load (VOLL) index as a metric and leverages a cost-benefit method and a DC load-flow model to achieve a risk-aware economic balance between incurred costs of TSO. The method considers credible contingencies along with forecast errors of renewable generation and loads as scenarios. Last but not least, it applies the

developed method to a real-world transmission grid, namely the transmission gird of Switzerland operated by Swissgrid, to illustrate its effectiveness.

Chapter 3 presents a hot-start linearized power flow model for transmission networks while accounting for active/reactive power losses of the grid and shunt susceptance of branches. Above all, it takes into account the impact of different bus types (i.e. slack, PV and PQ buses) on the linearization and takes advantage at most of the existing information, i.e. the solution of AC power flow problem for the base case opearting point. To this end, it first linearizes all non-linear power flow equations through extracting the first-order Taylor series expansion of the power flow equations. Then, it provides a linear formulation to explicitly characterize all transmission grid's constraints as linear functions of the nodal injections. It is worth mentioning that this linearized power flow model is exploited in chapter 4 to construct a grid-cognizant TSO-DSO coordination framework.

Chapter 4 first designs a holistic coordination framework between TSO and DSOs to empower them exchange bi-direction active and reactive power flexibility without having to reveal their confidential grids data. Then, it relies on the designed framework and offers a decision making tool for TSOs to help them optimally book their required active and reactive power flexibility from both power plants and distribution networks. This decision making problem is mathematically formulated as a two-stage linear stochastic optimization problem by employing mathematical techniques along with the linearized power flow model developed in chapter 3. Finally, the performance of the proposed framework and decision making tool is evaluated considering a real-world transmission network, i.e. the Swiss transmission network.

Chapter 5 first offers a comprehensive survey on the the existing power flow models. Then, it selects the best power flow model for managing the power flexibility of DERs located in active distribution networks (ADNs). The selected power flow model is exploited in chapter 6 and chapter 7. It is worth highlighting that the linearized power flow model presented in chapter 3 is also applicable for managing the power flexibility of DERs located in ADNs. However, this thesis introduces two linear power flow models (i.e. chapters 3 and 5) to be able to deal with all kinds of distribution networks. It is worth noting that section 5.4 elaborates on different features of the power flow models presented in chapters 3 and 5.

Chapter 6 introduces a method to characterize the capability area of an active distribution network (ADN) for providing both active and reactive power flexibility to the upper-layer grid (i.e., sub-transmission and transmission systems) at their point of common coupling (PCC). It is the first-ever method tackling the problem while considering the forecast errors of loads and stochastic generation, as well as the operational constraints of the grid and DERs. The method leverages a linearized load flow model and constructs a set of linear scenario-based robust optimization problems to estimate

the flexibility provision capability (FPC) area of the ADN. Above all, this chapter proves that, under certain assumptions, the FPC area is convex. The chapter finally evaluates the performance of the proposed method on a modified version of the IEEE 33-bus distribution test system.

Chapter 7 presents a two-stage active distribution network (ADN) management method to empower ADN operators to steer their ADN during the real-time operation in such a way that they can deliver the requested power flexibility of the upper-layer grid operator at their point of common coupling (PCC). The **first stage** is carried out minutes-ahead real-time operation. It updates the power set-points of DERs considering their offer curves as well as the uncertainties stem from the short-term forecast errors of demand and renewable generation profiles. The inter-temporal constraints and losses of the grid are accounted for by exploiting a linearized dynamic optimal power flow model, whereby the first stage is implemented as a linear scenario-based optimization problem. The **second stage** is carried out during real-time operation. It relies on a linear optimization problem, thereby adjusting the power flexibility injection of a utility-scale battery energy storage system (ESS) to mitigate the imbalance at the PCC inherent in the above-mentioned uncertainties. Notably, the chapter tests the performance of the proposed method on a real ADN located in the city of Aigle in southwest of Switzerland.

Considering the large amount of subjects treated by the thesis, the literature survey is integrated at the beginning of each Chapter.

1.3 Contributions

The original contributions of the thesis can be enumerated as following:

Chapter 2

1. Establishing a framework to model aggregated flexibility of distribution networks (AFENs) from TSO's perspective. This modeling framework is envisaged to facilitate a tighter collaboration between TSO and DSOs.
2. Introducing a risk-aware decision making tool to quantify the TSO's required size of active power flexibility from both DPPs and AFENs in a sequential energy and flexibility market structure. It benefits from mathematical techniques to extract the linear counterparts of the non-linear terms of the problem. Accordingly, it constructs a tractable linear algorithm, formulated as a two-stage linear stochastic optimization problem, that achieves an economic balance between costs and benefits of the active power flexibility.
3. Constructing the case study model of the swiss transmission network (used for planing and operational studies) on the basis of the data provided by swissgrid.

4. Evaluating the economic and technical benefits of Swissgrid, the operator of the Switzerland's transmission network, from the active power flexibility provision of AFENs.

Chapter 3

1. Linearizing power flow equations while accounting for:
   - Impact of different bus types, i.e. slack, PV and PQ buses;
   - Active and reactive power losses of the transmission grid;
   - Shunt susceptance of branches.
2. Explicitly characterizing the following quantities as linear functions of the active power injections of PV and PQ buses as well as reactive power injections of PQ buses:
   - Voltage magnitudes of all buses;
   - Apparent power flow of all branches;
   - Active/reactive power injections of slack bus;
   - Reactive power injections of PV buses.

Chapter 4

1. Designing a holistic TSO-DSO coordination framework where TSO and DSOs establish their collaboration on the basis of the FPC areas (the concept of FPC area is introduced in chapter 6). This framework facilitates the TSO and DSO collaboration, thereby, boosting unlocking the potential active/reactive power flexibility of DERs.
2. Developing a decision making tool for TSOs to help them optimally book their required active and reactive power flexibility via FPC areas.
3. Leveraging the linearized AC power flow model developed in chapter 3, it is able to account for grid's active and reactive power losses and, most notably, the nodal voltage magnitude constraints. Therefore, it can ensure that power plants accomplish their voltage regulation task against all uncertainties and contingencies without reaching their maximum/minimum reactive power limits. Accordingly, it helps TSOs steer their grids far from risks associated with under-voltage/over-voltage issues triggering voltage collapse.
4. Empowering TSO to take advantage of all existing power flexibility resources including dispatchable power plants and DERs located in distribution networks.
5. Following the sequential energy and flexibility market structure, thus, it is a tailored tool for most of European TSOs.
6. Evaluating the efficiency of the developed framework and decision making tool on a real-world transmission network, i.e. the Swiss transmission network operated by Swissgrid.

Chapter 5

1. Selecting the best power flow model for managing the power flexibility of DERs located in ADNs.

Chapter6

1. Developing a linear tractable algorithm to estimate the flexibility provision capability (FPC) area [1] of an ADN while considering the grid's/DERs' constraints as well as the uncertainties of demand and renewable generation. To deal with uncertainties, it first introduces a novel search methodology in the P-Q plane to explore the boundaries of the ADN's FPC area. Then, it relies on mathematical techniques to formulates the problem as a set of linear scenario-based robust optimization problems
2. Introducing a closed-form formula to determine the number of scenarios that should be taken into account in the above-mentioned linear scenario-based robust optimization problem for modeling the uncertainties of demand and renewable generation.
3. Mathematically proving that, assuming convex capabilities curves of DERs and a linearized power flow model, the estimated FPC area is feasible and convex.

Chapter7

1. Introducing a two-stage ADN management method to exploit/aggregate the power flexibility of DERs with the aim of providing an specific amount of active/reactive power flexibility to the upper-layer grid at the ADN's PCC. It first extracts linear models for the ESS's constraints, DERs'offer curves and objective function. Then, it casts the first stage of the method as a scenario-based linear dynamic power flow model. In addition to the technical constraints of the grid, DERs and the ESS; this model takes into account the grid's power losses and temporal variations and uncertainties of demand/renewable generation. Finally, it casts the second stage of the method as a optimization-based control strategy (formulated as a linear optimization problem) for the ESS.
2. Introducing a novel ESS management method. The method divides the net power injection of the ESS into two terms to elaborately preserve the ESS's state of energy (SOE) as well as take advantage at most of the power flexibility of the ESS.
3. Developing a machine learning-based approach (on the basis of k-nearest neighbors algorithm) to predict the active power generation of PV units and

[1] The flexibility provision capability (FPC) curve of an ADN is defined as a curve characterizing the extreme amount of active and reactive power flexibility that the ADN can provide to the upper-layer grid. The area surrounded by the FPC curve is called FPC area.

active power consumption of loads located in a distribution network of the city Aigle.

4. Illustrating the performance of the proposed method on a real distribution network located in the city of Aigle in southwest of Switzerland.

1.4 List of Publications

The work presented in this thesis has been reported by the following publications:

Journal Papers:

- M. Kalantar-Neyestanaki, F. Sossan, M. Bozorg, R. Cherkaoui, "Characterizing the Reserve Provision Capability Area of Active Distribution Networks: A Linear Robust Optimization Method," *IEEE Transactions on Smart Grid*, vol. 11, no. 3, pp. 2464–2475, November 2019 [17].
- M. Kalantar-Neyestanaki, R. Cherkaoui, "Coordinating Distributed Energy Resources and Utility-Scale Battery Energy Storage System for Power Flexibility Provision Under Uncertainty," *IEEE Transactions on Sustainable Energy*, vol. 12, pp. 1853–1863, Oct. 2021 [18].

Journal Papers Under Revision:

- M. Kalantar-Neyestanaki, R. Cherkaoui, "Risk-Aware Active Power Flexibility Allocation from TSO-DSO Interconnections: The Switzerland's Transmission Network," *Under review at IEEE Systems Journal.*
- M. Kalantar-Neyestanaki, R. Cherkaoui, "Grid-Cognizant TSO and DSO Coordination Framework for Active and Reactive Power Flexibility Exchange: The Swiss Case Study," *Under review at IEEE Transactions on Power Systems.*

Conference Papers:

- M. Kalantar-Neyestanaki, M. Bozorg, F. Sossan, R. Cherkaoui, "Allocation of Frequency Control Reserve from Aggregated Resources of Active Distribution Systems," Power System Computational Conference (PSCC), pp. 1-8, Dublin, Irland, June 11^{th}-15^{th}, 2018 [19].
- M. Kalantar-Neyestanaki, M. Bozorg, F. Sossan, R. Cherkaoui, "Allocation of Active Power Reserve from Active Distribution Networks Using a Cost-Benefit Approach: Application to Swissgrid Network," IEEE PowerTech, pp. 1-6, Milan, Italy, June 23^{rd}-27^{th}, 2019 [20].

Part I

Part I- Transmission System Operator (TSO) Side: Quantifying the TSO's Demand for Power Flexibility

2 Risk-Aware Active Power Flexibility Allocation from TSO-DSO Interconnections: The Switzerland's Transmission Network

> Our universe is a sea of energy - free, clean energy. It is all out there waiting for us to set sail upon it.
>
> — Robert Adams

Active power flexibility is defined as additional bi-directional active power a resource can provide to the grid by adjusting its operating point. Considering the increasing penetration of distributed energy resources (DERs) in distribution networks, DERs' active power flexibility could be aggregated and provided to the transmission system. In this context, the chapter is intended to:

1. Establish a framework for modeling aggregated flexibility of distribution networks (AFENs) as seen from transmission system operator's (TSO's) perspective.
2. Develop a two-stage linear stochastic optimization model to optimally book the TSO's required size of active power flexibility from AFENs and dispatchable power plants (DPPs). The model leverages a cost-benefit method and a DC load-flow model to minimize the TSO's total cost, namely the sum of:
   (a) Expected cost of active power flexibility allocation from AFENs and DPPs;
   (b) Expected cost of energy not supplied.

   To achieve a risk-aware economic balance between these two incurred costs of TSO, the model relies on the value of lost load (VOLL) index as a metric. The method considers credible contingencies along with forecast errors of renewable

generation and loads as scenarios. Finally, the method is applied to the transmission system of Switzerland, operated by Swissgrid, to illustrate its effectiveness.

Keywords: Active power flexibility, cost-benefit approach, distributed energy resource (DER), stochastic optimization, risk-aware decision making, two-stage optimization transmission Networks, TSO/DSO interface.

Nomenclature

Abbreviations

AFEN	Aggregated FlExibility of Distribution Networks
CHF	Confederation Helvetica (Swiss) Franc
DER	Distributed Energy Resources
DPP	Dispatchable Power Plants
SPP	Stochastic Power Plants
DDG	Dispatchable Distributed Generator
ESS	Energy Storage System
H&N	*Here-and-Now*
TSO	Transmission System Operator
VOLL	Value of Lost Load
W&S	*Wait-and-See*

Indices and Sets

g	Index of dispatchable/stochastic power plants.
i, j	Index of buses.
k	Index of AFENs.
l	Index of loads.
n	Index of offered blocks of flexibility.
s	Index of scenarios.
$t, t^{'}$	Index of time periods.
$\mathbb{A}$	Set of AFENs.

$\mathbb{A}_i$	Set of AFENs connected to bus i.
$\mathbb{B}$	Set of indices of all buses.
$\mathbb{B}_i$	Set of indices of all buses connected to bus i.
$\mathbb{DPP}$	Set of dispatchable power plants (DPPs).
$\mathbb{DPP}_i$	Set of DPPs connected to bus i.
$\mathbb{L}_i$	Set of loads connected to bus i.
$\mathbb{N}$	Set of offered blocks of flexibility.
$\mathbb{SPP}_i$	Set of stochastic power plants (SPPs) connected to bus i.
$\mathbb{S}$	Set of scenarios.
$\mathbb{T}$	Set of time periods forming the time horizon.

Auxiliary Variables (at Distribution level)

$f_{kts}^{\text{DDG+}}$,$f_{kts}^{\text{DDG−}}$	Upward and downward active power flexibility that TSO deploys from the aggregated dispatchable distributed generator (DDG) of AFEN k in time period t and scenario s [MW].
$f_{kts}^{\text{EES+}}$, $f_{kts}^{\text{ESS−}}$	Upward and downward active power flexibility that TSO deploys from the aggregated energy storage system (ESS) of AFEN k in time period t and scenario s [MW].
$f_{kts}^{\text{FL+}}$, $f_{kts}^{\text{FL−}}$	Upward and downward active power flexibility that TSO deploys from the aggregated flexible load of AFEN k in time period t and scenario s [MW].

Auxiliary Parameters (at Distribution level)

$\text{P}_{kt}^{\text{DDG}}$	Scheduled active power for the aggregated DDG of AFEN k in time period t [MW].
$\text{P}_{kt}^{\text{ESS}}$	Scheduled active power for the aggregated ESS of AFEN k in time period t [MW].
P_{kt}^{L}	Scheduled active power for the net load (including firm and flexible loads and non-dispatchable DGs) of AFEN k in time period t [MW].

Variables (at Transmission level)

$f_{gts}^{\mathrm{G}+}, f_{gts}^{\mathrm{G}-}$	Upward and downward (P-constrained) active power flexibility that TSO deploys from dispatchable power plant (DPP) g in time period t and scenario s [MW].
$f_{kts}^{\mathrm{P}+}, f_{kts}^{\mathrm{P}-}$	Upward and downward P-constrained active power flexibility that TSO deploys from AFEN k in time period t and scenario s [MW].
$f_{kts}^{\mathrm{PE}+}, f_{kts}^{\mathrm{PE}-}$	Upward and downward P&E-constrained active power flexibility that TSO deploys from AFEN k in time period t and scenario s [MW].
$F_{g}^{\mathrm{G}+}, F_{g}^{\mathrm{G}-}$	Size of the upward and downward active power flexibility that TSO books from DPP g [MW].
$F_{k}^{\mathrm{P}+}, F_{k}^{\mathrm{P}-}$	Size of the upward and downward P-constrained active power flexibility that TSO books from AFEN k [MW].
$F_{k}^{\mathrm{PE}+}, F_{k}^{\mathrm{PE}-}$	Size of the upward and downward P&E-constrained active power flexibility that TSO books from AFEN k [MW].
$P_{kts}^{\mathrm{SL}}, P_{lts}^{\mathrm{SL}}$	Involuntary shed load of AFEN k/load l in time period t and scenario s [MW].
θ_{its}	Voltage angle at bus i in time period t and scenario s [rad].

Parameters (at Transmission level)

$\mathrm{A}_{gts}^{\mathrm{G}}$	Binary parameter where 1 means power plant g is available in time period t and scenario s, otherwise 0.
$\mathrm{A}_{ijts}^{\mathrm{L}}$	Binary parameter where 1 means the transmission line connecting bus i to bus j is available in time period t and scenario s.
B_{ij}	Series susceptance of the transmission line connecting bus i to bus j [p.u.].
$\mathrm{E}_{k}^{\mathrm{PE}+,\max}$, $\mathrm{E}_{k}^{\mathrm{PE}-,\max}$	Energy limit of the total upward and downward P&E-constrained active power flexibility that AFEN k offers to the TSO [MWh].
$\mathrm{F}_{gn}^{\mathrm{G}+,\max}$, $\mathrm{F}_{gn}^{\mathrm{G}-,\max}$	Power limit of the nth block of the upward and downward (P-constrained) active power flexibility that DPP g offers to the TSO [MW].
$\mathrm{F}_{kn}^{\mathrm{P}+,\max}$, $\mathrm{F}_{kn}^{\mathrm{P}-,\max}$	Power limit of the nth block of the upward and downward P-constrained active power flexibility that AFEN k offers to the TSO [MW].
$\mathrm{F}_{kn}^{\mathrm{PE}+,\max}$, $\mathrm{F}_{kn}^{\mathrm{PE}-,\max}$	Power limit of the nth block of the upward and downward P&E-constrained active power flexibility that AFEN k offers to the TSO [MW].

P_{ij}^{max}	Rated power limit of the transmission line connecting buses i to j [MW].
P_{kt}, P_{lt}, P_{gt}	Scheduled active power for consumption of AFEN k/load l and generation of power plant g in time period t [MW].
$VOLL_i$	Value of lost load for energy not supplied at bus i [CHF/(MWh)].
ΔP_{gts}, ΔP_{lts}	Deviation from the scheduled active power for stochastic power plant (SPP) g/load l in time period t and scenario s [MW].
π_{gn}^{G+}, π_{gn}^{G-}	Price offer of DPP g for nth block of the upward and downward (P-constrained) active power flexibility, i.e. $F_{gn}^{G+,max}$/$F_{gn}^{G-,max}$ [CHF/MW].
π_{kn}^{P+}, π_{kn}^{P-}	Price offer of AFEN k for nth block of the upward and downward P-constrained active power flexibility, i.e. $F_{kn}^{P+,max}$/$F_{kn}^{P-,max}$ [CHF/MW].
π_{kn}^{PE+}, π_{kn}^{PE-}	Price offer of AFEN k for nth block of the upward and downward P&E-constrained active power flexibility, i.e. $F_{kn}^{PE+,max}$/$F_{kn}^{PE-,max}$ [CHF/MW].
π_t^+, π_t^-	Price of the deployed upward/downward active power flexibility in time period t [CHF/(MWh)].
ρ_s	Probability of occurrence of scenario s.
τ	Duration of each time period [hour].
$\mathscr{H}$	Duration of the time horizon [hour].

2.1 State of the Art

Environmental challenges along with the recent progress in renewable energy technologies are leading towards a green electricity generation future [21–23]. For example, in Switzerland with around 38% nuclear electricity generation, it has been planned to phase out nuclear plants by 2050, thereby opening the way for electricity generation from renewable energy sources [24]. Nonetheless, in order to achieve this goal, a rapt attention should be devoted to the power flexibility provision issue to guarantee voltage/frequency regulation in the presence of significant amount of stochastic renewable energy resources like solar and wind [25–28].

Tracking the evolution of distribution networks from passive to active ones illustrates that they are hosting more and more distributed energy resources (DERs) [13]. In order to keep the security and quality of supply in this emerging architecture, a solution is to aggregate the power flexibility of DERs located in distribution networks to provide it to the transmission grid [25], [29], [17]. This solution necessitates a tighter collaboration between DSOs, i.e. distribution system operators, and TSOs, i.e. transmission system

operators, to exchange such a flexibility [14]. The active power flexibility can be defined as additional bi-directional active power a given resource can provide to the grid by regulating its operating point, i.e. increasing or decreasing its active power consumption/generation [25], [17]. The question that naturally arises in this context is:

What is the optimal size of active power flexibility that a TSO must book from power flexibility providers (including aggregated flexibility of distribution networks) over a specified time horizon (next day or week)?

It is notable that TSO incurs costs due to booking and deploying active power flexibility while benefiting from it in terms of the expected cost reduction of energy not supplied. Therefore, the optimum solution should make a balance between the costs and benefits of the booked active power flexibility.

Across the world, TSOs procure their required active power flexibility through either integrated market structure, i.e. joint energy and flexibility[1] market, or sequential market structure [30–32]. Integrated market structure corresponds to the case where both energy and flexibility markets are simultaneously cleared/organized. However, sequential market structure corresponds to the case where energy and flexibility markets are sequentially (and separately) cleared/organized. The former is the current structure used in North America while the latter is the structure implemented in Switzerland and some other European countries. The main focus of this chapter is the Switzerland's flexibility market; thus, it opts for the sequential structure and try to facilitate the participation of aggregated resources of distribution networks in this market.

Traditional practices [33–38] quantify the TSO's required size of active power flexibility based on either deterministic or probabilistic criterion while relying just on the active power flexibility of dispatchable power plants (DPPs) only and neglecting the potential active power flexibility available in the distribution networks. Deterministic approaches ignore the stochastic nature of the contingencies and uncertainties, thereby setting the adequate size of active power flexibility equal to a pre-defined amount such as the capacity of the largest online generating unit or a fraction of the peak load [33]. Although deterministic approaches can be easily implemented, they cannot provide any information about the risk of the system. To deal with this issue, the probabilistic approaches are designed which consider the stochastic nature of the contingencies and uncertainties. These approaches fall into either statistic-based or optimization-based methods. The former neglects the transmission network constraints and quantifies the adequate size of active power flexibility based on the statistical assessments of the historical contingencies such as generators outage and forecast errors, whereby they try to satisfy a target risk level [34], [35]. The latter formulates the problem as an optimization problem aiming to determine the optimum

[1] Reserve and flexibility terms are interchangeably used throughout the chapter.

size of active power flexibility in such a way that a desired level of reliability metrics, such as loss of load probability (LOLP) and/or expected energy not supplied (EENS), are respected [36–38].

2.2 Motivations

In general, all above-mentioned methods may end up to a sub-optimal solution because they suffer from a couple of limitations:

- They just incorporate a risk criterion in their problem, thereby minimizing the TSO's incurred cost due to booking and deploying active power flexibility instead of balancing costs and benefits of the active power flexibility.
- They neglect the capability of distribution networks for active power flexibility provision, most notably, some of them neglect grid's constraints.
- They follow integrated energy and flexibility market structure whereas flexibility market of Switzerland is fully separated from the energy market.

These restrictions found in [33–38] paved the way to the method proposed in this chapter. In order to quantify the TSO's required size of active power flexibility, this chapter develops:

- A framework to help TSOs to take advantage of the aggregated flexibility of distribution networks (AFENs), whereby it tries to facilitate a tighter collaboration between TSO and DSOs.
- A two-stage stochastic optimization model where the scenarios include forecast errors of stochastic renewable generation and demand as well as transmission lines/power plants outages. It should be noted that the proposed method is applicable to any time horizon.

To the best of our knowledge, quantifying the TSO's required size of active power flexibility from both DPPs and AFENs is a problem whose treatment is missing in the literature.

It should be highlighted that the developed method explicitly and implicitly brings various benefits to different stakeholders:

- It lays a ground where AFENs can offer their potential active power flexibility to the TSO. In this way, it helps to unlock the potential power flexibility of DERs, thereby, generating a profit for DERs owners.

- Thanks to unlocking the potential power flexibility of DERs, it improves the security/reliability of the whole electric power system while decreasing the cost associated with flexibility allocation. The whole community including all stakeholders enjoy from these two benefits , i.e. higher reliability (security in supply) along with lower cost.
- It may help TSOs to avoid/postpone transmission grid expansion thanks to introducing new flexibility providers (i.e. AFENs) distributed throughout the transmission grid.
- It helps TSOs to take advantage of the flexibility of DERs located in distribution networks.
- It helps TSO to economically allocate its required active power flexibility while preserving the reliability of its network.
- It quantifies the technical and economic benefits of AFENs. As a result, it reveals the benefit of AFENs and promotes all stakeholders to invest more on this novel flexibility provision structure.

2.3 Problem Statement

This chapter follows sequential energy and flexibility market structure where energy and flexibility markets are sequentially cleared. More specifically, the day-ahead energy market is firstly cleared and accordingly the scheduled operating point of all entities (i.e. P_{gt}, P_{kt}, P_{lt}) are determined with the time resolution of τ. Then, the active power flexibility is allocated in two stages [39, 40] as sketched in the timeline of Fig. 2.1:

1. **Flexibility Booking Stage** (*here-and-now (H&N)* decisions): A week or a day prior to the real-time operation, all active power flexibility providers firstly evaluate the amount of active power flexibility that they are able to provide to the TSO over a selected time horizon, whereby they submit their flexibility offers (consisting of the size and price) to the TSO. Then, the TSO solves an optimization problem to quantify and book its required size of active power flexibility from each provider. In this stage, no real product is exchanged between TSO and active power flexibility providers but TSO pays the cost of its booked active power flexibility. In this way, TSO ensures the availability of an adequate amount of active power flexibility throughout the selected time horizon.
2. **Flexibility deployment Stage** (*wait-and-see (W&S) decisions*): This stage pertains to the real-time operation where the actual amount of the TSO's required active power flexibility turns out. In case of need, the TSO asks the active power flexibility providers to activate all/a part of the active power flexibility already

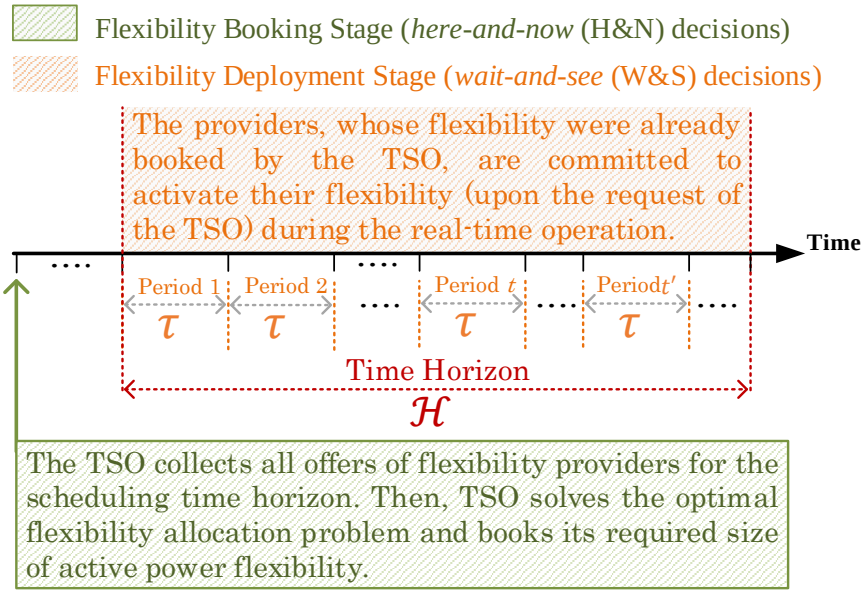

Figure 2.1: The general procedure of active power flexibility allocation.

booked. Accordingly, TSO pays the cost of activated flexibility in addition to the cost of booked flexibility already payed.

Following the presented sequential energy and flexibility market structure where energy market is separately cleared before the flexibility market, the chapter assumes that the outcome of the energy market is known/given. More specifically, the scheduled operating point of all entities (i.e. P_{gt}, P_{kt}, P_{lt}) are known for each time period t. Then, the chapter introduces a method to help TSOs to make an optimal decision in the first stage of the flexibility allocation procedure, i.e. flexibility booking stage. To this end, this chapter leverages a cost-benefit method [41] and develops a risk-aware optimization model for TSOs. It is mathematically formulated as a two-stage stochastic optimization problem and empowers TSO to determine the optimal size of active power flexibility that it should book from all providers throughout the time horizon, so that the total cost of TSO is minimized[2]. Although the method presented in this chapter is generic, it relies on the following considerations:

- The time horizon ($\mathscr{H}$) is formed of a number of time periods, each with duration of τ.
- In each individual time period t, the active power schedule of the power plants, AFENs and loads are known (P_{gt}, P_{kt}, P_{lt}).

[2]Due to the presence of time-coupling constraints associated with energy-constrained resources, the flexibility booking problem must be solved considering all time periods belonging to the time horizon $\mathscr{H}$

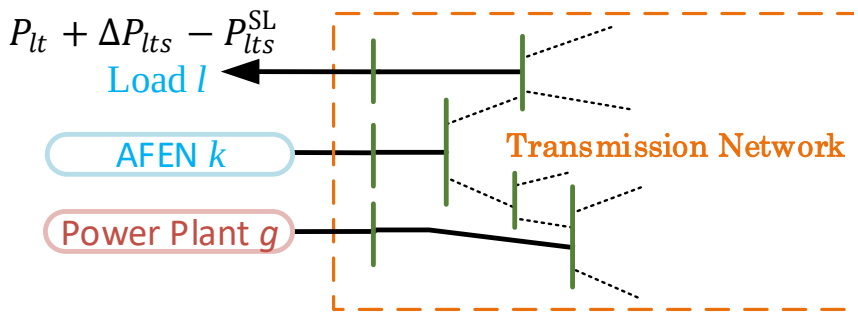

Figure 2.2: All entities of the power system form the TSO's viewpoint.

- The size of booked active power flexibility from each provider is a unique value for the whole time horizon.

2.4 Contributions & Novelties

Original contributions and novelties of this chapter are fourfold:

- It introduces a framework to model aggregated flexibility of distribution networks (AFENs) from TSO's perspective, whereby it tries to facilitate a tighter collaboration between TSO and DSOs.
- It extracts linear equivalent counterparts for nonlinear terms of the objective function, whereby, it offers a linear risk-aware optimization model to quantify the TSO's required size of active power flexibility (over a desired time horizon, e.g. next day) in a sequential energy and flexibility market structure. In this way, it mathematically balances costs and benefits of the active power flexibility.
- In addition to the active power flexibility of DPPs, it considers the active power flexibility of AFENs, thereby quantifying the TSO's required size of active power flexibility from both DPPs and AFENs.
- For a real transmission grid, i.e. the Switzerland's transmission grid, it evaluates the TSO's economic/technical benefits resulting from the active power flexibility provision of AFENs.

2.5 Resource Modeling Framework

Different entities such as AFENs, stochastic power plants (SPPs), dispatchable power plant (DPPs) and loads are connected to the transmission network as shown in Fig. 2.2. In the following, these entities are modeled from TSO's viewpoint:

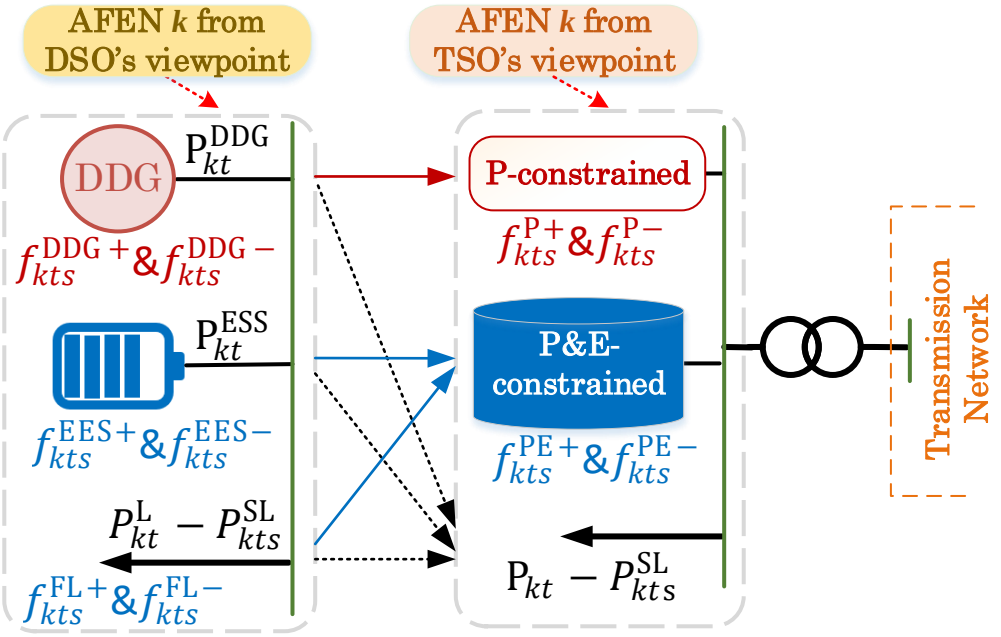

Figure 2.3: The model of AFEN k in time period t and scenario s from DSO's/TSO's viewpoint.

2.5.1 Modeling the AFENs

In the emerging distribution networks, the number of DERs including distributed generators (DGs), energy storage systems (ESSs) and flexible loads is progressively increasing. DGs accommodated in distribution networks fall into dispatchable and non-dispatchable sources. Dispatchable DGs are able to provide active power flexibility to the grid, whereas non-dispatchable DGs (e.g., wind and solar units) whose active power generation is subject to uncertainties increase the demand for power flexibility. In addition to the dispatchable DGs, flexible loads and ESSs are also able to provide active power flexibility to the grid. Thanks to aggregators[3] who organize and aggregate DERs, a new entity entitled AFEN is formed. In this way, the TSO can take advantage of the active power flexibility of DERs. The model of an AFEN from DSO's and TSO's viewpoint is shown in Fig. 2.3.

- **From DSO's viewpoint**: an AFEN consists of an aggregated dispatchable DG (DDG), an aggregated ESS and an aggregated load, as show in Fig. 2.3. In addition to the flexible loads, which are sources of flexibility, the aggregated load embraces the non-dispatchable DGs (negative loads) and firm loads, which are sources of uncertainties. It is assumed that deviations from scheduled active power of non-dispatchable DGs and loads are compensated by exploiting the local flexibility

[3] A third market player so-called aggregator who organizes and aggregates DERs to provide active power flexibility to the transmission network.

of the AFEN. The corresponding flexibility of these aggregated resources (i.e. $f_{kts}^{\mathrm{DDG+}}, f_{kts}^{\mathrm{DDG-}}, f_{kts}^{\mathrm{ESS+}}, f_{kts}^{\mathrm{ESS-}}, f_{kts}^{\mathrm{FL+}}, f_{kts}^{\mathrm{FL-}}$) are defined as auxiliary variables. It should be noted that these auxiliary variables are only under the control of the aggregator but not the TSO. Therefore, they are translated to the variables which can be controlled by the TSO, i.e. $f_{kts}^{\mathrm{P+}}, f_{kts}^{\mathrm{P-}}, f_{kts}^{\mathrm{PE+}}, f_{kts}^{\mathrm{PE-}}$. The relationships between both sets of variables are:

$$f_{kts}^{\mathrm{P+}} = f_{kts}^{\mathrm{DDG+}} \qquad \forall k \in \mathbb{A}, \forall t \in \mathbb{T}, \forall s \in \mathbb{S}, \tag{2.1}$$

$$f_{kts}^{\mathrm{P-}} = f_{kts}^{\mathrm{DDG-}} \qquad \forall k \in \mathbb{A}, \forall t \in \mathbb{T}, \forall s \in \mathbb{S}, \tag{2.2}$$

$$f_{kts}^{\mathrm{PE+}} = f_{kts}^{\mathrm{EES+}} + f_{kts}^{\mathrm{FL+}} \qquad \forall k \in \mathbb{A}, \forall t \in \mathbb{T}, \forall s \in \mathbb{S}, \tag{2.3}$$

$$f_{kts}^{\mathrm{PE-}} = f_{kts}^{\mathrm{EES-}} + f_{kts}^{\mathrm{FL-}} \qquad \forall k \in \mathbb{A}, \forall t \in \mathbb{T}, \forall s \in \mathbb{S}, \tag{2.4}$$

- **From TSO's viewpoint**: an AFEN is formed of 1- a P-constrained[4] active power flexibility source ($f_{kts}^{\mathrm{P+}}, f_{kts}^{\mathrm{P-}}$), 2- a P&E-constrained[5] active power flexibility source ($f_{kts}^{\mathrm{PE+}}, f_{kts}^{\mathrm{PE-}}$), along with 3- an equivalent load, as illustrated in Fig. 2.3. They respectively represent 1- the part of active power flexibility restricted only by the power limits ($\sum_n \mathrm{F}_{kn}^{\mathrm{P+,max}}, \sum_n \mathrm{F}_{kn}^{\mathrm{P-,max}}$) like those of dispatchable DGs, 2- the part of active power flexibility restricted by both power limits ($\sum_n \mathrm{F}_{kn}^{\mathrm{PE+,max}}, \sum_n \mathrm{F}_{kn}^{\mathrm{PE-,max}}$) and energy limits ($\mathrm{E}_{k}^{\mathrm{PE+,max}}, \mathrm{E}_{k}^{\mathrm{PE-,max}}$) similar to those of flexible loads and ESSs, 3- the net active power schedule for the AFEN expressed as:

$$\mathrm{P}_{kt} = -\mathrm{P}_{kt}^{\mathrm{DDG}} - \mathrm{P}_{kt}^{\mathrm{ESS}} + \mathrm{P}_{kt}^{\mathrm{L}} \qquad \forall k \in \mathbb{A}, \forall t \in \mathbb{T}, \tag{2.5}$$

note that a part of P_{kt} might involuntary be shed in time period t and scenario s, it is indicated by $\mathrm{P}_{kts}^{\mathrm{SL}}$. The variables on the left side of (2.1)-(2.4) represent the active power flexibility that TSO deploys from AFEN k in time period t and scenario s. The boundaries of these variables throughout the time horizon ($\sum_n \mathrm{F}_{kn}^{\mathrm{P+,max}}$, $\sum_n \mathrm{F}_{kn}^{\mathrm{P-,max}}$, $\sum_n \mathrm{F}_{kn}^{\mathrm{PE+,max}}$, $\sum_n \mathrm{F}_{kn}^{\mathrm{PE-,max}}$, $\mathrm{E}_{k}^{\mathrm{PE+,max}}$, $\mathrm{E}_{k}^{\mathrm{PE-,max}}$) are offered by AFEN k to the TSO. Then, TSO solves the optimal flexibility allocation problem defined in Section 2.6. The output of this problem quantifies the optimal size of active power flexibility ($\mathrm{F}_{k}^{\mathrm{P+}}$, $\mathrm{F}_{k}^{\mathrm{P-}}$, $\mathrm{F}_{k}^{\mathrm{PE+}}$, $\mathrm{F}_{k}^{\mathrm{PE-}}$) that TSO should book from each AFEN throughout the time horizon to minimize its total cost.

2.5.2 Modeling the Dispatchable/Stochastic Power Plants

The models of both dispatchable power plants (DPPs) and stochastic power plants (SPPs) are shown in Fig. 2.4. DPPs are able not only to follow their (typically day-ahead) defined schedule but also to provide active power flexibility which is restricted just by the power limits. However, SPPs, such as wind and solar power plants, may deviate

[4] Power constrained.
[5] Power and Energy constrained.

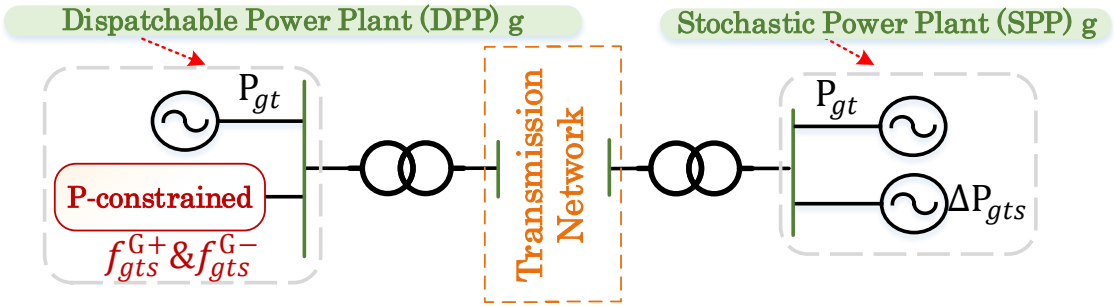

Figure 2.4: The model of dispatchable/stochastic power plant g from TSO viewpoint in time period t and scenario s.

from their schedule because of predictions errors thereby are sources of uncertainties.

2.6 Risk-Aware Flexibility Allocation Model

This Section relies on the resource modeling framework presented in Section 2.5 and leverage a cost-benefit method [41] to construct a risk-aware flexibility allocation model for TSOs. It follows the flexibility allocation procedure introduced in Section 2.3 and minimizes TSO's cost on the basis of a two-stage linear stochastic optimization model. The H&N stage models the flexibility market where the TSO's required size of active power flexibility is booked. Its decision variables, i.e. $\Psi^{H\&N} = \{F_g^{G+}, F_g^{G-}, F_k^{P+}, F_k^{P-}, F_k^{PE+}, F_k^{PE-}\}$ do not depend on any particular scenario and these decisions are made prior to the real-time operation. Then, W&S stage models constraints of power system. Its decision variables, i.e. $\Psi^{W\&S} = \{f_{gts}^{G+}, f_{gts}^{G-}, f_{kts}^{P+}, f_{kts}^{P-}, f_{kts}^{PE+}, f_{kts}^{PE-}, \delta_{its}, P_{kts}^{SL}, P_{lts}^{SL}\}$, pertain to the real-time operation thereby depending on each particular scenario. The mathematical formulation of the model is presented in the following:

2.6.1 Objective Function

The TSO objective is to minimize its total cost, i.e. C^{TSO}, which is formed of the cost associated with H&N stage and the expected cost associated with W&S stage:

$$\min_{\Psi^{H\&N} \bigcup \Psi^{W\&S}} C^{TSO} = C^{H\&N} + \sum_{t \in \mathbb{T}} EC_t^{W\&S}, \tag{2.6}$$

1. $C^{H\&N}$ is the cost of TSO due to booking upward/downward active power flexibility in H&N stage, i.e. prior to the real-time operation. It is formed of the sum of TSO's cost due to booking upward/downward active power flexibility from P-constrained (C_k^{P+}/C_k^{P-}) and P&E-constrained (C_k^{PE+}/C_k^{PE-}) resources of AFENs as

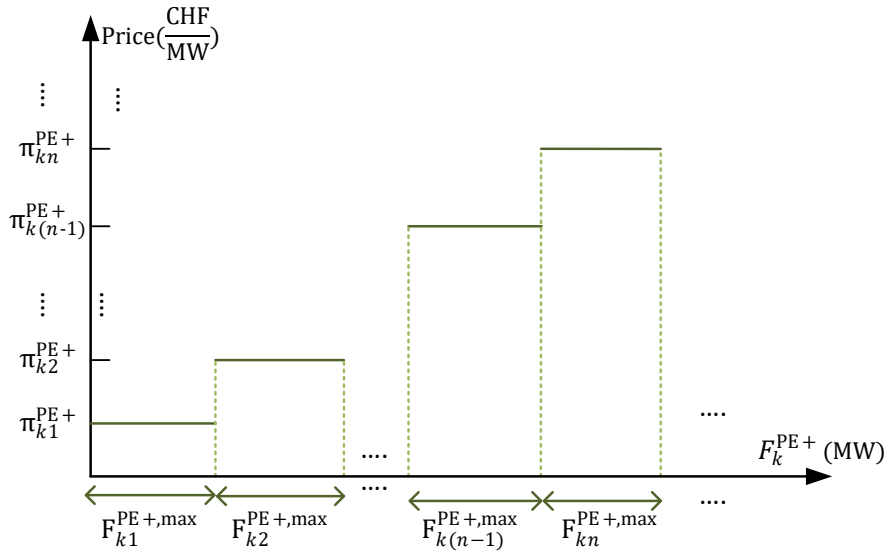

Figure 2.5: Offer curve of AFEN k for its size of upward PE-constrained active power flexibility.

well as DPPs ($C^{\text{G+}}_g / C^{\text{G-}}_g$):

$$C^{\text{H\&N}} = \sum_{g \in \mathbb{DP}} (C^{\text{G+}}_g + C^{\text{G-}}_g) + \sum_{k \in \mathbb{A}} (C^{\text{P+}}_k + C^{\text{P-}}_k + C^{\text{PE+}}_k + C^{\text{PE-}}_k), \tag{2.7}$$

in which all terms are piece-wise linear functions thanks to the piece-wise constant offer curves of the active power flexibility providers. However, each of these terms has a linear equivalent. For the sake of brevity, the following only extracts the linear equivalent for the term associated with TSO's cost due to booking upward active power flexibility from P&E-constrained resources of AFEN k in H&N stage, i.e. $C^{\text{PE+}}_k$. To this end, let's consider the offer curve of AFEN k for its upward P&E-constrained active power flexibility as shown in Fig. 2.5. The area under the offer curve defines $C^{\text{PE+}}_k$ which is a piece-wise linear function of $F^{\text{PE+}}_k$. The nth piece of $C^{\text{PE+}}_k$ is called $C^{\text{PE+}}_{kn}$ and corresponds to $\sum_{n'=1}^{n-1} \text{F}^{\text{PE+,max}}_{kn'} \leq F^{\text{PE+}}_k \leq \sum_{n'=1}^{n} \text{F}^{\text{PE+,max}}_{kn'}$. $C^{\text{PE+}}_{kn}$ can be mathematically expressed as:

$$C^{\text{PE+}}_{kn} = \pi^{\text{PE+}}_{kn} F^{\text{PE+}}_k + \sum_{n'=1}^{n-1} (\pi^{\text{PE+}}_{kn'} - \pi^{\text{PE+}}_{kn}) \text{F}^{\text{PE+,max}}_{kn'}. \tag{2.8}$$

$C^{\text{PE+}}_k$ is an increasing piece-wise linear function thanks to the fact that the offer curves are increasing functions. Therefore, minimizing $C^{\text{PE+}}_k$ over all pieces is equivalent to:

$$\min \gamma^{\text{PE+}}_k, \tag{2.9}$$

subject to

$$C^{\text{PE+}}_{kn} \leq \gamma^{\text{PE+}}_k \qquad \forall n \in \mathbb{N}, \tag{2.10}$$

where $\gamma_k^{\mathrm{PE+}}$ is an auxiliary variable. In the same way, the linear counterparts of the other terms of (2.7) can be extracted by introducing auxiliary variables $\gamma_k^{\mathrm{G+}}$, $\gamma_k^{\mathrm{G-}}$, $\gamma_k^{\mathrm{P+}}$, $\gamma_k^{\mathrm{P+}}$, $\gamma_k^{\mathrm{PE-}}$. Consequently, $C^{\mathrm{H\&N}}$ can be linearly expressed as:

$$C^{\mathrm{H\&N}} = \sum_{g\in\mathbb{DP}} (\gamma_g^{\mathrm{G+}} + \gamma_g^{\mathrm{G-}}) + \sum_{k\in\mathbb{A}} (\gamma_k^{\mathrm{P+}} + \gamma_k^{\mathrm{P-}} + \gamma_k^{\mathrm{PE+}} + \gamma_k^{\mathrm{PE-}}), \tag{2.11}$$

$$\gamma_g^{\mathrm{G+}} \geq C_{gn}^{\mathrm{G+}}, \qquad \forall g \in \mathbb{DP},\ \forall n \in \mathbb{N} \tag{2.12}$$

$$\gamma_g^{\mathrm{G-}} \geq C_{gn}^{\mathrm{G-}}, \qquad \forall g \in \mathbb{DP},\ \forall n \in \mathbb{N} \tag{2.13}$$

$$\gamma_k^{\mathrm{P+}} \geq C_{kn}^{\mathrm{P+}}, \qquad \forall k \in \mathbb{A},\quad \forall n \in \mathbb{N} \tag{2.14}$$

$$\gamma_k^{\mathrm{P-}} \geq C_{kn}^{\mathrm{P-}}, \qquad \forall k \in \mathbb{A},\quad \forall n \in \mathbb{N} \tag{2.15}$$

$$\gamma_k^{\mathrm{PE+}} \geq C_{kn}^{\mathrm{PE+}}, \qquad \forall k \in \mathbb{A},\quad \forall n \in \mathbb{N} \tag{2.16}$$

$$\gamma_k^{\mathrm{PE-}} \geq C_{kn}^{\mathrm{PE-}}, \qquad \forall k \in \mathbb{A},\quad \forall n \in \mathbb{N} \tag{2.17}$$

where $C_{gn}^{\mathrm{G+}}$, $C_{gn}^{\mathrm{G-}}$, $C_{kn}^{\mathrm{P+}}$, $C_{kn}^{\mathrm{P-}}$, $C_{kn}^{\mathrm{PE+}}$, $C_{kn}^{\mathrm{PE-}}$ respectively indicate the nth piece of $C_g^{\mathrm{G+}}$, $C_g^{\mathrm{G-}}$, $C_k^{\mathrm{P+}}$, $C_k^{\mathrm{P-}}$, $C_k^{\mathrm{PE+}}$, $C_k^{\mathrm{PE-}}$. All of them can be calculated similar to the way that $C_{kn}^{\mathrm{PE+}}$ was calculated in (2.8).

2. $EC_t^{\mathrm{W\&S}}$ is the expected cost of TSO in W&S (real-time operation) stage over time period t due to deploying upward/downward active power flexibility, i.e. $EC_t^{\mathrm{Flexibility}}$, and load curtailment, i.e. $EC_t^{\mathrm{Curtailment}}$:

$$EC_t^{\mathrm{W\&S}} = EC_t^{\mathrm{Flexibility}} + EC_t^{\mathrm{Curtailment}} \tag{2.18}$$

where $EC_t^{\mathrm{Flexibility}}$ is the expected cost of TSO due to deploying upward/downward active power flexibility from DPPs and AFENs (P-constrained as well as P&E-constrained sources) during the real-time operation over time period t:

$$\begin{aligned} EC_t^{\mathrm{Flexibility}} = &\sum_{s\in\mathbb{S}} \tau\rho_s\pi_t^{+}[\sum_{g\in\mathbb{DP}} f_{gts}^{\mathrm{G+}} + \sum_{k\in\mathbb{A}} \left(f_{kts}^{\mathrm{P+}} + f_{kts}^{\mathrm{PE+}}\right)] + \\ &+ \sum_{s\in\mathbb{S}} \tau\rho_s\pi_t^{-}[\sum_{g\in\mathbb{DP}} f_{gts}^{\mathrm{G-}} + \sum_{k\in\mathbb{A}} \left(f_{kts}^{\mathrm{P-}} + f_{kts}^{\mathrm{PE-}}\right)] \end{aligned} \tag{2.19}$$

and $EC_t^{\mathrm{Curtailment}}$ is the expected cost of TSO due to demand curtailment of AFENs and loads during the real-time operation over time period t:

$$EC_t^{\mathrm{Curtailment}} = \sum_{s\in\mathbb{S}} \sum_{i\in\mathbb{B}} \tau\rho_s \mathrm{VOLL}_i [\sum_{l\in\mathbb{L}_i} P_{lts}^{\mathrm{SL}} + \sum_{k\in\mathbb{A}_i} P_{kts}^{\mathrm{SL}}] \tag{2.20}$$

Note that expressions (2.11) and (2.19) characterize the cost of active power flexibility while expression (2.20) relies on the value of lost load (VOLL) index to economically quantify the TSO's risk whose reduction characterizes the benefit of the active power flexibility. In other words, the objective function aims at booking active power flexibility while balancing the costs and benefits incurred by the active power flexibility. In this way, it prevents over-booking, which is uneconomic, and under-booking, which is

unreliable.

2.6.2 Constraints of H&N Stage

The size of upward/downward active power flexibility that TSO books from DPPs and AFENs should respect the size of flexibility offered by providers:

$$0 \leq F_g^{\mathrm{G}+} \leq \sum_{n\in\mathbb{N}} \mathrm{F}_{gn}^{\mathrm{G}+,\max} \qquad \forall g \in \mathbb{DP} \tag{2.21}$$

$$0 \leq F_g^{\mathrm{G}-} \leq \sum_{n\in\mathbb{N}} \mathrm{F}_{gn}^{\mathrm{G}-,\max} \qquad \forall g \in \mathbb{DP} \tag{2.22}$$

$$0 \leq F_k^{\mathrm{P}+} \leq \sum_{n\in\mathbb{N}} \mathrm{F}_{kn}^{\mathrm{P}+,\max} \qquad \forall k \in \mathbb{A} \tag{2.23}$$

$$0 \leq F_k^{\mathrm{P}-} \leq \sum_{n\in\mathbb{N}} \mathrm{F}_{kn}^{\mathrm{P}-,\max} \qquad \forall k \in \mathbb{A} \tag{2.24}$$

$$0 \leq F_k^{\mathrm{PE}+} \leq \sum_{n\in\mathbb{N}} \mathrm{F}_{kn}^{\mathrm{PE}+,\max} \qquad \forall k \in \mathbb{A} \tag{2.25}$$

$$0 \leq F_k^{\mathrm{PE}-} \leq \sum_{n\in\mathbb{N}} \mathrm{F}_{kn}^{\mathrm{PE}-,\max} \qquad \forall k \in \mathbb{A} \tag{2.26}$$

2.6.3 Constraints of W&S Stage

During the real-time operation, the amount of upward/downward active power flexibility that TSO is allowed to deploy from DPPs and AFENs is restricted by the booked size of active power flexibility in H&N stage:

$$0 \leq f_{gts}^{\mathrm{G}+} \leq \mathrm{A}_{gts}^{\mathrm{G}} F_g^{\mathrm{G}+} \qquad \forall g \in \mathbb{DPP}, \forall t \in \mathbb{T}, \forall s \in \mathbb{S} \tag{2.27}$$

$$0 \leq f_{gts}^{\mathrm{G}-} \leq \mathrm{A}_{gts}^{\mathrm{G}} F_g^{\mathrm{G}-} \qquad \forall g \in \mathbb{DPP}, \forall t \in \mathbb{T}, \forall s \in \mathbb{S} \tag{2.28}$$

$$0 \leq f_{kts}^{\mathrm{P}+} \leq F_k^{\mathrm{P}+} \qquad \forall k \in \mathbb{A}, \forall t \in \mathbb{T}, \forall s \in \mathbb{S} \tag{2.29}$$

$$0 \leq f_{kts}^{\mathrm{P}-} \leq F_k^{\mathrm{P}-} \qquad \forall k \in \mathbb{A}, \forall t \in \mathbb{T}, \forall s \in \mathbb{S} \tag{2.30}$$

$$0 \leq f_{kts}^{\mathrm{PE}+} \leq F_k^{\mathrm{PE}+} \qquad \forall k \in \mathbb{A}, \forall t \in \mathbb{T}, \forall s \in \mathbb{S} \tag{2.31}$$

$$0 \leq f_{kts}^{\mathrm{PE}-} \leq F_k^{\mathrm{PE}-} \qquad \forall k \in \mathbb{A}, \forall t \in \mathbb{T}, \forall s \in \mathbb{S} \tag{2.32}$$

$$-\mathrm{E}_k^{\mathrm{PE}-,\max} \leq \sum_{t'=1}^{t} \left(f_{kt's}^{\mathrm{PE}+} - f_{kt's}^{\mathrm{PE}-} \right) \tau \leq \mathrm{E}_k^{\mathrm{PE}+,\max} \qquad \forall k \in \mathbb{A}, \forall t \in \mathbb{T}, \forall s \in \mathbb{S} \tag{2.33}$$

The transmission lines' flow limits as well as nodal active power balance in each time period are modeled based on the DC load-flow model:

$$-\mathrm{P}_{ij}^{\max} \leq \mathrm{A}_{ijts}^{\mathrm{L}} \mathrm{B}_{ij} \left(\theta_{its} - \theta_{jts} \right) \leq \mathrm{P}_{ij}^{\max}, \qquad \forall i,j \in \mathbb{B}, \forall t \in \mathbb{T}, \forall s \in \mathbb{S}, \tag{2.34}$$

$$\sum_{k\in\mathbb{A}_i}\left[-\left(\mathrm{P}_{kt}-\mathrm{P}^{\mathrm{SL}}_{kts}\right)+f^{\mathrm{P}+}_{kts}-f^{\mathrm{P}-}_{kts}+f^{\mathrm{PE}+}_{kts}-f^{\mathrm{PE}-}_{kts}\right]+\sum_{g\in\mathbb{DPP}_i}\left[\mathrm{A}^{\mathrm{G}}_{gts}\left(\mathrm{P}_{gt}+f^{\mathrm{G}+}_{gts}-f^{\mathrm{G}-}_{gts}\right)\right]+$$
$$+\sum_{g\in\mathbb{SPP}_i}\left[\mathrm{A}^{\mathrm{G}}_{gts}\left(\mathrm{P}_{gt}+\Delta\mathrm{P}_{gts}\right)\right]+\sum_{l\in\mathbb{L}_i}\left[-\left(\mathrm{P}_{lt}+\Delta\mathrm{P}_{lts}-P^{\mathrm{SL}}_{lts}\right)\right]=\sum_{j\in\mathbb{B}_i}\mathrm{A}^{\mathrm{L}}_{ijts}\,\mathrm{B}_{ij}\left(\theta_{its}-\theta_{jts}\right) \quad (2.35)$$
$$\forall i\in\mathbb{B},\forall t\in\mathbb{T},\ \forall s\in\mathbb{S},$$

$$\theta_{1ts}=0 \qquad \forall t\in\mathbb{T},\ \forall s\in\mathbb{S}. \quad (2.36)$$

where bus 1 is considered as the reference bus for the voltage angle of buses.

The two-stage stochastic optimization model is composed of the objective function (2.6) along with constraints (2.12)-(2.17), (2.21)-(2.36). This model can help TSOs to optimally book active power flexibility from not only DPPs but also AFENs while economically balancing the costs and benefits of the active power flexibility. It should be highlighted that constraint (2.33) couples all time periods to each other, thus, the presented two-stage optimization problem must be solved considering all time periods belonging the time horizon $\mathscr{H}$.

2.7 Case Study

The effectiveness of the proposed method is illustrated in the case of a real transmission grid, i.e. Switzerland's transmission grid operated by Swissgrid. In this study, it is assumed that stochastic renewable generation are substituted for nuclear generation. The topology of this grid is shown in Fig. 2.6, it consists of 212 buses at 220 kV and 380 kV which are connected together via 25 transmission-transformers and 284 transmission lines. This grid, located in the central part of Europe, is connected to Germany, France, Austria and Italy via 37 buses. In this study, these 37 interconnecting buses are modeled as a constant positive/negative injection in each time period. All buses of the grid can be classified into 5 categories based on the entity connected to them:

- DPP buses hosting DPPs;
- SPP buses hosting SPPs;
- Interconnecting buses, i.e buses connecting the grid to neighboring countries;
- AFENs buses hosting AFENs;
- Load buses hosting aggregated consumers;

Based on the time-line of the problem described in Section 2.3, the duration of $\mathscr{H}$ and τ are respectively considered 24 hours and 1 hour which models 24-hour of next day. Each 1-hour time period corresponds to a single scheduled operating point.

All grid's parameters and scheduled operating points of the grid over the 24-hour of study are provided by Swissgrid. Fig. 2.7 shows the total active power generation

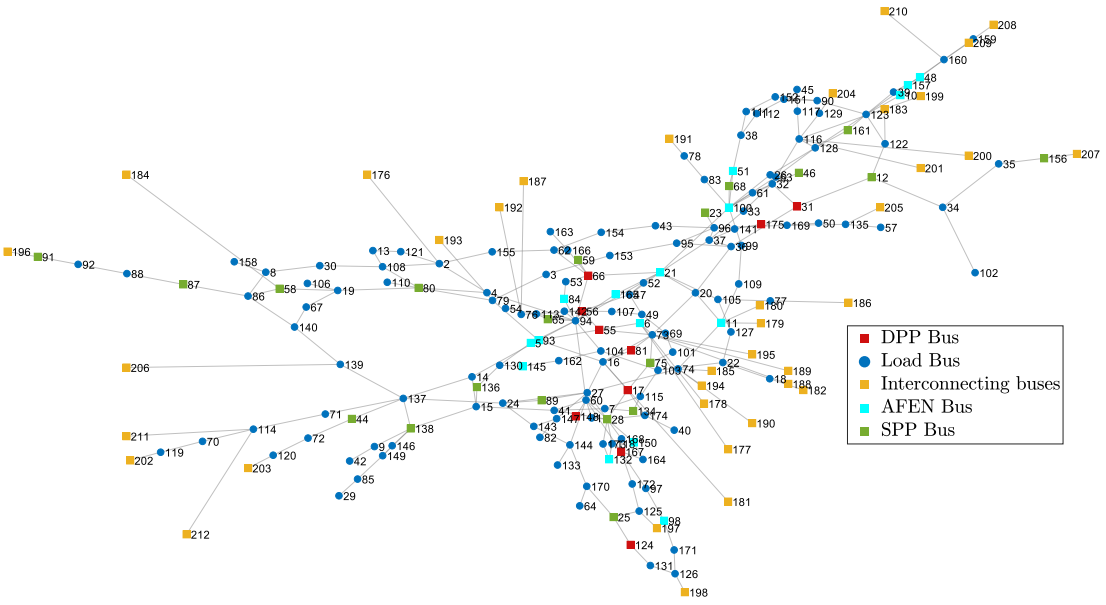

Figure 2.6: Swissgrid network topology.

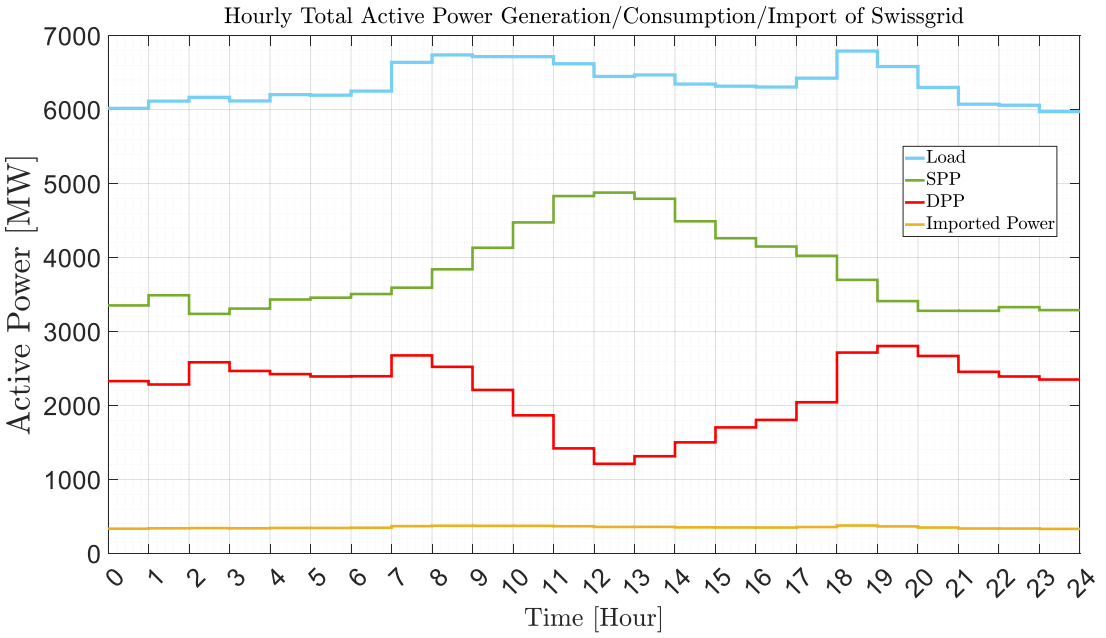

Figure 2.7: Total active power generation, consumption and import of the transmission network during 24 hours of study.

of DPPs and SPPs along with the total imported power from neighboring networks and the total consumption of the loads throughout all 24 time periods. The total energy consumption of the network is 152.6 GWh throughout all 24 time periods and stochastic generation covers 60% of it.

Active power generation of stochastic renewable generation and active power demand of loads are associated with uncertainties due to forecast errors, i.e. ΔP_{gts} and i.e. ΔP_{lts}. These uncertainties are assumed to be independent and identically distributed [42]. Therefore, ΔP_{gts} of stochastic renewable generation are sampled from Gaussian distributions with 0 mean and such that the root mean square error (RMSE) of the total stochastic renewable generation of Switzerland is 10% of the total predicted one. In the same way, ΔP_{lts} of loads are sampled from Gaussian distributions with 0 mean and such that the RMSE of the total demand of Switzerland is 5% of the total predicted one. Following the elaborated approach, 500 scenarios are generated to model uncertainties.

2.7.1 Constructing the Offer Curves of Flexibility Providers on the basis of the Siwssgrid's Flexibility Market Reports

Swissgrid regularly publishes the outcomes of its flexibility market including the prices/volumes of deployed and booked active power flexibility [43–45]. After processing this data, this chapter assumes the price of upward/downward deployed active power flexibility, i.e. π_t^+ and π_t^-, equal to the annual average price of the respective product over 2019:

$$\pi_t^+ = 102 \text{ Euro/MWh} \qquad \forall t \in \mathbb{T} \tag{2.37}$$

$$\pi_t^- = 35 \text{ Euro/MWh} \qquad \forall t \in \mathbb{T} \tag{2.38}$$

To determine the offer curves of DPPs and AFENs for their upward/downward active power flexibility (i.e. $\pi_{gn}^{G+}, \pi_{gn}^{G-}, \pi_{kn}^{P+}, \pi_{kn}^{P-}, \pi_{kn}^{PE+}, \pi_{kn}^{PE-}$), the prices and volumes of upward/-downward booked active power flexibility of the Swissgrid over 2019 are processed (separately for upward and downward booked active power flexibility) as:

1. Prices are firstly sorted in ascending order.
2. The sorted prices are segmented into 20 equi-volume groups where the first group consists of the lowest prices, ..., and the 20th group consists of the highest prices.
3. Weighted average price of each group is calculated considering the volume associated with each price. Accordingly, it results in 20 ascending prices.
4. An increasing piece-wise constant function is constructed relying on the 20 prices achieved in the former step (i.e. step 3). It is assumed that this function has equi-length pieces with length of 10 MW. This function is considered as the offer curve.

This procedure results in the offer curves for upward and downward active power

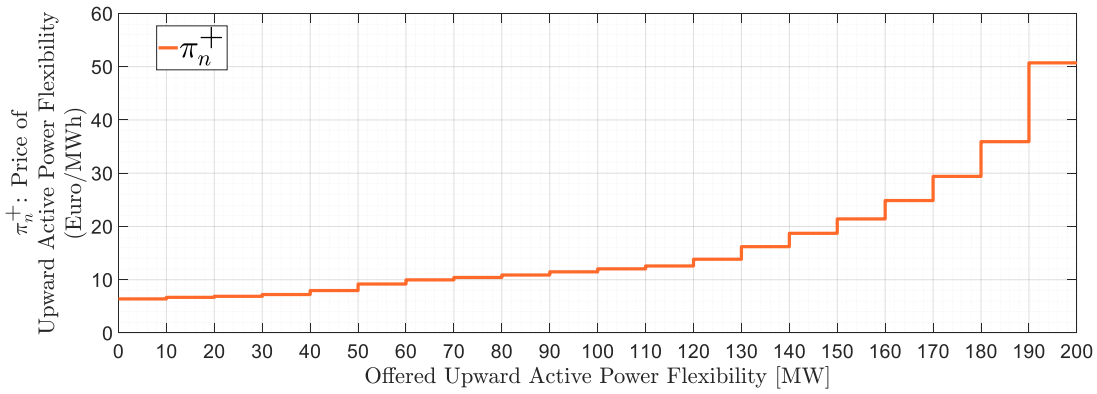

Figure 2.8: Constructed offer curve for upward active power flexibility.

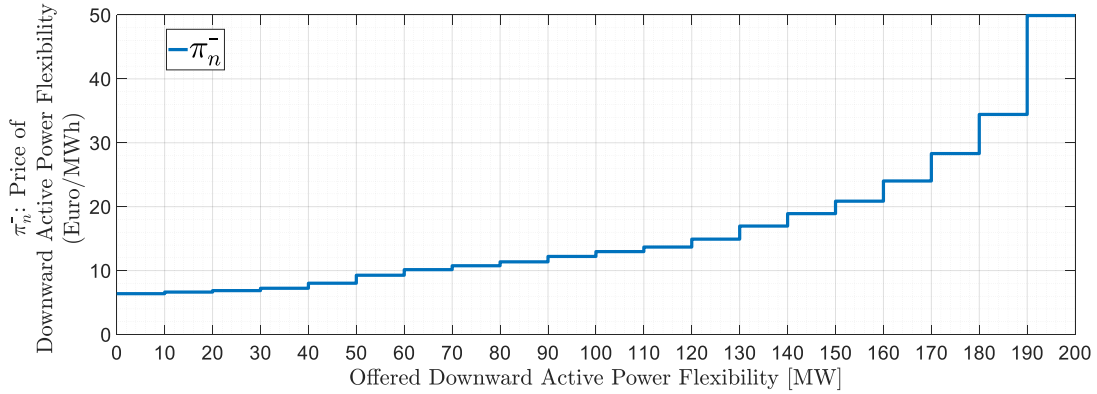

Figure 2.9: Constructed offer curve for downward active power flexibility.

Table 2.1: Size of the upward/downward active power flexibility offered by DPPs to the TSO.

Bus Number of DPP	17	31	55	56	66	81	124	148	167	175
$\sum_n F_{gn}^{G+,max}$	40	150	110	117	29	91	52	45	19	26
$\sum_n F_{gn}^{G-,max}$	78	123	195	150	110	124	58	60	105	130

flexibility represented in Fig. 2.8 and Fig. 2.9. To give the same priority to all power flexibility providers, this chapter supposes that all flexibility providers respectively offer their upward and downward active power flexibility following the offer curves illustrated in Fig. 2.8 and Fig. 2.9. However, it should be noted that each power flexibility provider can come up with its own size of offer. In this respect, the size of active power flexibility offered by DPPs and AFENs are respectively reported in Table 2.1 and Table 2.2.

Table 2.2: Size of the upward/downward active power flexibility offered by AFENs to the TSO.

Bus Number	$\sum_n \mathrm{F}_{kn}^{\mathrm{P+,max}}$	$\sum_n \mathrm{F}_{kn}^{\mathrm{P-,max}}$	$\sum_n \mathrm{F}_{kn}^{\mathrm{PE+,max}}$	$\sum_n \mathrm{F}_{kn}^{\mathrm{PE-,max}}$	$\mathrm{E}_{k}^{\mathrm{PE+,max}}$	$\mathrm{E}_{k}^{\mathrm{PE-,max}}$
5	35	35	18	18	72	62
6	87	87	43	43	45	40
10	30	30	16	16	90	76
11	30	30	15	15	45	50
21	39	39	19	19	37	40
48	25	25	12	12	50	44
51	24	24	12	12	70	64
84	34	34	17	17	65	70
93	43	43	21	21	45	50
98	32	32	16	16	35	44
100	55	55	27	27	94	76
132	38	38	19	19	95	78
145	32	32	16	16	30	24
150	25	25	12	12	56	60
157	28	28	14	14	68	57
165	32	32	16	16	35	38

2.8 Investigating the Performance of the Method

This section aims to evaluate the performance of the presented risk-aware flexibility allocation method by applying it to the case study constructed in section 2.7. In this respect, the problem is modeled using YALMIP-MATLAB [46] and solved with GUROBI [47] on a Windows based system with a 2.9 GHz Intel Core-i7 CPU and 32 GB of RAM.

2.8.1 Estimating the Value of Lost Load (VOLL)

In the absence of a standardized methodology for computing VOLL [48], this section aims to pinpoint a reliable and credible value for VOLL, thereby preventing from over-estimating/under-estimating VOLL that causes TSO to operate its grid in an uneconomic/unreliable manner. In this respect, the impact of the opted VOLL on the reliability of the network (i.e. EENS) and the total cost of TSO (i.e. C^{TSO}) is shown in Fig. 2.10. It corroborates that the reliability of the network improves when VOLL

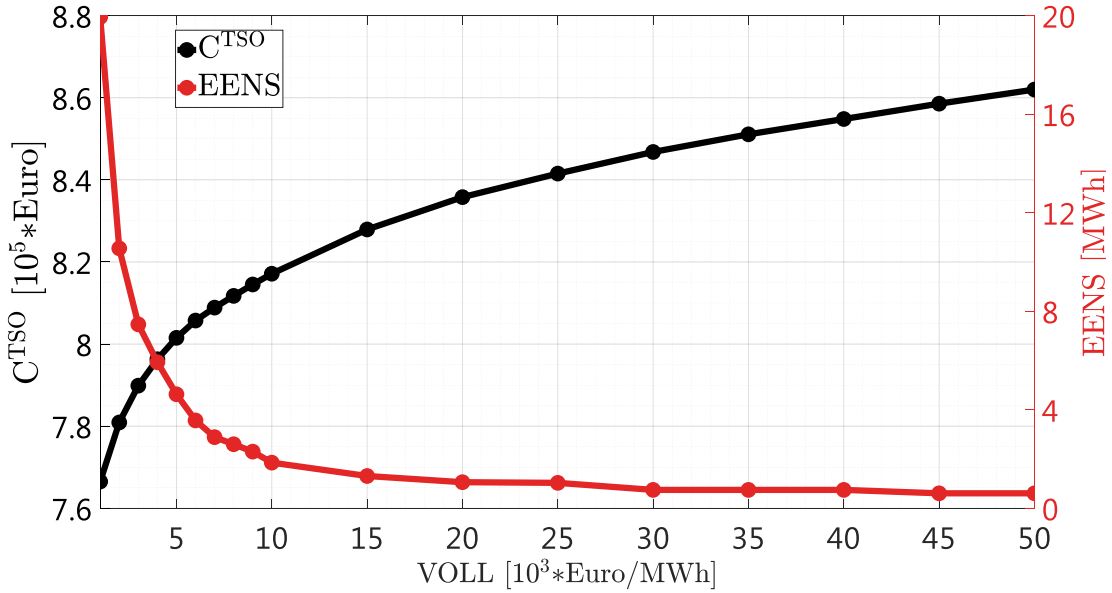

Figure 2.10: Impact of the opted VOLL on the reliability of the grid and C^{TSO}.

increases. More specifically, EENS considerably falls when VOLL increases up to 20000 Euro/MWh, however, above 20000 Euro/MWh, EENS almost levels off while C^{TSO} constantly increases by increasing VOLL. Therefore, it can be concluded that the credible value for VOLL is 20000 Euro/MWh where the TSO operates its grid both reliably and economically. Above all, opting VOLL = 20000 Euro/MWh leads to EENS = 1.31 MWh/day that satisfies the reliability criterion used by some European TSOs, i.e. EENS ≤ 0.002% of the net demand.

2.8.2 Optimal Allocation of Active Power Flexibility

The risk-aware flexibility allocation problem (2.6)-(2.36) is solved given that VOLL is set to 20000 Euro/MWh. The TSO's size of booked upward/downward active power flexibility from each provider is shown in Fig. 2.11. As it can be seen, the method homogeneously books active power flexibility from all providers to prevent from congestion during the real time grid operation.

EENS of the TSO over all 24 time periods is represented in Fig. 2.12. It illustrates that the method accepts a higher EENS at some time periods in such a way that the total cost of TSO over the total scheduling time horizon is minimized. Therefore, the method can be considered as a holistic decision making tool for TSO that takes into account the whole time horizon. In this way, the method prevents from over-booking/under-booking of active power flexibility that gives rise to uneconomic/unreliable operation of the grid.

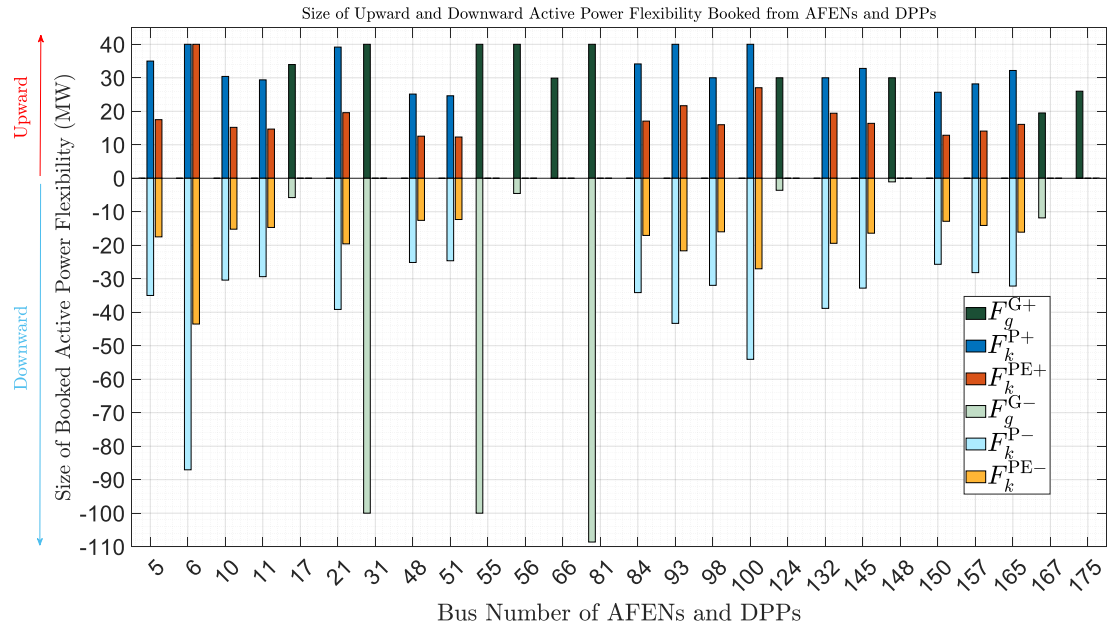

Figure 2.11: TSO's size of booked active power flexibility from AFENs and DPPs.

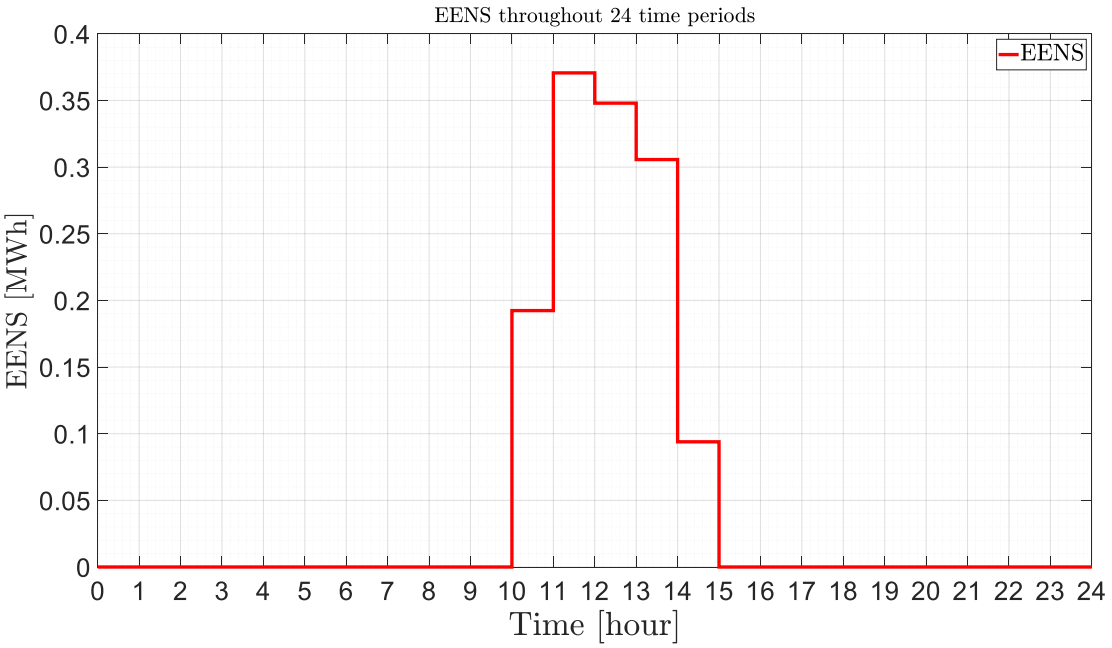

Figure 2.12: EENS of the TSO throughout all 24 time periods.

2.8.3 Investigating the Computational Burden of the Method

This section sets out to elaborate on the computational burden of the method. In this respect, it should be highlighted that YALMIP-MATLAB interface [46] and GUROBI

optimization solver [47] are selected to implement the method on a Windows based system with a 2.9 GHz Intel Core-i7 CPU and 32 GB of RAM. Then, the cast optimization problem is solved considering a time horizon with duration of 24 hours embracing of 24 time periods. The execution time of the problem is 35 minutes for a real-world transmission network, i.e. the electric transmission network of Switzerland, while considering 500 scenarios. It verifies the tractability of the developed two-stage linear model for large-scale networks. This affordable computation burden of the method is achieved thanks to the linear tractable formulation presented for the method. The tractability and agility of the method make it as an applicable and practical solution for large real-world transmission networks. Moreover, the computation time of the method can even be improved if this method is implemented on industry-grade computers and benefited from parallelization techniques.

2.8.4 Economic and Technical Benefits of AFENs

To economically and technically quantify the benefits of AFENs' flexibility, lets first introduce $EC^{\text{Flexibility}}$ as the TSO's total expected cost due to deploying upward/downward active power flexibility over all 24 time periods as:

$$EC^{\text{Flexibility}} = \sum_{t \in \mathbb{T}} EC_t^{\text{Flexibility}} \tag{2.39}$$

and $EC^{\text{Curtailment}}$ as the TSO's total expected cost due to demand curtailment over all 24 time periods as:

$$EC^{\text{Curtailment}} = \sum_{t \in \mathbb{T}} EC_t^{\text{Curtailment}} \tag{2.40}$$

then, the size of active power flexibility offered by AFENs are changed from 0% to 100% of the reported values in Table 2.2. Fig. 2.13 shows the EENS and total cost of the TSO as functions of the size of AFENs' flexibility. As it can be seen, AFENs' flexibility significantly improves the reliability of the network (i.e. EENS) and reduces the total cost of the TSO (i.e. C^{TSO}). It upholds that the reliability of the network improves when AFENs flexibility increases. More specifically, EENS considerably falls when AFENs' flexibility increases up to 60%, however, above 60%, EENS does not significantly change. To figure out why EENS levels off when AFENs' flexibility goes beyond 60%, the impact of AFENs' flexibility on $C^{\text{H\&N}}$ and $EC^{\text{Flexibility}}$ is examined. As illustrated in Fig. 2.14, when AFENs' flexibility increases, $C^{\text{H\&N}}$ constantly increases due to the fact that the TSO books greater deal of active power flexibility to decrease its EENS and accordingly $EC^{\text{Curtailment}}$ (TSO suffers from the shortage of power flexibility). However, when AFENs' flexibility goes beyond 60%, the TSO faces with the oversupply of power flexibility, thus, TSO starts replacing its high price booked flexibility with the low price one. Accordingly, $C^{\text{H\&N}}$ starts falling. Moreover, it should be noted that when AFENs' flexibility increases,

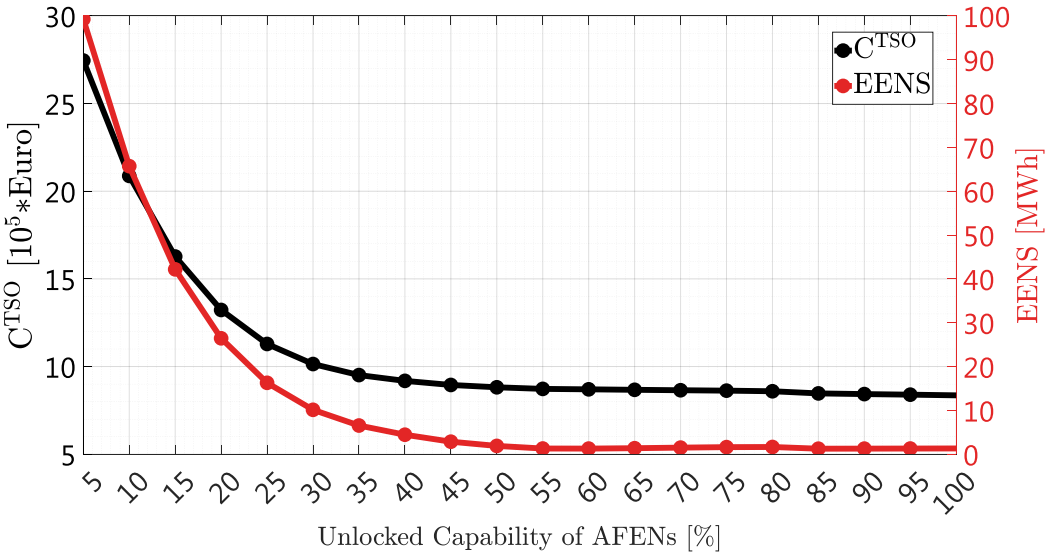

Figure 2.13: Quantifying the benefit of AFENs on the TSO's cost and EENS.

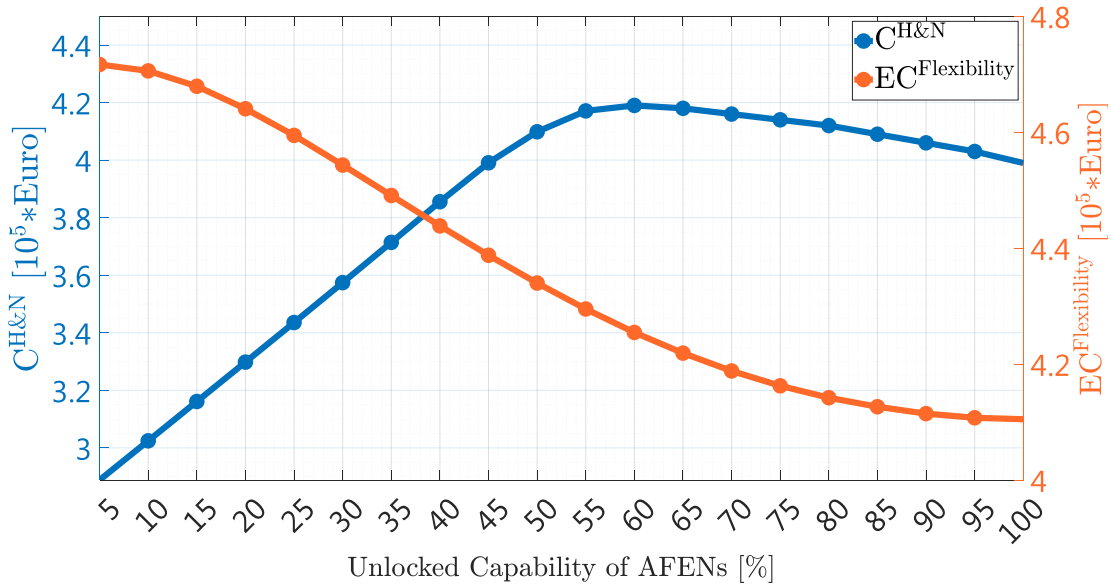

Figure 2.14: Impact of AFENs' flexibility on $C^{\text{H\&N}}$ and $EC^{\text{Flexibility}}$.

$EC^{\text{Flexibility}}$ constantly decreases thanks to the fact that the TSO can deploy its required power flexibility from more buses distributed throughout the grid, thereby more easily (by deploying less amount of power flexibility) mitigating the impact of uncertainties during the real-time grid operation.

Last but not least, Fig. 2.13 and Fig. 2.14 demonstrate the ability of the developed method to quantify the economic and technical benefits of the AFENs, whereby, TSO

can establish promoting policies such as providing incentives to empower AFENs for flexibility provision. Finally, it can be concluded that the provision of active power flexibility by AFENs not only decreases the total cost of TSO, but it also improves the reliability of the transmission network.

2.8.5 Impact of the Precision of Stochastic Generation Prediction on the TSO's Costs and Reliability

The amount of power flexibility that TSO books from different flexibility providers (and its associated cost) depends on the amount of uncertainties stemming from demand and stochastic generation. On the other hand, the magnitude of these uncertainties is largely affected by the precision of the prediction approach used to predict demand and stochastic generation. In this respect, this section aims to investigate the impact of precision of stochastic generation prediction on the TSO's cost and TSO's reliability. In this way, it quantifies the economic and technical benefits of precise stochastic generation prediction for TSO. To this end, it changes the RMSE of the total stochastic (renewable) generation of Switzerland from 7% to 20% of the total predicted one.

The impact of the precision of stochastic generation prediction on the total cost of TSO (i.e. C^{TSO}), and on the reliability of the transmission system, (i.e. EENS), is shown in Fig. 2.15. Fig. 2.15 reveals that both C^{TSO} and EENS constantly increase when RMSE of stochastic generation prediction increases, i.e. precision of prediction decreases. However, EENS significantly increases when RMSE goes beyond 16%. To discover the reason behind this significant increase, Fig. 2.16 illustrates the cost of TSO due to booking flexibility, i.e. $C^{\text{H\&N}}$ along with expected cost of TSO due to deploying flexibility, i.e. $EC^{\text{Flexibility}}$. As it can be seen, when RMSE increases up to 16%, $C^{\text{H\&N}}$ and $EC^{\text{Flexibility}}$ constantly rise because the TSO books and deploys greater deal of power flexibility to preserve the security of its grid against increasing uncertainties. To put it simply, TSO needs greater deal of power flexibility to 1-satisfy grid's constraints, 2-restrict the load not supplied and accordingly 3-restrict the expected cost of TSO related to load not supplied, i.e. $EC^{\text{Curtailment}}$. However, when RMSE goes beyond 16%, the TSO faces with the shortage of power flexibility, i.e. the TSO's required power flexibility is greater than the offered power flexibility of flexibility providers. Therefore, TSO completely books all offered active power flexibility, and as a result, $C^{\text{H\&N}}$ stays constant for RMSE beyond 16%. This shortage of power flexibility gives rise to surge in EENS and accordingly $EC^{\text{Curtailment}}$ and C^{TSO} because TSO cannot deal with severe, i.e. large uncertainties. On the other hand, it should be noted that $EC^{\text{Flexibility}}$ still rises even for RMSE beyond 16% due to the fact that the TSO needs to deal with larger uncertainties on average.

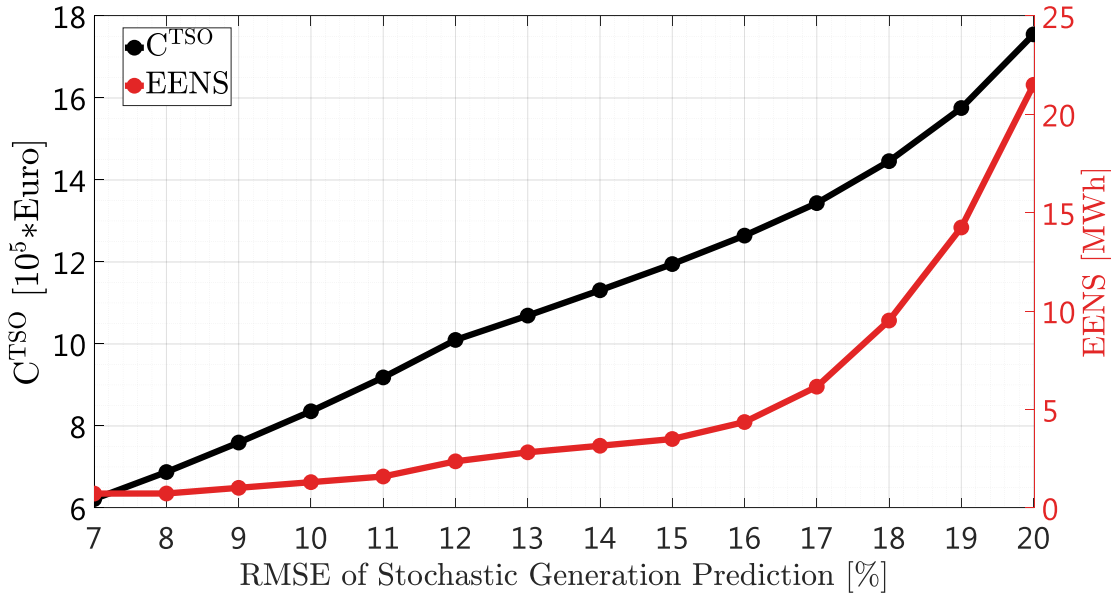

Figure 2.15: Impact of RMSE of stochastic generation prediction on the TSO's cost and EENS.

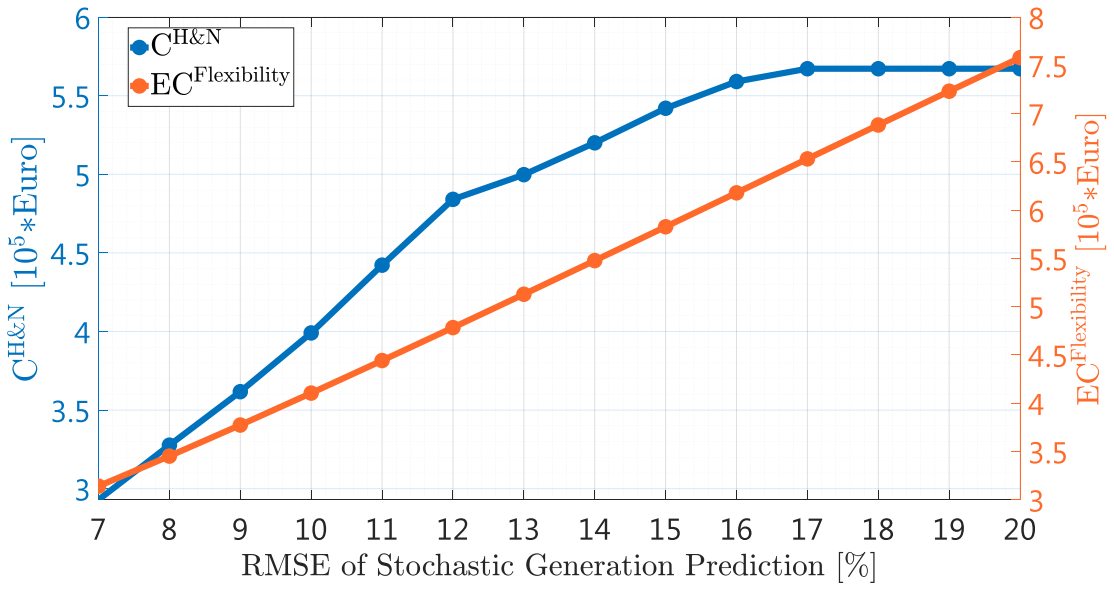

Figure 2.16: Impact of RMSE of stochastic generation prediction on $C^{\text{H\&N}}$ and $EC^{\text{Flexibility}}$.

2.9 Conclusion

This chapter first develops a modeling framework to model aggregated flexibility of distribution networks (AFENs) from TSO's viewpoint, whereby, the flexibility of DERs

located in distribution networks are empowered to participate in the flexibility market of TSO as an aggregated entity. Relying on the modeling framework of AFENs, the chapter constructs a risk-aware active power flexibility allocation model for TSO. This model follows a sequential market structure to suit the Switzerland's flexibility market that is separated from energy market. The model is mathematically formulated as a two-stage linear stochastic optimization problem where a cost-benefit approach is exploited to realize a balance between costs and benefits of the flexibility. This model is envisaged to help TSOs to take advantage of the flexibility of DERs located in distribution networks.

Finally, this chapter selects a real-world transmission grid, i.e. the Switzerland's transmission grid operated by Swissgrid as a case study. Then, the effectiveness of the developed risk-aware flexibility allocation method is investigated on a 24-hour time horizon. The achieved results illustrate the tractability of the method for a large-scale transmission grid. Moreover, economic and technical analysis concretely indicate that the provision of flexibility by AFENs improves the TSO's security despite the reduction of TSO's costs.

All in all, it can be concluded that the chapter succeeded to realize a twofold goal:

- Firstly, it developed a novel approach to modernize the traditional top-to-down flexibility provision mechanism to a bi-directional flexibility provision structure.
- Secondly, it demonstrated the benefits of this novel TSO-DSO collaboration approach.

3 Linearized Power Flow Model for Transmission Networks

> Truth is ever to be found in simplicity, and not in the multiplicity and confusion of things.
>
> — Isaac Newton

Transmission system operators (TSOs) can securely steer their grid if and only if they accurately embed their grids constraints (i.e. power flow equations) in their decision making processes. However, power flow equations describing the state of the grid are non-linear and non-convex, thus, embedding them in the TSO's decision making problems gives rise to intractable problems entailing high computational burden in case of real-world transmission systems. To deal with this complexity, a variety of linear power flow models have been offered, thereby, empowering TSOs to cast their decision making problems as linear optimization (i.e. optimal power flow) problems that can be efficiently solved by taking advantage of the maturity and agility of the existing linear programming solvers. However, available linear power flow models broadly rely on simplification and approximation instead of linearizing the original non-linear power flow equations. In other words, these linear models do not take advantage at most of the existing information. To bridge this gap, this chapter sets out to offer a hot-start [1] linearized power flow model while employing no approximation and simplification. Therefore, the offered power flow model takes advantage at most of the existing information, i.e the solution of AC power flow problem for the given

[1] Hot-start power flow models associated with the cases where the operating point of the grid (and the solution of AC power flow problem for this operating point) is given. Hot-start models provide a linear approximation of the power flow problem to analyze the behavior of the grid around this given operating point called base case (i.e. scheduled) operating point.

base case operating point. More specifically, this power flow model is founded on linearizing all non-linear power flow equations through extracting the first-order Taylor series expansion of power flow equations. This power flow model provides a linear formulation for all constraints associated with the TSO's grid. To put it simply, it offers explicit linear functions to express the following variables as linear functions of the nodal active power injections of PV and PQ buses as well as reactive power injections of PQ buses:

- Voltage magnitudes of all buses;
- Apparent power flow of all branches;
- Active/reactive power injections of slack bus.
- Reactive power injections of PV buses.

Above all, this linear power flow model takes into account shunt susceptance of branches as well as active/reactive power losses of the transmission grid. This linearized power flow model is exploited in chapter 4 to construct a grid-cognizant TSO-DSO coordination framework. Indeed, this coordination framework is mathematically formulated as an optimization problem embracing the power flow constraints. This kind of optimization problem is widely known as optimal power flow (OPF) problem.

Keywords: DC power flow model, linearized power flow model, optimal power flow (OPF), power flow equations, Taylor series expansion, electric transmission systems, transmission system operator (TSO).

Nomenclature

Indices and Sets

i	Index for Buses.
l	Index for transmission lines.
$\mathbb{B}$	Set of all buses.
$\mathbb{B}_{V\Theta}$	Set of Vθ bus.
$\mathbb{B}_{PV}$	Set of PV buses.
$\mathbb{B}_{PQ}$	Set of PQ buses.
$\mathbb{L}$	Set of transmission lines.

Variables (Scalars)

I_i^{Inj}	Phasor of the current injected to bus i [p.u.].
P_i	Total active power injection of bus i.
Q_i	Total reactive power injection of bus i.
S_i	Total complex power injection of bus i (i.e. $P_i + \sqrt{-1}Q_i$).
S_l^{From}	Complex power flow entering the from-end of branch l.
$\|S_l^{\mathrm{From}}\|$	Apparent power flow entering the from-end of branch l.
S_l^{To}	Complex power flow entering the to-end of branch l.
$\|S_1^{\mathrm{To}}\|$	Apparent power flow entering the to-end of branch l.
V_i	Voltage phasor of bus i.
$\|V_i\|$	Voltage magnitude of bus i.
θ_i	Voltage phase angle of bus i.
ΔP_i	Deviation of the active power injection of bus i from its base case value, i.e. $\widehat{\mathrm{P}}_i$.
ΔQ_i	Deviation of the reactive power injection of bus i from its base case value, i.e. $\widehat{\mathrm{Q}}_i$.
ΔS_i	Deviation of the complex power injection of bus i from its base case value, i.e. $\widehat{\mathrm{S}}_i$.
$\Delta\theta_i$	Deviation of the voltage phase angle of bus i from its base case operating point.
$\Delta\|V_i\|$	Deviation of the voltage magnitude of bus i from its base case value, i.e. $\|\widehat{\mathrm{V}}\|_i$.
$\Delta\|S_l^{\mathrm{From}}\|$	Deviation of the apparent power flow entering the from-end of branch l from its base case value.
$\Delta\|S_l^{\mathrm{To}}\|$	Deviation of the apparent power flow entering the to-end of branch l from its base case value.

Variables (Vectors)

$\boldsymbol{I}^{\mathrm{Inj}}$	$= [I_1^{\mathrm{Inj}}, \ldots, I_{\mathrm{n_B}}^{\mathrm{Inj}}]^{\mathrm{T}}$.
$\boldsymbol{P}$	$= \left[P_1, \ldots, P_{\mathrm{n_B}} \right]^{\mathrm{T}}$.

$\boldsymbol{Q}$	$= \left[Q_1 , \ldots, Q_{\mathrm{n_{\mathbb{B}}}} \right]^{\mathrm{T}}$.
$\boldsymbol{S}$	$= \left[S_1 , \ldots, S_{\mathrm{n_{\mathbb{B}}}} \right]^{\mathrm{T}}$.
$\boldsymbol{S}^{\mathrm{From}}$	$= \left[S_1^{\mathrm{From}} , \ldots., S_{\mathrm{n_{\mathbb{L}}}}^{\mathrm{From}} \right]^{\mathrm{T}}$.
$\Vert\boldsymbol{S}^{\mathrm{From}}\Vert$	$= \left[\Vert S_1^{\mathrm{From}}\Vert , \ldots., \Vert S_{\mathrm{n_{\mathbb{L}}}}^{\mathrm{From}}\Vert \right]^{\mathrm{T}}$.
$\boldsymbol{S}^{\mathrm{To}}$	$= \left[S_1^{\mathrm{To}} , \ldots., S_{\mathrm{n_{\mathbb{L}}}}^{\mathrm{To}} \right]^{\mathrm{T}}$.
$\Vert\boldsymbol{S}^{\mathrm{To}}\Vert$	$= \left[\Vert S_1^{\mathrm{To}}\Vert , \ldots., \Vert S_{\mathrm{n_{\mathbb{L}}}}^{\mathrm{To}}\Vert \right]^{\mathrm{T}}$.
$\boldsymbol{V}$	$= [V_1 , \ldots, V_{\mathrm{n_{\mathbb{B}}}}]^{\mathrm{T}}$.
$\Vert\boldsymbol{V}\Vert$	$= \left[\Vert V_1\Vert , \ldots, \Vert V_{\mathrm{n_{\mathbb{B}}}}\Vert \right]^{\mathrm{T}}$.
$\boldsymbol{\theta}$	$= [\theta_1 , \ldots, \theta_{\mathrm{n_{\mathbb{B}}}}]^{\mathrm{T}}$.
$\boldsymbol{\Delta P}$	$= \left[\Delta P_1 , \ldots, \Delta P_{\mathrm{n_{\mathbb{B}}}} \right]^{\mathrm{T}}$.
$\boldsymbol{\Delta Q}$	$= \left[\Delta Q_1 , \ldots, \Delta Q_{\mathrm{n_{\mathbb{B}}}} \right]^{\mathrm{T}}$.
$\boldsymbol{\Delta S}$	$= \left[\Delta S_1 , \ldots, \Delta S_{\mathrm{n_{\mathbb{B}}}} \right]^{\mathrm{T}}$.
$\boldsymbol{\Delta}\Vert\boldsymbol{S}^{\mathrm{From}}\Vert$	$= \left[\Delta\Vert S_1^{\mathrm{From}}\Vert , \ldots., \Delta\Vert S_{\mathrm{n_{\mathbb{L}}}}^{\mathrm{From}}\Vert \right]^{\mathrm{T}}$.
$\boldsymbol{\Delta}\Vert\boldsymbol{S}^{\mathrm{To}}\Vert$	$= \left[\Delta\Vert S_1^{\mathrm{To}}\Vert , \ldots., \Delta\Vert S_{\mathrm{n_{\mathbb{L}}}}^{\mathrm{To}}\Vert \right]^{\mathrm{T}}$.
$\boldsymbol{\Delta}\Vert\boldsymbol{V}\Vert$	$= \left[\Delta\Vert V_1\Vert , \ldots, \Delta\Vert V_{\mathrm{n_{\mathbb{B}}}}\Vert \right]^{\mathrm{T}}$.
$\Delta\boldsymbol{\theta}$	$= \left[\Delta\theta_1 , \ldots, \Delta\theta_{\mathrm{n_{\mathbb{B}}}} \right]^{\mathrm{T}}$.

Parameters (Pertained to the Base Case Operating Point)

$\widehat{\mathrm{P}}_i$	Total active power injection of bus i for the base case operating point.
$\widehat{\mathrm{Q}}_i$	Total reactive power injection of bus i for the base case operating point.
$\widehat{\mathrm{S}}_i$	Total complex power injection of bus i for the base case operating point (i.e. $\widehat{\mathrm{P}}_i + \sqrt{-1}\widehat{\mathrm{Q}}_i$).
$\Vert\widehat{\mathrm{S}}_l^{\mathrm{From}}\Vert$	Apparent power flow entering the from-end of branch l for the base case operating point.
$\Vert\widehat{\mathrm{S}}_l^{\mathrm{To}}\Vert$	Apparent power flow entering the to-end of branch l for the base case operating point.
$\Vert\widehat{\mathrm{V}}\Vert_i$	Voltage magnitude of bus i for the base case operating point.
$\widehat{\mathrm{V}}_i$	Voltage phasor of bus i for the base case operating point ($\widehat{\mathrm{V}}_i = \Vert\widehat{\mathrm{V}}\Vert_i \sphericalangle \widehat{\Theta}_i$).
$\widehat{\Theta}_i$	Voltage phase angle of bus i for the base case operating point.

$\widehat{\mathbf{P}}$ $= \left[\widehat{\mathrm{P}}_1 , \ldots, \widehat{\mathrm{P}}_{\mathrm{n}_{\mathbb{B}}} \right]^{\mathrm{T}}$.

$\widehat{\mathbf{Q}}$ $= \left[\widehat{\mathrm{Q}}_1 , \ldots, \widehat{\mathrm{Q}}_{\mathrm{n}_{\mathbb{B}}} \right]^{\mathrm{T}}$.

$\widehat{\mathbf{S}}$ $= \left[\widehat{\mathrm{S}}_1 , \ldots, \widehat{\mathrm{S}}_{\mathrm{n}_{\mathbb{B}}} \right]^{\mathrm{T}}$.

$\|\widehat{\boldsymbol{S}}^{\mathrm{From}}\|$ $= \left[\|\widehat{\mathrm{S}}_1^{\mathrm{From}}\| , \ldots, \|\widehat{\mathrm{S}}_{\mathrm{n}_{\mathbb{L}}}^{\mathrm{From}}\| \right]^{\mathrm{T}}$.

$\|\widehat{\boldsymbol{S}}^{\mathrm{To}}\|$ $= \left[\|\widehat{\mathrm{S}}_1^{\mathrm{To}}\| , \ldots, \|\widehat{\mathrm{S}}_{\mathrm{n}_{\mathbb{L}}}^{\mathrm{To}}\| \right]^{\mathrm{T}}$.

$\widehat{\mathbf{V}}$ $= \left[\widehat{\mathrm{V}}_1 , \ldots, \widehat{\mathrm{V}}_{\mathrm{n}_{\mathbb{B}}} \right]^{\mathrm{T}}$.

$\|\widehat{\mathbf{V}}\|$ $= \left[\|\widehat{\mathrm{V}}\|_1 , \ldots, \|\widehat{\mathrm{V}}_{\mathrm{n}_{\mathbb{B}}}\| \right]^{\mathrm{T}}$.

$\widehat{\boldsymbol{\Theta}}$ $= \left[\widehat{\Theta}_1 , \ldots, \widehat{\Theta}_{\mathrm{n}_{\mathbb{B}}} \right]^{\mathrm{T}}$.

Parameters (Pertained to the Grid)

$\mathrm{n}_{\mathbb{B}}$ Number of buses.

$\mathrm{n}_{\mathbb{L}}$ Number of transmission lines/transformers.

$\mathrm{n}_{\mathbb{PV}}$ Number of PV buses.

$\mathrm{n}_{\mathbb{PQ}}$ Number of PQ buses.

$\mathbf{A}$ Branch to node incidence matrix.

$\mathbf{A}^{\mathrm{From}}$ Branch to from-node incidence matrix.

$\mathbf{A}^{\mathrm{To}}$ Branch to to-node incidence matrix.

$\mathrm{S}_l^{\mathrm{Max}}$ Maximum power flow limit of branch l [p.u.].

$\mathrm{V}_i^{\mathrm{Max}}$ Maximum voltage limit of bus i [p.u.].

$\mathrm{V}_i^{\mathrm{Min}}$ Minimum voltage limit of bus i [p.u.].

y_l Shunt admittance of branch l.

z_l Series impedance of branch l.

$\mathbf{S}^{\mathrm{Max}}$ $= \left[\mathrm{S}_1^{\mathrm{Max}} , \ldots . , \mathrm{S}_{\mathrm{n}_{\mathbb{L}}}^{\mathrm{Max}} \right]^{T}$.

$\mathbf{V}^{\mathrm{Max}}$ $= \left[\mathrm{V}_1^{\mathrm{Max}} , \ldots, \mathrm{V}_{\mathrm{n}_{\mathbb{B}}}^{\mathrm{Max}} \right]^{\mathrm{T}}$.

$\mathbf{Y}$ Admittance matrix of the transmission network.

$\mathbf{Y}^{\mathrm{Sh}}$ $= \left[y_1, \ldots, y_{N_{\mathbb{L}}} \right]^{\mathrm{T}}$.

$\mathbf{Z}^{\mathrm{Se}}$ $= \left[z_1, \ldots, z_{N_{\mathbb{L}}} \right]^{\mathrm{T}}$.

3.1 State of the Art

Power flow equations are indispensable part of modeling, planning, operation and control of electric power systems [49]. Since the invention of modern computers in 1960's, researchers have developed a variety of methods [50], [51] to tackle these non-linear non-convex algebraic equations. The set of power flow equations stating the steady-state transmission of power in an AC electric power system is widely recognized as power flow problem [49]. Power flow problem aims to determine the voltage magnitude and voltage phase angle of all buses, thereby determining all other electric quantities of the grid like power flow of lines. Complexity of the power flow problem has led researchers to come up with approximate models [52–65]. Among all exiting power flow models for transmission networks, DC power flow model has been the most favorite/utilized one thanks to its linear and simple formulation [49], [52]. It is worth noting that DC power flow model has been established on the basis of three assumptions:

- Voltage magnitude of all buses are identical and equal to 1 p.u.
- Series resistance (R) of all branches as well as shunt susceptance of all branches are ignored, i.e. assumed equal to 0.
- The difference between voltage phase angle of buses are small, thus, $\sin(\theta_1 - \theta_2) \approx \theta_1 - \theta_2$.

Considering the widespread utilization of DC power flow model for different applications, the performance of DC power flow model has been analyzed in multiple works [52, 53, 66–70]. Work in [66] draws an experimental comparison between the performance of DC power flow model and AC power flow model for contingency and reliability analysis. It concludes that DC power flow model might lead to results that are quite far away from the results achieved from AC power flow model. Accuracy of DC power flow model for determining locational marginal price (LMP) is investigated in [67]. It concludes that, in general, the accuracy of DC power flow model for calculating LMP is acceptable. However, there might be some buses where the accuracy of the calculated LMP is poor. [68] investigates the performance of DC power flow model for cascade failure simulations. It reaches to the conclusion that DC power flow model might result in inaccurate and optimistic cascade predictions. [69] leverages convex relaxation techniques and introduces a method to determine the upper bound for the approximation error of DC power flow model. Assumptions of DC power flow model have been individually investigated in [70], most notably, this work quantifies the error resulted form those assumptions. To improve the performance of DC power flow model, [52, 53] offer modified versions of DC power flow to account for active power losses of the transmission lines. Moreover, they compare the performance of these variant of DC power flow model with each other.

The feasibility of DC optimal power flow problem (OPF) is investigated in [71]. In other words, it mathematically checks whether solution of DC OPF (and also modified DC OPFs) is AC feasible or not. This work shows that under light assumptions, the feasible region of DC OPF (and even modified DC OPFs) has no intersection with feasible region of AC OPF. Therefore, solution of DC OPF and its modified versions are AC infeasible. Moreover, it truly highlights that the DC power flow model is not a linearized version of AC power flow and it is just an approximation for AC power flow. However, DC power flow model is often misunderstood as a linearized version of AC power flow equations.

To overcome the drawbacks of DC power flow model and its modified versions, researchers have recently offered linear power flow models considering reactive power flow and grid's losses [59–65]. The work in [59] develops a linear power flow model in polar coordinates by 1-defining a number of tangential lines to form a convex envelop of the cosine function, and 2-approximating the sin function using the first order Taylor series expansion. Considering the way that the cosine function is approximated, this linear approximation of the power flow model is solely applicable in cases where the objective function of the OPF embraces the terms associated to the convexified cosine function. Moreover, this model fails to linearly model maximum power flow limit of branches.

Works in [60] and [61] constructs a linearized power flow model through extracting first order Taylor series expansion of non-linear power flow equations while 1-regarding nodal voltage magnitudes and nodal voltage phase angles as independent variables, 2-assuming the nodal voltage magnitudes are close to 1 p.u. (i.e. $V \approx 1 p.u.$), 3-approximating $\sin(\theta) \approx \theta$ and $\cos(\theta) \approx 1$. Assumptions 2 and 3 cause that the constructed model cannot account for active/reactive power losses of the gird. To resolve this issue, it adds new terms (coming from the second order approximation of $\cos(\theta)$, namely θ^2) to embed active/reactive power losses of the transmission lines in the power flow model. Then, it offers an approach to linearize θ^2. However, this approach is only valid for the cases where the objective function of the OPF problem is increasing in respect to the grid's losses. Moreover, it fails to linearly model maximum power flow limit of branches.

The work in [62] considers 1-the square of the nodal voltage magnitude (i.e. ${V_i}^2$, ${V_j}^2$) and 2-the nodal voltage phase angle multiplied by the square of the nodal voltage magnitude (i.e. ${V_i}^2\theta_i, {V_j}^2\theta_j$) as the independent variables. Then, it builds a linear approximation of the power flow equations by 1-introducing a heuristic parameter and approximating $\sin(\theta_i) \approx 0.95\theta_i$, $\sin(\theta_j) \approx 0.95\theta_j$, $\cos(\theta_i) \approx 0.95$, $\cos(\theta_j) \approx 0.95$, and 2-approximating $V_i \approx V_j$, and 3-approximating $V_i^2\theta_i \approx V_i\theta_i$, $V_j^2\theta_j \approx V_j\theta_j$. However, this work fails to linearly model maximum power flow limit of branches and it has not also reported its performance for reactive power flow of branches and nodal voltage magnitude. Moreover, it exploits some heuristic parameters with no mathematical

support.

The work in [64] considers the real and imaginary parts of the nodal voltage phasor as independent variables. Then, it only extracts the first order Taylor series expansion of the power flow equation without detailing how to solve them.

The work in [63] mathematically investigates all possible linear power flow models that can be constructed by considering the nodal voltage magnitude and nodal voltage phase angle as the independent variables. Among this kind of linear models, it finds that the best model featuring the minimum linearization error is the one extracted on the basis of the first order Taylor expansion of the non-linear power flow equations while 1-square of the nodal voltage magnitude (i.e. ${V_i}^2$, ${V_j}^2$), and 2-the voltage phase angle difference between from-end bus and to-end bus of branches (i.e. $\theta_i - \theta_j$) are regarded as the independent variables. However, this linearization approach suffers from the fact that the selected independent variables (i.e. $\theta_i - \theta_j$) are only independent in the case of radial grids and they are not independent in the case of meshed grids. Accordingly, the mathematical reasoning of [63] is only valid for radial grids. To put it simply, this model provides a linearized version of the AC power flow model solely in the case of radial grids. In the case of meshed grid, this model is only a linear approximation of the AC power flow model, nonetheless, it is misinterpreted as the linearized version.

Linear power flow models can be categorized into:

- Hot-Start Linear Power Flow Models: The operating point of the system along with the solution of AC power flow problem for this operating point are given. This operating point is called base case (i.e. scheduled) operating point. Relying on this additional information, hot-start models provide a linear approximation of the power flow problem to analyze the behavior of the grid around the base case operating point. Hot-start models are utilized in applications associated with the short-term grid operation where an initial AC power flow solution is available.
- Cold-Start Linear Power Flow Models: No base case operating point is available. Cold-start models provide a linear approximation of the power flow problem to find the operating point of the system. These models are utilized in short-term operation planning and long-term grid planning.

Almost all above-mentioned linear power flow models are mainly designated to deal with cold-start power flow problem. Therefore, they employ various approximations and construct a linear approximation of the power flow problem, instead of linearizing power flow problem (and taking advantage of all available information). These approximations result in models that cannot fully benefit from the avalabile information in

hot-start problems.

3.2 Contributions & Novelties

To the best knowledge of the author, the existing literature lacks a correct linearized version (with no approximation) of the power flow problem that takes advantage at most of the existing information associated with the base case operating point, i.e. the solution of AC power flow problem for the base case operating point. In this context, this chapter offers a hot-start power flow model benefiting from linear formulation with affordable computational burden. The main contributions of the chapter are:

1. It linearizes power flow equations (with using no simplification and approximation) while accounting for:
    - Both active and reactive powers;
    - Both nodal voltage magnitude and nodal voltage phase angle;
    - Impact of different bus types, i.e. slack, PV and PQ buses;
    - Active and reactive power losses of the transmission grid;
    - Shunt susceptance of branches.
2. It explicitly characterizes the following quantities (and accordingly all grid's constraints) as linear functions of the active power injections of PV and PQ buses as well as reactive power injections of PQ buses:
    - Voltage magnitudes of PQ buses (It should be noted that the voltage magnitude of slack bus and PV buses are given/known);
    - Voltage phase angle of PV and PQ buses (It should be noted that the voltage phase angle of slack bus is given/known);
    - Apparent power flow of branches;
    - Active power injection of slack bus (It should be noted that active power injection of PV buses and PQ buses are given/known);
    - Reactive power injection of slack bus and PV buses (It should be noted that reactive power injection of PQ buses are given/known).

3.3 Notation

This section elaborates on the notation which is used to linearize non-linear and non-convex power flow equations around a given operating point called base case (i.e. scheduled) operating point. It considers a typical transmission network consisting of $n_{\mathbb{B}}$ buses categorized into 3 groups:

1. Vθ bus: This bus is often referred as slack or reference bus. The main features of this bus are that:
   - Both voltage magnitude and voltage phase angle of this bus are known and fixed.
   - Active and reactive power injections of this bus are unknown.

   Although this chapter assumes a single slack bus with fixed and known voltage, the presented formulation can be extended to the cases where there are several slack buses.
2. PV buses: The main features of these buses are that:
   - Voltage magnitudes of these buses are known and fixed, however, their voltage phase angles are unknown.
   - Active power injections of these buses are known, however, their reactive power injections are unknown.
3. PQ buses: The main features of these buses are that:
   - Neither voltage phase angles nor voltage magnitudes of these buses are known.
   - Both active and reactive power injections of these buses are known.

To simplify mathematical representation of the linearized power flow model, without loss of generality, it is assumed that the indices of buses are assigned in such way that the introduced 3 groups of buses respectively come after each other:

$$\mathbb{B} = \begin{bmatrix} 1 \\ 2 \\ \vdots \\ n_{\mathbb{B}} \end{bmatrix} = \begin{bmatrix} \mathbb{B}_{V\theta} \\ \mathbb{B}_{PV} \\ \mathbb{B}_{PQ} \end{bmatrix}, \tag{3.1}$$

where $\mathbb{B}$ is a vector with dimension $n_{\mathbb{B}} \times 1$ representing the set of all $n_{\mathbb{B}}$ buses of the transmission network; $\mathbb{B}_{V\theta} = [1]$ is a vector with dimension 1×1 representing the set of Vθ buses (single slack bus); $\mathbb{B}_{PV} = [2, 3, \ldots, n_{PV} + 1]^T$ is a vector with dimension $n_{PV} \times 1$ representing the set of PV buses; $\mathbb{B}_{PQ} = [n_{PV}+2, n_{PV}+3, \ldots, n_{\mathbb{B}}]^T$ is a vector with dimension $n_{PQ} \times 1$ representing the set of PQ buses.

To state power flow equations in vector-matrix form, lets boldface letters are used for matrices and vectors; $(.)^T$ for transposition; $(.)^*$ for element-wise conjugate of a vector/matrix; $\|.\|$ for element-wise Euclidean norm of a vector/matrix; $\mathbb{R}$ for set of real numbers; $\mathbb{C}$ for set of complex numbers. For a complex number $c \in \mathbb{C}$, $\Re\{c\}$, $\Im\{c\}$ and c^*

indicate its real part, imaginary part and its conjugate, respectively. $\boldsymbol{P} = \left[P_1 , \ldots, P_{\mathrm{n_{\mathbb{B}}}} \right]^{\mathrm{T}}$, $\widehat{\mathbf{P}} = \left[\widehat{\mathrm{P}}_1 , \ldots, \widehat{\mathrm{P}}_{\mathrm{n_{\mathbb{B}}}} \right]^{\mathrm{T}}$, $\boldsymbol{\Delta P} = \left[\Delta P_1 , \ldots, \Delta P_{\mathrm{n_{\mathbb{B}}}} \right]^{\mathrm{T}}$, $\boldsymbol{Q} = [Q_1 , \ldots, Q_{\mathrm{n_{\mathbb{B}}}}]^{\mathrm{T}}$, $\widehat{\mathbf{Q}} = \left[\widehat{\mathrm{Q}}_1 , \ldots, \widehat{\mathrm{Q}}_{\mathrm{n_{\mathbb{B}}}} \right]^{\mathrm{T}}$, $\boldsymbol{\Delta Q} = \left[\Delta Q_1 , \ldots, \Delta Q_{\mathrm{n_{\mathbb{B}}}} \right]^{\mathrm{T}}$, $\|\boldsymbol{V}\| = \left[\|V_1\| , \ldots, \|V_{\mathrm{n_{\mathbb{B}}}}\| \right]^{\mathrm{T}}$, $\|\widehat{\mathbf{V}}\| = \left[\|\widehat{\mathrm{V}}\|_1 , \ldots, \|\widehat{\mathrm{V}}_{\mathrm{n_{\mathbb{B}}}}\| \right]^{\mathrm{T}}$, $\boldsymbol{\Delta}\|\boldsymbol{V}\| = \left[\Delta\|V_1\| , \ldots, \Delta\|V_{\mathrm{n_{\mathbb{B}}}}\| \right]^{\mathrm{T}}$, $\mathbf{V}^{\mathrm{Max}} = \left[\mathrm{V}_1^{\mathrm{Max}} , \ldots, \mathrm{V}_{\mathrm{n_{\mathbb{B}}}}^{\mathrm{Max}}\right]^{\mathrm{T}}$, $\mathbf{V}^{\mathrm{Min}} = \left[\mathrm{V}_1^{\mathrm{Min}} , \ldots, \mathrm{V}_{\mathrm{n_{\mathbb{B}}}}^{\mathrm{Min}}\right]^{\mathrm{T}}$, $\boldsymbol{\theta} = [\theta_1 , \ldots, \theta_{\mathrm{n_{\mathbb{B}}}}]^{\mathrm{T}}$, $\widehat{\boldsymbol{\Theta}} = \left[\widehat{\Theta}_1 , \ldots, \widehat{\Theta}_{\mathrm{n_{\mathbb{B}}}} \right]^{\mathrm{T}}$, $\Delta\boldsymbol{\theta} = \left[\Delta\theta_1 , \ldots, \Delta\theta_{\mathrm{n_{\mathbb{B}}}} \right]^{\mathrm{T}}$ are vectors in $\mathbb{R}^{\mathrm{n_{\mathbb{B}}}\times 1}$; $\boldsymbol{V} = [V_1 , \ldots, V_{\mathrm{n_{\mathbb{B}}}}]^{\mathrm{T}}$, $\widehat{\mathbf{V}} = \left[\widehat{\mathrm{V}}_1 , \ldots, \widehat{\mathrm{V}}_{\mathrm{n_{\mathbb{B}}}} \right]^{\mathrm{T}}$, $\boldsymbol{I}^{\mathrm{Inj}} = [I_1^{\mathrm{Inj}} , \ldots, I_{\mathrm{n_{\mathbb{B}}}}^{\mathrm{Inj}}]^{\mathrm{T}}$ are vectors in $\mathbb{C}^{\mathrm{n_{\mathbb{B}}}\times 1}$ collecting the respective electrical quantities of buses. l is the index for transmission lines/transformers; $\mathbb{L}$ is the set of transmission lines/transformers; $\mathrm{n_{\mathbb{L}}}$ is the number of transmission lines/transformers; $\mathbf{Z}^{\mathrm{Se}} = \left[z_1,\ldots, z_{N_{\mathbb{L}}}\right]^{\mathrm{T}}$ and $\mathbf{Y}^{\mathrm{Sh}} = \left[y_1,\ldots, y_{N_{\mathbb{L}}}\right]^{\mathrm{T}}$ are vectors in $\mathbb{C}^{\mathrm{N_{\mathbb{L}}}\times 1}$, in which z_l and y_l represent the series impedance and shunt admittance of branch l, respectively. $\|\boldsymbol{S}^{\mathrm{From}}\| = \left[\|S_1^{\mathrm{From}}\| , \ldots., \|S_{\mathrm{n_{\mathbb{L}}}}^{\mathrm{From}}\| \right]^{\mathrm{T}}$, $\|\widehat{\boldsymbol{S}}^{\mathrm{From}}\| = \left[\|\widehat{\mathrm{S}}_1^{\mathrm{From}}\| , \ldots, \|\widehat{\mathrm{S}}_{\mathrm{n_{\mathbb{L}}}}^{\mathrm{From}}\| \right]^{\mathrm{T}}$, $\boldsymbol{\Delta}\|\boldsymbol{S}^{\mathrm{From}}\| = \left[\Delta\|S_1^{\mathrm{From}}\| , \ldots., \Delta\|S_{\mathrm{n_{\mathbb{L}}}}^{\mathrm{From}}\| \right]^{\mathrm{T}}$, $\|\boldsymbol{S}^{\mathrm{To}}\| = \left[\|S_1^{\mathrm{To}}\| , \ldots., \|S_{\mathrm{n_{\mathbb{L}}}}^{\mathrm{To}}\| \right]^{\mathrm{T}}$, $\|\widehat{\boldsymbol{S}}^{\mathrm{To}}\| = [\|\widehat{\mathrm{S}}_1^{\mathrm{To}}\| , \ldots, \|\widehat{\mathrm{S}}_{\mathrm{n_{\mathbb{L}}}}^{\mathrm{To}}\|]^{\mathrm{T}}$, $\boldsymbol{\Delta}\|\boldsymbol{S}\|^{\mathrm{To}} = \left[\Delta\|S_1^{\mathrm{To}}\| , \ldots., \Delta\|S_{\mathrm{n_{\mathbb{L}}}}^{\mathrm{To}}\| \right]^{\mathrm{T}}$ and $\mathbf{S}^{\mathrm{Max}} = \left[\mathrm{S}_1^{\mathrm{Max}} , \ldots. , \mathrm{S}_{\mathrm{n_{\mathbb{L}}}}^{\mathrm{Max}} \right]^{T}$ are vectors in $\mathbb{R}^{\mathrm{N_{\mathbb{L}}}\times 1}$; $\boldsymbol{S}^{\mathrm{From}} = \left[S_1^{\mathrm{From}} , \ldots., S_{\mathrm{n_{\mathbb{L}}}}^{\mathrm{From}} \right]^{\mathrm{T}}$ and $\boldsymbol{S}^{\mathrm{To}} = \left[S_1^{\mathrm{To}} , \ldots., S_{\mathrm{n_{\mathbb{L}}}}^{\mathrm{To}} \right]^{\mathrm{T}}$ are vectors $\mathbb{C}^{\mathrm{N_{\mathbb{L}}}\times 1}$ collecting the respective electrical quantities of branches. For two vectors $\mathbf{x}$ and $\mathbf{y}$ (with the same dimension), $\mathbf{x}./\mathbf{y}$ returns element-wise division of two vectors; $\dfrac{\partial \boldsymbol{x}}{\partial \boldsymbol{y}}$ returns the first partial derivatives of $\mathbf{x}$ with respect to $\mathbf{y}$. For a vector $\mathbf{x}$, diag($\mathbf{x}$) returns a matrix with the elements of x in its diagonal. For a vector $\mathbf{x} = [x_1, x_2, \ldots, x_{\mathrm{n_{\mathbb{B}}}}]$ with dimension $\mathrm{n_{\mathbb{B}}} \times 1$:

- $[\mathbf{x}]_{\mathrm{V}\theta}$ returns a vector with dimension 1 gathering the element of x associated to Vθ bus:

$$[\mathbf{x}]_{\mathrm{V}\theta} = [x_1]. \tag{3.2}$$

- $[\mathbf{x}]_{\mathrm{PV}}$ returns a vector with dimension $\mathrm{n_{PV}} \times 1$ gathering the elements of x associated to PV buses:

$$[\mathbf{x}]_{\mathrm{V}\theta} = [x_2, x_3, \ldots, x_{\mathrm{n_{PV}}+1}]^{\mathrm{T}}. \tag{3.3}$$

- $[\mathbf{x}]_{\mathrm{PQ}}$ returns a vector with dimension $\mathrm{n_{PQ}} \times 1$ gathering the elements of x associated to PQ buses:

$$[\mathbf{x}]_{\mathrm{V}\theta} = [x_{\mathrm{n_{PV}}+2}, x_{\mathrm{n_{PV}}+3}, \ldots, x_{\mathrm{n_{\mathbb{B}}}}]^{\mathrm{T}}. \tag{3.4}$$

Accordingly, $\mathbf{x}$ can be expressed based on $[\mathbf{x}]_{\mathrm{V}\theta}$, $[\mathbf{x}]_{\mathrm{PV}}$ and $[\mathbf{x}]_{\mathrm{PQ}}$ as:

$$\mathbf{x} = \begin{bmatrix} [\mathbf{x}]_{\mathrm{V}\theta} \\ [\mathbf{x}]_{\mathrm{PV}} \\ [\mathbf{x}]_{\mathrm{PQ}} \end{bmatrix}. \tag{3.5}$$

3.4 Power Flow Equations

It should be noted that the state of the grid and accordingly all electrical quantities pertained to the base case operating point (i.e. all vectors $\|\widehat{\mathbf{V}}\|$, $\widehat{\mathbf{\Theta}}$, $\widehat{\mathbf{P}}$, $\widehat{\mathbf{Q}}$, $\widehat{\boldsymbol{S}}^{\text{From}}$, $\widehat{\boldsymbol{S}}^{\text{To}}$, $\|\widehat{\boldsymbol{S}}^{\text{From}}\|$, $\|\widehat{\boldsymbol{S}}^{\text{To}}\|$) are known/given[2]. As a result, each electrical variable pertained to the grid (i.e. $\|\boldsymbol{V}\|$, $\boldsymbol{\theta}$, $\boldsymbol{P}$, $\boldsymbol{Q}$, $\|\boldsymbol{S}^{\text{From}}\|$, $\|\boldsymbol{S}^{\text{To}}\|$) can be expressed as the sum of two terms:

1. the value of the respective variable for the base case operating point (i.e. $\|\widehat{\mathbf{V}}\|$, $\widehat{\mathbf{\Theta}}$, $\widehat{\mathbf{P}}$, $\widehat{\mathbf{Q}}$, $\|\widehat{\boldsymbol{S}}^{\text{From}}\|$, $\|\widehat{\boldsymbol{S}}^{\text{To}}\|$).
2. the deviation of the respective variable from its base case value (i.e. $\boldsymbol{\Delta}\|\boldsymbol{V}\|$, $\boldsymbol{\Delta\theta}$, $\boldsymbol{\Delta P}$, $\boldsymbol{\Delta Q}$, $\boldsymbol{\Delta}\|\boldsymbol{S}\|^{\text{From}}$, $\boldsymbol{\Delta}\|\boldsymbol{S}\|^{\text{To}}$).

$$\|\boldsymbol{V}\| = \|\widehat{\mathbf{V}}\| + \boldsymbol{\Delta}\|\boldsymbol{V}\|, \tag{3.6}$$

$$\boldsymbol{\theta} = \widehat{\mathbf{\Theta}} + \boldsymbol{\Delta\theta}, \tag{3.7}$$

$$\boldsymbol{P} = \widehat{\mathbf{P}} + \boldsymbol{\Delta P}, \tag{3.8}$$

$$\boldsymbol{Q} = \widehat{\mathbf{Q}} + \boldsymbol{\Delta Q}, \tag{3.9}$$

$$\|\boldsymbol{S}^{\text{From}}\| = \|\widehat{\boldsymbol{S}}^{\text{From}}\| + \boldsymbol{\Delta}\|\boldsymbol{S}\|^{\text{From}}, \tag{3.10}$$

$$\|\boldsymbol{S}^{\text{To}}\| = \|\widehat{\boldsymbol{S}}^{\text{To}}\| + \boldsymbol{\Delta}\|\boldsymbol{S}\|^{\text{To}}, \tag{3.11}$$

Remark 1: Considering the fact that Vθ bus controls its active power injection to prevent its voltage phase angle from any deviations, thus $[\boldsymbol{\theta}]_{\text{V}\theta} = [\widehat{\mathbf{\Theta}}]_{\text{V}\theta}$ and $[\boldsymbol{\Delta\theta}]_{\text{V}\theta} = 0$.

Remark 2: Considering the fact that Vθ bus and PV buses control their reactive power injections to prevent their voltage magnitude from any deviations, thus $[\|\boldsymbol{V}\|]_{\text{V}\theta} = [\|\widehat{\mathbf{V}}\|]_{\text{V}\theta}$, $[\boldsymbol{\Delta}\|\boldsymbol{V}\|]_{\text{V}\theta} = 0$, $[\|\boldsymbol{V}\|]_{\text{PV}} = [\|\widehat{\mathbf{V}}\|]_{\text{PV}}$ and $[\boldsymbol{\Delta}\|\boldsymbol{V}\|]_{\text{PV}} = 0$.

Combination of two expressions (3.8) and (3.9) yields:

$$\boldsymbol{S} = \widehat{\mathbf{S}} + \boldsymbol{\Delta S}, \tag{3.12}$$

where $\boldsymbol{S}$ is a vector with dimension $\text{n}_{\mathbb{B}} \times 1$ representing the nodal complex power injection of all buses; $\widehat{\mathbf{S}}$ represents the nodal complex power injection for the base-case operating point which can be calculated as:

$$\widehat{\mathbf{S}} = \widehat{\mathbf{P}} + \sqrt{-1}\,\widehat{\mathbf{Q}}. \tag{3.13}$$

and $\boldsymbol{\Delta S}$ represents the deviation of the nodal complex power injection from its base case value which can be calculated as:

$$\boldsymbol{\Delta S} = \boldsymbol{\Delta P} + \sqrt{-1}\,\boldsymbol{\Delta Q}. \tag{3.14}$$

[2] Power flow equations are linearized around a given base case (i.e. scheduled) operating point.

Then, the power flow equations can be cast in vector-matrix form as:

$$\boldsymbol{S} = \text{diag}(\boldsymbol{V})\boldsymbol{I}^{\text{Inj}^*} = \text{diag}(\boldsymbol{I}^{\text{Inj}^*})\boldsymbol{V}, \tag{3.15}$$

$$\boldsymbol{I}^{\text{Inj}} = \mathbf{Y}\boldsymbol{V}, \tag{3.16}$$

Assuming that remarks 1 and 2 are valid and $[\boldsymbol{P}]_{\text{PV}}$, $[\boldsymbol{P}]_{\text{PQ}}$, $[\boldsymbol{Q}]_{\text{PQ}}$ are known. The power flow problem aims to determine the value of state variables of the grid, i.e. $[\boldsymbol{\theta}]_{\text{PV}}$, $[\|\boldsymbol{V}\|]_{\text{PQ}}$, $[\boldsymbol{\theta}]_{\text{PQ}}$, thereby determining the value of all other electrical quantities of the grid such as $[\boldsymbol{P}]_{\text{V}\theta}$, $[\boldsymbol{Q}]_{\text{V}\theta}$, $[\boldsymbol{Q}]_{\text{PV}}$, $\boldsymbol{S}^{\text{From}}$ and $\boldsymbol{S}^{\text{To}}$, $\|\boldsymbol{S}^{\text{From}}\|$ and $\|\boldsymbol{S}^{\text{To}}\|$.

Given the values of the grid's state variables (i.e.$[\boldsymbol{\theta}]_{\text{PV}}$, $[\|\boldsymbol{V}\|]_{\text{PQ}}$, $[\boldsymbol{\theta}]_{\text{PQ}}$):

1. The value of $[\boldsymbol{P}]_{\text{V}\theta}$, $[\boldsymbol{Q}]_{\text{V}\theta}$ and $[\boldsymbol{Q}]_{\text{PV}}$ can be calculated following (3.15) and (3.16).
2. The power flow of branches can be determined as detailed in the following:

Matrix $\mathbf{A} \in \mathbb{R}^{n_{\mathbb{L}} \times n_{\mathbb{B}}}$ (is formed of -1, 0, 1) indicates branch to node incidence matrix . This matrix is composed of two parts:

$$\mathbf{A} = \mathbf{A}^{\text{From}} + \mathbf{A}^{\text{To}} \tag{3.17}$$

where $\mathbf{A}^{\text{From}}$ is a matrix consisting of 0, 1 representing branch to from-node incidence matrix and $\mathbf{A}^{\text{To}}$ is a matrix consisting of 0, -1 representing branch to to-node incidence matrix.

Complex power flow entering the from-end of branches, i.e. $\boldsymbol{S}^{\text{From}} \in \mathbb{C}^{n_{\mathbb{L}} \times 1}$, and complex power flow entering the to-end of branches, i.e. $\boldsymbol{S}^{\text{To}} \in \mathbb{C}^{n_{\mathbb{L}} \times 1}$ can be calculated as:

$$\boldsymbol{S}^{\text{From}} = \text{diag}(\mathbf{A}^{\text{From}}\boldsymbol{V})\,(\mathbf{Y}^{\text{From}}\boldsymbol{V})^*, \tag{3.18}$$

$$\boldsymbol{S}^{\text{To}} = -\text{diag}(\mathbf{A}^{\text{To}}\boldsymbol{V})\,(\mathbf{Y}^{\text{To}}\boldsymbol{V})^*, \tag{3.19}$$

where $\mathbf{Y}^{\text{From}} \in \mathbb{C}^{n_{\mathbb{L}} \times n_{\mathbb{B}}}$ and $\mathbf{Y}^{\text{To}} \in \mathbb{C}^{n_{\mathbb{L}} \times n_{\mathbb{B}}}$ can be calculated as:

$$\mathbf{Y}^{\text{From}} = (\text{diag}\,(\mathbf{Y}^{\text{Sh}}/2)\,\mathbf{A}^{\text{From}} + \text{diag}\,(\mathbf{Z}^{\text{Se}})^{-1}\,\mathbf{A}) \tag{3.20}$$

$$\mathbf{Y}^{\text{To}} = -(\text{diag}\,(\mathbf{Y}^{\text{Sh}}/2)\,\mathbf{A}^{\text{To}} + \text{diag}\,(\mathbf{Z}^{\text{Se}})^{-1}\,\mathbf{A}) \tag{3.21}$$

Consequently, the apparent power flow entering the from-end of branches, i.e. $\|\boldsymbol{S}^{\text{From}}\| \in \mathbb{R}^{n_{\mathbb{L}} \times 1}$, and the apparent power flow entering the to-end of branches, i.e. $\|\boldsymbol{S}^{\text{To}}\| \in \mathbb{R}^{n_{\mathbb{L}} \times 1}$ can be easily calculated by extracting the element-wise Euclidean norm of $\boldsymbol{S}^{\text{From}}$ and $\boldsymbol{S}^{\text{To}}$, respectively.

3.5 Linearizing Power Flow Equations

The power flow equations are linearized around the given base case operating point (i.e. $\|\widehat{\mathbf{V}}\|, \widehat{\boldsymbol{\Theta}}$) assuming that remark 3 is valid:

Remark 3: Power flow equations (3.15) and (3.16) are respected for the base case operating point.

To linearize power flow equations, let calculate the first partial derivatives of $\boldsymbol{V}$ with respect to $\|\boldsymbol{V}\|$ and $\boldsymbol{\theta}$ (i.e. state variables):

$$\frac{\partial \boldsymbol{V}}{\partial \|\boldsymbol{V}\|} = \text{diag}(\, \boldsymbol{V} \,./\, \|\boldsymbol{V}\| \,), \tag{3.22}$$

$$\frac{\partial \boldsymbol{V}}{\partial \boldsymbol{\theta}} = \sqrt{-1}\, \text{diag}(\, \boldsymbol{V} \,), \tag{3.23}$$

The first partial derivatives of $\boldsymbol{I}^{\text{Inj}}$ with respect to $\|\boldsymbol{V}\|$ and $\boldsymbol{\theta}$ can be easily extracted by combining expressions (3.16), (3.22) and (3.23):

$$\frac{\partial \boldsymbol{I}^{\text{Inj}}}{\partial \|\boldsymbol{V}\|} = \mathbf{Y} \frac{\partial \boldsymbol{V}}{\partial \|\boldsymbol{V}\|} = \mathbf{Y}\, \text{diag}(\, \boldsymbol{V} \,./\, \|\boldsymbol{V}\| \,), \tag{3.24}$$

$$\frac{\partial \boldsymbol{I}^{\text{Inj}}}{\partial \boldsymbol{\theta}} = \mathbf{Y} \frac{\partial \boldsymbol{V}}{\partial \boldsymbol{\theta}} = \sqrt{-1}\, \mathbf{Y}\, \text{diag}(\, \boldsymbol{V} \,), \tag{3.25}$$

Finally, the first partial derivatives of $\boldsymbol{S}$ with respect to $\|\boldsymbol{V}\|$ and $\boldsymbol{\theta}$ can be derived by combining expressions (3.15) and (3.22)-(3.25):

$$\begin{aligned} \frac{\partial \boldsymbol{S}}{\partial \|\boldsymbol{V}\|} &= \text{diag}(\, \boldsymbol{I}^{\text{Inj}^*} \,) \frac{\partial \boldsymbol{V}}{\partial \|\boldsymbol{V}\|} + \text{diag}(\, \boldsymbol{V} \,)(\, \frac{\partial \boldsymbol{I}^{\text{Inj}}}{\partial \|\boldsymbol{V}\|} \,)^* = \\ &= \text{diag}(\, \boldsymbol{I}^{\text{Inj}^*} \,)\text{diag}(\, \boldsymbol{V} \,./\, \|\boldsymbol{V}\| \,) + \text{diag}(\, \boldsymbol{V} \,)\, \mathbf{Y}^*\, \text{diag}(\, \boldsymbol{V}^* \,./\, \|\boldsymbol{V}\| \,), \end{aligned} \tag{3.26}$$

$$\begin{aligned} \frac{\partial \boldsymbol{S}}{\partial \boldsymbol{\theta}} &= \text{diag}(\, \boldsymbol{I}^{\text{Inj}^*} \,) \frac{\partial \boldsymbol{V}}{\partial \boldsymbol{\theta}} + \text{diag}(\, \boldsymbol{V} \,)(\, \frac{\partial \boldsymbol{I}^{\text{Inj}}}{\partial \boldsymbol{\theta}} \,)^* = \\ &= \text{diag}(\, \boldsymbol{I}^{\text{Inj}^*} \,)\, \sqrt{-1}\, \text{diag}(\, \boldsymbol{V} \,) + \text{diag}(\, \boldsymbol{V} \,)\, \mathbf{Y}^*\, \sqrt{-1}\, \text{diag}(\, \boldsymbol{V}^* \,), \end{aligned} \tag{3.27}$$

It is worth highlighting that $\frac{\partial \boldsymbol{V}}{\partial \|\boldsymbol{V}\|}$, $\frac{\partial \boldsymbol{V}}{\partial \boldsymbol{\theta}}$, $\frac{\partial \boldsymbol{S}}{\partial \|\boldsymbol{V}\|}$ and $\frac{\partial \boldsymbol{S}}{\partial \boldsymbol{\theta}}$ are matrices in $\mathbb{C}^{n_{\mathbb{B}} \times n_{\mathbb{B}}}$. $\frac{\partial \boldsymbol{I}^{\text{Inj}}}{\partial \|\boldsymbol{V}\|}$ and $\frac{\partial \boldsymbol{I}^{\text{Inj}}}{\partial \boldsymbol{\theta}}$ are matrices in $\mathbb{C}^{n_{\mathbb{L}} \times n_{\mathbb{B}}}$.

The first order Taylor expansion of $\boldsymbol{S}$ with respect to the state variables $\|\boldsymbol{V}\|$ and $\boldsymbol{\theta}$ can be written as:

$$\boldsymbol{S} = \widehat{\mathbf{S}} + \left.\frac{\partial \boldsymbol{S}}{\partial \|\boldsymbol{V}\|}\right|_{\widehat{\boldsymbol{\theta}},\, \|\widehat{\mathbf{V}}\|} \boldsymbol{\Delta}\|\boldsymbol{V}\| + \left.\frac{\partial \boldsymbol{S}}{\partial \boldsymbol{\theta}}\right|_{\widehat{\boldsymbol{\theta}},\, \|\widehat{\mathbf{V}}\|} \boldsymbol{\Delta}\boldsymbol{\theta}, \tag{3.28}$$

Substituting expressions (3.12)-(3.14), (3.26) and (3.27) into expression (3.28) results in

the following vector-matrix equation:

$$\begin{bmatrix} \boldsymbol{\Delta P} \\ \boldsymbol{\Delta Q} \end{bmatrix} = \mathbf{J}^{full}\Big|_{\widehat{\boldsymbol{\Theta}},\, \| \widehat{\mathbf{V}} \|} \begin{bmatrix} \boldsymbol{\Delta\theta} \\ \boldsymbol{\Delta}\|\boldsymbol{V}\| \end{bmatrix} \tag{3.29}$$

where matrix $\mathbf{J}^{full}$ is:

$$\mathbf{J}^{full} := \begin{bmatrix} \dfrac{\partial \boldsymbol{P}}{\partial \boldsymbol{\theta}} & \dfrac{\partial \boldsymbol{P}}{\partial \|\boldsymbol{V}\|} \\ \dfrac{\partial \boldsymbol{Q}}{\partial \boldsymbol{\theta}} & \dfrac{\partial \boldsymbol{Q}}{\partial \|\boldsymbol{V}\|} \end{bmatrix} = \begin{bmatrix} \Re\left\{\dfrac{\partial \boldsymbol{S}}{\partial \boldsymbol{\theta}}\right\} & \Re\left\{\dfrac{\partial \boldsymbol{S}}{\partial \|\boldsymbol{V}\|}\right\} \\ \Im\left\{\dfrac{\partial \boldsymbol{S}}{\partial \boldsymbol{\theta}}\right\} & \Im\left\{\dfrac{\partial \boldsymbol{S}}{\partial \|\boldsymbol{V}\|}\right\} \end{bmatrix} \in \mathbb{R}^{2n_{\mathbb{B}} \times 2n_{\mathbb{B}}} \tag{3.30}$$

Thus, elements of $\mathbf{J}^{full}$ can be calculated on the basis of (3.26) and (3.27). Considering the fact that only values of $[\boldsymbol{\Delta P}]_{\mathrm{PV}}$, $[\boldsymbol{\Delta P}]_{\mathrm{PQ}}$ and $[\boldsymbol{\Delta Q}]_{\mathrm{PQ}}$ are known, therefore, expression (3.29) is reconfigured with the purpose of determining the value of unknown state variables $[\boldsymbol{\theta}]_{\mathrm{PV}}$, $[\|\boldsymbol{V}\|]_{\mathrm{PQ}}$ and $[\boldsymbol{\theta}]_{\mathrm{PQ}}$:

$$\begin{bmatrix} [\boldsymbol{\Delta P}]_{\mathrm{PV}} \\ [\boldsymbol{\Delta P}]_{\mathrm{PQ}} \\ [\boldsymbol{\Delta Q}]_{\mathrm{PQ}} \end{bmatrix} = \mathbf{J}\Big|_{\widehat{\boldsymbol{\Theta}},\, \| \widehat{\mathbf{V}} \|} \begin{bmatrix} [\boldsymbol{\Delta\theta}]_{\mathrm{PV}} \\ [\boldsymbol{\Delta\theta}]_{\mathrm{PQ}} \\ [\boldsymbol{\Delta}\|\boldsymbol{V}\|]_{\mathrm{PQ}} \end{bmatrix} \tag{3.31}$$

where matrix $\mathbf{J} \in \mathbb{R}^{(n_{\mathrm{PV}}+2n_{\mathrm{PQ}}) \times (n_{\mathrm{PV}}+2n_{\mathrm{PQ}})}$ can be calculated as:

$$\mathbf{J} := \begin{bmatrix} \dfrac{\partial [\boldsymbol{P}]_{\mathrm{PV}}}{\partial [\boldsymbol{\theta}]_{\mathrm{PV}}} & \dfrac{\partial [\boldsymbol{P}]_{\mathrm{PV}}}{\partial [\boldsymbol{\theta}]_{\mathrm{PQ}}} & \dfrac{\partial [\boldsymbol{P}]_{\mathrm{PV}}}{\partial [\|\boldsymbol{V}\|]_{\mathrm{PQ}}} \\ \dfrac{\partial [\boldsymbol{P}]_{\mathrm{PQ}}}{\partial [\boldsymbol{\theta}]_{\mathrm{PV}}} & \dfrac{\partial [\boldsymbol{P}]_{\mathrm{PQ}}}{\partial [\boldsymbol{\theta}]_{\mathrm{PQ}}} & \dfrac{\partial [\boldsymbol{P}]_{\mathrm{PQ}}}{\partial [\|\boldsymbol{V}\|]_{\mathrm{PQ}}} \\ \dfrac{\partial [\boldsymbol{Q}]_{\mathrm{PQ}}}{\partial [\boldsymbol{\theta}]_{\mathrm{PV}}} & \dfrac{\partial [\boldsymbol{Q}]_{\mathrm{PQ}}}{\partial [\boldsymbol{\theta}]_{\mathrm{PQ}}} & \dfrac{\partial [\boldsymbol{Q}]_{\mathrm{PQ}}}{\partial [\|\boldsymbol{V}\|]_{\mathrm{PQ}}} \end{bmatrix} = \begin{bmatrix} \Re\left\{\dfrac{\partial [\boldsymbol{S}]_{\mathrm{PV}}}{\partial [\boldsymbol{\theta}]_{\mathrm{PV}}}\right\} & \Re\left\{\dfrac{\partial [\boldsymbol{S}]_{\mathrm{PV}}}{\partial [\boldsymbol{\theta}]_{\mathrm{PQ}}}\right\} & \Re\left\{\dfrac{\partial [\boldsymbol{S}]_{\mathrm{PV}}}{\partial [\|\boldsymbol{V}\|]_{\mathrm{PQ}}}\right\} \\ \Re\left\{\dfrac{\partial [\boldsymbol{S}]_{\mathrm{PQ}}}{\partial [\boldsymbol{\theta}]_{\mathrm{PV}}}\right\} & \Re\left\{\dfrac{\partial [\boldsymbol{S}]_{\mathrm{PQ}}}{\partial [\boldsymbol{\theta}]_{\mathrm{PQ}}}\right\} & \Re\left\{\dfrac{\partial [\boldsymbol{S}]_{\mathrm{PQ}}}{\partial [\|\boldsymbol{V}\|]_{\mathrm{PQ}}}\right\} \\ \Im\left\{\dfrac{\partial [\boldsymbol{S}]_{\mathrm{PQ}}}{\partial [\boldsymbol{\theta}]_{\mathrm{PV}}}\right\} & \Im\left\{\dfrac{\partial [\boldsymbol{S}]_{\mathrm{PQ}}}{\partial [\boldsymbol{\theta}]_{\mathrm{PQ}}}\right\} & \Im\left\{\dfrac{\partial [\boldsymbol{S}]_{\mathrm{PQ}}}{\partial [\|\boldsymbol{V}\|]_{\mathrm{PQ}}}\right\} \end{bmatrix} \tag{3.32}$$

thus, elements of $\mathbf{J}$ can be calculated on the basis of (3.26) and (3.27). All elements of the vector located in the left-hand side of equation (3.31) are known, thus, unknown state variables $[\boldsymbol{\theta}]_{\mathrm{PV}}$, $[\|\boldsymbol{V}\|]_{\mathrm{PQ}}$ and $[\boldsymbol{\theta}]_{\mathrm{PQ}}$ can be calculated by multiplying inverse of $\mathbf{J}$ in (3.31) which yields:

$$\begin{bmatrix} [\boldsymbol{\Delta\theta}]_{\mathrm{PV}} \\ [\boldsymbol{\Delta\theta}]_{\mathrm{PQ}} \\ [\boldsymbol{\Delta}\|\boldsymbol{V}\|]_{\mathrm{PQ}} \end{bmatrix} = \boldsymbol{\Gamma}\Big|_{\widehat{\boldsymbol{\Theta}},\, \| \widehat{\mathbf{V}} \|} \begin{bmatrix} [\boldsymbol{\Delta P}]_{\mathrm{PV}} \\ [\boldsymbol{\Delta P}]_{\mathrm{PQ}} \\ [\boldsymbol{\Delta Q}]_{\mathrm{PQ}} \end{bmatrix} \tag{3.33}$$

where matrix $\boldsymbol{\Gamma} \in \mathbb{R}^{(n_{\mathrm{PV}}+2n_{\mathrm{PQ}}) \times (n_{\mathrm{PV}}+2n_{\mathrm{PQ}})}$ is equal to $\mathbf{J}^{-1}$.

3.5.1 Linear Formulation for Nodal Voltage Magnitude

Considering the fact that all elements of the vector located in the right-hand side of equation (3.33) are known, thus the value of all elements belonging to vector $[\|\boldsymbol{\Delta V}\|]_{\mathrm{PQ}}$ can be easily calculated as:

$$[\boldsymbol{\Delta}\|\boldsymbol{V}\|]_{\mathrm{PQ}} = \mathbb{V}\begin{bmatrix}[\boldsymbol{\Delta P}]_{\mathrm{PV}}\\ [\boldsymbol{\Delta P}]_{\mathrm{PQ}}\\ [\boldsymbol{\Delta Q}]_{\mathrm{PQ}}\end{bmatrix} \tag{3.34}$$

where $\mathbb{V} \in \mathbb{R}^{n_{\mathrm{PQ}}\times(n_{\mathrm{PV}}+2n_{\mathrm{PQ}})}$ is a sub-matrix of $\boldsymbol{\Gamma}\Big|_{\hat{\boldsymbol{\theta}},\,\|\hat{\mathbf{V}}\|}$ formed of the last n_{PQ} rows of $\boldsymbol{\Gamma}\Big|_{\hat{\boldsymbol{\theta}},\,\|\hat{\mathbf{V}}\|}$.

By substituting $[\boldsymbol{\Delta}\|\boldsymbol{V}\|]_{\mathrm{PQ}}$ from (3.34) into (3.6), the voltage magnitudes of all PQ buses can be expressed as a linear function of $[\boldsymbol{\Delta P}]_{\mathrm{PV}}$, $[\boldsymbol{\Delta P}]_{\mathrm{PQ}}$, and $[\boldsymbol{\Delta Q}]_{\mathrm{PQ}}$:

$$[\|\boldsymbol{V}\|]_{\mathrm{PQ}} = \mathbb{V}^0 \;+\; \mathbb{V}\begin{bmatrix}[\boldsymbol{\Delta P}]_{\mathrm{PV}}\\ [\boldsymbol{\Delta P}]_{\mathrm{PQ}}\\ [\boldsymbol{\Delta Q}]_{\mathrm{PQ}}\end{bmatrix} \tag{3.35}$$

where $\mathbb{V}^0 \in \mathbb{R}^{n_{\mathrm{PQ}}\times 1}$ is a constant vector that can be calculated as:

$$\mathbb{V}^0 \;=\; [\|\,\hat{\mathbf{V}}\|]_{\mathrm{PQ}} \tag{3.36}$$

and $\mathbb{V}$ is a constant matrix in $\mathbb{R}^{n_{\mathrm{PQ}}\times(n_{\mathrm{PV}}+2n_{\mathrm{PQ}})}$ as detailed above.

It is worth reminding that the voltage magnitudes of the other buses, i.e. Vθ bus and PV buses are known and fixed as characterized in Remark 2. Finally, nodal voltage magnitude limits of PQ buses are linearly modeled as:

$$[\mathbf{V}^{\mathrm{Min}}]_{\mathrm{PQ}} \le \mathbb{V}^0 \;+\; \mathbb{V}\Big|_{\hat{\boldsymbol{\theta}},\,\|\hat{\mathbf{V}}\|}\begin{bmatrix}[\boldsymbol{\Delta P}]_{\mathrm{PV}}\\ [\boldsymbol{\Delta P}]_{\mathrm{PQ}}\\ [\boldsymbol{\Delta Q}]_{\mathrm{PQ}}\end{bmatrix} \le [\mathbf{V}^{\mathrm{Max}}]_{\mathrm{PQ}} \tag{3.37}$$

3.5.2 Linear Formulation for Active Power Injection of Vθ bus

Vθ bus, i.e. slack bus, adjusts its active power injection so that its voltage phase angle is fixed. Therefore, active power injection of Vθ bus depends on the nodal active/reactive power injections of the other buses. Considering Remarks 1 and 2 as well as expressions

(3.29) and (3.30), $[\boldsymbol{\Delta P}]_{\mathrm{V}\theta}$ can be characterized as a liner function of $[\boldsymbol{\Delta\theta}]_{\mathrm{PV}}$, $[\boldsymbol{\Delta\theta}]_{\mathrm{PQ}}$ and $[\boldsymbol{\Delta}\|\boldsymbol{V}\|]_{\mathrm{PQ}}$ as:

$$[\boldsymbol{\Delta P}]_{\mathrm{V}\theta} = \mathbb{P}^{\mathrm{A}}\Big|_{\widehat{\boldsymbol{\theta}},\,\|\widehat{\mathbf{V}}\|} \begin{bmatrix} [\boldsymbol{\Delta\theta}]_{\mathrm{PV}} \\ [\boldsymbol{\Delta\theta}]_{\mathrm{PQ}} \\ [\boldsymbol{\Delta}\|\boldsymbol{V}\|]_{\mathrm{PQ}} \end{bmatrix} \tag{3.38}$$

where $\mathbb{P}^{\mathrm{A}} \in \mathbb{R}^{1\times(\mathrm{n_{PV}}+2\mathrm{n_{PQ}})}$ is a sub-matrix of $\mathbf{J}^{full}$ composed of:

$$\mathbb{P}^{\mathrm{A}} := \begin{bmatrix} \dfrac{\partial[\boldsymbol{P}]_{\mathrm{V}\theta}}{\partial[\boldsymbol{\theta}]_{\mathrm{PV}}} & \dfrac{\partial[\boldsymbol{P}]_{\mathrm{V}\theta}}{\partial[\boldsymbol{\theta}]_{\mathrm{PQ}}} & \dfrac{\partial[\boldsymbol{P}]_{\mathrm{V}\theta}}{\partial[\|\boldsymbol{V}\|]_{\mathrm{PQ}}} \end{bmatrix} = \begin{bmatrix} \Re\left\{\dfrac{\partial[\boldsymbol{S}]_{\mathrm{V}\theta}}{\partial[\boldsymbol{\theta}]_{\mathrm{PV}}}\right\} & \Re\left\{\dfrac{\partial[\boldsymbol{S}]_{\mathrm{V}\theta}}{\partial[\boldsymbol{\theta}]_{\mathrm{PQ}}}\right\} & \Re\left\{\dfrac{\partial[\boldsymbol{S}]_{\mathrm{V}\theta}}{\partial[\|\boldsymbol{V}\|]_{\mathrm{PQ}}}\right\} \end{bmatrix} \tag{3.39}$$

thus, elements of $\mathbb{P}^{\mathrm{A}}$ can be calculated on the basis of (3.26) and (3.27).

Substituting $[[\boldsymbol{\Delta\theta}]_{\mathrm{PV}},\ [\boldsymbol{\Delta\theta}]_{\mathrm{PQ}},\ [\boldsymbol{\Delta}\|\boldsymbol{V}\|]_{\mathrm{PQ}}]^{\mathrm{T}}$ from (3.33) into (3.38) results in the following linear function that characterizes $[\boldsymbol{\Delta P}]_{\mathrm{V}\theta}$ as a linear function of $[\boldsymbol{\Delta P}]_{\mathrm{PV}}$, $[\boldsymbol{\Delta P}]_{\mathrm{PQ}}$, and $[\boldsymbol{\Delta Q}]_{\mathrm{PQ}}$:

$$[\boldsymbol{\Delta P}]_{\mathrm{V}\theta} = \mathbb{P}^{\mathrm{A}}\Big|_{\widehat{\boldsymbol{\theta}},\,\|\widehat{\mathbf{V}}\|} \Gamma\Big|_{\widehat{\boldsymbol{\theta}},\,\|\widehat{\mathbf{V}}\|} \begin{bmatrix} [\boldsymbol{\Delta P}]_{\mathrm{PV}} \\ [\boldsymbol{\Delta P}]_{\mathrm{PQ}} \\ [\boldsymbol{\Delta Q}]_{\mathrm{PQ}} \end{bmatrix} \tag{3.40}$$

Accordingly, active power injection of the slack bus, i.e. $[\boldsymbol{P}]_{\mathrm{V}\theta}$, can be characterized as a linear function of $[\boldsymbol{\Delta P}]_{\mathrm{PV}}$, $[\boldsymbol{\Delta P}]_{\mathrm{PQ}}$, and $[\boldsymbol{\Delta Q}]_{\mathrm{PQ}}$ by replacing $[\boldsymbol{\Delta P}]_{\mathrm{V}\theta}$ from (3.40) into (3.8):

$$[\boldsymbol{P}]_{\mathrm{V}\theta} = \mathbb{P}^{0} + \mathbb{P} \begin{bmatrix} [\boldsymbol{\Delta P}]_{\mathrm{PV}} \\ [\boldsymbol{\Delta P}]_{\mathrm{PQ}} \\ [\boldsymbol{\Delta Q}]_{\mathrm{PQ}} \end{bmatrix} \tag{3.41}$$

where $\mathbb{P}^{0} \in \mathbb{R}$ is a constant vector that can be calculated as:

$$\mathbb{P}^{0} = [\,\widehat{\mathbf{P}}]_{\mathrm{V}\theta} \tag{3.42}$$

and $\mathbb{P}$ is a constant matrix in $\mathbb{R}^{1\times(\mathrm{n_{PV}}+2\mathrm{n_{PQ}})}$ and can be easily calculated as:

$$\mathbb{P} = \mathbb{P}^{\mathrm{A}}\Big|_{\widehat{\boldsymbol{\theta}},\,\|\widehat{\mathbf{V}}\|} \Gamma\Big|_{\widehat{\boldsymbol{\theta}},\,\|\widehat{\mathbf{V}}\|} \tag{3.43}$$

3.5.3 Linear Formulation for Reactive Power Injections of Vθ and PV buses

Vθ bus and PV buses regulate their reactive power injections so that their voltage magnitudes are fixed. Therefore, reactive power injections of Vθ and PV buses depend on the nodal active/reactive power injections of the other buses. Considering Remarks 1 and 2 as well as expressions (3.29) and (3.30), $[\boldsymbol{\Delta Q}]_{\mathrm{V}\theta}$ and $[\boldsymbol{\Delta Q}]_{\mathrm{PV}}$ can be expressed as

a liner function of $[\boldsymbol{\Delta\theta}]_{\mathrm{PV}}$, $[\boldsymbol{\Delta\theta}]_{\mathrm{PQ}}$ and $[\boldsymbol{\Delta}\|\boldsymbol{V}\|]_{\mathrm{PQ}}$

$$\begin{bmatrix} [\boldsymbol{\Delta Q}]_{\mathrm{V}\theta} \\ [\boldsymbol{\Delta Q}]_{\mathrm{PV}} \end{bmatrix} = \mathbb{Q}^{\mathrm{A}}\Big|_{\widehat{\boldsymbol{\Theta}},\,\|\widehat{\mathbf{V}}\|} \begin{bmatrix} [\boldsymbol{\Delta\theta}]_{\mathrm{PV}} \\ [\boldsymbol{\Delta\theta}]_{\mathrm{PQ}} \\ [\boldsymbol{\Delta}\|\boldsymbol{V}\|]_{\mathrm{PQ}} \end{bmatrix} \tag{3.44}$$

where $\mathbb{Q}^{\mathrm{A}} \in \mathbb{R}^{(n_{\mathrm{PV}}+1)\times(n_{\mathrm{PV}}+2n_{\mathrm{PQ}})}$ is a sub-matrix of $\mathbf{J}^{full}$ composed of:

$$\mathbb{Q}^{\mathrm{A}} := \begin{bmatrix} \frac{\partial [\boldsymbol{Q}]_{\mathrm{V}\theta}}{\partial [\boldsymbol{\theta}]_{\mathrm{PV}}} & \frac{\partial [\boldsymbol{Q}]_{\mathrm{V}\theta}}{\partial [\boldsymbol{\theta}]_{\mathrm{PQ}}} & \frac{\partial [\boldsymbol{Q}]_{\mathrm{V}\theta}}{\partial [\|\boldsymbol{V}\|]_{\mathrm{PQ}}} \\ \frac{\partial [\boldsymbol{Q}]_{\mathrm{PV}}}{\partial [\boldsymbol{\theta}]_{\mathrm{PV}}} & \frac{\partial [\boldsymbol{Q}]_{\mathrm{PV}}}{\partial [\boldsymbol{\theta}]_{\mathrm{PQ}}} & \frac{\partial [\boldsymbol{Q}]_{\mathrm{PV}}}{\partial [\|\boldsymbol{V}\|]_{\mathrm{PQ}}} \end{bmatrix} = \begin{bmatrix} \Im\left\{\frac{\partial [\boldsymbol{S}]_{\mathrm{V}\theta}}{\partial [\boldsymbol{\theta}]_{\mathrm{PV}}}\right\} & \Im\left\{\frac{\partial [\boldsymbol{S}]_{\mathrm{V}\theta}}{\partial [\boldsymbol{\theta}]_{\mathrm{PQ}}}\right\} & \Im\left\{\frac{\partial [\boldsymbol{S}]_{\mathrm{V}\theta}}{\partial [\|\boldsymbol{V}\|]_{\mathrm{PQ}}}\right\} \\ \Im\left\{\frac{\partial [\boldsymbol{S}]_{\mathrm{PV}}}{\partial [\boldsymbol{\theta}]_{\mathrm{PV}}}\right\} & \Im\left\{\frac{\partial [\boldsymbol{S}]_{\mathrm{PV}}}{\partial [\boldsymbol{\theta}]_{\mathrm{PQ}}}\right\} & \Im\left\{\frac{\partial [\boldsymbol{S}]_{\mathrm{PV}}}{\partial [\|\boldsymbol{V}\|]_{\mathrm{PQ}}}\right\} \end{bmatrix} \tag{3.45}$$

thus, all elements of $\mathbb{Q}^{\mathrm{A}}$ can be calculated on the basis of (3.26) and (3.27).

Replacing $[[\boldsymbol{\Delta\theta}]_{\mathrm{PV}}, [\boldsymbol{\Delta\theta}]_{\mathrm{PQ}}, [\boldsymbol{\Delta}\|\boldsymbol{V}\|]_{\mathrm{PQ}}]^{\mathrm{T}}$ from (3.33) into (3.44) leads to the following linear function that characterizes $[[\boldsymbol{\Delta Q}]_{\mathrm{V}\theta}, [\boldsymbol{\Delta Q}]_{\mathrm{PV}}]^{\mathrm{T}}$ as a linear function of $[\boldsymbol{\Delta P}]_{\mathrm{PV}}$, $[\boldsymbol{\Delta P}]_{\mathrm{PQ}}$, and $[\boldsymbol{\Delta Q}]_{\mathrm{PQ}}$:

$$\begin{bmatrix} [\boldsymbol{\Delta Q}]_{\mathrm{V}\theta} \\ [\boldsymbol{\Delta Q}]_{\mathrm{PV}} \end{bmatrix} = \mathbb{Q}^{\mathrm{A}}\Big|_{\widehat{\boldsymbol{\Theta}},\,\|\widehat{\mathbf{V}}\|} \Gamma\Big|_{\widehat{\boldsymbol{\Theta}},\,\|\widehat{\mathbf{V}}\|} \begin{bmatrix} [\boldsymbol{\Delta P}]_{\mathrm{PV}} \\ [\boldsymbol{\Delta P}]_{\mathrm{PQ}} \\ [\boldsymbol{\Delta Q}]_{\mathrm{PQ}} \end{bmatrix} \tag{3.46}$$

Consequently, reactive power injections of Vθ and PV buses, i.e. $[[\boldsymbol{Q}]_{\mathrm{V}\theta}, [\boldsymbol{Q}]_{\mathrm{PV}}]^{\mathrm{T}}$, can be characterized as a linear function of $[\boldsymbol{\Delta P}]_{\mathrm{PV}}$, $[\boldsymbol{\Delta P}]_{\mathrm{PQ}}$, and $[\boldsymbol{\Delta Q}]_{\mathrm{PQ}}$ by replacing $[\,[\boldsymbol{\Delta Q}]_{\mathrm{V}\theta}, [\boldsymbol{\Delta Q}]_{\mathrm{PV}}]^{\mathrm{T}}$ from (3.46) into (3.9):

$$\begin{bmatrix} [\boldsymbol{Q}]_{\mathrm{V}\theta} \\ [\boldsymbol{Q}]_{\mathrm{PV}} \end{bmatrix} = \mathbb{Q}^{0} + \mathbb{Q} \begin{bmatrix} [\boldsymbol{\Delta P}]_{\mathrm{PV}} \\ [\boldsymbol{\Delta P}]_{\mathrm{PQ}} \\ [\boldsymbol{\Delta Q}]_{\mathrm{PQ}} \end{bmatrix} \tag{3.47}$$

where $\mathbb{Q}^{0} \in \mathbb{R}^{(n_{\mathrm{PV}}+1)\times 1}$ is a constant vector that can be calculated as:

$$\mathbb{Q}^{0} = \begin{bmatrix} [\,\widehat{\mathbf{Q}}]_{\mathrm{V}\theta} \\ [\,\widehat{\mathbf{Q}}]_{\mathrm{PV}} \end{bmatrix} \tag{3.48}$$

and $\mathbb{Q}$ is a constant matrix in $\mathbb{R}^{(n_{\mathrm{PV}}+1)\times(n_{\mathrm{PV}}+2n_{\mathrm{PQ}})}$ and can be easily calculated as:

$$\mathbb{Q} = \mathbb{Q}^{\mathrm{A}}\Big|_{\widehat{\boldsymbol{\Theta}},\,\|\widehat{\mathbf{V}}\|} \Gamma\Big|_{\widehat{\boldsymbol{\Theta}},\,\|\widehat{\mathbf{V}}\|} \tag{3.49}$$

3.5.4 Linear Formulation for Complex Power Flow of Branches

3.5.4.1 From-end

Considering (3.18), the first partial derivatives of $\boldsymbol{S}^{\text{From}}$ with respect to $\|\boldsymbol{V}\|$ and $\boldsymbol{\theta}$ can be easily extracted as:

$$\frac{\partial \boldsymbol{S}^{\text{From}}}{\partial \|\boldsymbol{V}\|} = \text{diag}(\mathbf{A}^{\text{From}}\ \boldsymbol{V})\ \mathbf{Y}^{\text{From}^*}\ (\frac{\partial \boldsymbol{V}}{\partial \|\boldsymbol{V}\|})^* + \text{diag}(\mathbf{Y}^{\text{From}^*}\ \boldsymbol{V}^*)\ \mathbf{A}^{\text{From}}\ (\frac{\partial \boldsymbol{V}}{\partial \|\boldsymbol{V}\|}), \tag{3.50}$$

$$\frac{\partial \boldsymbol{S}^{\text{From}}}{\partial \boldsymbol{\theta}} = \text{diag}(\mathbf{A}^{\text{From}}\ \boldsymbol{V})\ \mathbf{Y}^{\text{From}^*}\ (\frac{\partial \boldsymbol{V}}{\partial \boldsymbol{\theta}})^* + \text{diag}(\mathbf{Y}^{\text{From}^*}\ \boldsymbol{V}^*)\ \mathbf{A}^{\text{From}}\ (\frac{\partial \boldsymbol{V}}{\partial \boldsymbol{\theta}}), \tag{3.51}$$

Replacing $(\frac{\partial \boldsymbol{V}}{\partial \|\boldsymbol{V}\|})$ from (3.22) into (3.50) along with replacing $(\frac{\partial \boldsymbol{V}}{\partial \boldsymbol{\theta}})$ from (3.23) into (3.51) yields:

$$\frac{\partial \boldsymbol{S}^{\text{From}}}{\partial \|\boldsymbol{V}\|} = \text{diag}(\mathbf{A}^{\text{From}}\ \boldsymbol{V})\ \mathbf{Y}^{\text{From}^*}\ \text{diag}(\ \boldsymbol{V}^*\ ./\ \|\boldsymbol{V}\|\ ) + \text{diag}(\mathbf{Y}^{\text{From}^*}\ \boldsymbol{V}^*)\ \mathbf{A}^{\text{From}}\ \text{diag}(\ \boldsymbol{V}\ ./\ \|\boldsymbol{V}\|\ ), \tag{3.52}$$

$$\frac{\partial \boldsymbol{S}^{\text{From}}}{\partial \boldsymbol{\theta}} = \text{diag}(\mathbf{A}^{\text{From}}\ \boldsymbol{V})\ \mathbf{Y}^{\text{From}^*}\ \sqrt{-1}\ \text{diag}(\ \boldsymbol{V}^*\ ) + \text{diag}(\mathbf{Y}^{\text{From}^*}\ \boldsymbol{V}^*)\ \mathbf{A}^{\text{From}}\ \sqrt{-1}\ \text{diag}(\ \boldsymbol{V}\ ), \tag{3.53}$$

In order to extract the first partial derivatives of $\|\boldsymbol{S}^{\text{From}}\|$ with respect to $\|\boldsymbol{V}\|$ and $\boldsymbol{\theta}$, let first introduce two different ways for calculating the square of the apparent power flow entering the from-end of branches, i.e. $\|\boldsymbol{S}^{\text{From}}\|^2 \in \mathbb{R}^{n_{\mathbb{L}}\times 1}$:

$$\|\ \boldsymbol{S}^{\text{From}}\|^{\ 2} = \text{diag}(\|\ \boldsymbol{S}^{\text{From}}\ \|)\ \|\ \boldsymbol{S}^{\text{From}}\ \| \tag{3.54}$$

$$\|\ \boldsymbol{S}^{\text{From}}\|^{\ 2} = \text{diag}(\ \boldsymbol{S}^{\text{From}}\ )\ \ \boldsymbol{S}^{\text{From}^*}, \tag{3.55}$$

The first partial derivatives of (3.54) with respect to $\|\boldsymbol{V}\|$ results in:

$$\begin{aligned}\frac{\partial\|\ \boldsymbol{S}^{\text{From}}\ \|^2}{\partial\|\boldsymbol{V}\|} &= \text{diag}(\|\ \boldsymbol{S}^{\text{From}}\ \|)\ \frac{\partial\|\ \boldsymbol{S}^{\text{From}}\ \|}{\partial\|\boldsymbol{V}\|} + \text{diag}(\|\ \boldsymbol{S}^{\text{From}}\ \|)\ \frac{\partial\|\ \boldsymbol{S}^{\text{From}}\ \|}{\partial\|\boldsymbol{V}\|} \\ &= 2\ \text{diag}(\|\ \boldsymbol{S}^{\text{From}}\ \|)\ \frac{\partial\|\ \boldsymbol{S}^{\text{From}}\ \|}{\partial\|\boldsymbol{V}\|}\end{aligned} \tag{3.56}$$

The first partial derivatives of (3.55) with respect to $\|\boldsymbol{V}\|$ results in:

$$\begin{aligned}\frac{\partial\|\ \boldsymbol{S}^{\text{From}}\ \|^2}{\partial\|\boldsymbol{V}\|} &= \text{diag}(\ \boldsymbol{S}^{\text{From}}\ )\ (\frac{\partial \boldsymbol{S}^{\text{From}}}{\partial\|\boldsymbol{V}\|})^* + \text{diag}(\ \boldsymbol{S}^{\text{From}^*}\ )\ \frac{\partial \boldsymbol{S}^{\text{From}}}{\partial\|\boldsymbol{V}\|} \\ &= 2\ \Re\left\{\text{diag}(\ \boldsymbol{S}^{\text{From}^*}\ )\ \frac{\partial \boldsymbol{S}^{\text{From}}}{\partial\|\boldsymbol{V}\|}\right\}\end{aligned} \tag{3.57}$$

Considering the fact that the left-hand sides of equations (3.56) and (3.57) are the same, thus, the right-hand sides of these equations are equal:

$$2\,\mathrm{diag}(\|\,\boldsymbol{S}^{\mathrm{From}}\,\|)\,\frac{\partial\|\,\boldsymbol{S}^{\mathrm{From}}\,\|}{\partial\|\boldsymbol{V}\|}\;=\;2\,\Re\Big\{\mathrm{diag}(\,\boldsymbol{S}^{\mathrm{From}\,*}\,)\,\frac{\partial\boldsymbol{S}^{\mathrm{From}}}{\partial\|\boldsymbol{V}\|}\Big\}\tag{3.58}$$

Multiplying both sides of (3.58) by $0.5\mathrm{diag}(\|\,\boldsymbol{S}^{\mathrm{From}}\,\|)^{-1}$ yields:

$$\frac{\partial\|\,\boldsymbol{S}^{\mathrm{From}}\,\|}{\partial\|\boldsymbol{V}\|}\;=\;\mathrm{diag}(\|\,\boldsymbol{S}^{\mathrm{From}}\,\|)^{-1}\,\Re\Big\{\mathrm{diag}(\,\boldsymbol{S}^{\mathrm{From}\,*}\,)\,\frac{\partial\boldsymbol{S}^{\mathrm{From}}}{\partial\|\boldsymbol{V}\|}\Big\}\tag{3.59}$$

In the same way, the first partial derivatives of $\|\boldsymbol{S}^{\mathrm{From}}\|$ with respect to $\boldsymbol{\theta}$ can be calculated:

$$\frac{\partial\|\,\boldsymbol{S}^{\mathrm{From}}\,\|}{\partial\boldsymbol{\theta}}\;=\;\mathrm{diag}(\|\,\boldsymbol{S}^{\mathrm{From}}\,\|)^{-1}\,\Re\Big\{\mathrm{diag}(\,\boldsymbol{S}^{\mathrm{From}\,*}\,)\,\frac{\partial\boldsymbol{S}^{\mathrm{From}}}{\partial\boldsymbol{\theta}}\Big\}\tag{3.60}$$

It is worth highlighting that $\frac{\partial\boldsymbol{S}^{\mathrm{From}}}{\partial\|\boldsymbol{V}\|}$ and $\frac{\partial\boldsymbol{S}^{\mathrm{From}}}{\partial\boldsymbol{\theta}}$ are matrices in $\mathbb{C}^{n_{\mathbb{L}}\times n_{\mathbb{B}}}$, whereas $\frac{\partial\|\,\boldsymbol{S}^{\mathrm{From}}\,\|}{\partial\|\boldsymbol{V}\|}$ and $\frac{\partial\|\,\boldsymbol{S}^{\mathrm{From}}\,\|}{\partial\boldsymbol{\theta}}$ are matrices in $\mathbb{R}^{n_{\mathbb{L}}\times n_{\mathbb{B}}}$.

The first order Taylor expansion of $\|\,\boldsymbol{S}^{\mathrm{From}}\|$ with respect to the state variables $\|\boldsymbol{V}\|$ and $\boldsymbol{\theta}$ can be written as:

$$\|\boldsymbol{S}^{\mathrm{From}}\|\;=\;\|\widehat{\mathbf{S}}^{\mathrm{From}}\|\;+\;\frac{\partial\|\boldsymbol{S}^{\mathrm{From}}\|}{\partial\|\boldsymbol{V}\|}\bigg|_{\widehat{\boldsymbol{\theta}},\,\|\,\widehat{\mathbf{V}}\|}\boldsymbol{\Delta}\|\boldsymbol{V}\|\;+\;\frac{\partial\|\boldsymbol{S}^{\mathrm{From}}\|}{\partial\boldsymbol{\theta}}\bigg|_{\widehat{\boldsymbol{\theta}},\,\|\,\widehat{\mathbf{V}}\|}\boldsymbol{\Delta}\boldsymbol{\theta},\tag{3.61}$$

Considering Remarks 1 and 2 along with substituting expressions (3.10), (3.52), (3.53), (3.59), (3.60) into expression (3.61) result in the following vector-matrix equation:

$$\boldsymbol{\Delta}\|\boldsymbol{S}^{\mathrm{From}}\|=\mathbb{S}^{\mathrm{From,A}}\bigg|_{\widehat{\boldsymbol{\theta}},\,\|\,\widehat{\mathbf{V}}\|}\begin{bmatrix}[\boldsymbol{\Delta}\boldsymbol{\theta}]_{\mathrm{PV}}\\ [\boldsymbol{\Delta}\boldsymbol{\theta}]_{\mathrm{PQ}}\\ [\boldsymbol{\Delta}\|\boldsymbol{V}\|]_{\mathrm{PQ}}\end{bmatrix}\tag{3.62}$$

where $\mathbb{S}^{\mathrm{From,A}}\in\mathbb{C}^{n_{\mathbb{L}}\times(n_{\mathrm{PV}}+2n_{\mathrm{PV}})}$ is composed of:

$$\mathbb{S}^{\mathrm{From,A}}:=\begin{bmatrix}\frac{\partial\|\boldsymbol{S}^{\mathrm{From}}\|}{\partial[\boldsymbol{\theta}]_{\mathrm{PV}}} & \frac{\partial\|\boldsymbol{S}^{\mathrm{From}}\|}{\partial[\boldsymbol{\theta}]_{\mathrm{PQ}}} & \frac{\partial\|\boldsymbol{S}^{\mathrm{From}}\|}{\partial[\|\boldsymbol{V}\|]_{\mathrm{PQ}}}\end{bmatrix}\tag{3.63}$$

thus, all elements of $\mathbb{S}^{\mathrm{From,A}}$ can be calculated on the basis of (3.59) and (3.60).

Substituting $[[\boldsymbol{\Delta}\boldsymbol{\theta}]_{\mathrm{PV}},\,[\boldsymbol{\Delta}\boldsymbol{\theta}]_{\mathrm{PQ}},\,[\boldsymbol{\Delta}\|\boldsymbol{V}\|]_{\mathrm{PQ}}]^{\mathrm{T}}$ from (3.33) into (3.62) results in the following linear function that characterizes $\boldsymbol{\Delta}\|\boldsymbol{S}^{\mathrm{From}}\|$ as a linear function of $[\boldsymbol{\Delta}\boldsymbol{P}]_{\mathrm{PV}}$, $[\boldsymbol{\Delta}\boldsymbol{P}]_{\mathrm{PQ}}$, and

$[\boldsymbol{\Delta Q}]_{\mathrm{PQ}}$:

$$\boldsymbol{\Delta}\|\boldsymbol{S}^{\mathrm{From}}\| = \mathbb{S}^{\mathrm{From,A}}\Big|_{\widehat{\boldsymbol{\theta}},\,\|\widehat{\mathbf{V}}\|}\;\Gamma\Big|_{\widehat{\boldsymbol{\theta}},\,\|\widehat{\mathbf{V}}\|}\begin{bmatrix}[\boldsymbol{\Delta P}]_{\mathrm{PV}}\\ [\boldsymbol{\Delta P}]_{\mathrm{PQ}}\\ [\boldsymbol{\Delta Q}]_{\mathrm{PQ}}\end{bmatrix} \tag{3.64}$$

Accordingly, apparent power flow entering the from-end of branches, i.e. $\|\boldsymbol{S}^{\mathrm{From}}\|$, can be characterized as a linear function of $[\boldsymbol{\Delta P}]_{\mathrm{PV}}$, $[\boldsymbol{\Delta P}]_{\mathrm{PQ}}$, and $[\boldsymbol{\Delta Q}]_{\mathrm{PQ}}$ by replacing $\boldsymbol{\Delta}\|\boldsymbol{S}^{\mathrm{From}}\|$ from (3.64) into (3.10):

$$\|\boldsymbol{S}^{\mathrm{From}}\| = \mathbb{S}^{\mathrm{From,0}} + \mathbb{S}^{\mathrm{From}}\begin{bmatrix}[\boldsymbol{\Delta P}]_{\mathrm{PV}}\\ [\boldsymbol{\Delta P}]_{\mathrm{PQ}}\\ [\boldsymbol{\Delta Q}]_{\mathrm{PQ}}\end{bmatrix} \tag{3.65}$$

where $\mathbb{S}^{\mathrm{From,0}} \in \mathbb{R}^{n_{\mathbb{L}}\times 1}$ is a constant vector that can be calculated as:

$$\mathbb{S}^{\mathrm{From,0}} = \|\widehat{\mathbf{S}}^{\mathrm{From}}\| \tag{3.66}$$

and $\mathbb{S}^{\mathrm{From}}$ is a constant matrix in $\mathbb{R}^{n_{\mathbb{L}}\times(n_{\mathrm{PV}}+2n_{\mathrm{PQ}})}$ and can be easily calculated as:

$$\mathbb{S}^{\mathrm{From}} = \mathbb{S}^{\mathrm{From,A}}\Big|_{\widehat{\boldsymbol{\theta}},\,\|\widehat{\mathbf{V}}\|}\;\Gamma\Big|_{\widehat{\boldsymbol{\theta}},\,\|\widehat{\mathbf{V}}\|} \tag{3.67}$$

3.5.4.2 To-end

In the same way of 3.5.4.1, apparent power flow entering the to-end of branches, i.e. $\|\boldsymbol{S}^{\mathrm{To}}\|$, can be characterized as a linear function of $[\boldsymbol{\Delta P}]_{\mathrm{PV}}$, $[\boldsymbol{\Delta P}]_{\mathrm{PQ}}$, and $[\boldsymbol{\Delta Q}]_{\mathrm{PQ}}$ as:

$$\|\boldsymbol{S}^{\mathrm{To}}\| = \mathbb{S}^{\mathrm{To,0}} + \mathbb{S}^{\mathrm{To}}\begin{bmatrix}[\boldsymbol{\Delta P}]_{\mathrm{PV}}\\ [\boldsymbol{\Delta P}]_{\mathrm{PQ}}\\ [\boldsymbol{\Delta Q}]_{\mathrm{PQ}}\end{bmatrix} \tag{3.68}$$

where $\mathbb{S}^{\mathrm{To,0}} \in \mathbb{R}^{n_{\mathbb{L}}\times 1}$ is a constant vector that can be calculated as:

$$\mathbb{S}^{\mathrm{To,0}} = \|\widehat{\mathbf{S}}^{\mathrm{To}}\| \tag{3.69}$$

and $\mathbb{S}^{\mathrm{To}}$ is a constant matrix in $\mathbb{R}^{n_{\mathbb{L}}\times(n_{\mathrm{PV}}+2n_{\mathrm{PQ}})}$ and can be calculated as:

$$\mathbb{S}^{\mathrm{To}} = \mathbb{S}^{\mathrm{To,A}}\Big|_{\widehat{\boldsymbol{\theta}},\,\|\widehat{\mathbf{V}}\|}\;\Gamma\Big|_{\widehat{\boldsymbol{\theta}},\,\|\widehat{\mathbf{V}}\|} \tag{3.70}$$

where $\mathbb{S}^{\mathrm{To,A}} \in \mathbb{C}^{n_{\mathbb{L}} \times (n_{\mathrm{PV}}+2n_{\mathrm{PV}})}$ is composed of:

$$\mathbb{S}^{\mathrm{To,A}} := \begin{bmatrix} \dfrac{\partial \| \boldsymbol{S}^{\mathrm{To}} \|}{\partial [\boldsymbol{\theta}]_{\mathrm{PV}}} & \dfrac{\partial \| \boldsymbol{S}^{\mathrm{To}} \|}{\partial [\boldsymbol{\theta}]_{\mathrm{PQ}}} & \dfrac{\partial \| \boldsymbol{S}^{\mathrm{To}} \|}{\partial [\| \boldsymbol{V} \|]_{\mathrm{PQ}}} \end{bmatrix} \tag{3.71}$$

where elements of $\mathbb{S}^{\mathrm{To,A}}$ can be calculated as:

$$\frac{\partial \| \boldsymbol{S}^{\mathrm{To}} \|}{\partial \| \boldsymbol{V} \|} = \mathrm{diag}(\| \boldsymbol{S}^{\mathrm{To}} \|)^{-1} \, \Re \Big\{ \mathrm{diag}(\boldsymbol{S}^{\mathrm{To}*}) \, \frac{\partial \boldsymbol{S}^{\mathrm{To}}}{\partial \| \boldsymbol{V} \|} \Big\} \tag{3.72}$$

$$\frac{\partial \| \boldsymbol{S}^{\mathrm{To}} \|}{\partial \boldsymbol{\theta}} = \mathrm{diag}(\| \boldsymbol{S}^{\mathrm{To}} \|)^{-1} \, \Re \Big\{ \mathrm{diag}(\boldsymbol{S}^{\mathrm{To}*}) \, \frac{\partial \boldsymbol{S}^{\mathrm{To}}}{\partial \boldsymbol{\theta}} \Big\} \tag{3.73}$$

where the first partial derivatives of $\boldsymbol{S}^{\mathrm{To}}$ with respect to $\| \boldsymbol{V} \|$ and $\boldsymbol{\theta}$ can be extracted as:

$$\frac{\partial \boldsymbol{S}^{\mathrm{To}}}{\partial \| \boldsymbol{V} \|} = -\mathrm{diag}(\mathbf{A}^{\mathrm{To}} \, \boldsymbol{V}) \; \mathbf{Y}^{\mathrm{To}*} \; \mathrm{diag}(\boldsymbol{V}^* \, ./ \, \| \boldsymbol{V} \|) - \mathrm{diag}(\mathbf{Y}^{\mathrm{To}*} \, \boldsymbol{V}^*) \, \mathbf{A}^{\mathrm{To}} \, \mathrm{diag}(\boldsymbol{V} \, ./ \, \| \boldsymbol{V} \|), \tag{3.74}$$

$$\frac{\partial \boldsymbol{S}^{\mathrm{To}}}{\partial \boldsymbol{\theta}} = -\mathrm{diag}(\mathbf{A}^{\mathrm{To}} \, \boldsymbol{V}) \; \mathbf{Y}^{\mathrm{To}*} \; \sqrt{-1} \, \mathrm{diag}(\boldsymbol{V}^*) - \mathrm{diag}(\mathbf{Y}^{\mathrm{To}*} \, \boldsymbol{V}^*) \, \mathbf{A}^{\mathrm{To}} \, \sqrt{-1} \, \mathrm{diag}(\boldsymbol{V}), \tag{3.75}$$

It is worth highlighting that $\dfrac{\partial \boldsymbol{S}^{\mathrm{To}}}{\partial \| \boldsymbol{V} \|}$ and $\dfrac{\partial \boldsymbol{S}^{\mathrm{To}}}{\partial \boldsymbol{\theta}}$ are matrices in $\mathbb{C}^{n_{\mathbb{L}} \times n_{\mathbb{B}}}$, whereas $\dfrac{\partial \| \boldsymbol{S}^{\mathrm{To}} \|}{\partial \| \boldsymbol{V} \|}$ and $\dfrac{\partial \| \boldsymbol{S}^{\mathrm{To}} \|}{\partial \boldsymbol{\theta}}$ are matrices in $\mathbb{R}^{n_{\mathbb{L}} \times n_{\mathbb{B}}}$.

Hence, following (3.65) and (3.68), maximum power flow limit of transmission lines/-transformers can be linearly expressed as:

$$0 \leq \mathbb{S}^{\mathrm{From},0} + \mathbb{S}^{\mathrm{From}} \begin{bmatrix} [\boldsymbol{\Delta P}]_{\mathrm{PV}} \\ [\boldsymbol{\Delta P}]_{\mathrm{PQ}} \\ [\boldsymbol{\Delta Q}]_{\mathrm{PQ}} \end{bmatrix} \leq \mathbf{S}^{\mathrm{Max}} \tag{3.76}$$

$$0 \leq \mathbb{S}^{\mathrm{To},0} + \mathbb{S}^{\mathrm{To}} \begin{bmatrix} [\boldsymbol{\Delta P}]_{\mathrm{PV}} \\ [\boldsymbol{\Delta P}]_{\mathrm{PQ}} \\ [\boldsymbol{\Delta Q}]_{\mathrm{PQ}} \end{bmatrix} \leq \mathbf{S}^{\mathrm{Max}} \tag{3.77}$$

3.6 Conclusion

This chapter established a hot-start linearized power flow model while employing no approximation and simplification. Accordingly, the established power flow model takes advantage at most of the existing information, i.e the solution of AC power flow problem for the base case operating point. This linearized power flow model explicitly characterizes all grid constraints, including nodal voltage magnitude limits and maximum power flow limit of branches, as linear functions of the nodal injections. Above all, it takes into account shunt susceptance of branches as well as active/reactive power

losses of the transmission grid. In sum, this linearized power flow model empowers TSOs to achieve a clear perspective about their grid while having low computational burden thanks to its linear formulation. Last but not least, this linearized power flow model prepares a ground for constructing a grid-aware TSO-DSO coordination framework in chapter 4.

4 Grid-Cognizant TSO and DSO Coordination Framework for Active and Reactive Power Flexibility Exchange: The Swiss Case Study

All truths are easy to understand once they are discovered; the point is to discover them.
— Galileo Galilei

This chapter first designs a holistic coordination framework between transmission system operator (TSO) and distribution system operators (DSOs) to modernize traditional top-to-down (from transmission system to distribution systems) power flexibility provision mechanism to a bi-directional power flexibility provision mechanism between TSO and DSOs. More specifically, the designed framework empowers TSO and DSOs to exchange both active and reactive power flexibility without having to reveal their confidential grids data. Above all, the framework allows TSO to take advantage of the potential active and reactive power flexibility of the proliferating number of distributed energy resources (DERs) installed in distribution systems. Leveraging the designed framework along with the linearized power flow model developed in chapter 3, the chapter finally offers a two-stage mixed-integer linear stochastic optimization method to help TSO optimally book its required active and reactive power flexibility from both power plants and distribution systems. In particular, the offered method considers the constraints and active/reactive power losses of the transmission network. The performance of the proposed framework is evaluated considering a real-world transmission network, i.e. the Swiss transmission network.

Keywords: TSO-DSO collaboration, transmission network, active and reactive power flexibility, frequency and voltage control services, ancillary services, two-stage mixed-integer linear stochastic optimization, distributed energy resources.

Nomenclature

Indices and Sets

d	Index for (flexible and inflexible) distribution networks.
g	Index for (stochastic and dispatchable) power plants.
i, j	Index for buses.
l	Index for transmission lines/transformers.
n	Index for the offered FPC areas to the TSO.
r	Index for the reference (slack) bus.
s	Index for scenarios modeling uncertainties.
t, t'	Index for time intervals.
B	Set of all buses excluding the reference bus.
B^{G}	Set of buses hosting power plants (including the reference bus r).
B^{D}	Set of buses without power plants.
D	Set of all distribution networks ($\mathrm{D} = \mathrm{D}^{\mathrm{Flex}} \bigcup \mathrm{D}^{\mathrm{Inflex}}$).
$\mathrm{D}^{\mathrm{Flex}}$	Set of flexible distribution networks.
$\mathrm{D}_i^{\mathrm{Flex}}$	Set of flexible distribution networks connected to bus i.
$\mathrm{D}^{\mathrm{Inflex}}$	Set of inflexible distribution networks.
$\mathrm{D}_i^{\mathrm{Inflex}}$	Set of inflexible distribution networks connected to bus i.
G	Set of all power plants ($\mathrm{G} = \mathrm{G}^{\mathrm{Flex}} \bigcup \mathrm{G}^{\mathrm{Inflex}}$).
$\mathrm{G}^{\mathrm{Flex}}$	Set of flexible power plants, i.e. dispatchable power plants like hydro plants.
$\mathrm{G}_i^{\mathrm{Flex}}$	Set of flexible power plants connected to bus i.
$\mathrm{G}^{\mathrm{Inflex}}$	Set of inflexible power plants, i.e. stochastic power plants like solar/wind plants.
$\mathrm{G}_i^{\mathrm{Inflex}}$	Set of inflexible power plants connected to bus i.
L	Set of transmission lines/transformers.
O_{d}	Set of offered FPC areas to the TSO by flexible distribution network d.
O_{g}	Set of offered FPC areas to the TSO by flexible dispatchable power plant g.

S	Set of scenarios.
T	Set of time intervals belonging to the time horizon H.

Variables

f^{P}_{dts}, f^{Q}_{dts}	Active and reactive power flexibility that TSO deploys from flexible distribution networks d ($d \in \mathrm{D}^{\mathrm{Flex}}$) during time interval t and scenario s.
f^{P}_{gts}	Active power flexibility that TSO deploys from flexible distribution networks g ($g \in \mathrm{G}^{\mathrm{Flex}}$) during time interval t and scenario s.
$F^{\mathrm{P+,TSO}}_{dt}$, $F^{\mathrm{P-,TSO}}_{dt}$	The TSO's booked upward and downward active power flexibility from flexible distribution network d for time interval t (boundaries of $\mathscr{A}^{\mathrm{TSO}}_{dt}$).
$F^{\mathrm{Q+,TSO}}_{dt}$, $F^{\mathrm{Q-,TSO}}_{dt}$	The TSO's booked upward and downward reactive power flexibility from flexible distribution network d for time interval t (boundaries of $\mathscr{A}^{\mathrm{TSO}}_{dt}$).
$F^{\mathrm{P+,TSO}}_{gt}$, $F^{\mathrm{P-,TSO}}_{gt}$	The TSO's booked upward and downward active power flexibility from flexible power plant g for time interval t (boundaries of $\mathscr{A}^{\mathrm{TSO}}_{gt}$).
P^{LNS}_{dts}	Load not supplied (i.e. curtailed) of distribution network d in time interval t and scenario s.

Parameters

$\mathscr{A}_{dtn}$	The n^{th} Offered FPC area of flexible distribution network d for time interval t.
$\mathscr{A}^{\mathrm{TSO}}_{dt}$	FPC area that TSO books from flexible distribution network d for time interval t.
$\mathscr{A}_{gtn}$	The n^{th} Offered FPC area of flexible power plant g for time interval t.
$\mathscr{A}^{\mathrm{TSO}}_{gt}$	FPC area that TSO books from flexible power plant g for time interval t.
$\widehat{\mathrm{P}}_{dt}$, $\widehat{\mathrm{Q}}_{dt}$	Scheduled active and reactive power absorption of distribution network d ($d \in \mathrm{D}$) from its TSO-DSO interface.
$\widehat{\mathrm{P}}_{gt}$	Scheduled/predicted active power generation of dispatchable/stochastic power plant g ($g \in \mathrm{G}$).
$\mathrm{Q}^{\mathrm{Max}}_{gt}$, $\mathrm{Q}^{\mathrm{Min}}_{gt}$	Maximum and minimum reactive power generation limit of power plant g.
$\mathrm{t}_{\mathrm{DSO}}$	The time (in hour) prior to the beginning of the time horizon H when each flexible distribution network offers its FPC areas to the TSO.

t_{TSO}	The time (in hour) prior to the beginning of the time horizon H when the TSO books its required FPC area from flexibility providers.
$\|\widehat{V}_{gt}\|$	The TSO's defined set-point for the voltage magnitude of the interconnecting bus of the power plant g ($g \in G$).
VOLL	Value of lost load for energy not supplied.
$\pi^{P+}_{dtn}, \pi^{P-}_{dtn}$, $\pi^{Q+}_{dtn}, \pi^{Q-}_{dtn}$	Offered booking prices of flexible distribution network d for its FPC area $\mathscr{A}_{dtn}$.
π^{P+}_{gtn}, π^{P-}_{gtn}	Offered booking prices of flexible power plant g for its active power flexibility belonging to $\mathscr{A}_{gtn}$.
π'^{P+}_{t}, π'^{P-}_{t}, π'^{Q+}_{t}, π'^{Q-}_{t}	Price of deployed upward active, downward active, upward reactive and downward reactive power flexibility during the real-time grid operation.
ΔP_{dts}, ΔQ_{dts}	The deviated active/reactive power absorption of inflexible distribution network d ($d \in D^{Inflex}$) from its scheduled operating point, i.e. $\widehat{P}_{dt}$ and $\widehat{Q}_{dt}$.
ΔP_{gts},	The deviated active power generation of inflexible power plant g ($g \in G^{Inflex}$) from its predicted power generation, i.e. $\widehat{P}_{gt}$.
ΔP_{its}, ΔQ_{its}	Net deviation of the active/reactive power injection of bus i from its scheduled operating point in time interval t and scenario s.
τ	Duration of each time interval [hour].
ρ_s	Probability of occurrence of scenario s.

4.1 Motivations

Electricity generation from renewable energy sources (RES) including wind and solar energy is attaining significant levels in almost all electric power systems around the globe [72]. Although this massive integration of RES helps to alleviate environmental concerns, it might jeopardize the security of electric power systems and set off a variety of challenges for grid operators mainly due to simultaneous realization of:

- surge in uncertainties stemming from stochastic power generation of RES.
- fall in available power flexibility owing to the phase-out of conventional dispatchable power plants.

Active (and respectively reactive) power flexibility refers to the additional bi-directional active (reactive) power a resource can provides to the grid by regulating its operating point. Grid operators respectively leverage active and reactive power flexibility to regulate frequency and voltage throughout the grid, most importantly, to counteract the impact of uncertainties and contingencies. Given that the conventional power plants have been the main sources of active/reactive power flexibility (main providers of frequency/voltage control services), their decommissioning is diminishing the available sources of power flexibility [73, 74]. In this emerging architecture, grid operators are encountering non-traditional problems, thereby requiring supplementary active/reactive power flexibility to securely steer the grid and guarantee power quality, voltage/frequency regulation, and congestion management [75]. For instance, the main reason of immense blackouts, such as South Australia [76] and Southern California [77] blackouts, was voltage collapse resulting from lack of reactive power flexibility needed to prevent further voltage drop. Moreover, spikes in the price of power flexibility are appearing more frequently in recent years [78]. These unprecedented issues all together bear testimony to the importance of the reliable and adequate provision of both active and reactive power flexibility.

4.2 State of the Art

To avoid lack of power flexibility, a promising solution widely recognized in the literature is to unlock and tap the power flexibility of proliferating distributed energy resources (DERs) located in distribution level. In this respect, the existing literature offers three mainstreams of methods. The first mainstream of methods restrict themselves exclusively to the distribution level and strive to unlock and deploy the active/reactive power flexibility of DERs to deal with local issues at distribution networks. Work in [79] developed a two-stage hierarchical optimization model to deploy the power flexibility of DERs in order to mitigate the congestion in distribution networks. [80] proposed a communication-free coordination approach to manage the power flexibility of DERs, thereby, providing frequency control service to the local network. Work in [81] presented two algorithms namely rule-based algorithm and optimization-based algorithm to capture the power flexibility of DERs and provide voltage control service to the distribution network.

In contrast, the second mainstream of methods broaden their scope of application. They set out to coordinate and aggregate the active/reactive power flexibility of DERs located in distribution level with the purpose of providing it to the transmission network at the TSO-DSO interface. In this respect, [29] and [17] introduced the concept of flexibility provision capability (FPC) curve/area. FPC curve of a distribution network is a curve in P-Q plane characterizing the extreme amount of the active and reactive power flexibility that the distribution network can provide to the transmission network at its TSO-DSO interface. The area surrounded by the FPC curve is called FPC

area. Moreover, work in [17] constructed a set of robust optimization problems to robustly predict the FPC area of a distribution network while considering grid/DERs constraints and uncertainties of demand/stochastic generation. Therefore, it ensures that, during real-time grid operation, the DSO can provide to the TSO any amount of active and reactive power flexibility corresponding to the points located inside its FPC area without deteriorating the security of the distribution network. Relying on this method, a day prior to the real-time grid operation, each DSO can firstly predict and then offer to the TSO its FPC area associated with each time interval of the next day. Work in [18] turned its attention to the real-time grid operation stage and proposed a two-stage distribution network control strategy to empower DSOs optimally procure the active/reactive power flexibility of DERs in order to satisfy at best both active and reactive power flexibility request of the TSO. Works in [82–86] concentrated on the reactive power flexibility provision to the TSO. To this end, [82] introduced a centralized control scheme and evaluated the financial incentives required for encouraging distribution networks to participate in this control scheme. In line with [82], [83] and [84] developed a model-free control scheme to aggregate the reactive power flexibility of dispersed small-scale photovoltaic systems or battery storage located in distribution level, whereas [85] and [86] defined a centralized optimization-based control scheme to tap the reactive power flexibility of utility-scale DERs and provide it to the TSO.

The third mainstream of methods have less been well addressed. This mainstream aims to improve the coordination between TSO and DSO in such a way that the TSO can also benefit from the active/reactive power flexibility of DERs installed in distribution level. Work in [20] offered an active power flexibility allocation method to optimally book the TSO's required size of active power flexibility from not only power plants but also distribution systems. To deal with active power imbalance during the real-time grid operation at the transmission level, work in [87] offered an optimal power flow approach to help TSO optimally deploy the power flexibility of distribution networks, thereby counteracting the impact of the active power imbalance at the transmission system.

4.3 Contributions & Novelties

To the best knowledge of the author, the existing literature lacks a TSO-DSO coordination framework to enable TSO and DSOs exchange both active and reactive power flexibility with each other. In this context, the main contributions of the chapter are:

- It designs a holistic TSO-DSO coordination framework where TSO and DSOs establish their collaboration on the basis of the FPC areas. This framework facilitates the TSO and DSO collaboration, thereby, boosting unlocking the potential active/reactive power flexibility of DERs.

- It develops a decision making tool for TSOs to help them optimally book their required active and reactive power flexibility via FPC areas. Leveraging a linearized AC power flow model, it is able to account for grid's active and reactive power losses and, most notably, the nodal voltage magnitude constraints. Therefore, it can ensure that power plants accomplish their voltage regulation task against all uncertainties and contingencies without reaching their maximum/minimum reactive power limits. Accordingly, it helps TSOs steer their grids far from risks associated with under-voltage/over-voltage issues triggering voltage collapse.
- It allows TSO to take advantage of all existing power flexibility resources including dispatchable power plants and DERs located in distribution networks.
- It follows the sequential energy and flexibility market structure, thus, it is a tailored tool for most of European TSOs.
- It evaluates the efficiency of the developed framework and decision making tool on a real-world transmission network, i.e. the Swiss transmission network operated by Swissgrid.

4.4 TSO-DSO Coordination Framework

The emerging smart grids enable new automated control strategies for managing proliferating number of DERs installed in distribution networks. These novel control strategists are able to aggregate the potential active/reactive power flexibility of the DERs and provide it to the transmission network at the TSO-DSO interface while respecting all constraints of the distribution network [17,18]. More specifically, these kind of methods have been revolutionizing the paradigm of treating distribution networks as sources of uncertainties to sources of active/reactive power flexibility. Accordingly, distribution networks can be categorized into **flexible** and **inflexible** ones.

1. **Flexible distribution networks**: They coordinate and deploy the power flexibility of DERs to tackle the local flexibility demand at the distribution network, furthermore, they offer the surplus power flexibility of those DERs to the transmission network at their TSO-DSO interface.
2. **Inflexible distribution networks**: They are managed in a traditional way where the DERs' power flexibility is not unlocked and tapped. Therefore, instead of providing power flexibility to the transmission network, these inflexible distribution networks are sources of uncertainties which require power flexibility.

An efficient TSO-DSO coordination framework is needed to help TSO benefit from the power flexibility of DERs installed in distribution level, thereby improving the security of the whole electric power system. However, TSO and DSOs are independent

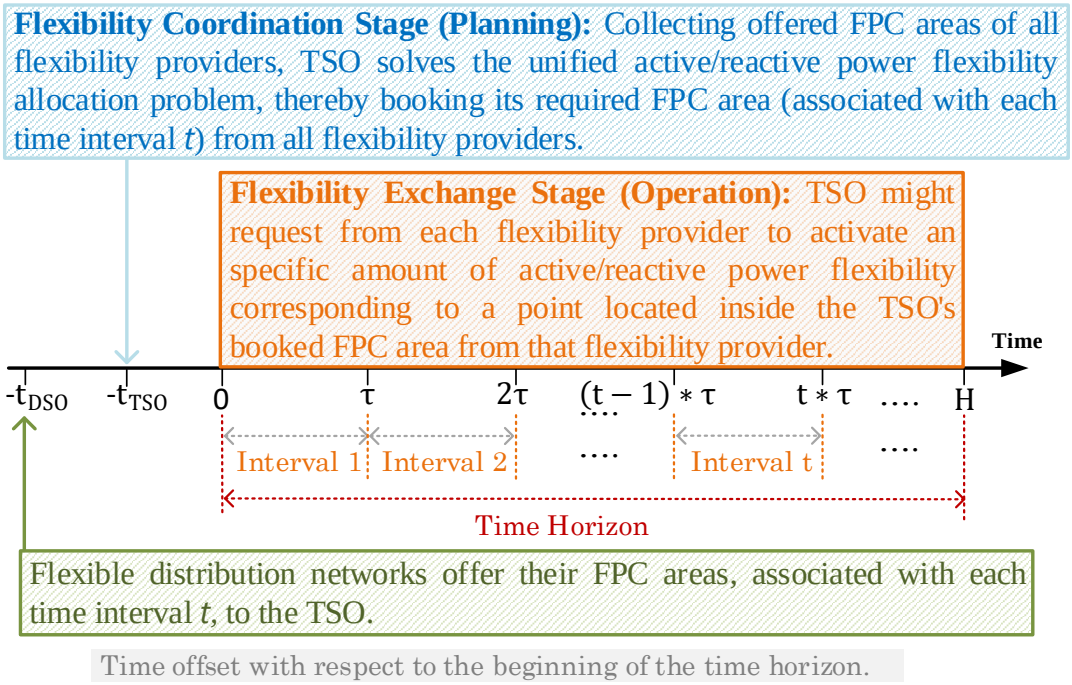

Figure 4.1: Timeline of the designed TSO-DSO coordination framework.

operators/organizations, they therefore prefer to exchange such an active/reactive flexibility while sharing as less as possible data with each other. To address this issue, this paper leverages the concept of FPC area, introduced in [17], and develops a holistic TSO-DSO collaboration framework. This framework allows TSO and DSO to easily coordinate their flexibility demand/capability with each other using FPC areas, thereby exchanging active/reactive power flexibility without revealing their confidential girds data. On the other hand, the common-practice for steering the electric power systems is that the grid operators schedule the operation of their grid prior to the real-time grid operation, e.g. day-ahead or hours-ahead. In line with this widely accepted procedure, this paper organizes the TSO-DSO coordination in two stages. These two stages are elaborated by referring to a time horizon with duration of H (e.g. 24-hour of the next day) embracing a number of time intervals each with duration of τ as shown in Fig. 4.1:

1. **Flexibility Coordination Stage (Planning):** t_{DSO} hours prior to the beginning of the time horizon H, each flexible distribution network exploits the methodology introduced in [17] and predicts its FPC areas associated with each time interval t. Accordingly, for each time interval t, it offers a set of FPC areas with different prices to the TSO as shown in Fig. 4.2. After collecting the offered FPC areas of all flexibility providers including flexible distribution networks and flexible power plants[1], at t_{TSO} hours prior to the beginning of the time horizon H, the TSO books its required FPC area from each flexibility provider for each time interval t.

[1] Dispatchable power plants which are able to provide power flexibility to the TSO.

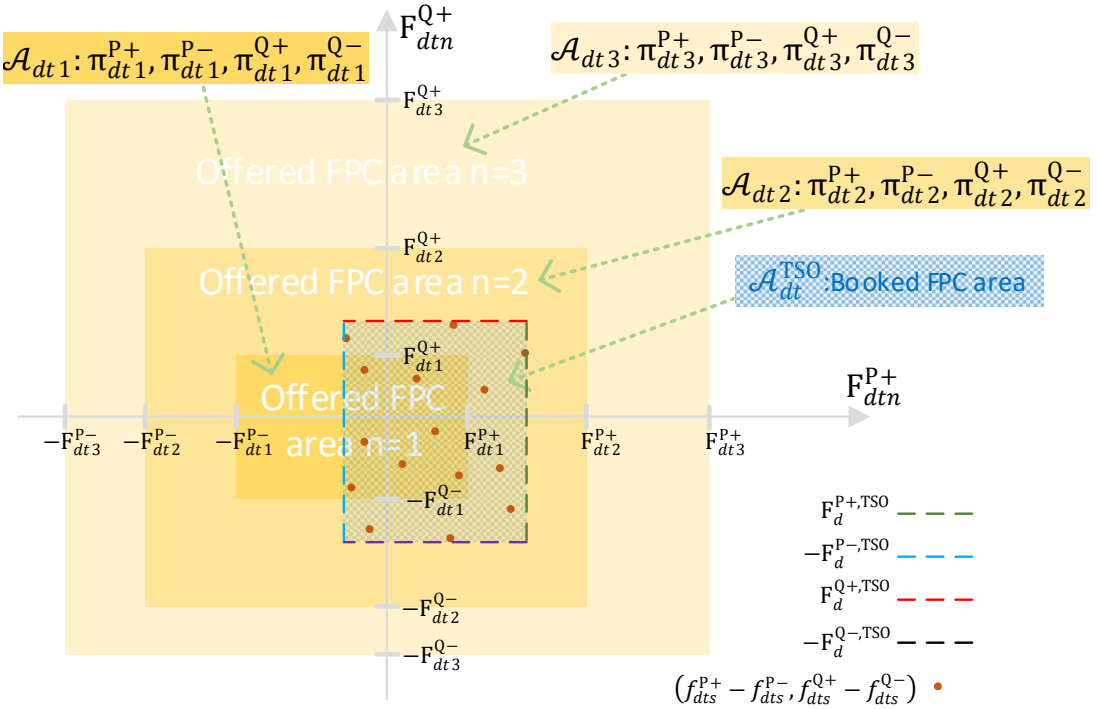

Figure 4.2: Offered FPC areas of flexible distribution network d for time interval t.

2. **Flexibility Exchange Stage (Operation):** During real-time grid operation, the TSO might require active/reactive power flexibility to securely steer its grid against uncertainties and contingencies. Considering its grid situation, the TSO might request from each flexibility provider to activate (provide) an specific amount of active/reactive power flexibility corresponding to a point (any red point shown in Fig. 4.2) located inside the TSO's booked FPC area from that flexibility provider.

4.5 Unified Active & Reactive Power Flexibility Allocation

This section implements the TSO's unified active and reactive power flexibility allocation problem as a two-stage decision making process where "flexibility coordination stage" corresponds with *here&now* decisions and "flexibility exchange stage" with *wiat&see* decisions. As a result, it extracts a two-stage mixed-integer linear stochastic optimization formulation for the problem. In this regard, let i and j be the indices for buses; r the index for the reference (slack) bus; B the set of all buses excluding the reference bus; B^G the set of buses hosting power plants (including the reference bus r); B^D the set of buses without power plants; l the index for transmission lines/-transformers; L the set of transmission lines/transformers; t and t' the indices for time intervals; T the set of time intervals belonging to the time horizon H; s the index for scenarios modeling the forecast errors of demand and renewable generation; S the set

of scenarios; d the index for (flexible and inflexible) distribution networks; $\mathrm{D}^{\mathrm{Flex}}$ the set of flexible distribution networks; $\mathrm{D}^{\mathrm{Inflex}}$ the set of inflexible distribution networks; D the set of all distribution networks ($\mathrm{D} = \mathrm{D}^{\mathrm{Flex}} \bigcup \mathrm{D}^{\mathrm{Inflex}}$); g the index for (stochastic and dispatchable) power plants; $\mathrm{G}^{\mathrm{Flex}}$ the set of flexible power plants, i.e. dispatchable power plants like hydro plants; $\mathrm{G}^{\mathrm{Inflex}}$ the set of inflexible power plants, i.e. stochastic power plants like solar/wind plants; G the set of all power plants ($\mathrm{G} = \mathrm{G}^{\mathrm{Flex}} \bigcup \mathrm{G}^{\mathrm{Inflex}}$); $\mathrm{D}_i^{\mathrm{Flex}}$ / $\mathrm{D}_i^{\mathrm{Inflex}}$ the set of flexible/inflexible distribution networks connected to bus i; $\mathrm{G}_i^{\mathrm{Flex}}$ / $\mathrm{G}_i^{\mathrm{Inflex}}$ the set of flexible/inflexible power plants connected to bus i; n the index for the offered FPC areas to the TSO; $\mathrm{O_d}$ / $\mathrm{O_g}$ the set of offered FPC areas to the TSO by flexible distribution network d / flexible dispatchable power plant g. Superscripts $*^{\mathrm{P+}}$, $*^{\mathrm{P-}}$. $*^{\mathrm{Q+}}$, $*^{\mathrm{Q-}}$ are respectively used to indicate the quantity of $*$ associated with upward active, downward active, upward reactive and downward reactive power flexibility. Operator $|.|$ denotes the element-wise absolute values of its argument. Then, the problem is formulated relying on the following considerations:

1) Sequential Energy & Flexibility Market

It follows the sequential energy and flexibility market structure where the outcome of the day-ahead energy market is known. Thus, for each time interval t belonging to the time horizon H:

- The scheduled active and reactive power absorption of distribution network d (for all $d \in \mathrm{D}$) from its TSO-DSO interface, i.e. $\widehat{\mathrm{P}}_{dt}$ and $\widehat{\mathrm{Q}}_{dt}$, are known.
- The scheduled/predicted active power generation of dispatchable/stochastic power plant g (for all $g \in \mathrm{G}$) are known, i.e. $\widehat{\mathrm{P}}_{gt}$. Moreover, the TSO's defined set-point for the voltage magnitude of the interconnecting bus of that plant, i.e. $|\widehat{\mathrm{V}}_{gt}|$, is known.

2) Flexibility Coordination Stage

For each time interval t:

- Flexible distribution network d offers a set of FPC areas, i.e. $\mathscr{A}_{dtn}$, with different booking prices i.e. $\pi_{dtn}^{\mathrm{P+}}, \pi_{dtn}^{\mathrm{P-}}, \pi_{dtn}^{\mathrm{Q+}}, \pi_{dtn}^{\mathrm{Q-}}$ to the TSO. Afterwards, TSO books its required FPC area from flexible distribution network d, i.e. $\mathscr{A}_{dt}^{\mathrm{TSO}}$. It is noteworthy that $\mathscr{A}_{dtn}$ (and respectively $\mathscr{A}_{dt}^{\mathrm{TSO}}$) is characterized by its 4 non-negative boundaries, namely offered (booked) upward and downward active/reactive power flexibility, i.e. $\mathrm{F}_{dtn}^{\mathrm{P+}}$, $\mathrm{F}_{dtn}^{\mathrm{P-}}$, $\mathrm{F}_{dtn}^{\mathrm{Q+}}$ and $\mathrm{F}_{dtn}^{\mathrm{Q-}}$ ($F_{dt}^{\mathrm{P+,TSO}}$, $F_{dt}^{\mathrm{P-,TSO}}$, $F_{dt}^{\mathrm{Q+,TSO}}$ and $F_{dt}^{\mathrm{Q-,TSO}}$);
- Power plant g (for all $g \in \mathrm{G}$), during the real-time grid operation, is responsible to automatically regulate its reactive power injection in such a way that the voltage magnitude of its interconnecting bus is preserved equal to the voltage set-point

defined by the TSO, i.e. $|\widehat{\mathrm{V}}_{gt}|$. Therefore, the optimal power flexibility allocation problem treats all buses hosting power plants ($i \in \mathrm{B}^{\mathrm{G}}$) as PV buses, to put it simply, their reactive power injections depend on the nodal injections of the other buses (as characterized in (4.30)) and their voltage magnitudes are fixed equal to their respective set-points, i.e. $|\widehat{\mathrm{V}}_{gt}|$. Accordingly, it is assumed that there are long-term contracts between TSO and power plants where power plants are committed to accomplish automatic voltage regulation during the real-time grid operation without any additional cost. As a consequence, the TSO needs to neither book (in flexibility coordination stage) nor request from power plants to activate their reactive power flexibility (in flexibility exchange stage).

- Flexible power plant g offers a set of FPC areas, i.e. $\mathscr{A}_{gtn}$, with different booking prices i.e. $\pi^{\mathrm{P}+}_{gtn}, \pi^{\mathrm{P}-}_{gtn}$ to the TSO. Afterwards, TSO books its required FPC area from flexible power plant g, i.e. $\mathscr{A}^{\mathrm{TSO}}_{gt}$. It is noteworthy that $\mathscr{A}_{gtn}$ (and respectively $\mathscr{A}^{\mathrm{TSO}}_{gt}$) is characterized by its 4 non-negative boundaries, namely offered (booked) upward and downward active power flexibility, i.e. $\mathrm{F}^{\mathrm{P}+}_{gtn}$ and $\mathrm{F}^{\mathrm{P}-}_{gtn}$ ($F^{\mathrm{P}+,\mathrm{TSO}}_{gt}$ and $F^{\mathrm{P}-,\mathrm{TSO}}_{gt}$) along with minimum and maximum reactive power generation limit of power plant g, i.e. $\mathrm{Q}^{\mathrm{Min}}_{gt}$ and $\mathrm{Q}^{\mathrm{Max}}_{gt}$.

3) Flexibility Exchange Stage

In time interval t and scenario s:

- Flexible distribution networks d (for all $d \in \mathrm{D}^{\mathrm{Flex}}$) is able not only to follow its scheduled operating point, i.e. $\widehat{\mathrm{P}}_{dt}$ and $\widehat{\mathrm{Q}}_{dt}$, but also to provide active and reactive power flexibility to the transmission network at its TSO-DSO interface i.e. f^{P}_{dts} and f^{Q}_{dts}. f^{P}_{dts} (and respectively f^{Q}_{dts}) is formed of the sum of two non-negative components called upward, i.e. $f^{\mathrm{P}+}_{dts}$, and downward, i.e. $f^{\mathrm{P}-}_{dts}$ active power flexibility (upward, i.e. $f^{\mathrm{Q}+}_{dts}$, and downward, i.e. $f^{\mathrm{Q}-}_{dts}$ reactive power flexibility) as:

$$f^{\mathrm{P}}_{dts} = f^{\mathrm{P}+}_{dts} - f^{\mathrm{P}-}_{dts}. \tag{4.1}$$

$$f^{\mathrm{Q}}_{dts} = f^{\mathrm{Q}+}_{dts} - f^{\mathrm{Q}-}_{dts}. \tag{4.2}$$

- In contrasts to the flexible distribution networks, inflexible distribution network d (for all $d \in \mathrm{D}^{\mathrm{Inflex}}$) is sources of active and reactive power uncertainties, i.e. $\Delta\mathrm{P}_{dts}$ and $\Delta\mathrm{Q}_{dts}$. Therefore, it may deviate from its scheduled operating point, i.e. $\widehat{\mathrm{P}}_{dt}$ and $\widehat{\mathrm{Q}}_{dt}$.

- Dispatchable power plant g (for all $g \in \mathrm{G}^{\mathrm{Flex}}$) can provide active power flexibility to the transmission network i.e. f^{P}_{gts}. f^{P}_{gts} is formed of the sum of two non-negative components called upward, i.e. $f^{\mathrm{P}+}_{gts}$, and downward, i.e. $f^{\mathrm{P}-}_{gts}$ active power flexibility as:

$$f^{\mathrm{P}}_{gts} = f^{\mathrm{P}+}_{gts} - f^{\mathrm{P}-}_{gts}. \tag{4.3}$$

- Stochastic power plant g (for all $g \in \mathrm{G}^{\mathrm{Inflex}}$) is source of active power uncertainties, i.e. $\Delta \mathrm{P}_{gts}$. Therefore, it may deviate from its predicted power generation, i.e. $\widehat{\mathrm{P}}_{gt}$.

It is worth noting that the TSO's unified active/reactive power flexibility allocation problem is separately solved for each individual time interval and in the same way. For this reason, the formulation in the following refers to one time slot only, and it is applied identically to each time slot of the time horizon.

4.5.1 Objective function

The objective function is designed to help TSO optimally steer its grid, thereby minimizing the cost of TSO, i.e. C_t^{TSO}, over each time interval t in both flexibility coordination (planning) and flexibility exchange (operation) stages:

$$\min C_t^{\mathrm{TSO}} = C_t^{\mathrm{Planning}} + EC_t^{\mathrm{Operation}}, \tag{4.4}$$

1) C_t^{Planning} represents the cost of TSO over time interval t in coordination stage where the TSO books FPC areas. More specifically, it specifies the TSO's cost associated with booking FPC areas $\mathscr{A}_{dt}^{\mathrm{TSO}}$ and $\mathscr{A}_{gt}^{\mathrm{TSO}}$:

$$\begin{aligned} C_t^{\mathrm{Planning}} = & \sum_{d \in \mathrm{D}^{\mathrm{Flex}}} \left[\pi_{dt}^{\mathrm{P+}} F_{dt}^{\mathrm{P+,TSO}} + \pi_{dt}^{\mathrm{P-}} F_{dt}^{\mathrm{P-,TSO}} + \pi_{dt}^{\mathrm{Q+}} F_{dt}^{\mathrm{Q+,TSO}} + \pi_{dt}^{\mathrm{Q-}} F_{dt}^{\mathrm{Q-,TSO}}\right] + \\ & + \sum_{g \in \mathrm{G}^{\mathrm{Flex}}} \left[\pi_{gt}^{\mathrm{P+}} F_{gt}^{\mathrm{P+,TSO}} + \pi_{gt}^{\mathrm{P-}} F_{gt}^{\mathrm{P-,TSO}}\right], \end{aligned} \tag{4.5}$$

where $\pi_{dt}^{\mathrm{P+}}$, $\pi_{dt}^{\mathrm{P-}}$, $\pi_{dt}^{\mathrm{Q+}}$, $\pi_{dt}^{\mathrm{Q-}}$, $\pi_{gt}^{\mathrm{P+}}$ and $\pi_{gt}^{\mathrm{P-}}$ are the booking prices associated with $\mathscr{A}_{dt}^{\mathrm{TSO}}$ and $\mathscr{A}_{gt}^{\mathrm{TSO}}$ and can be calculated as detailed in (4.15).

2) $EC_t^{\mathrm{Operation}}$ represents the expected cost of TSO over time interval t in flexibility exchange stage where the TSO deploys active/reactive power flexibility to preserve the power quality of its grid and avoid curtailing demand. Accordingly, it embraces two parts:

$$EC_t^{\mathrm{Operation}} = EC_t^{\mathrm{Flexibility}} + EC_t^{\mathrm{LNS}} \tag{4.6}$$

where $EC_t^{\mathrm{Flexibility}}$ represents TSO's expected cost due to deploying upward/downward

active/reactive power flexibility in time interval t:

$$\begin{aligned} EC_t^{\text{Flexibility}} = & \sum_{s\in\mathbb{S}} \tau\rho_s \pi'^{\text{P+}}_t [\sum_{d\in \text{D}^{\text{Flex}}} f^{\text{P+}}_{dts} + \sum_{g\in \text{G}^{\text{Flex}}} f^{\text{P+}}_{gts}] + \\ & + \sum_{s\in\mathbb{S}} \tau\rho_s \pi'^{\text{P-}}_t [\sum_{d\in \text{D}^{\text{Flex}}} f^{\text{P-}}_{dts} + \sum_{g\in \text{G}^{\text{Flex}}} f^{\text{P-}}_{gts}] + \\ & + \sum_{s\in\mathbb{S}} \tau\rho_s \pi'^{\text{Q+}}_t [\sum_{d\in \text{D}^{\text{Flex}}} f^{\text{Q+}}_{dts}] + \\ & + \sum_{s\in\mathbb{S}} \tau\rho_s \pi'^{\text{Q-}}_t [\sum_{d\in \text{D}^{\text{Flex}}} f^{\text{Q-}}_{dts}] \end{aligned} \tag{4.7}$$

where ρ_s is the probability of occurrence of scenario s; $\pi'^{\text{P+}}_t$, $\pi'^{\text{P-}}_t$, $\pi'^{\text{Q+}}_t$ and $\pi'^{\text{Q-}}_t$ are prices for deploying upward active, downward active, upward reactive and downward reactive power flexibility during the real-time grid operation. EC_t^{LNS} represents the TSO's expected cost pertained to the load not supplied in time interval t:

$$EC_t^{\text{LNS}} = \text{VOLL} \sum_{s\in\mathbb{S}} \tau\rho_s \sum_{d\in \text{D}} P^{\text{LNS}}_{dts} \tag{4.8}$$

where VOLL is value of lost load for energy not supplied; P^{LNS}_{dts} is the load not supplied (i.e. curtailed) of distribution network d in time interval t and scenario s.

4.5.2 Constraints Associated with Flexibility Coordination Stage

For each offered FPC area $\mathscr{A}_{dtn}$ (and respectively $\mathscr{A}_{gtn}$), a binary variable u_{dtn} (u_{gtn}) is designated to characterize the booking prices associated with $\mathscr{A}^{\text{TSO}}_{dt}$ ($\mathscr{A}^{\text{TSO}}_{gt}$), thereby determining the coefficients used in (4.5). For the sake of brevity, the following just elaborates the way that binary variable u_{dtn} can be mathematically modeled. However, binary variable u_{gtn} can also be modeled in the same way. Binary variable u_{dtn} takes 1 if $\mathscr{A}_{dtn}$ is the smallest offered FPC area that $\mathscr{A}^{\text{TSO}}_{dt} \subset \mathscr{A}_{dtn}$ and 0 otherwise. In order to mathematically express this logical relationship, lets first introduce the auxiliary binary variable u'_{dtn} denoting whether $\mathscr{A}^{\text{TSO}}_{dt} \subset \mathscr{A}_{dtn}$ or not. u'_{dtn} can be mathematically modeled as:

$$u'_{dtn} = u'^{\text{P+}}_{dtn}\, u'^{\text{P-}}_{dtn}\, u'^{\text{Q+}}_{dtn}\, u'^{\text{Q-}}_{dtn} \tag{4.9}$$

where binary variable $u'^{\text{P+}}_{dtn}$ (and similarly $u'^{\text{P-}}_{dtn}$, $u'^{\text{Q+}}_{dtn}$ and $u'^{\text{Q-}}_{dtn}$) indicates whether $F^{\text{P+,TSO}}_{dt} - \text{F}^{\text{P+}}_{dtn} \le 0$ or not, i.e. $u'^{\text{P+}}_{dtn} = 1 \leftrightarrow F^{\text{P+,TSO}}_{dt} - \text{F}^{\text{P+}}_{dtn} \le 0$. These logical relationships can be mathematically expressed as [88]:

$$\text{m}^{\text{P+}}_{dtn} u'^{\text{P+}}_{dtn} + \varepsilon \le F^{\text{P+,TSO}}_{dt} - \text{F}^{\text{P+}}_{dtn} \le \text{M}^{\text{P+}}_{dtn}(1 - u'^{\text{P+}}_{dtn}) \tag{4.10}$$

$$\text{m}^{\text{P-}}_{dtn} u'^{\text{P-}}_{dtn} + \varepsilon \le F^{\text{P-,TSO}}_{dt} - \text{F}^{\text{P-}}_{dtn} \le \text{M}^{\text{P-}}_{dtn}(1 - u'^{\text{P-}}_{dtn}) \tag{4.11}$$

$$\text{m}^{\text{Q+}}_{dtn} u'^{\text{Q+}}_{dtn} + \varepsilon \le F^{\text{Q+,TSO}}_{dt} - \text{F}^{\text{Q+}}_{dtn} \le \text{M}^{\text{Q+}}_{dtn}(1 - u'^{\text{Q+}}_{dtn}) \tag{4.12}$$

$$\text{m}^{\text{Q-}}_{dtn} u'^{\text{Q-}}_{dtn} + \varepsilon \le F^{\text{Q-,TSO}}_{dt} - \text{F}^{\text{Q-}}_{dtn} \le \text{M}^{\text{Q-}}_{dtn}(1 - u'^{\text{Q-}}_{dtn}) \tag{4.13}$$

where parameters $\mathrm{m}^{\mathrm{P+}}_{dtn}$, $\mathrm{m}^{\mathrm{P-}}_{dtn}$, $\mathrm{m}^{\mathrm{Q+}}_{dtn}$ and $\mathrm{m}^{\mathrm{Q-}}_{dtn}$ are respectively the lower bounds for $F^{\mathrm{P+,TSO}}_{dt} - \mathrm{F}^{\mathrm{P+}}_{dtn}$, $F^{\mathrm{P-,TSO}}_{dt} - \mathrm{F}^{\mathrm{P-}}_{dtn}$, $F^{\mathrm{Q+,TSO}}_{dt} - \mathrm{F}^{\mathrm{Q+}}_{dtn}$, and $F^{\mathrm{Q-,TSO}}_{dt} - \mathrm{F}^{\mathrm{Q-}}_{dtn}$. Parameters $\mathrm{M}^{\mathrm{P+}}_{dtn}$, $\mathrm{M}^{\mathrm{P-}}_{dtn}$, $\mathrm{M}^{\mathrm{Q+}}_{dtn}$ and $\mathrm{M}^{\mathrm{Q-}}_{dtn}$ are respectively the upper bounds for $F^{\mathrm{P+,TSO}}_{dt} - \mathrm{F}^{\mathrm{P+}}_{dtn}$, $F^{\mathrm{P-,TSO}}_{dt} - \mathrm{F}^{\mathrm{P-}}_{dtn}$, $F^{\mathrm{Q+,TSO}}_{dt} - \mathrm{F}^{\mathrm{Q+}}_{dtn}$, and $F^{\mathrm{Q-,TSO}}_{dt} - \mathrm{F}^{\mathrm{Q-}}_{dtn}$. These bounds can be easily determined referring to Fig. 4.2, as calculated in (4.22)-(4.23). It is worth noting that commercial solvers, more specifically classical optimization approaches, are not able to deal with strict inequality constraints. To tackle this issue, a very small number, ε, is added to the left-hand side constraints to convert strict inequality constraints ($<$) to non-strict inequality constraints ($\leq$). Finally, the binary variable u_{dtn} is characterized via constraints (4.14) where among all offers, i.e. $n \in \mathrm{O_d}$, the smallest $\mathscr{A}_{dtn}$ having $u'_{dtn} = 1$ is detected:

$$u_{dtn} = \begin{cases} u'_{dt1} & \text{if } n = 1 \\ u'_{dtn}(1 - u'_{dt(n-1)}) & \text{if } n \geq 2 \end{cases} \tag{4.14}$$

Accordingly, the booking price for upward active power flexibility from flexible distribution network d in time interval t can be easily characterized as:

$$\pi^{\mathrm{P+}}_{dt} = \sum_{n \in \mathrm{N}} \pi^{\mathrm{P+}}_{dtn} u_{dtn} \tag{4.15}$$

In the same way, the other booking prices used in (4.5), i.e. $\pi^{\mathrm{P-}}_{dt}$, $\pi^{\mathrm{Q+}}_{dt}$, $\pi^{\mathrm{Q-}}_{dt}$, $\pi^{\mathrm{P+}}_{gt}$ and $\pi^{\mathrm{P-}}_{gt}$, can be calculated.

For each time interval t and for each flexibility provider, the TSO is allowed to book at most the largest offered FPC area. To put it simply, $\mathscr{A}^{\mathrm{TSO}}_{dt}$ (and respectively $\mathscr{A}^{\mathrm{TSO}}_{gt}$) is restricted by $\mathscr{A}_{dtn'}$ ($\mathscr{A}_{gtn'}$) where index n' corresponds to the largest offered FPC area of flexible distribution network d (flexible power plant g) for time interval t:

$$0 \leq F^{\mathrm{P+,TSO}}_{dt} \leq \mathrm{F}^{\mathrm{P+}}_{dtn'} \tag{4.16}$$
$$0 \leq F^{\mathrm{P-,TSO}}_{dt} \leq \mathrm{F}^{\mathrm{P-}}_{dtn'} \tag{4.17}$$
$$0 \leq F^{\mathrm{Q+,TSO}}_{dt} \leq \mathrm{F}^{\mathrm{Q+}}_{dtn'} \tag{4.18}$$
$$0 \leq F^{\mathrm{Q-,TSO}}_{dt} \leq \mathrm{F}^{\mathrm{Q-}}_{dtn'} \tag{4.19}$$
$$0 \leq F^{\mathrm{P+,TSO}}_{gt} \leq \mathrm{F}^{\mathrm{P+}}_{gtn'} \tag{4.20}$$
$$0 \leq F^{\mathrm{P-,TSO}}_{gt} \leq \mathrm{F}^{\mathrm{P-}}_{gtn'} \tag{4.21}$$

Considering (4.16)-(4.19), upper and lower bounds for $F^{\mathrm{P+,TSO}}_{dt} - \mathrm{F}^{\mathrm{P+}}_{dtn}$, i.e. $\mathrm{M}^{\mathrm{P+}}_{dtn}$ and $\mathrm{m}^{\mathrm{P+}}_{dtn}$ (and similarly $\mathrm{m}^{\mathrm{P-}}_{dtn}$, $\mathrm{M}^{\mathrm{P-}}_{dtn}$, $\mathrm{m}^{\mathrm{Q+}}_{dtn}$, $\mathrm{M}^{\mathrm{Q+}}_{dtn}$, $\mathrm{m}^{\mathrm{Q-}}_{dtn}$, $\mathrm{M}^{\mathrm{Q-}}_{dtn}$) can be easily calculated as:

$$\mathrm{M}^{\mathrm{P+}}_{dtn} = \mathrm{F}^{\mathrm{P+}}_{dtn'} - \mathrm{F}^{\mathrm{P+}}_{dtn} \tag{4.22}$$
$$\mathrm{m}^{\mathrm{P+}}_{dtn} = -\mathrm{F}^{\mathrm{P+}}_{dtn} - \varepsilon \tag{4.23}$$

4.5.3 Constraints Associated with Flexibility Exchange Stage

During the real-time grid operation, the TSO is allowed to deploy any amount of active/reactive power flexibility belonging to its booked FPC areas, i.e. $\mathscr{A}_{dt}^{\mathrm{TSO}}$ and $\mathscr{A}_{gt}^{\mathrm{TSO}}$:

$$-F_{dt}^{\mathrm{P-,TSO}} \leq f_{dts}^{\mathrm{P}} \leq F_{dt}^{\mathrm{P+,TSO}} \tag{4.24}$$

$$-F_{dt}^{\mathrm{Q-,TSO}} \leq f_{dts}^{\mathrm{Q}} \leq F_{dt}^{\mathrm{Q+,TSO}} \tag{4.25}$$

$$-F_{gt}^{\mathrm{P-,TSO}} \leq f_{gts}^{\mathrm{P}} \leq F_{gt}^{\mathrm{P+,TSO}} \tag{4.26}$$

Furthermore, to avoid under/over-voltage issues, the TSO must ensure that each power plant g can accomplish its voltage regulation task without reaching its maximum/minimum reactive power generation limits, i.e. $\mathrm{Q}_{gt}^{\mathrm{Max}}$ / $\mathrm{Q}_{gt}^{\mathrm{Min}}$, (for all $g \in \mathrm{G}, t \in \mathrm{T}, s \in \mathrm{S}$):

$$-\mathrm{Q}_{gt}^{\mathrm{Min}} \leq Q_{gts} \leq \mathrm{Q}_{gt}^{\mathrm{Max}}, \tag{4.27}$$

where Q_{gts}, characterized in (4.30), denotes the reactive power generation of power plant g in time interval t and scenario s.

4.5.3.1 Modeling the Constraints of the Grid

This section is intended to linearly model all grid constraints. To this end, two variables ΔP_{its} and ΔQ_{its} are firstly introduced:

- For each bus i in B, the net deviation of the nodal active power injection from its scheduled operating point in time interval t and scenario s can be calculated as:

$$\Delta P_{its} = \sum_{d \in \mathrm{D}_i^{\mathrm{Flex}}} f_{dts}^{\mathrm{P}} + \sum_{d \in \mathrm{D}_i^{\mathrm{Inflex}}} \Delta \mathrm{P}_{dts} + \sum_{g \in \mathrm{G}_i^{\mathrm{Flex}}} f_{gts}^{\mathrm{P}} + \sum_{g \in \mathrm{G}_i^{\mathrm{Inflex}}} \Delta \mathrm{P}_{gts}, \tag{4.28}$$

- For each bus i in B^{D}, the net deviation of the nodal reactive power injection from its scheduled operating point in time interval t and scenario s can be calculated as:

$$\Delta Q_{its} = \sum_{d \in \mathrm{D}_i^{\mathrm{Flex}}} f_{dts}^{\mathrm{Q}} + \sum_{d \in \mathrm{D}_i^{\mathrm{Inflex}}} \Delta \mathrm{Q}_{dts}, \tag{4.29}$$

Relying on a linearized AC power flow model, the following four sets of variables are expressed as linear functions of ΔP_{its} (calculated in (4.28)) and ΔQ_{its} (calculated in (4.29)):

1) Reactive Power Generation of Power Plants:

Considering the fact that each power plant controls its reactive power injection in such a way that the voltage magnitude of its interconnecting bus is preserved equal to the

voltage set-point defined by the TSO, i.e. $|\widehat{\mathrm{V}}_{gt}|$. Therefore, for each power plant g, its reactive power injection in time interval t and scenario s, i.e. Q_{gts}, depends on ΔP_{its} (calculated in (4.28)) and ΔQ_{its} (calculated in (4.29)) and can be expressed as a linear function with constant coefficients $\mathbb{Q}^{0}_{gt}$, $\mathbb{Q}^{\mathrm{P}}_{git}$ and $\mathbb{Q}^{\mathrm{Q}}_{git}$:

$$Q_{gts} = \mathbb{Q}^{0}_{gt} + \sum_{i \in \mathrm{B}} \mathbb{Q}^{\mathrm{P}}_{git}\, \Delta P_{its} + \sum_{i \in \mathrm{B}^{\mathrm{D}}} \mathbb{Q}^{\mathrm{Q}}_{git}\, \Delta Q_{its}, \tag{4.30}$$

2) Active Power Flexibility Provision of the Slack power plant:

The slack power plant g, connected to the reference bus r, provides active power flexibility so that the voltage phase angle of its interconnecting bus is fixed to zero. Therefore, its active power flexibility provision in time interval t and scenario s, i.e. f^{P}_{gts}, depends on ΔP_{its} (calculated in (4.28)) and ΔQ_{its} (calculated in (4.29)) and can be expressed as a linear function with constant coefficients $\mathbb{P}^{0}_{gt}$, $\mathbb{P}^{\mathrm{P}}_{git}$ and $\mathbb{P}^{\mathrm{Q}}_{git}$ (just for g connected to the reference bus r):

$$f^{\mathrm{P}}_{gts} = \mathbb{P}^{0}_{gt} + \sum_{i \in \mathrm{B}} \mathbb{P}^{\mathrm{P}}_{git}\, \Delta P_{its} + \sum_{i \in \mathrm{B}^{\mathrm{D}}} \mathbb{P}^{\mathrm{Q}}_{git}\, \Delta Q_{its}, \tag{4.31}$$

It should be noted that the active power flexibility provision of all flexible power plants, i.e. f^{P}_{gts}, excluding the slack power plant are independent optimization variables and their optimal values are determined by solving the optimization problem.

3) Nodal Voltage Magnitude:

For each bus i in B^{D}, the nodal voltage magnitude in time interval t and scenario s, i.e. $|V_{its}|$, can be expressed as a linear function with constant coefficients $\mathbb{V}^{0}_{it}$, $\mathbb{V}^{\mathrm{P}}_{ijt}$ and $\mathbb{V}^{\mathrm{Q}}_{ijt}$:

$$|V_{its}| = \mathbb{V}^{0}_{it} + \sum_{j \in \mathrm{B}} \mathbb{V}^{\mathrm{P}}_{ijt}\, \Delta P_{jts} + \sum_{j \in \mathrm{B}^{\mathrm{D}}} \mathbb{V}^{\mathrm{Q}}_{ijt}\, \Delta Q_{jts}, \tag{4.32}$$

Therefore, the nodal voltage magnitude constraints are linearly characterized as (for all $i \in \mathrm{B}^{\mathrm{D}}, t \in \mathrm{T}, s \in \mathrm{S}$):

$$\mathrm{V}^{\mathrm{Min}}_{i} \leq |V_{its}| \leq \mathrm{V}^{\mathrm{Max}}_{i}, \tag{4.33}$$

where $\mathrm{V}^{\mathrm{Min}}_{i}$ and $\mathrm{V}^{\mathrm{Max}}_{i}$ respectively denote the minimum and maximum allowable voltage magnitude of node i. It is noteworthy that the voltage magnitude of the other buses (i.e. $i \in \mathrm{B}^{\mathrm{G}}$) are fixed to their defined voltage set-point, i.e. $|\widehat{\mathrm{V}}_{gt}|$.

4) Apparent Power Flow in Branches

The apparent power flow entering the from-end (and respectively the to-end) of transmission line/transformer l in time interval t and scenario s can be expressed as linear

function of ΔP_{its} (calculated in (4.28)) and ΔQ_{its} (calculated in (4.29)) with constant coefficients $\mathbb{S}^{\mathrm{F,0}}_{lt}$, $\mathbb{S}^{\mathrm{F,P}}_{lit}$ and $\mathbb{S}^{\mathrm{F,Q}}_{lit}$ ($\mathbb{S}^{\mathrm{T,0}}_{lt}$, $\mathbb{S}^{\mathrm{T,P}}_{lit}$ and $\mathbb{S}^{\mathrm{T,Q}}_{lit}$):

$$S^{\mathrm{F}}_{lts} = \mathbb{S}^{\mathrm{F,0}}_{lt} + \sum_{i\in \mathrm{B}} \mathbb{S}^{\mathrm{F,P}}_{lit}\, \Delta P_{its} + \sum_{i\in \mathrm{B^D}} \mathbb{S}^{\mathrm{F,Q}}_{lit}\, \Delta Q_{its}, \tag{4.34}$$

$$S^{\mathrm{T}}_{lts} = \mathbb{S}^{\mathrm{T,0}}_{lt} + \sum_{i\in \mathrm{B}} \mathbb{S}^{\mathrm{T,P}}_{lit}\, \Delta P_{its} + \sum_{i\in \mathrm{B^D}} \mathbb{S}^{\mathrm{T,Q}}_{lit}\, \Delta Q_{its}, \tag{4.35}$$

Hence, maximum power flow limit of transmission lines/ transformer l can be linearly expressed (for all $l \in \mathrm{L}$, $t \in \mathrm{T}$, $s \in \mathrm{S}$):

$$0 \leq S^{\mathrm{F}}_{lts} \leq \mathrm{S}^{\mathrm{Max}}_{l}, \tag{4.36}$$

$$0 \leq S^{\mathrm{T}}_{lts} \leq \mathrm{S}^{\mathrm{Max}}_{l}, \tag{4.37}$$

where $\mathrm{S}^{\mathrm{Max}}_{l}$ denotes the maximum power flow limit of transmission lines/transformer l.

Objective function (4.4) along with constraints (4.1)-(4.3), (4.5)-(4.8), (4.10)-(4.21), (4.24)-(4.37) and the linear equivalent counterparts of (4.5) and (4.9), introduced in the section 4.5.4 and section 4.5.5, casts the problem as a two-stage mixed integer stochastic optimization problem. Optimization variables pertained to the flexibility coordination stage, i.e. *here&now* decision variables, are:

$$\begin{aligned}&\{F^{\mathrm{P+,TSO}}_{dt}, F^{\mathrm{P-,TSO}}_{dt}, F^{\mathrm{Q+,TSO}}_{dt}, F^{\mathrm{Q-,TSO}}_{dt}, F^{\mathrm{P+,TSO}}_{gt}, F^{\mathrm{P-,TSO}}_{gt}, u_{dtn},\\ &u'_{dtn}, u'^{\mathrm{P+}}_{dtn}, u'^{\mathrm{P-}}_{dtn}, u'^{\mathrm{Q+}}_{dtn}, u'^{\mathrm{Q-}}_{dtn}, u_{gtn}, u'_{gtn}, u'^{\mathrm{P+}}_{gtn}, u'^{\mathrm{P-}}_{gtn}\}\end{aligned} \tag{4.38}$$

and optimization variables pertained to the flexibility exchange stage, i.e. *wait&see* decision variables, are:

$$\{f^{\mathrm{P+}}_{dts}, f^{\mathrm{P-}}_{dts}, f^{\mathrm{Q+}}_{dts}, f^{\mathrm{Q-}}_{dts}, f^{\mathrm{P+}}_{gts}, f^{\mathrm{P-}}_{gts}, Q_{gts}, P^{\mathrm{NS}}_{dts}, |V_{its}|, S^{\mathrm{F}}_{lts}, S^{\mathrm{T}}_{lts}\} \tag{4.39}$$

4.5.4 Extracting a Linear Equivalent Counterpart for Non-linear Expression (4.5)

Product of binary variable u and continuous variable x results in a non-linear term, i.e. ux. This non-linear term has a linear equivalent counterpart consisting of an auxiliary continuous variable, i.e. y, and two linear constraints:

$$ux^{\mathrm{Min}} \leq y \leq ux^{\mathrm{Max}}, \tag{4.40}$$

$$-(1-u)x^{\mathrm{Max}} \leq y - x \leq -(1-u)x^{\mathrm{Min}}, \tag{4.41}$$

where parameters x^{Min} and x^{Max} denotes the lower and upper bounds of x. Constraints (4.40) and (4.41) together enforce y become equal x if and only if binary variable u is 1 and 0 otherwise. Therefore, non-linear term ux can be replaced by continuous

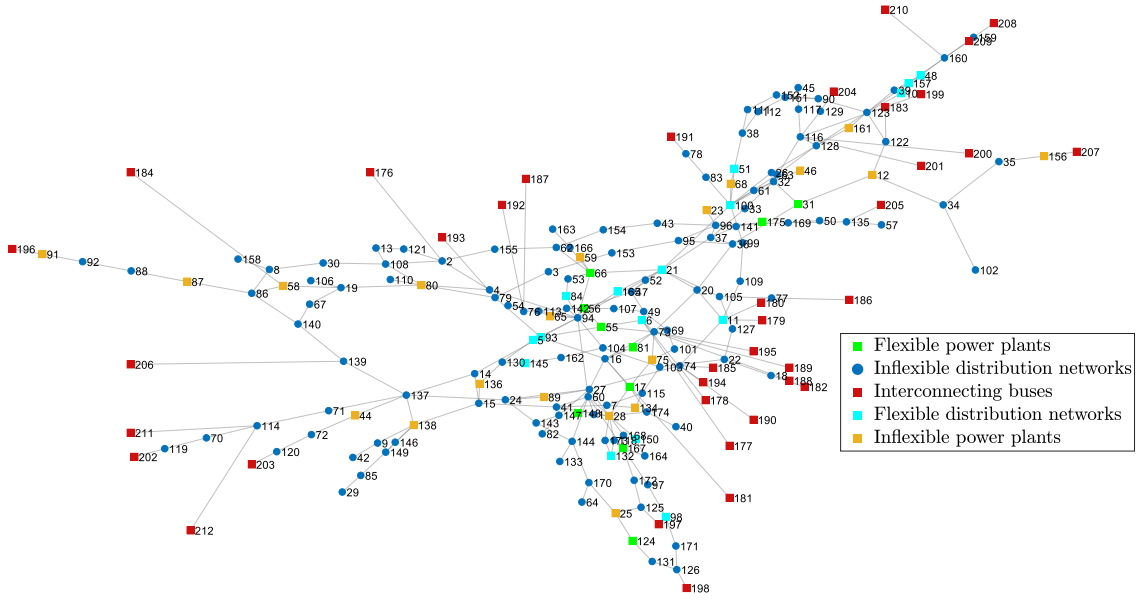

Figure 4.3: Single line diagram of the Swiss electric transmission network.

auxiliary variable y bound via (4.40) and (4.41).

4.5.5 Extracting a Linear Equivalent Counterpart for Non-linear Expression (4.9)

Product of N binary variables u_k, i.e. $\prod_{k=1}^{N} u_k$ suffers from non-linearity. However, this non-linear term has a liner equivalent counterpart formed of a continuous auxiliary variable z and $N+1$ linear constraints:

$$0 \leq z \leq u_k, \qquad \forall k = 1,2,..,N \tag{4.42}$$

$$\sum_{k=1}^{N} u_k - N + 1 \leq z, \tag{4.43}$$

Constraints (4.42) and (4.43) together enforce z take 1 if an only if all binary variables u_k are 1 and 0 otherwise. Therefore, non-linear term $\prod_{k=1}^{N} u_k$ can be replaced by continuous auxiliary variable z bound via (4.42) and (4.43).

4.6 Case Study

The electric transmission network of Switzerland, 6700 km in length, is selected as the case study. This grid is formed of 284 transmission lines and 25 transmission transformers interconnecting 212 buses at two voltage levels 380 kV and 220 kV. This grid is connected to the electric transmission networks of Italy, France, Austria and

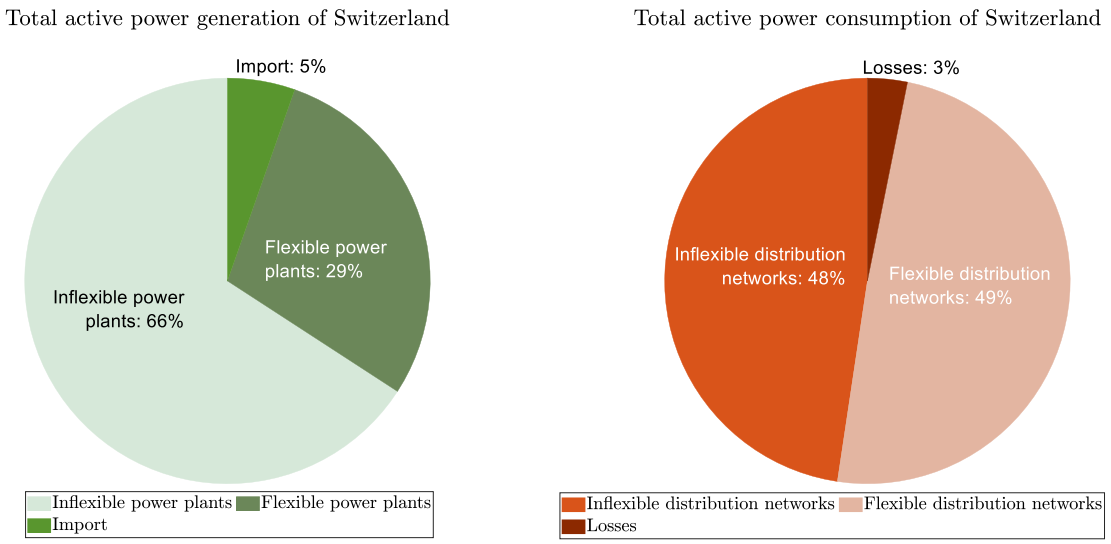

Figure 4.4: Share of different entities from active power consumption/generation of Switzerland.

Germany via 37 interconnecting buses. This case study is constructed on the basis of data provided by Swissgrid, given that nuclear generation has been totally replaced by renewable stochastic generation. Fig. 4.3 illustrates the single line diagram of this grid whose buses are colored in 5 different colors considering the entity they are hosting:

- Flexible (dispatchable) power plants;
- Inflexible (stochastic) power plants;
- Buses connecting the grid to the neighboring grids, i.e. interconnecting buses;
- Flexible distribution networks;
- Inflexible distribution networks;

Following the time-line of the problem depicted in Fig. 4.1, the duration of each time interval, i.e. τ, and the duration of the time horizon, i.e $\mathscr{H}$, are respectively considered 1 hour and 24 hours which model 24-hour of the next day. Moreover, t_{DSO} and t_{TSO} are respectively considered 2 hours and 1 hour prior to the beginning of the time horizon $\mathscr{H}$. Then, the performance of the proposed TSO-DSO coordination framework is investigated over a time interval where the total active power consumption of Switzerland including transmission grid's losses is 6959 MW. This demand is formed of 3 parts, namely demand of flexible distribution networks, inflexible distribution networks and transmission grid's losses as shown in Fig. 4.4. This demand is supplied thanks to the imported power from neighboring countries as well as generated power

of flexible/inflexible power plants as detailed in Fig. 4.4. As it can be seen, renewable generation contributes to 66% of the total generation of Switzerland. The power factor of both flexible and inflexible distribution networks range between 0.9 and 1. Inflexible distribution networks are assumed as constant power factor loads, while flexible distribution networks might change their power factor with the purpose of providing active/reactive power flexibility. Active power generation of inflexible power plants and active power demand of inflexible distribution networks are associated with uncertainties due to forecast errors, i.e. $\Delta \mathrm{P}_{gts}$ and i.e. $\Delta \mathrm{P}_{dts}$. These uncertainties are assumed to be independent and identically distributed [42]. Therefore, $\Delta \mathrm{P}_{gts}$ of inflexible power plants are sampled from Gaussian distributions with 0 mean and such that the root mean square error (RMSE) of the total stochastic (renewable) generation of Switzerland is 10% of the total predicted one. In the same way, $\Delta \mathrm{P}_{dts}$ of inflexible distribution networks are sampled from Gaussian distributions with 0 mean and such that the RMSE of the total demand of Switzerland is 5% of the total predicted one. Accordingly, the uncertainties associated with reactive power consumption of inflexible distribution networks, i.e. $\Delta \mathrm{Q}_{dts}$, are determined considering the constant power factor of inflexible distribution networks and $\Delta \mathrm{P}_{dts}$. Following the elaborated approach, 1000 scenarios are generated to model uncertainties.

4.6.1 Extracting Prices of Active/Reactive Power Flexibility from Siwssgrid's Flexibility Market Reports

Swissgrid regularly publishes the results of its flexibility market, i.e. the price of its deployed and booked active power flexibility [43–45, 89]. After processing this data, this chapter assumes the price of upward/downward deployed active power flexibility, i.e. $\pi'^{\mathrm{P}+}_t$ and $\pi'^{\mathrm{P}-}_t$, equal to the annual average price of the respective product over 2019:

$$\pi'^{\mathrm{P}+}_t = 102 \text{ Euro/MWh} \tag{4.44}$$

$$\pi'^{\mathrm{P}-}_t = 35 \text{ Euro/MWh}, \tag{4.45}$$

The price of upward/downward deployed reactive power flexibility, i.e. $\pi'^{\mathrm{Q}+}_t$ and $\pi'^{\mathrm{Q}-}_t$, are selected equal to the 3 Euro/MVArh as reported in [89].

To simplify the visualization of the results, this chapter supposes that all flexibility providers offer two FPC areas to the TSO. The first FPC area (the smaller FPC area) of each provider, i.e. $n = 1$, corresponds to 50% of its flexibility provision capability while the second FPC area (the larger FPC area), i.e. $n = 2$, corresponds to 100% of its flexibility provision capability. Moreover, it is assumed that all providers offer their first FPC areas with the same price (low price) and they offer their second FPC areas with the same price (high price). To determine the booking prices of FPC areas, i.e. $\pi^{\mathrm{P}+}_{dtn}$, $\pi^{\mathrm{P}-}_{dtn}$, $\pi^{\mathrm{Q}+}_{dtn}$, $\pi^{\mathrm{Q}-}_{dtn}$, $\pi^{\mathrm{P}+}_{gtn}$ and $\pi^{\mathrm{P}-}_{gtn}$, the prices of upward/downward booked active power flexibility of

Swissgrid over 2019 are processed and they are clustered into two groups representing the low and high prices. Accordingly, the booking prices of upward/downward active power flexibility for the first FPC area, i.e. $n = 1$, (and respectively the second FPC area, i.e. $n = 2$,) are considered equal to the annual average price of the respective product for low (and respectively high) price cluster over 2019. To put it simply, for all $d \in \mathrm{D}^{\mathrm{Flex}}$ and for all $g \in \mathrm{G}^{\mathrm{Flex}}$:

$$\pi^{\mathrm{P}+}_{dtn} = \pi^{\mathrm{P}+}_{gtn} = \begin{cases} 8.7 \ \text{Euro/MWh} & \text{if } n = 1 \\ 23.5 \ \text{Euro/MWh} & \text{if } n = 2 \end{cases} \tag{4.46}$$

$$\pi^{\mathrm{P}-}_{dtn} = \pi^{\mathrm{P}-}_{gtn} = \begin{cases} 8.6 \ \text{Euro/MWh} & \text{if } n = 1 \\ 22.9 \ \text{Euro/MWh} & \text{if } n = 2 \end{cases} \tag{4.47}$$

In the absence of data associated with booking prices of upward/downward reactive power flexibility, this chapter considers the booking prices of upward and downward reactive power flexibility respectively equal to 0.1 of the booking price of upward and downward active power flexibility:

$$\pi^{\mathrm{Q}+}_{dtn} = \begin{cases} 0.87 \ \text{Euro/MWh} & \text{if } n = 1 \\ 2.35 \ \text{Euro/MWh} & \text{if } n = 2 \end{cases} \tag{4.48}$$

$$\pi^{\mathrm{Q}-}_{dtn} = \begin{cases} 0.86 \ \text{Euro/MWh} & \text{if } n = 1 \\ 2.29 \ \text{Euro/MWh} & \text{if } n = 2 \end{cases} \tag{4.49}$$

4.7 Investigating the Performance of the Method

This section sets out to evaluate the performance of the designed TSO-DSO coordination framework (presented in section 4.4) along with the TSO's unified active reactive power flexibility allocation method (formulated section 4.5) by applying it to the case study constructed in section 4.6. In this respect, value of lost load (VOLL) is chosen equal to 40000 Euro/MWh and minimum/maximum nodal voltage limits are considered equal to 0.95 pu and 1.05 pu. Then, YALMIP-MATLAB interface [46] is leveraged to cast the problem and GUROBI optimization solver [47] is selected to solve the problem on a Windows based system with a 2.9 GHz Intel core-i7 CPU and 32 GB of RAM.

4.7.1 TSO-DSO Coordination for Optimal Allocation of Power Flexibility

Based on the designed TSO-DSO coordination framework, first, all flexibility providers offer their FPC areas to the TSO, i.e. $\mathscr{A}_{gtn}$ and $\mathscr{A}_{dtn}$. These offered FPC areas are

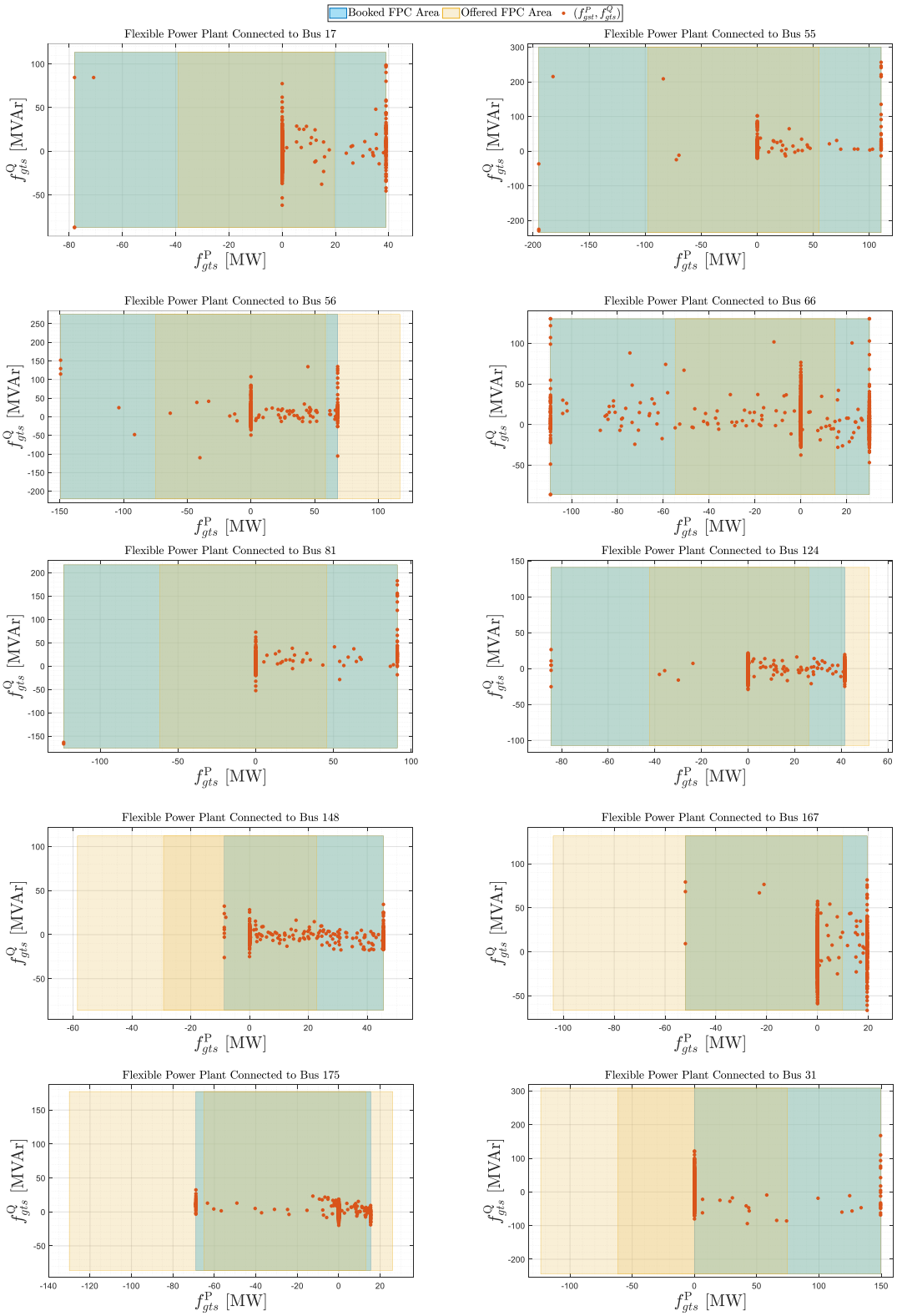

Figure 4.5: Offered FPC areas of flexible power plants (i.e. $\mathscr{A}_{gtn}$) as well as the TSO's booked FPC areas from flexible power plants (i.e. i.e. $\mathscr{A}^{\text{TSO}}_{gt}$).

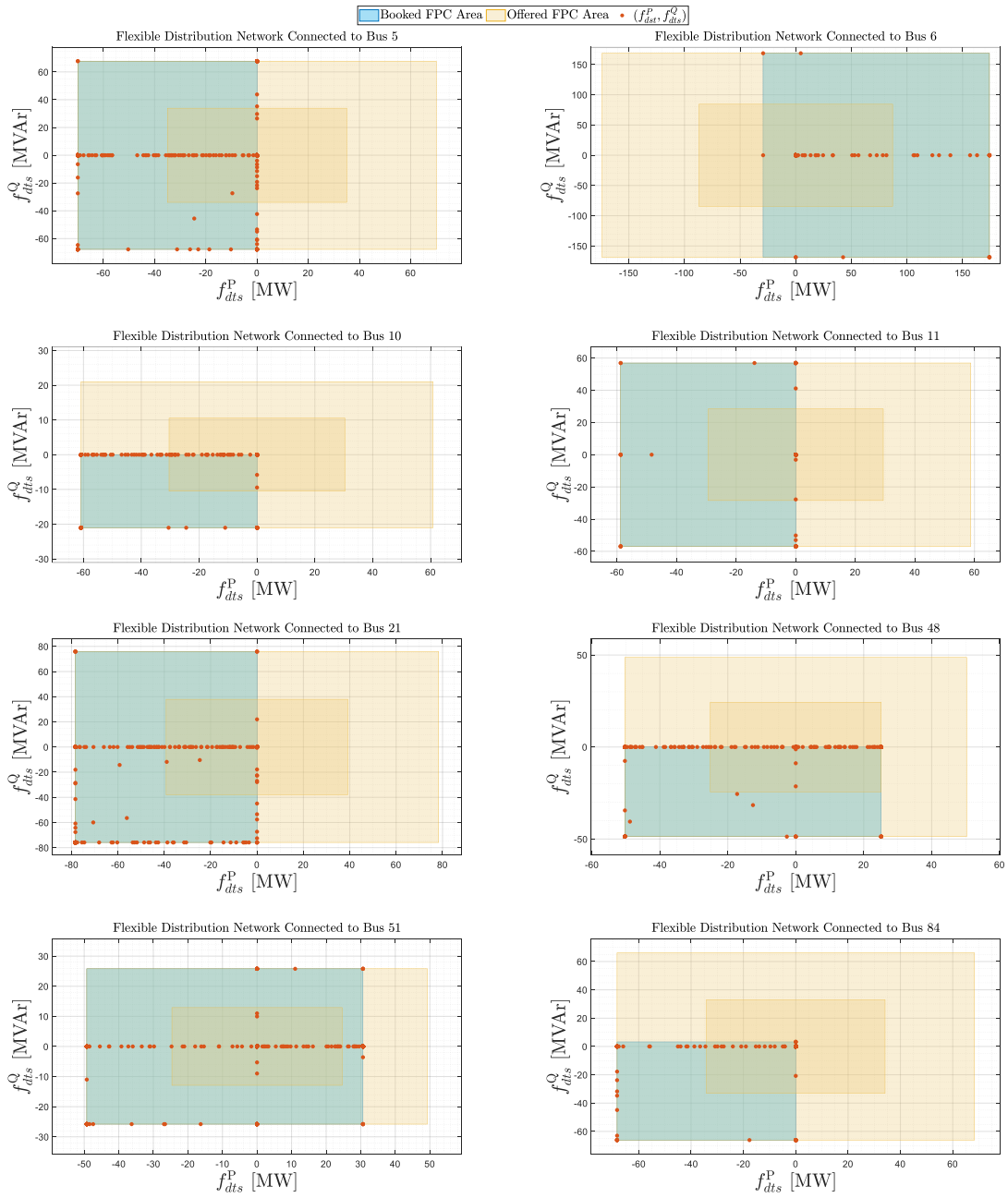

Figure 4.6: Part1: Offered FPC areas of flexible distribution networks (i.e. $\mathscr{A}_{dtn}$) as well as the TSO's booked FPC areas from flexible distribution networks (i.e. i.e. $\mathscr{A}_{dt}^{\text{TSO}}$).

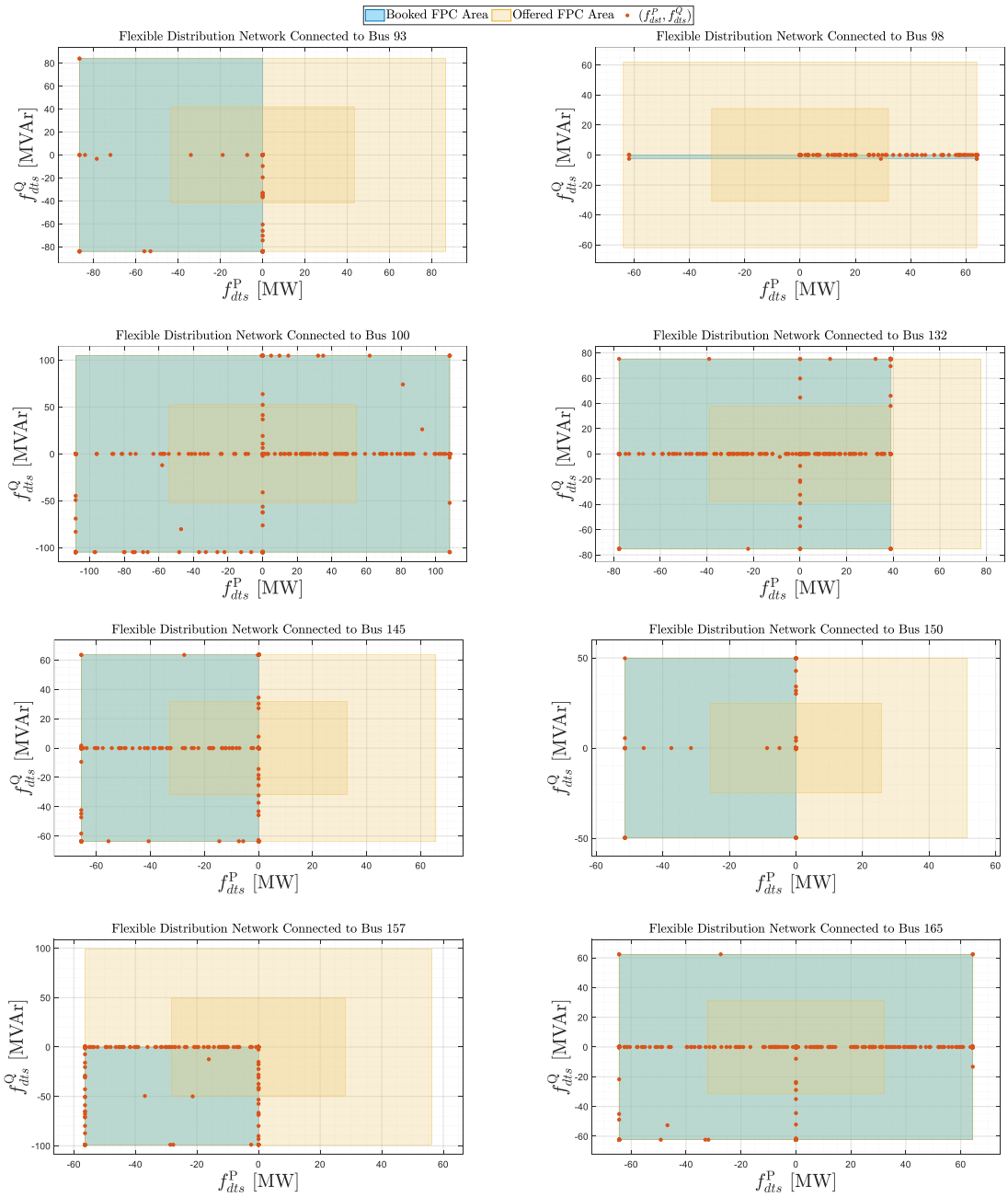

Figure 4.7: Part2: Offered FPC areas of flexible distribution networks (i.e. $\mathscr{A}_{dtn}$) as well as the TSO's booked FPC areas from flexible distribution networks (i.e. i.e. $\mathscr{A}_{dt}^{\text{TSO}}$).

illustrated in dark and light yellow colors in Fig. 4.5, Fig. 4.6 and Fig. 4.7. Then, TSO feeds these offered FPC areas into its two-stage mixed integer stochastic optimization problem (formulated in section4.5). Consequently, TSO books its required FPC area from each provider to be able to securely steer its grid considering uncertainties modeled via scenarios. The TSO's booked FPC area from each flexibility provider is illustrated in blue color in Fig. 4.5, Fig. 4.6 and Fig. 4.7. Moreover, each dark orange point in Fig. 4.5, Fig. 4.6 and Fig. 4.7 represents the amount of active/reactive power flexibility that TSO needs to deploy from the respective flexibility provider over each individual scenario to supply demand while respecting grid's constraints.

Above all, the expected energy not supplied of the Swissgrid is expected to be 2.6738 MWh, i.e 0.038% of the total demand of the network.

It is worth noting that in contrast to the free of charge reactive power flexibility of power plants, booking/deploying reactive power flexibility from flexible distribution networks involves additional cost for TSO. However, the achieved results (illustrated in Fig. 4.5, Fig. 4.6 and Fig. 4.7) reveal that TSO needs to book and deploy reactive power flexibility from flexible distribution networks in addition to the one coming from power plants. Moreover, the achieved results reveal that the TSO books active power flexibility from both flexible power plants and flexible distribution networks, although all flexible power plants and flexible distribution networks are offering the same prices for their active power flexibility. In sum, the achieved results highlight that flexible distribution networks play an important role in providing the required power flexibility of TSO, especially, in electric power system with high share of stochastic generation.

4.7.2 Impact of the Precision of Stochastic Generation Prediction on the TSO's Costs and Reliability

The amount of power flexibility that TSO books from different flexibility providers (and its associated cost) depends on the amount of uncertainties stemming from demand and stochastic generation. On the other hand, the magnitude of these uncertainties is largely affected by the precision of the prediction approach used to predict demand and stochastic generation. In this respect, this section aims to investigate the impact of precision of stochastic generation prediction on the TSO's cost and TSO's reliability. In this way, it quantifies the economic and technical benefits of precise stochastic generation prediction for TSO. To this end, it changes the RMSE of the total stochastic (renewable) generation of Switzerland from 7% to 20% of the total predicted one.

The impact of the precision of stochastic generation prediction on the total cost of TSO, i.e. $C_t^{\text{TSO}} = C_t^{\text{Planning}} + EC_t^{\text{Flexibility}} + EC_t^{\text{LNS}}$, and on the reliability of the transmission system, i.e. expected energy not supplied (EENS), are shown in Fig. 4.8. Fig. 4.8 reveals

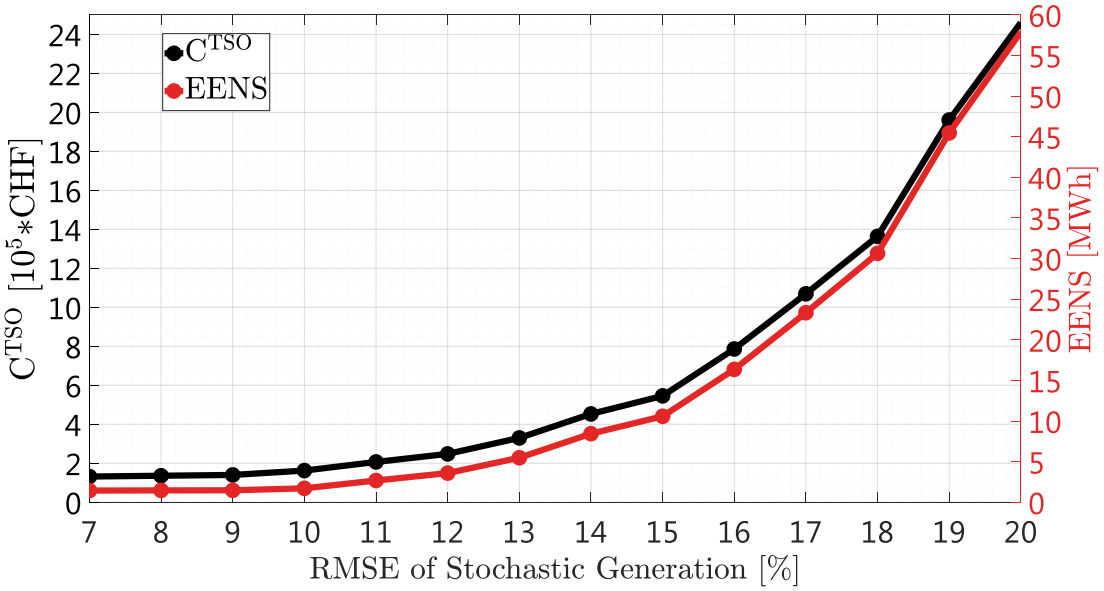

Figure 4.8: Impact of RMSE of stochastic generation prediction on the TSO's cost and EENS.

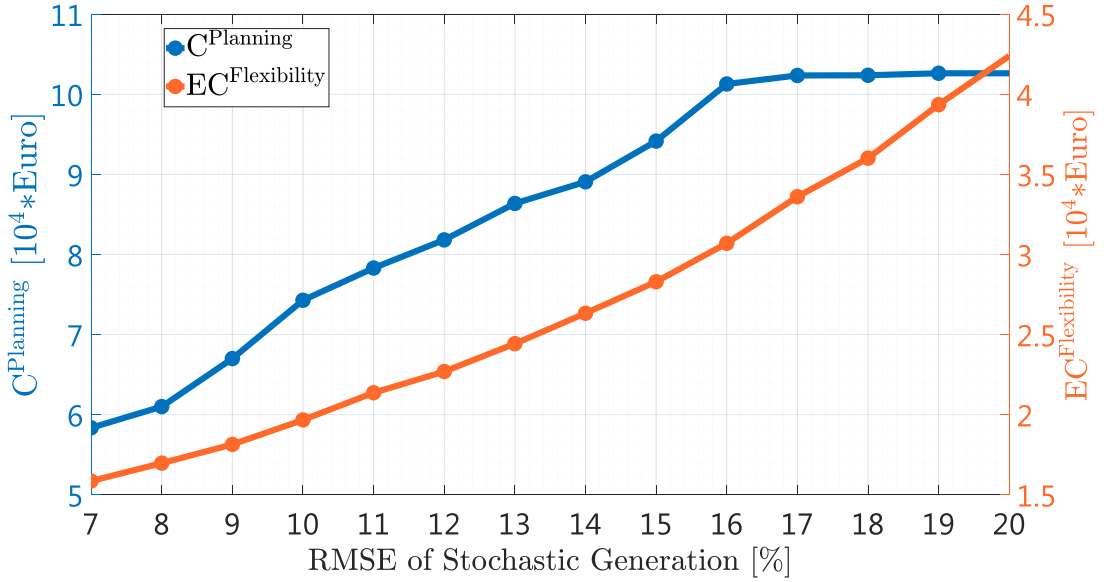

Figure 4.9: Impact of RMSE of stochastic generation prediction on C^{Planning} and $EC_t^{\text{Flexibility}}$.

that both C_t^{TSO} and EENS constantly increase when RMSE of stochastic generation prediction increases, i.e. precision of prediction decreases. However, C_t^{TSO} and EENS significantly increase when RMSE goes beyond 15%. To discover the reason behind this significant increase, Fig. 4.9 illustrates the cost of TSO due to booking flexibility, i.e. C_t^{Planning} along with expected cost of TSO due to deploying flexibility, i.e. $EC_t^{\text{Flexibility}}$.

As it can be seen, when RMSE increases up to 15%, C_t^{Planning} and $EC_t^{\text{Flexibility}}$ constantly rise because the TSO books and deploys greater deal of power flexibility to preserve the security of its grid against increasing uncertainties. To put it simply, TSO needs greater deal of power flexibility to 1-satisfy grid's constraints, 2-deal with increase and decrease of grid's active/reactive power losses, 3-restrict the load not supplied and accordingly 4-restrict the expected cost of TSO related to load not supplied, i.e. EC_t^{LNS}. However, when RMSE goes beyond 15%, the TSO faces with the shortage of power flexibility, i.e. the TSO's required power flexibility is greater than the offered power flexibility of flexibility providers. Therefore, TSO completely books all offered FPC areas, and as a result, C_t^{Planning} stays constant for RMSE beyond 15%. This shortage of power flexibility gives rise to surge in EENS and accordingly EC_t^{LNS} and C_t^{TSO} because TSO cannot deal with severe, i.e. large uncertainties. On the other hand, it should be noted that $EC_t^{\text{Flexibility}}$ still rises even for RMSE beyond 15% due to the fact that the TSO needs to deal with larger uncertainties on average.

Last but not least, it should be highlighted that Fig. 4.8 is very informative not only for Swissgrid but also for other TSOs due to the fact that the above-mentioned analysis has been carried out on the basis of the prices extracted from the Swissgrid's flexibility market (detailed in section 4.6.1). For example, TSO's can use this figure as an indicator to find out whether it is economic to invest on their prediction framework to improve the precision of their prediction or not.

4.7.3 Investigating the Computational Burden of the Method

This section is intended to elaborate on the computational burden of the method. To this end, it should be highlighted that YALMIP-MATLAB interface [46] and GUROBI optimization solver [47] are selected to implement the method on a Windows based system with a 2.9 GHz Intel Core-i7 CPU and 32 GB of RAM. The computation time of the method for a real-world electric transmission network, i.e. the electric transmission network of Switzerland, is 408 seconds while considering 1000 scenarios. This low computation burden of the method is achieved thanks to the linear tractable formulation presented for the method. The tractability and agility of the method make it as an applicable and practical solution for large real-world transmission networks. Moreover, the computation time of the method can even be improved if this method is implemented on industry-grade computers and benefited from parallelization techniques.

4.7.4 On the Feasibility of the Optimal Allocated Power Flexibility

The proposed method models grid's constraints using a linearized power flow model, thus, the achieved results might not fully respect grid constraints. In this respect, the achieved optimal solution of the problem for each individual scenario is used to

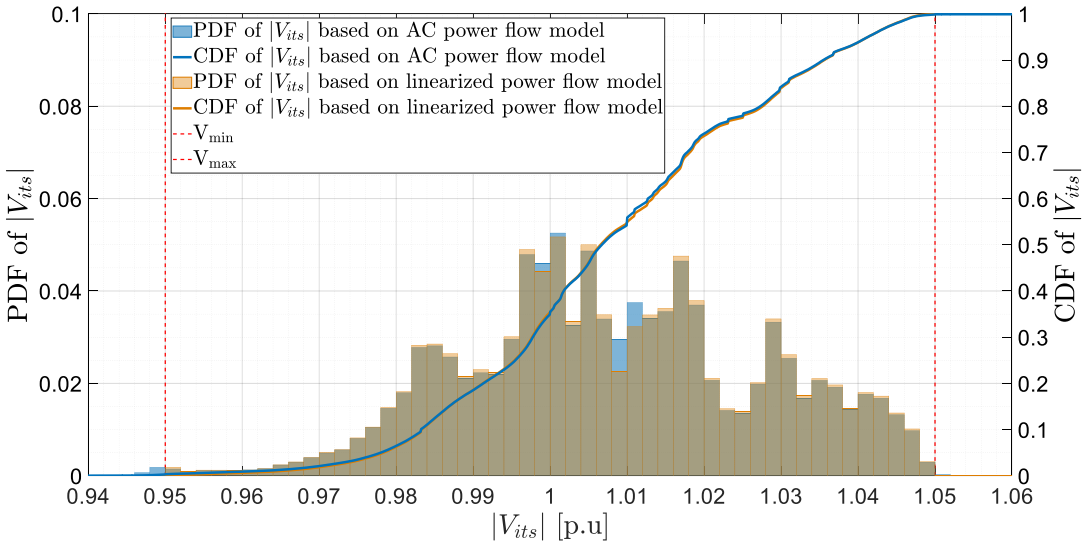

Figure 4.10: Probability/Cumulative density function of the voltage magnitudes of all buses over all scenarios extracted from the AC power flow model versus the one extracted from the proposed method.

calculate the following quantities on the basis of both linearized power flow model (detailed in 4.5.3.1) and AC power flow model:

- Nodal voltage magnitude, i.e. $|V_{its}|$;
- Apparent power flow entering from-end and to-end of branches, i.e. S^{F}_{lts} and S^{T}_{lts};

Then, considering all scenarios, the probability/cumulative density function (PDF/CDF) of the nodal voltage magnitude calculated on basis of linearized power flow model, i.e. (4.32) are compared with the PDF/CDF of the nodal voltage magnitude calculated on the basis of AC power flow model. As shown in Fig. 4.10, the CDF/PDF of $|V_{its}|$ derived from linearized power flow model highly matches the one derived from the AC power flow model, moreover, the voltage magnitude constraint is slightly violated for less than 0.42% of the cases. The similar analysis is drawn for S^{F}_{lts} and S^{T}_{lts} and active/reactive power. As depicted in Fig. 4.11, Fig. 4.12, the CDF/PDF of S^{F}_{lts} and S^{T}_{lts} derived from linearized power flow model highly matches the the respective quantity derived from the AC power flow model, moreover, the maximum power flow limit of branches is slightly violated for less than 1.06% of the cases.

4.8 Conclusion

This chapter firstly established a novel TSO-DSO coordination framework with the purpose of enabling TSO and DSO to exchange bi-directional active/reactive power

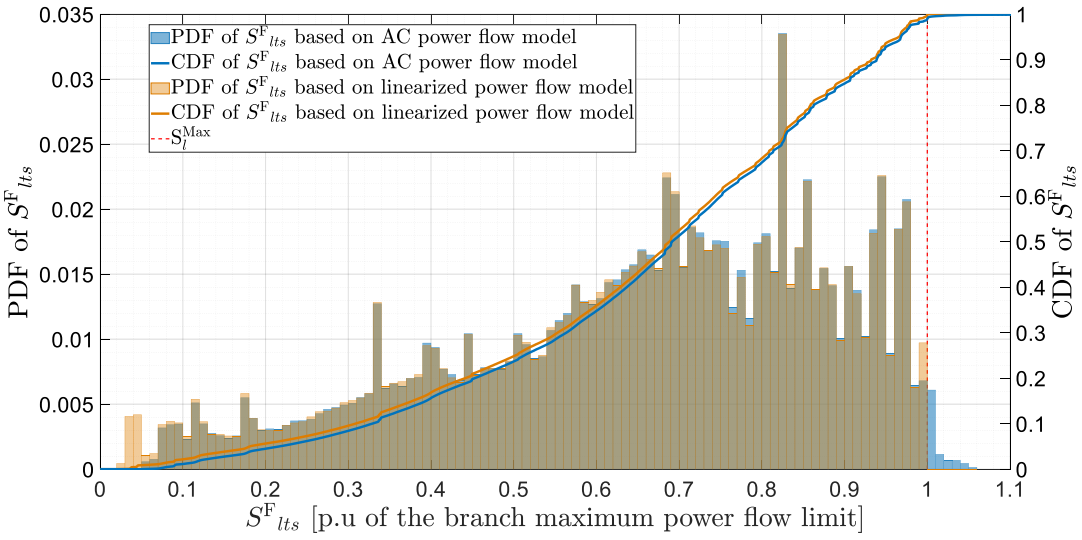

Figure 4.11: Probability/Cumulative density function of the apparent power flow entering the from-end of branches over all scenarios extracted from the AC power flow model versus the one extracted from the proposed method.

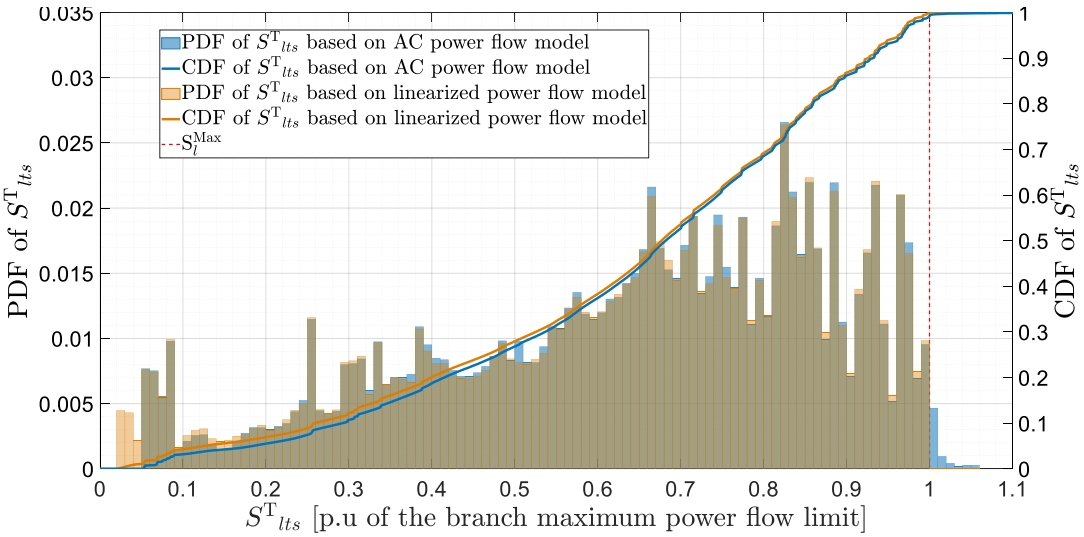

Figure 4.12: Probability/Cumulative density function of the apparent power flow entering the to-end of branches over all scenarios extracted from the AC power flow model versus the one extracted from the proposed method.

flexibility with each other. Therefore, both active and reactive power flexibility of DERs located in flexible distribution networks can be provided to the TSO. The privileged feature of this framework is that TSO and DSO can implement it without having to disclose their confidential grids data. Moreover, this framework follows a sequential market structure to suit the Switzerland's flexibility market that is separate from the

energy market. Then, this chapter mathematically models this framework as a two-stage mixed integer stochastic optimization problem. In addition to maximum power flow limit of branches, this model considers the nodal voltage magnitude limit as well as grid's losses.

Last but not least, this chapter opted a real-world electric transmission network, i.e. the Swiss transmission network, as a case study. The achieved results bear testimony to the paramount importance of the active and reactive power flexibility of flexible distribution networks in electric power systems with high share of stochastic generation. To securely steer the grid against increasing uncertainties, TSO needs both active and reactive power flexibility of flexible distribution networks.

Part II

Part II- Distribution System Operator (DSO) Side: Characterizing the DSO's Capability for Providing Power Flexibility

5 Linearized Power Flow Model for Meshed and Radial Active Distribution Networks

> The visible world is the invisible organization of energy.
>
> — Heinz Pagels

Power flow model is a fundamental building block to mathematically formulate a wide range of problems including optimal planning, operation and control of transmission/distribution systems. Accordingly, finding a tailored power flow model is an indispensable task in developing an efficient method to optimally manage active distribution networks (ADNs). In this context, this chapter firstly provide a comprehensive survey on the the existing power flow models. Then, it relies on the method developed in [90], [91] and presents a method to linearly formulate power flow constraints for both meshed and radial ADNs[1]. This method linearizes all non-linear power flow equations thereby offering a linear formulation for all constraints associated with the ADN's grid. More specifically, it expresses:

- Voltage magnitudes of all nodes of the ADN ;
- Current phasor as well as current magnitude of all branches of the ADN;
- The active/reactive power flexibility absorbed by the ADN at the point of common coupling point (PCC) with the upper-layer grid;

[1] It is worth highlighting that the linearized power flow model presented in chapter 3 is also applicable for balanced meshed and radial distribution networks. However, this thesis introduces two linear power flow models (i.e. chapters 3 and 5) to be able to deal with all kinds of distribution networks. Please refer to section 5.4 for detailed discussion about the power flow models presented in chapters 3 and 5.

as linear functions of the nodal active/reactive power injections.

It is worth noting that this linearized power flow model is used in chapter 6 and chapter 7. Indeed, these two chapters are mathematically formulated as optimization problems embracing the power flow constraints. This kind of optimization problems are widely known as optimal power flow (OPF) problem.

Keywords: Bus injection model, branch flow model, convexification, fixed-point linearization, heuristic approaches, interior point method, linearized power flow model, optimal power flow (OPF), power flow model.

Nomenclature

Indices and Sets

$0'$	Index for the point of common coupling (PCC) node between the ADN and the upper-layer grid.
i, j	Index for nodes excluding $0'$.
l	Index for branches.
n	Index for the linear boundaries modeling the maximum current flow limit of a branch.
s	Index for scenarios.
t	Index for time intervals.
$\mathbb{B}$	Set of nodes of ADN excluding $0'$.
$\mathbb{F}_l$	Set of the linear boundaries modeling the maximum current flow limit of branch l.
$\mathbb{L}$	Set of branches of ADN.
$\mathbb{S}$	Set of scenarios.

Variables

$f^{\mathrm{P}}_{0'ts}$, $f^{\mathrm{Q}}_{0'ts}$	Active/reactive power flexibility absorbed by the ADN from the upper-layer grid during time slot t and scenario s [p.u.].
I_{lts}	Current phasor of branch l during time slot t and scenario s [p.u.].
I^{Real}_{lts}, I^{Imag}_{lts}	Real/imaginary part of I_{lts} [p.u.].

$\|I_{lts}\|$	Magnitude of I_{lts} [p.u.].
I^{Inj}_{its}	Phasor of the current injected to node i [p.u.].
$P_{0'ts}$, $Q_{0'ts}$	Total active/reactive power absorbed by the ADN at its PCC during time slot t and scenario s [p.u.].
V_{jts}	Voltage phasor of node j during time slot t and scenario s [p.u.].
ΔP_{its}, ΔQ_{its}	Net deviation of the active/reactive power injection at node i from its scheduled value (i.e. its base case operating point) during time slot t and scenario s [p.u.].

Parameters

$\mathbf{F}^{0}_{nl}$, $\mathbf{F}^{\text{Real}}_{nl}$, $\mathbf{F}^{\text{Imag}}_{nl}$	Constant terms of the linear functions ($n \in \mathbb{C}_l$) modeling the maximum current flow limit of branch l based on I^{Real}_{lts} and I^{Imag}_{lts}.
$\mathrm{I}^{\text{Max}}_{l}$	Maximum current limit of branch l [p.u.].
$\mathrm{N}_{\mathbb{B}}$	Number of nodes of ADN excluding $0'$.
$\mathrm{N}_{\mathbb{L}}$	Number of branches of ADN.
N_{s}	Number of scenarios belonging to set $\mathbb{S}$.
$\widehat{\mathrm{P}}_{0't}$, $\widehat{\mathrm{Q}}_{0't}$	ADN's scheduled (i.e. base case operating point) active/reactive power absorption from the upper-layer grid at its PCC during time slot t [p.u.].
$\widehat{\mathrm{P}}_{it}$, $\widehat{\mathrm{Q}}_{it}$	Total scheduled (base case operating point) active/reactive power injection at node i during time slot t [p.u.].
$\widehat{\mathrm{V}}_{it}$	Voltage phasor of node i during time slot t for the base case operating point [p.u.].
$\mathrm{V}^{\text{Max}}_{j}$	Maximum voltage limit of node j [p.u.].
$\mathrm{V}^{\text{Min}}_{j}$	Minimum voltage limit of node j [p.u.].
y_l	Shunt admittance of branch l.
$\mathbf{Y}$	Admittance matrix of the ADN.
z_l	Series impedance of branch l.

5.1 State of the Art

AC power flow constraints form the backbone of all methods addressing the optimal operation and control of active distribution networks (ADNs). Specifically, AC power

flow constraints characterize Kirchhoff's current and voltage laws, nodal active/reactive power balance and branches' power flow limits. They are naturally nonlinear and non-convex. Accordingly, power system engineers have traditionally strived to develop efficient approaches to deal with these complex constraints. Since the inception of research on optimal power flow (OPF) problem, i.e. Carpentier's formulation in 1962 [92], there have been a great deal of research on OPF as surveyed in [93–98]. Totally, four mainstreams can be recognized in the existing literature:

5.1.1 Mathematical Algorithms for Solving the Non-Convex OPF

A variety of optimization algorithms including gradient method [99], Newton's method [100], interior point method [101–103] have been employed to find the optimal solution of the OPF problem. These algorithms are mainly founded on the basis of the Karush-Kuhn-Tucker (KKT) necessary conditions. Therefore, these algorithms can only guarantee a local optimal solution and may fail to find the global optimum solution due to the non-convexity of the OPF problem.

5.1.2 Heuristic Approaches for Solving the Non-Convex OPF

In [97], a survey on the application of the heuristic approaches for solving the OPF problem is presented. A wide range of heuristic approaches such as genetic algorithm [104], particle swarm [105], artificial neural network [106] and tabu search algorithm [107] have been exploited to deal with the OPF problem. These approaches suffer from two principal drawbacks. Firstly, they naturally perform exhaustive search, therefore, their computational complexity scale poorly with the size of grid. Secondly, they cannot guarantee the global optimum solution of the OPF problem.

5.1.3 Convexification of the OPF

Different relaxation techniques have been proposed to convexify the OPF problem. In general, they can be categorized into two types, namely bus injection models and branch flow models [108] and [109]. The former relies on the nodal variables including nodal voltages and nodal currents/power injections, whereas, the latter focuses on the branches' current and power flows.

5.1.3.1 Bus Injection Models

Considering nodal variables, [110] and [111] formulated the OPF problem as a quadratically constrained quadratic program and then approximated it by a semi-definite program. However, they did not determine when the semi-definite relaxation is exact.

Instead of solving the OPF problem directly, [112] suggested solving the dual OPF problem which is a convex semi-definite program. Furthermore, it presented a necessary and sufficient condition to guarantee zero duality gap, under which the global optimum solution of the OPF problem is recoverable from the optimum solution of the dual problem. In [113], a number of examples were presented to reveal the limitations of the semi-definite relaxation proposed in [112]. It showed when the line-flow limit is strict, the duality gap becomes non-zero, thus, the solution achieved by semi-definite relaxation is not exact and meaningful.

5.1.3.2 Branch Flow Models

Branch flow model was firstly introduced in [114], [115] for optimal sizing and placement of switched capacitors in radial distribution networks. This model is commonly known as "DistFlow model". Then, [116–118] focused on radial distribution networks and derived different variant of DistFlow model by applying different relaxations. All works in [114–118] rely on angle relaxation. Angle relaxation (ar-OPF) is a kind of relaxation where the angle of voltages and currents are eliminated form the OPF equations. This kind of relaxation is only applicable to the radial distribution networks as put forward in [119]. Finally, [119] and [120] constructed the comprehensive theory of branch flow model for both meshed and radial networks. In addition to angle relaxation, this theory exploited conic relaxation. Conic relaxation (cr-OPF) is a kind of relaxation where the quadratic equality constraints are converted to inequality constraints. Above all, [119] and [120] offered clear conditions, under which the relaxation is exact. Then, [121] focused on radial distribution networks and modified the OPF problem in such a way that the corresponding second-order cone program (SOCP) relaxation is exact under a milder condition in comparison with [119] and [120]. However, the model presented in [121] does not take into account the shunt capacitors of the equivalent two-port π line model thereby is not applicable in grids with coaxial underground cables. To deal with this shortcoming, the work in [122] and [123] developed a methodology relying on the augmented Lagrangian method that considers the shunt impedances. This method solves the original non-convex OPF problem in an iterative-manner. Although this method can be easily formulated in distributed manner, it suffers from high computation burden due to its iterative-manner. Finally, to overcome the shortcomings of [121–123], [124] embedded a new set of more conservative constraints in the OPF problem to ensure the optimality and feasibility of the relaxed OPF solution while considering the shunt impedances. This method benefits from lower computation burden in comparison with the former approaches. Furthermore, it presented sufficient condition under which the defined relaxed OPF is exact.

5.1.4 Linearized OPF

Linear power flow models can be constructed by either linearizing or providing a linear approximation of the non-linear power flow equations. Specifically, they linearly express some desired variables on the basis of their selected independent variables. These linear power flow models are widely used to reduce the computational burden associated with the nonlinear power flow models, thereby offering tractable, computationally efficient, and scalable models. In particular, they are appealing as the linear OPF problems can be efficiently solved by taking advantage of the maturity and agility of the existing linear programming solvers. In this way, large-scale practical problems can be easily solved.

In addition to a variety of linear power flow models surveyed in section 3.1, various linear power flow models have been constructed for distribution networks considering either rectangular or polar coordinates:

5.1.4.1 Linearization in Rectangular Coordinates

The work in [125] formulates all power flow equations on the basis of the imaginary and real parts of the nodal voltage phasors and nodal current injection phasors (i.e. rectangular coordinates). Then, it extracts the first-order Taylor series expansions of the power flow equations in rectangular coordinates. However, it fails to offer a linear formulation for all grid's constraints. To deal with this issue, it firstly models voltage magnitude limits of each bus and maximum current flow limit of each branch through defining an outer box constraint surrounding (i.e. relaxing) the original constraint in rectangle coordinates. Then, it proposes an iterative procedure to achieve a feasible solution. This iterative procedure consists of adding, in each iteration, multiple tangential cutting planes and penalty factors to the problem.

5.1.4.2 Linearization in Polar Coordinates

The work in [126] employs Gauss-Seidel method and Z-bus matrix to linearly express the nodal voltage magnitude and grid's power losses as linear functions of the nodal active/reactive power injections. The great advantage of this method is that it is independent of the Jacobian matrix. Therefore, as the operating point of the distribution network varies, the method is able to update the coefficients of the proposed linear functions without having to solve the full AC load-flow problem. [127] characterizes the feasible power flows as implicit algebraic relation between nodal voltage magnitude/phase angle and the nodal active/reactive power injections. Accordingly, it derives a linear power flow model by exploiting the first-order taylor expansion. In line with [126], [128] extends a linear power flow model for balanced distribution networks and provides sufficient conditions for the existence of a practical solution,

above all, it provides an upper bound on the maximum approximation error (i.e. error between the linear approximation and the AC power flow model). Finally works in [90] and [91] extend the model presented in [126] and construct a comprehensive linear power flow model tailored for multiphase radial/meshed distribution networks feeding either delta-connected or Wye-connected loads/sources at each multiphase bus. Most importantly, [91] relies on the fixed-point interpretation of the AC power flow model and provides explicit conditions for the existence and uniqueness of the load-flow solution, above all, it provides an upper bound on the maximum approximation error (i.e. error between the linear approximation and the AC power flow model).

5.2 Selecting the Best Power Flow Model for Modeling ADNs

This section is intended to find the best power flow model for managing the power flexibility of distributed energy resources (DERs) installed in ADNs. The opted model is exploited in chapter 6 and chapter 7 to model grid's constraints.

The **first** and **second mainstreams** of models, respectively presented in section 5.1.1 and 5.1.2, suffer from two drawbacks:

- Their non-linearity causes poor performance and high computational burden, consequently they are intractable.
- They cannot guarantee the global optimum solution of the OPF problem due to their non-convexity.

Although the **third mainstream** of models, presented in section 5.1.3, outperform the two above-mentioned mainstreams, they also cannot be used for managing the power flexibility. The following sets out the rational behind this fact:

1. The objective function of the optimization problems associated with the power flexibility management naturally consists of both upward/downward active power flexibility. Accordingly, the objective function is not increasing with respect to the grid's active power losses because the activation of either upward or downward power flexibility may decrease the grid's active power losses.
2. The third mainstream of models guarantee the global optimum solution of the OPF problem if and only if they satisfy the sufficient conditions for exactness of the relaxation (convexification). One of these condition is that the OPF problem have an increasing objective function with respect to the grid's power losses.
3. Finally, the first and second clauses together reveal that the **third mainstream** of models are not applicable for managing the power flexibility in ADNs.

The **fourth** mainstream of models, presented in 5.1.4, does not suffer from the disadvantages set out for the **first**, **second** and **third** mainstream of models. Among all models belonging to the fourth mainstream, the linearized power flow model presented in [90] and [91] is selected as the best model due to the following reasons:

- It is applicable to both meshed and radial ADNs.
- It is applicable to both balanced and unbalanced multiphase ADNs.
- It leverages fixed-point linearization approach which is computationally more efficient than first-order Taylor expansion of the power flow equations.
- Thanks to the fixed-point linearization, it provides a better global approximation (i.e precise over a wider range of nodal injection deviations).
- It provides an upper bound for the linearization error of the model.
- It is a mathematical rigorous model as set out in [91].
- It provides explicit linear functions to express the following variables as linear functions of the nodal active/reactive power injections:
  - Voltage magnitudes of all nodes of the ADN ;
  - Current phasor of all branches of the ADN;
  - The active/reactive power flexibility absorbed by the ADN at its PCC with the upper-layer grid.

To summarize, this thesis exploits the linearized power flow model of [90] and [91] to model ADN's constraints.

5.3 Mathematical formulation of the Linearized Power Flow Model

This section relies on the linearized power flow model of [90] and [91] to linearly formulate power flow constraints for both meshed and radial ADNs. This formulation is exploited in chapter 6 and chapter 7. For the sake of brevity, the method is presented considering a typical ADN consisting of a single slack node with fixed and known voltage that is its PCC node and $N_{\mathbb{B}}$ PQ nodes. The slack node is numbered $0'$ and the PQ nodes are numbered $1,2,\ldots,N_{\mathbb{B}}$. Then, power flow equations are expressed in a vector-matrix form. To this end, boldface letters are used for matrices and vectors; $(.)^{\mathrm{T}}$ for transposition; $\|.\|$ for the element-wise Euclidean norm of a vector/matrix; $\mathbb{R}$ for set of real numbers; $\mathbb{C}$ for set of complex numbers. For a complex number

$c \in \mathbb{C}$, $\Re\{c\}$, $\Im\{c\}$ and c^* indicate its real part, imaginary part and its conjugate, respectively. For a vector x, diag(x) returns a matrix with the elements of x in its diagonal. Let $\widehat{\mathbf{P}}_t = \left[\, \widehat{\mathrm{P}}_{1t}\,,\, \ldots,\, \widehat{\mathrm{P}}_{\mathrm{N}_{\mathbb{B}}t}\right]^{\mathrm{T}}$, $\boldsymbol{\Delta P}_{ts} = \left[\, \Delta P_{1ts}\,,\, \ldots,\, \Delta P_{\mathrm{N}_{\mathbb{B}}ts}\right]^{\mathrm{T}}$, $\widehat{\mathbf{Q}}_t = \left[\, \widehat{\mathrm{Q}}_{1t}\,,\, \ldots,\, \widehat{\mathrm{Q}}_{\mathrm{N}_{\mathbb{B}}t}\right]^{\mathrm{T}}$, $\boldsymbol{\Delta Q}_{ts} = \left[\, \Delta Q_{1ts}\,,\, \ldots,\, \Delta Q_{\mathrm{N}_{\mathbb{B}}ts}\right]^{\mathrm{T}}$, $\|\boldsymbol{V}_{ts}\| = \left[\, \|V_{1ts}\|\,,\, \ldots,\, \|V_{\mathrm{N}_{\mathbb{B}}ts}\|\right]^{\mathrm{T}}$, $\mathbf{V}^{\mathrm{Max}} = \left[\mathrm{V}_1^{\mathrm{Max}}\,,\, \ldots,\, \mathrm{V}_{\mathrm{N}_{\mathbb{B}}}^{\mathrm{Max}}\right]^{\mathrm{T}}$, $\mathbf{V}^{\mathrm{Min}} = \left[\mathrm{V}_1^{\mathrm{Min}}\,,\, \ldots,\, \mathrm{V}_{\mathrm{N}_{\mathbb{B}}}^{\mathrm{Min}}\right]^{\mathrm{T}}$ be vectors in $\mathbb{R}^{\mathrm{N}_{\mathbb{B}}\times 1}$ and $\boldsymbol{V}_{ts} = \left[\, V_{1ts}\,,\, \ldots,\, V_{\mathrm{N}_{\mathbb{B}}ts}\right]^{\mathrm{T}}$, $\widehat{\mathbf{V}}_t = \left[\, \widehat{\mathrm{V}}_{1t}\,,\, \ldots,\, \widehat{\mathrm{V}}_{\mathrm{N}_{\mathbb{B}}t}\right]^{\mathrm{T}}$, and $\boldsymbol{I}_{ts}^{\mathrm{Inj}} = [I_{1ts}^{\mathrm{Inj}}\,,\, \ldots, I_{\mathrm{N}_{\mathbb{B}}ts}^{\mathrm{Inj}}]^{\mathrm{T}}$ be vectors in $\mathbb{C}^{\mathrm{N}_{\mathbb{B}}\times 1}$ collecting the respective electrical quantities of PQ nodes. $\boldsymbol{I}_{ts} = \left[\, I_{1ts}\,,\, \ldots.,\, I_{\mathrm{N}_{\mathbb{L}}ts}\right]^{\mathrm{T}}$ be a vector in $\mathbb{C}^{N_{\mathbb{L}}\times 1}$ and $\mathbf{I}^{\mathrm{Max}} = \left[\, I_1^{\mathrm{Max}}\,,\, \ldots.,I_{\mathrm{N}_{\mathbb{L}}}^{\mathrm{Max}}\right]^{T}$ be vectors in $\mathbb{R}^{\mathrm{N}_{\mathbb{L}}\times 1}$ collecting the respective electrical quantities of branches. $\boldsymbol{S}_{ts}$ represents the net complex power injection vector of PQ nodes and can be expressed as follows:

$$\boldsymbol{S}_{ts} \;=\; \widehat{\mathbf{S}}_t \;+\; \boldsymbol{\Delta S}_{ts}, \tag{5.1}$$

where $\widehat{\mathbf{S}}_t$ and $\boldsymbol{\Delta S}_{ts}$ can be calculated as follows:

$$\widehat{\mathbf{S}}_t \;=\widehat{\mathbf{P}}_t \;+\; \sqrt{-1}\,\widehat{\mathbf{Q}}_t, \tag{5.2}$$

$$\boldsymbol{\Delta S}_{ts} \;=\boldsymbol{\Delta P}_{ts} \;+\; \sqrt{-1}\,\boldsymbol{\Delta Q}_{ts}. \tag{5.3}$$

Then, the power flow equations can be defined as the following set of equations. Assuming that $\mathrm{V}_{0'}$ and $\boldsymbol{S}_{ts}$ are known, they aim to find out the value of $\boldsymbol{V}_{ts}, P_{0'ts}$, and $Q_{0'ts}$:

$$\boldsymbol{S}_{ts} \;=\; \mathrm{diag}(\boldsymbol{V}_{ts})\;\boldsymbol{I}_{ts}^{\mathrm{Inj}^*}, \tag{5.4}$$

$$\boldsymbol{I}_{ts}^{\mathrm{Inj}} \;=\; \mathbf{Y}_{\mathrm{G}0'}\mathrm{V}_{0'} \;+\; \mathbf{Y}_{\mathrm{GG}}\;\boldsymbol{V}_{ts}, \tag{5.5}$$

$$P_{0'ts} \;+\; \sqrt{-1}\;Q_{0'ts} \;=\; \mathrm{V}_{0'}\;\left(\mathbf{Y}_{0'0'}\;\mathrm{V}_{0'} \;+\; \mathbf{Y}_{0'\mathrm{G}}\;\boldsymbol{V}_{ts}\right)^*, \tag{5.6}$$

where $\mathbf{Y}_{0'0'} \in \mathbb{C}$, $\mathbf{Y}_{0'\mathrm{G}} \in \mathbb{C}^{1\times \mathrm{N}_{\mathbb{B}}}$, $\mathbf{Y}_{\mathrm{G}0'} \in \mathbb{C}^{\mathrm{N}_{\mathbb{B}}\times 1}$ and $\mathbf{Y}_{\mathrm{GG}} \in \mathbb{C}^{\mathrm{N}_{\mathbb{B}}\times \mathrm{N}_{\mathbb{B}}}$ are the sub-matrices of the ADN's admittance matrix $\mathbf{Y}$:

$$\mathbf{Y} := \begin{bmatrix} \mathbf{Y}_{0'0'} & \mathbf{Y}_{0'\mathrm{G}} \\ \mathbf{Y}_{\mathrm{G}0'} & \mathbf{Y}_{\mathrm{GG}} \end{bmatrix} \in \mathbb{C}^{(\mathrm{N}_{\mathbb{B}}\;+\;1)\times(\mathrm{N}_{\mathbb{B}}\;+\;1)} \tag{5.7}$$

which can be built base on the topology of ADN considering the shunt capacitors/reactors as well as π-model of branches. By substituting $\boldsymbol{I}_{ts}^{\mathrm{Inj}}$ from (5.5) into (5.4) the following fixed-point equation for $\boldsymbol{V}_{ts}$ is achieved:

$$\boldsymbol{V}_{ts} \;=\; -\,\mathbf{Y}_{\mathrm{GG}}^{-1}\,\mathbf{Y}_{\mathrm{G}0'}\;V_{0'} \;+\; \mathbf{Y}_{\mathrm{GG}}^{-1}\,\mathrm{diag}\left(\boldsymbol{V}_{ts}^*\right)^{-1}\;\boldsymbol{S}_{ts}^* \tag{5.8}$$

where $\mathbf{Y}_{\mathrm{GG}}^{-1}\,\mathbf{Y}_{\mathrm{G}0'}\;V_{0'}$ is a vector in $\mathbb{C}^{\mathrm{N}_{\mathbb{B}}\times 1}$, entitled zero-load vector, indicating the voltage phasors of PQ nodes when the injection of all PQ nodes are zero. Reference [14] proved the existence and uniqueness of solution (5.8) for $\boldsymbol{V}_{ts}$. This equation can be linearized around the base case operating point, namely $\widehat{\mathbf{V}}_t$, which is the solution of power flow

equation for $\widehat{\mathbf{S}}_t$, as follows:

$$\boldsymbol{V}_{ts} \;=\; \mathbf{E}'^{0}_{t} \;+\; \mathbf{E}'_{t}\,\boldsymbol{X}_{ts} \tag{5.9}$$

where $\mathbf{X}_{ts}$ is a vector in $\mathbb{C}^{2\mathrm{N}_{\mathbb{B}}\times 1}$ defined as:

$$\boldsymbol{X}_{ts} \;=\; \begin{bmatrix} \boldsymbol{\Delta P}_{ts} \\ \boldsymbol{\Delta Q}_{ts} \end{bmatrix} \tag{5.10}$$

and $\mathbf{E}'_t{}^{0}$ is a constant vector in $\mathbb{C}^{\mathrm{N}_{\mathbb{B}}\times 1}$ and can be calculated as:

$$\mathbf{E}'^{0}_{t} \;=\; -\,\mathbf{Y}^{-1}_{\mathrm{GG}}\,\mathbf{Y}_{\mathrm{G0'}}\,\mathrm{V}_{0'} \;+\; \mathbf{Y}^{-1}_{\mathrm{GG}}\,\mathrm{diag}\left(\widehat{\mathbf{V}}^{*}_{t}\right)^{-1}\widehat{\mathbf{S}}^{*}_{t} \tag{5.11}$$

and $\mathbf{E}'_t$ is a constant matrix in $\mathbb{C}^{\mathrm{N}_{\mathbb{B}}\times 2\mathrm{N}_{\mathbb{B}}}$ consisting of two sub-matrices $\mathbf{E}'^{\mathrm{P}}_{t}$ and $\mathbf{E}'^{\mathrm{Q}}_{t}$ with dimension equal to $\mathbb{C}^{\mathrm{N}_{\mathbb{B}}\times\mathrm{N}_{\mathbb{B}}}$ calculated as:

$$\mathbf{E}'_t \;=\; \begin{bmatrix} \mathbf{E}'^{\mathrm{P}}_{t} & \mathbf{E}'^{\mathrm{Q}}_{t} \end{bmatrix} \tag{5.12}$$

$$\mathbf{E}'^{\mathrm{P}}_{t} \;=\; \mathbf{Y}^{-1}_{\mathrm{GG}}\,\mathrm{diag}\left(\widehat{\mathbf{V}}^{*}_{t}\right)^{-1} \tag{5.13}$$

$$\mathbf{E}'^{\mathrm{Q}}_{t} \;=\; \sqrt{-1}\,\mathbf{Y}^{-1}_{\mathrm{GG}}\,\mathrm{diag}\left(\widehat{\mathbf{V}}^{*}_{t}\right)^{-1} \tag{5.14}$$

Considering (5.9), the nodal voltage magnitude ($\|\boldsymbol{V}_{ts}\|$) can be calculated as:

$$\begin{aligned}
\|\boldsymbol{V}_{ts}\| \;&=\; \|\,\mathbf{E}'^{0}_{t} \;+\; \mathbf{E}'_{t}\,\boldsymbol{X}_{ts}\| \\
&=\; \|\mathrm{diag}(\mathbf{E}'^{0}_{t})\|\;\|\mathbf{1} \;+\; \mathrm{diag}(\mathbf{E}'^{0}_{t})^{-1}\,\mathbf{E}'_{t}\,\boldsymbol{X}_{ts}\| \\
&=\; \|\mathrm{diag}(\mathbf{E}'^{0}_{t})\|\;\|\mathbf{1} \;+\; \Re\{\mathrm{diag}(\mathbf{E}'^{0}_{t})^{-1}\,\mathbf{E}'_{t}\}\,\boldsymbol{X}_{ts} \;+\sqrt{-1}\,\Im\{\mathrm{diag}(\mathbf{E}'^{0}_{t})^{-1}\,\mathbf{E}'_{t}\}\,\boldsymbol{X}_{ts}\| \\
&\approx\; \|\mathrm{diag}(\mathbf{E}'^{0}_{t})\|\;(\mathbf{1} \;+\; \Re\{\mathrm{diag}(\mathbf{E}'^{0}_{t})^{-1}\,\mathbf{E}'_{t}\}\,\boldsymbol{X}_{ts})
\end{aligned} \tag{5.15}$$

where $\mathbf{1}$ indicates the $\mathrm{N}_{\mathbb{B}}\times 1$ vector of all ones and the approximation is valid under the assumption that:

$$\|\,\Im\{\mathrm{diag}(\mathbf{E}'^{0}_{t})^{-1}\,\mathbf{E}'_{t}\}\,\boldsymbol{X}_{ts}\|_{\infty} \ll \mathbf{1} \tag{5.16}$$

Considering (5.15), $\|\boldsymbol{V}_{ts}\|$ is linearly expressed as:

$$\|\boldsymbol{V}_{ts}\| \;=\; \mathbf{E}^{0}_{t} \;+\; \mathbf{E}_{t}\,\boldsymbol{X}_{ts} \tag{5.17}$$

where $\mathbf{E}^{0}_{t}$ is a constant vector in $\mathbb{R}^{\mathrm{N}_{\mathbb{B}}\times 1}$ and $\mathbf{E}_t$ is a constant matrix in $\mathbb{R}^{\mathrm{N}_{\mathbb{B}}\times\mathrm{N}_{\mathbb{B}}}$, calculated as:

$$\mathbf{E}^{0}_{t} \;=\; \|\mathrm{diag}(\mathbf{E}'^{0}_{t})\| \tag{5.18}$$

$$\mathbf{E}_{t} \;=\; \|\mathrm{diag}(\mathbf{E}'^{0}_{t})\|\Re\{\mathrm{diag}(\mathbf{E}'^{0}_{t})^{-1}\,\mathbf{E}'_{t}\} \tag{5.19}$$

Consequently, the nodal voltage magnitude limits of ADN can be linearly modeled as:

$$\mathbf{V}^{\text{Min}} \leq \mathbf{E}_t^0 + \mathbf{E}_t \boldsymbol{X}_{ts} \leq \mathbf{V}^{\text{Max}} \tag{5.20}$$

Total active and reactive power that ADN absorbs from the upper-layer grid at its PCC during time slot t and scenario s are:

$$P_{0'ts} = \widehat{\mathrm{P}}_{0't} + f^{\mathrm{P}}_{0'ts}, \tag{5.21}$$

$$Q_{0'ts} = \widehat{\mathrm{Q}}_{0't} + f^{\mathrm{Q}}_{0'ts}, \tag{5.22}$$

$P_{0'ts}$ and $Q_{0'ts}$ are formed of two terms:

- $\widehat{\mathrm{P}}_{0't}$ and $\widehat{\mathrm{Q}}_{0't}$: They indicate the ADN's scheduled (i.e. base-case operating point) active and reactive power absorption from the upper-layer grid at its PCC during time slot t.
- $f^{\mathrm{P}}_{0'ts}$ and $f^{\mathrm{Q}}_{0'ts}$: They indicate active and reactive power flexibility that ADN absorbs from the upper-layer grid during time slot t and scenario s.

The power flexibility of the ADN ($f^{\mathrm{P}}_{0'ts}$ and $f^{\mathrm{Q}}_{0'ts}$) can be expressed as a linear function of $\boldsymbol{X}_{ts}$ by combining equations (5.6), (5.9), (5.21) and (5.22) as:

$$f^{\mathrm{P}}_{0'ts} = \mathbf{P}_t^0 + \mathbf{P}_t^{\mathrm{PQ}} \boldsymbol{X}_{ts} \tag{5.23}$$

$$f^{\mathrm{Q}}_{0'ts} = \mathbf{Q}_t^0 + \mathbf{Q}_t^{\mathrm{PQ}} \boldsymbol{X}_{ts} \tag{5.24}$$

where $\mathbf{P}_t^0$ and $\mathbf{Q}_t^0$ are constants in $\mathbb{R}$, calculated as:

$$\mathbf{P}_t^0 = \Re\{\mathrm{V}_{0'}\, \mathbf{Y}^*_{0'0'}\, \mathrm{V}_{0'} + \mathrm{V}_{0'}\, \mathbf{Y}^*_{0'\mathrm{G}}\, \mathbf{E}'^{0\,*}_{\mathrm{t}}\} - \widehat{\mathrm{P}}_{0'\mathrm{t}} \tag{5.25}$$

$$\mathbf{Q}_t^0 = \Im\{\mathrm{V}_{0'}\, \mathbf{Y}^*_{0'0'}\, \mathrm{V}_{0'} + \mathrm{V}_{0'}\, \mathbf{Y}^*_{0'\mathrm{G}}\, \mathbf{E}'^{0\,*}_{\mathrm{t}}\} - \widehat{\mathrm{Q}}_{0'\mathrm{t}} \tag{5.26}$$

and $\mathbf{P}_t^{\mathrm{PQ}}$ and $\mathbf{Q}_t^{\mathrm{PQ}}$ are constant vectors in $\mathbb{R}^{1\times 2\mathrm{N}_{\mathbb{B}}}$, calculated as:

$$\mathbf{P}_t^{\mathrm{PQ}} = \Re\{\mathrm{V}_{0'}\, \mathbf{Y}^*_{0'\mathrm{G}}\, \mathbf{E}'^{\,*}_{\mathrm{t}}\} \tag{5.27}$$

$$\mathbf{Q}_t^{\mathrm{PQ}} = \Re\{\mathrm{V}_{0'}\, \mathbf{Y}^*_{0'\mathrm{G}}\, \mathbf{E}'^{\,*}_{\mathrm{t}}\} \tag{5.28}$$

These two vectors consist of two sub-vectors as:

$$\mathbf{P}_t^{\mathrm{PQ}} = \begin{bmatrix} \mathbf{P}_t^{\mathrm{P}} & \mathbf{P}_t^{\mathrm{Q}} \end{bmatrix} \tag{5.29}$$

$$\mathbf{Q}_t^{\mathrm{PQ}} = \begin{bmatrix} \mathbf{Q}_t^{\mathrm{P}} & \mathbf{Q}_t^{\mathrm{Q}} \end{bmatrix} \tag{5.30}$$

where $\mathbf{P}_t^{\mathrm{P}}$, $\mathbf{P}_t^{\mathrm{Q}}$, $\mathbf{Q}_t^{\mathrm{P}}$, and $\mathbf{Q}_t^{\mathrm{Q}}$ are constants vectors in $\mathbb{R}^{1\times \mathrm{N}_{\mathbb{B}}}$.

5.3.0.1 Maximum Current Flow Constraint of Branches

In order to calculate the branches' current phasors, let $\mathbf{Z}^{\mathrm{Se}} = \left[z_1, \ldots, z_{N_{\mathbb{L}}}\right]^{\mathrm{T}}$ and $\mathbf{Y}^{\mathrm{Sh}} = \left[y_1, \ldots, y_{N_{\mathbb{L}}}\right]^{\mathrm{T}}$ be vectors in $\mathbb{C}^{\mathrm{N_{\mathbb{L}}} \times 1}$, in which z_l and y_l represent the series impedance and shunt admittance of branch l, respectively. Then, $\boldsymbol{I}_{ts}$ can be expressed as:

$$\boldsymbol{I}_{ts} \;=\; (\mathrm{diag}\,(\mathbf{Y}^{\mathrm{Sh}}/2)\,\mathbf{A}^{\mathrm{From}} + \mathrm{diag}\,(\mathbf{Z}^{\mathrm{Se}})^{-1}\,\mathbf{A})\,\boldsymbol{V}_{ts} \tag{5.31}$$

where $\mathbf{A}$ is the branch to node incidence matrix and can be written as:

$$\mathbf{A} \;=\; \mathbf{A}^{\mathrm{From}} + \mathbf{A}^{\mathrm{To}} \tag{5.32}$$

in which $\mathbf{A}^{\mathrm{From}}$ is a matrix consisting of 0, 1 and $\mathbf{A}^{\mathrm{To}}$ is a matrix consisting of 0, -1. In other words, $\mathbf{A}^{\mathrm{From}}/\mathbf{A}^{\mathrm{To}}$ are the branch to from-node/to-node incidence matrices.

$\boldsymbol{I}_{ts}$ can be expressed as a linear function of $\boldsymbol{X}_{ts}$ by substituting (5.9) into (5.31), as:

$$\boldsymbol{I}_{ts} \;=\; \mathbf{H}_t^0 \;+\; \mathbf{H}_t\,\boldsymbol{X}_{ts} \tag{5.33}$$

where $\mathbf{H}_t^0$ is a constant vector in $\mathbb{C}^{\mathrm{N_{\mathbb{L}}} \times 1}$ and can be calculated as:

$$\mathbf{H}_t^0 \;=\; (\mathrm{diag}\,(\mathbf{Y}^{\mathrm{Sh}}/2)\,\mathbf{A}^{\mathrm{From}} + \mathrm{diag}\,(\mathbf{Z}^{\mathrm{Se}})^{-1}\,\mathbf{A})\mathbf{E}'^{0}_{t} \tag{5.34}$$

and $\mathbf{H}_t$ is a constant matrix in $\mathbb{C}^{\mathrm{N_{\mathbb{L}}} \times 2\mathrm{N_{\mathbb{B}}}}$ consisting of two sub-matrices $\mathbf{H}_t^{\mathrm{P}}$ and $\mathbf{H}_t^{\mathrm{Q}}$ with dimension equal to $\mathbb{C}^{\mathrm{N_{\mathbb{L}}} \times \mathrm{N_{\mathbb{B}}}}$ calculated as:

$$\mathbf{H}_t \;=\; \begin{bmatrix} \mathbf{H}_t^{\mathrm{P}} & \mathbf{H}_t^{\mathrm{Q}} \end{bmatrix} \tag{5.35}$$

$$\mathbf{H}_t^{\mathrm{P}} \;= (\mathrm{diag}\,(\mathbf{Y}^{\mathrm{Sh}}/2)\,\mathbf{A}^{\mathrm{From}} + \mathrm{diag}\,(\mathbf{Z}^{\mathrm{Se}})^{-1}\,\mathbf{A})\,\mathbf{E}'^{\mathrm{P}}_{t} \tag{5.36}$$

$$\mathbf{H}_t^{\mathrm{Q}} \;= (\mathrm{diag}\,(\mathbf{Y}^{\mathrm{Sh}}/2)\,\mathbf{A}^{\mathrm{From}} + \mathrm{diag}\,(\mathbf{Z}^{\mathrm{Se}})^{-1}\,\mathbf{A})\,\mathbf{E}'^{\mathrm{Q}}_{t} \tag{5.37}$$

The maximum allowable current flow of branch l can be expressed as the following nonlinear constraint:

$$\|I_{lts}\|^2 = I_{lts}^{\mathrm{Real}\,2} + I_{lts}^{\mathrm{Imag}\,2} \leq \mathrm{I}_l^{\mathrm{Max}\,2} \qquad \forall\, l \in \mathbb{L},\ \forall\, s \in \mathbb{S}. \tag{5.38}$$

where I_{lts} is the current phasor of branch l during time slot t and scenario s; I_{lts}^{Real} and I_{lts}^{Imag} are real and imaginary parts of I_{lts}; $\|I_{lts}\|$ is the magnitude of I_{lts}; $\mathrm{I}_l^{\mathrm{Max}}$ is the maximum current limit of branch l. I_{lts} and consequently I_{lts}^{Real} and I_{lts}^{Imag} can be calculated as (5.33).

The nonlinear constraint (5.38) can be linearized based on a pre-defined number of linear boundaries approximating the real curve, as represented in Fig. 5.1:

$$\mathbf{F}_{nl}^{\mathrm{Real}}\,I_{lts}^{\mathrm{Real}} \;+\; \mathbf{F}_{nl}^{\mathrm{Imag}}\,I_{lts}^{\mathrm{Imag}} \;\leq\; \mathbf{F}_{nl}^{0} \qquad \forall\, l \in \mathbb{L}, \forall\, n \in \mathbb{F}_l,\ \forall\, s \in \mathbb{S}, \tag{5.39}$$

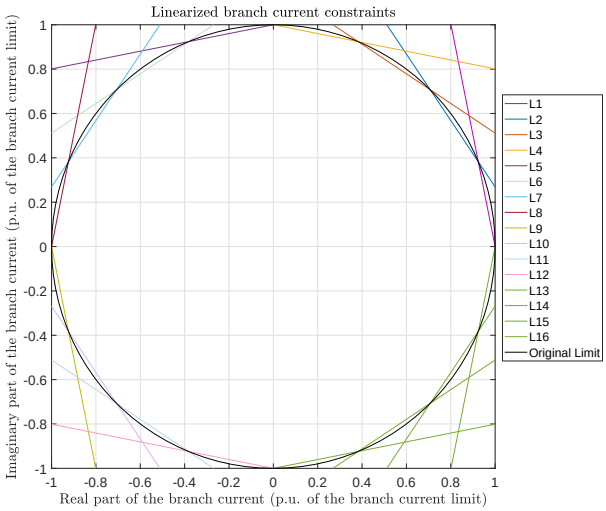

Figure 5.1: Linearized branch current constraint.

5.4 Remark on the Linearized Power Flow Models Constructed in Chapter 3 & Chapter 5

Chapter 3 established a linearized power flow model by deriving the first-order Taylor (FOT) series expansion of the non-linear power flow equations. In addition to transmission networks, this linearized power flow model is applicable for balanced radial and meshed distribution network consisting of even multiple slack and PV nodes in addition to PQ nodes. However, this model is not applicable for imbalance distribution networks. Further research is needed to extend this model and offer a holistic model that is applicable for even imbalanced distribution networks.

The current chapter (chapter 5)) offered a linearized power flow model by leveraging fixed-point linearization (FPL) approach. This linearized power flow model is applicable for balanced/unbalanced radial and meshed distribution networks consisting of only a single slack node and multiple PQ nodes. However, this model is not applicable for distribution networks consisting of single or multiple PV nodes.

Although both FOT and FPL approaches provide precise linear approximations, it should be noted that FOT approach mathematically offers the best local linear approximation, i.e. tangent plane at the linearization point. Thus, it is expected that the linear load flow model presented in chapter 3 provides the best approximation accuracy around the base case operating point. On the other hand, FPL provides a better approximation over a wide range of operating points from base case operating point to no load operating point. Thus, generally speaking, the linear power flow model presented in chapter 5 provides a better approximation accuracy over the above-mentioned range of operating points.

Finally, it can be concluded that this thesis introduced two linear power flow models to be able to deal with all kinds of distribution networks (balanced/unbalanced radial/meshed distribution networks with either single or multiple PV nodes). Considering the characteristics of the distribution network of interest, one of two presented linear power flow models is opted to model grid's constraints in chapter 6 and chapter 7.

5.5 Conclusion

This chapter provided a comprehensive survey on the the existing power flow models and accordingly selected the best tailored power flow model for managing the power flexibility of DERs installed in ADNs. In this way, this chapter tried to consolidate the foundations of the frameworks introduced in chapter 6 and chapter 7.

6 Characterizing the Flexibility Provision Capability Area of Active Distribution Networks: A Linear Robust Optimization Method

The laws of nature are written by the hand of God in the language of mathematics.

— Galileo Galilei

Distributed energy resources (DERs) installed in active distribution networks (ADNs) can be exploited to provide both active and reactive power flexibility to the upper-layer grid (i.e., sub-transmission and transmission systems) at their point of common coupling (PCC). This chapter introduces a method to determine the capability area of an ADN for the provision of both active and reactive power flexibility while considering the forecast errors of loads and stochastic generation, as well as the operational constraints of the grid and DERs. The method leverages a linearized load flow model and introduces a set of linear scenario-based robust optimization problems to estimate the flexibility provision capability (FPC) area of the ADN. It is proved that, under certain assumptions, the FPC area is convex. The performance of the proposed method is tested on a modified version of the IEEE 33-bus distribution test system.

Keywords: Active distribution network (ADN), distributed energy resources (DERs), flexibility provision capability (FPC) curve, flexibility provision capability (FPC) area, power flexibility, scenario-based robust optimization, TSO/DSO interface.

Nomenclature

Abbreviations

ADN	Active Distribution Network
DDG	Dispatchable Distributed Generator
DER	Distributed Energy Resource
DSO	Distribution System Operator
FPC	Flexibility Provision Capability
OPF	Optimal Power Flow
PCC	Point of Common Coupling
SDG	Stochastic Distributed Generator
TSO	Transmission System Operator

Indices and Sets

$0'$	Index for the common coupling node between the ADN and the upper-layer grid.
h	Index for stochastic distributed generators (SDGs).
i, j	Index for nodes excluding $0'$.
k	Index for dispatchable distributed generators (DDGs).
l	Index for branches.
m	Index for the linear boundaries modeling the capability curve of a DDG/SDG.
n	Index for the linear boundaries modeling the maximum current flow limit of a branch.
s	Index for scenarios.
t	Index for time intervals.
$\mathbb{B}$	Set of nodes of ADN excluding $0'$.
$\mathbb{C}_l$	Set of the linear boundaries modeling the maximum current flow limit of branch l.
$\mathbb{C}_k, \mathbb{C}_h$	Set of linear boundaries modeling the capability curve of DDG k, SDG h.
$\mathbb{DDG}$	Set of DDGs of ADN.
$\mathbb{DDG}_i$	Set of DDGs connected to node i.

$\mathbb{L}$	Set of branches of ADN.
$\mathbb{SDG}_i$	Set of SDGs connected to node i.
$\mathbb{S}$	Set of selected credible scenarios.
ψ	Set of optimization variables.
$\Omega(\psi), \Gamma(\psi)$	Set of inequality/equality constraints modeling the operational constraints of ADN and DERs.

Variables

$f_{kts}^{\mathrm{DDG,P}}$, $f_{kts}^{\mathrm{DDG,Q}}$	Active/reactive power flexibility injected by DDG k to the grid during time slot t and scenario s [p.u.].
$f_{0'ts}^{\mathrm{P}}$, $f_{0'ts}^{\mathrm{Q}}$	Active/reactive power flexibility absorbed by the ADN from the upper-layer grid during time slot t and scenario s [p.u.].
$F_{0't}^{\mathrm{P}}$, $F_{0't}^{\mathrm{Q}}$	Capacity of the active/reactive power flexibility absorbed by the ADN from the upper-layer grid during time slot t [p.u.].
$f_{hts}^{\mathrm{SDG,Q}}$	Reactive power flexibility injected by SDG h to the grid during time slot t and scenario s [p.u.].
I_{lts}	Current phasor of branch l during time slot t and scenario s [p.u.].
I_{lts}^{Real}, I_{lts}^{Imag}	Real/imaginary part of I_{lts} [p.u.].
$\|I_{lts}\|$	Magnitude of I_{lts} [p.u.].
$P_{0'ts}^{\mathrm{Net}}$, $Q_{0'ts}^{\mathrm{Net}}$	Total active/reactive power absorbed by the ADN at its connection point during time slot t and scenario s [p.u.].
V_{jts}	Voltage magnitude of node j during time slot t and scenario s [p.u.].
$\Delta P_{its}^{\mathrm{Net}}$, $\Delta Q_{its}^{\mathrm{Net}}$	Net deviation of the active/reactive power injection at node i from its base case operating point (i.e. scheduled operating point) during time slot t and scenario s [p.u.].

Parameters

a^{P}, a^{Q}	Constant terms defining the search direction in $F_{0't}^{\mathrm{P}} - F_{0't}^{\mathrm{Q}}$ coordinate plane.
$\mathbf{A}_{nl}^{0}$, $\mathbf{A}_{nl}^{\mathrm{Real}}$, $\mathbf{A}_{nl}^{\mathrm{Imag}}$	Constant terms of the linear functions ($n \in \mathbb{C}_l$) modeling the maximum current flow limit of branch l based on I_{lts}^{Real} and I_{lts}^{Imag}.
$\mathbf{D}_{mkt}^{0}$, $\mathbf{D}_{mk}^{P}$, $\mathbf{D}_{mk}^{\mathrm{Q}}$	Constant terms of the linear functions ($m \in \mathbb{C}_k$) modeling the capability curve of DDG k based on $f_{kts}^{\mathrm{P,DDG}}$ and $f_{kts}^{\mathrm{Q,DDG}}$.

$\mathbf{I}^{0,\text{Real}}_{lt}$, $\mathbf{I}^{\text{P,Real}}_{lit}$, $\mathbf{I}^{\text{Q,Real}}_{lit}$	Constant terms of the linear function expressing I^{Real}_{lts} based on $\Delta P^{\text{Net}}_{its}$ and $\Delta Q^{\text{Net}}_{its}$.
$\mathbf{I}^{0,\text{Imag}}_{lt}$, $\mathbf{I}^{\text{P,Imag}}_{lit}$, $\mathbf{I}^{\text{Q,Imag}}_{lit}$	Constant terms of the linear function expressing I^{Imag}_{lts} based on $\Delta P^{\text{Net}}_{its}$ and $\Delta Q^{\text{Net}}_{its}$.
$\text{I}^{\text{Max}}_{l}$	Maximum current limit of branch l [p.u.].
$\text{N}_{\mathbb{B}}$	Number of nodes of ADN excluding $0'$.
N^{DDG}, N^{SDG}	Number of DDGs/SDGs installed in ADN.
N_{s}	Number of scenarios belonging to set $\mathbb{S}$.
$\mathbf{R}^{0}_{mhts}$, $\mathbf{R}^{\text{P}}_{mhts}$, $\mathbf{R}^{\text{Q}}_{mhts}$	Constant terms of the linear functions ($m \in \mathbb{C}_h$) modeling the capability curve of SDG h based on $\Delta P^{\text{SDG}}_{hts}$ and $f^{\text{Q,SDG}}_{hts}$.
$\text{P}^{\text{Base}}_{0't}$, $\text{Q}^{\text{Base}}_{0't}$	ADN's scheduled (i.e. base case operating point) active/reactive power absorption from the upper-layer grid at their connection point during time slot t [p.u.].
$\text{P}^{\text{Base}}_{it}$, $\text{Q}^{\text{Base}}_{it}$	Total scheduled (base case operating point) active/reactive power injection at node i during time slot t [p.u.].
$\mathbf{P}^{0}_{t}$, $\mathbf{P}^{\text{P}}_{it}$, $\mathbf{P}^{\text{Q}}_{it}$	Constant terms of the linear function expressing $f^{\text{P}}_{0'ts}$ based on $\Delta P^{\text{Net}}_{its}$ and $\Delta Q^{\text{Net}}_{its}$.
$\mathbf{Q}^{0}_{t}$, $\mathbf{Q}^{\text{P}}_{it}$, $\mathbf{Q}^{\text{Q}}_{it}$	Constant terms of the linear function expressing $f^{\text{Q}}_{0'ts}$ based on $\Delta \text{P}^{\text{Net}}_{its}$ and $\Delta \text{Q}^{\text{Net}}_{its}$.
$\mathbf{V}^{0}_{it}$, $\mathbf{V}^{P}_{ijt}$, $\mathbf{V}^{Q}_{ijt}$	Constant terms of the linear function expressing V_{its} based on $\Delta P^{\text{Net}}_{jts}$ and $\Delta Q^{\text{Net}}_{jts}$.
$\text{V}^{\text{Max}}_{j}$	Maximum voltage limit of node j [p.u.].
$\text{V}^{\text{Min}}_{j}$	Minimum voltage limit of node j [p.u.].
t_0	The time (in hour) prior to the beginning of the scheduling time horizon when ADN's FPC area for each time slot of the scheduling time horizon is estimated.
T	Duration of the scheduling time horizon [hour].
τ	Duration of each time slot [hour].
θ	The angle between the selected direction and $\text{F}^{\text{P}}_{0't}$ axis.
$\Delta P^{\text{D}}_{its}$, $\Delta Q^{\text{D}}_{its}$	Deviation of the active/reactive power consumption of the load connected to node i from its scheduled operating point (i.e. base case operating point) during time slot t and scenario s [p.u.].
$\Delta P^{\text{SDG}}_{hts}$	Deviation of the active power generation of SDG h from its scheduled operating point (i.e. base case operating point) during time slot t and scenario s [p.u.].

6.1 State of the Art

The penetration of Renewable Energy sources (RESs) is significantly increasing in the electric power system. RESs, on the one hand, do not usually provide ancillary services, on the other hand, introduce uncertainties into the electric power system. Consequently, the grid operators need larger amount of ancillary services to counteract the impact of those uncertainties and preserve the security of supply [26], [27], [129], [130].

On the other hand, the number of distributed energy resources (DERs) is progressively increasing in active distribution networks (ADNs). A promising solution to preserve the quality/security of supply is aggregating the power flexibility of DERs located in ADNs to provide active/reactive power flexibility to the upper-layer grid [29], [131–133].

*The **active/reactive power flexibility** can be perceived as a service that a given resource can provide to the grid by regulating up or down its operating point, i.e. increasing or decreasing its active/reactive power consumption/generation* [17].

In this emerging architecture, further cooperation between operators of different levels of electric power systems, e.g., transmission system operators (TSOs) and distribution system operators (DSOs), is required to exchange such a power flexibility [14], [15, 134–136].

The question that arises is:
How much are the maximum active/reactive power flexibility an ADN can provide upon request at its point of common coupling (PCC) to the upper-layer grid?

In this context, the flexibility provision capability (FPC) curve of an ADN is defined as a curve characterizing the extreme amount of active and reactive power flexibility that ADN can provide to the upper-layer grid. The area surrounded by the FPC curve is called FPC area. This area is a function of the ADN's operating point, ADN's grid constraints (i.e. voltage and current constraints) and the capability limits of DERs located in the ADN.

In [131], a random sampling approach is proposed to determine the FPC area of an ADN. It first generates random points inside the capability curve of each DER and then, for each combination, applies a nonlinear load flow to determine the nodal voltages and lines currents. If they respect all grid constraints, the resulting power flow at the grid connection point is retained and used to compose the FPC area, otherwise it is discarded. The final output of this method is a set of feasible points instead of the perimeter of the ADN's FPC area (FPC curve). This approach is essentially an exhaustive search, therefore, its computational complexity scales poorly with the number of DERs in the ADN. Works in [29], [132], [133] propose to estimate the FPC curve of an ADN by

solving a non-convex non-linear optimal power flow (OPF) problem. In comparison with the random sampling approach, OPF-based methods are better suited to identify accurately the full FPC area while might require less computational effort. However, since OPFs are notoriously non-convex, also this approach lacks guaranteed tractability properties.

6.2 Motivations

In general, all the above-mentioned approaches suffer from the following limitations:

1. They do not model uncertainties. As known, renewable generation and demand at high level of disaggregation is highly volatile. Consequently, these methods can only forecast the FPC area of ADN for short-term horizons (i.e., few minutes ahead), where uncertainties can be neglected. As typical power system operations entail scheduling operation on longer time horizons (e.g. day-ahead and hours-ahead), accounting for uncertainties is a key to achieve a reliable estimation of the FPC;
2. They model the FPC area of DERs as a rectangular area, which might be unrealistic;
3. They estimate the FPC area by solving a non-convex optimization problem. Thus, they cannot mathematically ensure the global optimality;
4. They entail a high computational effort when the number of DERs is large.

The limitations found in [29], [131–133] inspired the motivations of this chapter. To overcome those limitations, this chapter introduces a tractable algorithm based on a linear scenario-based robust optimization problem to estimate the curve and the area of the FPC of an ADN while considering grid constraints and uncertainties of loads and stochastic generation. Grid constraints are modelled by leveraging recent advancements in linearized load flow models [90]- [91], whereas uncertainty of loads and stochastic generation are explicitly modelled with scenarios, which are used to enforce robust grid constraints and deliver realistic estimates of the FPC area. To comply with the current scheduling/operation paradigm of current power systems, the proposed method is applied to a long-term scheduling horizon T (e.g. day-ahead), where uncertainties play a salient role. This longer-term horizon method, compared to existing ones, entails considering a large number of scenarios to model the forecasting errors of demand and stochastic generation. It is shown that the proposed method can compute robust estimates of the FPC of ADNs in a reliable and efficient way.

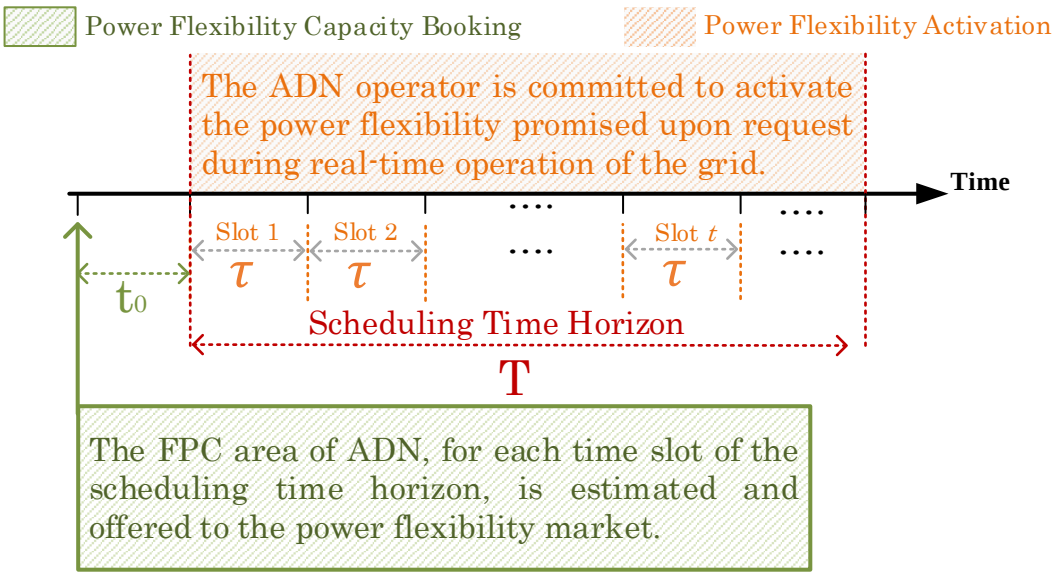

Figure 6.1: The general procedure for estimating the ADN's FPC area.

6.3 Problem Statement

Although specifications might vary from system to system, the procedure to manage (i.e. book/activate) power flexibility[1] in electrical grids generally consists in two steps:

1. **Power flexibility[3] booking (planning)**: This step is usually carried out (t_0 hours) prior to the real-time grid operations. For each time slot of the scheduling time horizon T, the TSO estimates its needs for power flexibility, and power flexibility providers estimate their capacity for providing power flexibility. Then, demand and offers are collected in the power flexibility capacity market[2] and the TSO books its required power flexibility by clearing the market. In this stage, no real product is exchanged between the TSO and the power flexibility providers.

2. **Power flexibility[3] activation (real-time operation)**: This step is carried out during the real-time operation. In case of need, the TSO sends its requests to the power flexibility providers who already succeeded to sell their power flexibility capacities in the power flexibility capacity market[4]. Then, those power flexibility providers activate all or a portion of the power flexibility capacities they have sold.

In line with the above-mentioned procedure, Fig. 6.1 shows the timeline of the problem. This chapter solely focuses on the first step, namely power flexibility[3] booking step.

[1] Power reserve.
[2] Power reserve capacity market.

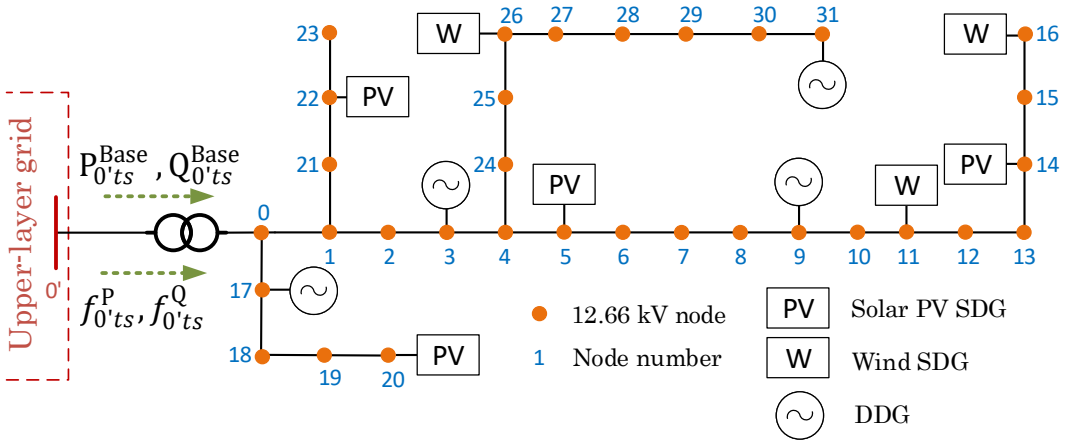

Figure 6.2: The single line diagram of the modified IEEE 33-bus distribution test system.

Accordingly, this chapter introduces a method to estimate the FPC area of an ADN for each individual time slot of the scheduling time horizon so that it can be offered to the power flexibility capacity market[4]. This method assumes that:

- The FPC area of an ADN for each time slot of the scheduling time horizon T is estimated t_0 hours before the beginning of the scheduling time horizon;
- The scheduling time horizon T consists of a number of time slots, each with duration of τ;
- The ADN's forecasted/scheduled operating point, i.e. $P^{Base}_{0't}$, $Q^{Base}_{0't}$, P^{Base}_{it} and Q^{Base}_{it} for each time slot is assumed to be known and it is called ADN's base case operating point.

This method is general and can accommodate any desired scheduling horizon with any duration of time slots by plugging-in suitable forecasts. Finally, it is worth noting that the FPC areas at various time slots are determined separately and in the same manner. Since there is no time-coupling constraint in the problem, the FPC areas are independent from each other. For this reason, this chapter proposes the formulation of the problem referring to one time slot only, and it is applied identically to each time slot of the time horizon.

Although references to the distribution grid of Fig. 6.2 are made throughout the chapter, the proposed formulation can accommodate any kind of grid (i.e., meshed or radial) with a single connection point to the upper-layer grid.

6.4 Contributions & Novelties

Original contributions of this chapter can be enumerated as:

1. It introduces a method to characterize the maximum ranges of active/reactive power flexibility an ADN can provide to the upper-layer grid at its PCC while considering the uncertainties of load and renewable generation (i.e. FPC area). To the best knowledge of the author, it is the first-ever work addressing this problem.
2. To deal with uncertainties, it offers a novel search methodology in the P-Q plane to explore the boundaries of the ADN's FPC area.
3. It develops linear models for the DERs' constraints and exploits the linearized load flow model proposed in [90, 91] to represent the grid's constraints (i.e., nodal voltage constraints and line current constraints), thereby succeeding in implementing the search methodology in the P-Q plane as a tractable linear algorithm with low complexity,.
4. Thanks to the presented linear models, it casts the search methodology in the P-Q plane as a set of linear scenario-based robust optimization problems. In addition to the technical constraints of the grid and DERs, this model takes into account the grid's power losses and uncertainties of demand/renewable generation.
5. Most notably, this tractable linear robust formulation is able to efficiently estimate the FPC area of an ADN for any desired time horizon with any duration.
6. It mathematically proves that, assuming convex capabilities curves of DERs and a linearized power flow model, the estimated FPC area is feasible and convex.
7. It presents a closed-form formula to determine the number of scenarios that should be taken into account in above-mentioned linear scenario-based robust optimization problem for modeling the uncertainties of demand and renewable generation.

6.5 Methodology

The power flow at the connection point of the ADN in Fig. 6.2 is:

$$P^{\mathrm{Net}}_{0't s} = \mathrm{P}^{\mathrm{Base}}_{0't} + f^{\mathrm{P}}_{0't s}, \tag{6.1}$$

$$Q^{\mathrm{Net}}_{0't s} = \mathrm{Q}^{\mathrm{Base}}_{0't} + f^{\mathrm{Q}}_{0't s}, \tag{6.2}$$

It is assumed that $\mathrm{P}^{\mathrm{Base}}_{0't}$ and $\mathrm{Q}^{\mathrm{Base}}_{0't}$ are known, then, this method estimates the FPC curve, i.e. the boundary of $f^{\mathrm{P}}_{0't s}$ and $f^{\mathrm{Q}}_{0't s}$, while considering grid constraints and uncertainties of loads and stochastic generation.

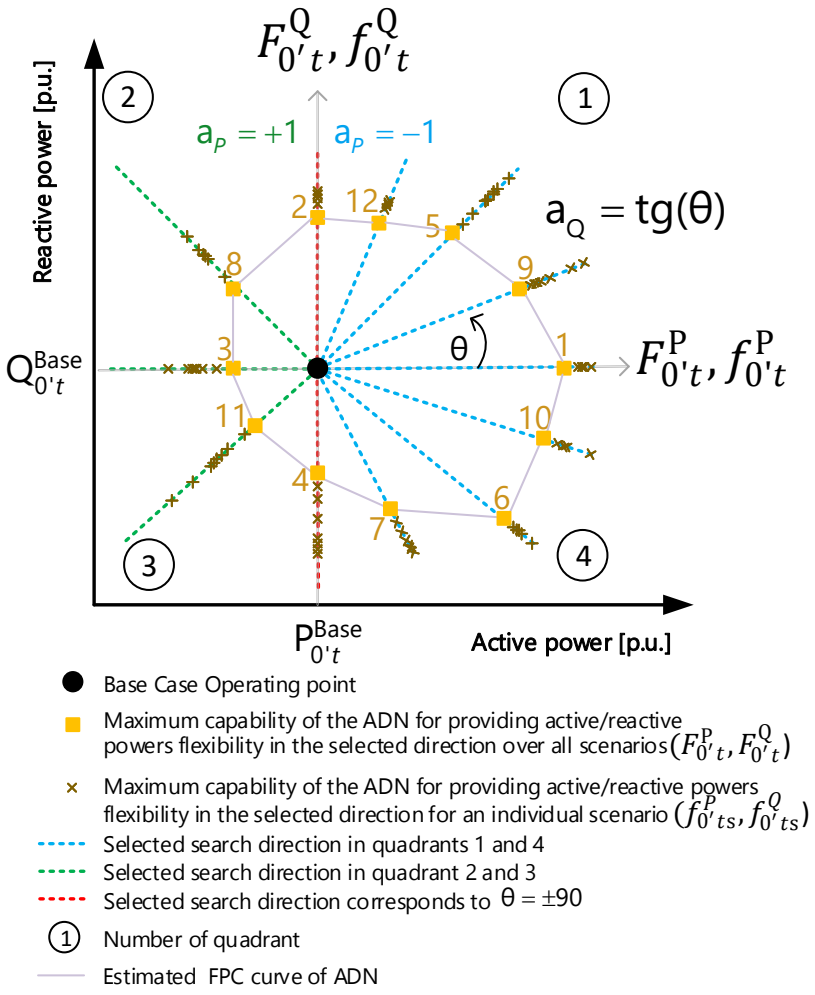

Figure 6.3: Typical estimated FPC area of an ADN.

The proposed method consists of three main parts:

- Definition of the search directions;
- Computation of the points of the FPC curve along the defined search directions;
- Estimation of the whole FPC curve.

These three steps are explained in the following by referring to Fig. 6.3, which exemplifies the FPC on the $F^{P}_{0't} - F^{Q}_{0't}$ plane.

1. **Definition of the search directions**: As shown in Fig. 6.3, the angle θ defines a search direction in the $F^{P}_{0't} - F^{Q}_{0't}$ plane and can take a value between $0°$ and $360°$.

It determines a_P and a_Q as follows:

$$a_P = \begin{cases} -1 & \text{if} \quad 0^\circ \leq \theta < 90^\circ \\ +1 & \text{if} \quad 90^\circ < \theta < 270^\circ \\ -1 & \text{if} \quad 270^\circ < \theta < 360^\circ \end{cases} \tag{6.3}$$

$$a_Q = \tan(\theta) \qquad 0^\circ \leq \theta < 360^\circ \tag{6.4}$$

a_P and a_Q are used in the second step, when solving the linear robust optimization problem. A set of search directions is defined with the following procedure:

(a) The minimum acceptable granularity for the final estimated FPC curve is defined. It determines the procedure termination criterion. The procedure is terminated when the Euclidean distances between all two consecutive estimated points on the FPC curve (yellow squares in Fig. 6.3) are smaller than the pre-defined granularity.

(b) Four search directions, corresponding to $\theta = 0^\circ, 90^\circ, 180^\circ, 270^\circ$, are defined. For each search direction, the linear robust optimization problem introduced in step 2 is solved, determining 4 points on the FPC curve.

(c) The search directions are ordered based on their increasing θ.

(d) The Euclidean distance between each couple of consecutive points for increasing θ on the FPC curve is calculated. If all the distances are smaller than the defined granularity in (a), the procedure ends and goes to final step 3; otherwise, the couple of consecutive points with the largest distance is selected, and the arithmetic mean of their search direction θ is used as the new search direction.

(e) For the new search direction in (d), the linear robust optimization problem of step 2, is solved.

(f) Jump to C.

The above-mentioned procedure is illustrated in Fig. 6.3, where the numbers on the FPC curve denote the sequence of the defined directions.

2. **Computation of the points of the FPC curve along the defined search directions**: For a defined θ, this step entails solving the optimization problem detailed in Section 6.6 to find the point on the FPC curve associated to that search direction.

3. **Estimation of the whole FPC curve**: Once the points of the FPC curve are defined, they are linearly interpolated to approximate the whole FPC curve, as shown in Fig. 6.3. As discussed and formally proven in Section 6.7, this is a valid approximation because the FPC curve determined by this method is convex by construction.

The flowchart of the presented method for estimating the ADN's FPC areas for all time slots of the scheduling time horizon is sketched in Fig. 6.4.

6.6 Linear Scenario-Based Robust Optimization Problem Formulation

6.6.1 Mathematical Formulation

This section describes the linear scenario-based robust optimization problem that determines a point on the FPC curve for a selected search direction. Assuming $\theta \neq 90°$ and $\theta \neq 270°$, coefficients a_P and a_Q are respectively calculated based on 6.3 and 6.4. The associated point of the FPC curve is calculated by solving the following optimization problem:

$$\min_{\psi} \; a_P \, F^P_{0't}, \tag{6.5}$$

subject to

$$f^Q_{0'ts} = a_Q f^P_{0'ts} \qquad \forall s \in \mathbb{S}, \tag{6.6}$$

$$a_P f^P_{0'ts} \leq a_P F^P_{0't} \leq 0 \qquad \forall s \in \mathbb{S}, \tag{6.7}$$

$$F^Q_{0't} = a_Q F^P_{0't} \qquad \forall s \in \mathbb{S}, \tag{6.8}$$

$$\Omega(\psi) \leq 0 \qquad \forall s \in \mathbb{S}, \tag{6.9}$$

$$\Gamma(\psi) = 0 \qquad \forall s \in \mathbb{S}, \tag{6.10}$$

where ψ denotes the set of optimization variables of the problem:

$$\psi = \{F^P_{0't}, F^Q_{0't}, f^P_{0'ts}, f^Q_{0'ts}, I^{Real}_{lts}, I^{Imag}_{lts}, V_{jts}, f^{DDG,P}_{kts}, f^{DDG,Q}_{kts}, f^{SDG,Q}_{hts}\}. \tag{6.11}$$

For $a_P = -1$, the objective function (6.5) minimizes $-F^P_{0't}$ or equivalently maximizes $F^P_{0't}$, whereas, for $a_P = +1$, it minimizes $F^P_{0't}$. Constraint (6.6) specifies the search direction in the $F^P_{0't}-F^Q_{0't}$ plane, as shown in Fig. 6.3. Since the objective function (6.5) consists of the active power flexibility capacity $F^P_{0't}$ only, constraint (6.6) achieves to steer the search in the direction of the $F^Q_{0't}$ axis also. In order to guarantee that the ADN can provide, in real-time operation, any amount of power flexibility corresponding to the points located in its FPC area in spite of uncertainties, this method computes robust estimates of the points on the FPC curve. In other words, $F^P_{0't}$ and $F^Q_{0't}$ (i.e., yellow squares in Fig. 6.3) are chosen as the most conservative $f^P_{0'ts}$ and $f^Q_{0'ts}$ (i.e., the innermost grey crosses in Fig. 6.3). This is performed by constraints (6.7) and (6.8). In (6.7), $a_P = -1$ corresponds to the quadrants 1 and 4 (positive values of $f^P_{0'ts}$ and $F^P_{0't}$), whereas $a_P = +1$ corresponds to the quadrants 2 and 3 (negative values of $f^P_{0'ts}$ and $F^P_{0't}$). Thanks to (6.6) and (6.7), the above-mentioned conservative manner for $F^Q_{0't}$ in particular can be

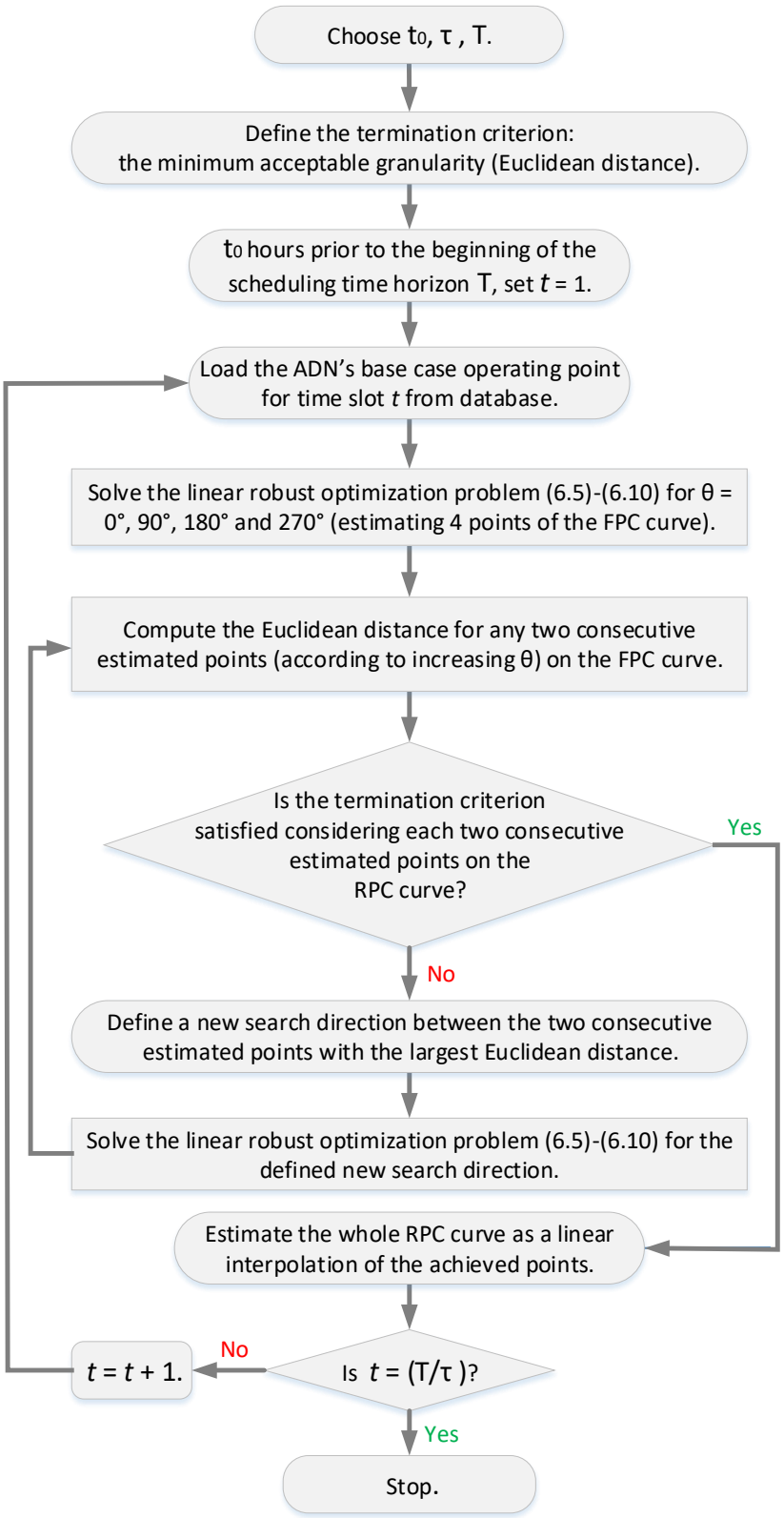

Figure 6.4: Flowchart showing the procedure for estimating the FPC area of ADN for each time slot of the scheduling time horizon.

modeled as constraint (6.8).

For search directions $\theta = 90°$ or $\theta = 270°$, the objective function and constraints (6.5)-(6.8) are modified as:

$$\min_{\psi} \; \mathrm{a}' \, F^{\mathrm{Q}}_{0't}, \tag{6.12}$$

subject to

$$f^{\mathrm{P}}_{0'ts} = 0 \qquad \forall s \in \mathbb{S}, \tag{6.13}$$

$$\mathrm{a}' f^{\mathrm{Q}}_{0'ts} \leq \mathrm{a}' F^{\mathrm{Q}}_{0't} \leq 0 \qquad \forall s \in \mathbb{S}, \tag{6.14}$$

$$F^{\mathrm{P}}_{0't} = 0 \qquad \forall s \in \mathbb{S}, \tag{6.15}$$

in (6.12)-(6.15), a′ is equal to -1 and +1 for $\theta = 90°$ and $\theta = 270°$, respectively.

Expressions (6.9) and (6.10) are linear and model the operational constraints of the ADN and DERs, as described in subsections 6.6.2 and 6.6.3.

The problem (6.5)-(6.10) is a linear scenario-based robust optimization problem that determines the point on the FPC curve associated to search direction θ. In this problem, index s corresponds to the scenarios modeling the forecast errors of loads ($\Delta \mathrm{P}^{\mathrm{D}}_{its}$, $\Delta \mathrm{Q}^{\mathrm{D}}_{its}$) and stochastic generation ($\Delta \mathrm{P}^{\mathrm{SDG}}_{hts}$).

In the following, the operational constraints of the ADN and DERs (6.9) and (6.10) are defined assuming that:

- Dispatchable distributed generators (DDGs) can provide both active/reactive power flexibility ($f^{\mathrm{DDG,P}}_{kts}$, $f^{\mathrm{DDG,Q}}_{kts}$);
- SDGs are sources of active power uncertainties ($\Delta \mathrm{P}^{\mathrm{SDG}}_{hts}$) and they can only provide reactive power flexibility ($f^{\mathrm{SDG,Q}}_{hts}$);
- Loads are sources of both active/reactive power uncertainties ($\Delta \mathrm{P}^{\mathrm{D}}_{its}$, $\Delta \mathrm{Q}^{\mathrm{D}}_{its}$).

6.6.2 Modeling the Technical Constraints of ADN

The linearized load flow model proposed in [90]- [91] is used to derive expressions of:

- The active/reactive power flexibility absorbed by the ADN from the upper-layer grid, at the ADN's PCC ($f^{\mathrm{P}}_{0'ts}$, $f^{\mathrm{Q}}_{0'ts}$);
- Voltage magnitudes of all nodes of the ADN (V_{its});
- Current phasor of all branches of the ADN (I_{lts});

as a linear function of nodal injections $\Delta \mathrm{P}^{\mathrm{Net}}_{its}$ and $\Delta \mathrm{Q}^{\mathrm{Net}}_{its}$.

The net deviation of the active/reactive power injection at node i from its base case operating point (for the selected time slot t) during the scenario s can be written as:

$$\Delta P^{\mathrm{Net}}_{its} = -\Delta \mathrm{P}^{\mathrm{D}}_{its} + \sum_{k \in \mathbb{DDG}_i} f^{\mathrm{DDG,P}}_{kts} + \sum_{h \in \mathbb{SDG}_i} \Delta \mathrm{P}^{\mathrm{SDG}}_{hts} \qquad \forall i \in \mathbb{B}, \tag{6.16}$$

$$\Delta Q^{\mathrm{Net}}_{its} = -\Delta \mathrm{Q}^{\mathrm{D}}_{its} + \sum_{k \in \mathbb{DDG}_i} f^{\mathrm{DDG,Q}}_{kts} + \sum_{h \in \mathbb{SDG}_i} f^{\mathrm{SDG}}_{hts} \qquad \forall i \in \mathbb{B}. \tag{6.17}$$

6.6.2.1 The Active/Reactive Power Flexibility at the PCC

The active power flexibility absorbed by the ADN from the upper-layer grid at the ADN's PCC can be expressed as a linear function of $\Delta \mathrm{P}^{\mathrm{Net}}_{its}$ and $\Delta \mathrm{Q}^{\mathrm{Net}}_{its}$ with constant coefficients $\mathbf{P}^{0}_{it}$, $\mathbf{P}^{\mathrm{P}}_{it}$ and $\mathbf{P}^{\mathrm{Q}}_{it}$:

$$f^{\mathrm{P}}_{0'ts} = \mathbf{P}^{0}_{t} + \sum_{i \in \mathbb{B}} \left(\mathbf{P}^{\mathrm{P}}_{it} \, \Delta P^{\mathrm{Net}}_{its} + \mathbf{P}^{\mathrm{Q}}_{it} \, \Delta Q^{\mathrm{Net}}_{its} \right) \qquad \forall s \in \mathbb{S}. \tag{6.18}$$

In the same way, the reactive power flexibility absorbed by the ADN from the upper-layer grid at the ADN's PCC can be expressed as a linear function of $\Delta \mathrm{P}^{\mathrm{Net}}_{its}$ and $\Delta \mathrm{Q}^{\mathrm{Net}}_{its}$ with constant coefficients $\mathbf{Q}^{0}_{it}$, $\mathbf{Q}^{\mathrm{P}}_{it}$ and $\mathbf{Q}^{\mathrm{Q}}_{it}$:

$$f^{\mathrm{Q}}_{0'ts} = \mathbf{Q}^{0}_{t} + \sum_{i \in \mathbb{B}} \left(\mathbf{Q}^{\mathrm{P}}_{it} \, \Delta P^{\mathrm{Net}}_{its} + \mathbf{Q}^{\mathrm{Q}}_{it} \, \Delta Q^{\mathrm{Net}}_{its} \right) \qquad \forall s \in \mathbb{S}. \tag{6.19}$$

6.6.2.2 Maximum Current Flow Constraint of Branches

The maximum allowable current flow of branch l can be expressed as the following nonlinear constraint:

$$\| I_{lts} \|^2 = I^{\mathrm{Real}^2}_{lts} + I^{\mathrm{Imag}^2}_{lts} \leq \mathrm{I}^{\mathrm{Max}^2}_{l} \qquad \forall l \in \mathbb{L}, \ \forall s \in \mathbb{S}. \tag{6.20}$$

where I_{lts} is the current phasor of branch l during time slot t and scenario s; I^{Real}_{lts} and I^{Imag}_{lts} are real and imaginary parts of I_{lts}; $\| I_{lts} \|$ is the magnitude of I_{lts}; $\mathrm{I}^{\mathrm{Max}}_{l}$ is the maximum current limit of branch l.

As represented in Fig. 6.5, the nonlinear constraint (6.20) can be linearized based on a pre-defined number of linear boundaries approximating the real curve:

$$\mathbf{A}^{\mathrm{Real}}_{nl} I^{\mathrm{Real}}_{lts} + \mathbf{A}^{\mathrm{Imag}}_{nl} I^{\mathrm{Imag}}_{lts} \leq \mathbf{A}^{0}_{nl} \qquad \forall l \in \mathbb{L}, \forall n \in \mathbb{C}_l, \ \forall s \in \mathbb{S}, \tag{6.21}$$

where the real (respectively imaginary) part of the current phasor of branch l[3] can

[3] The maximum current flow limit of branch l is modeled for its both sending and receiving ends.

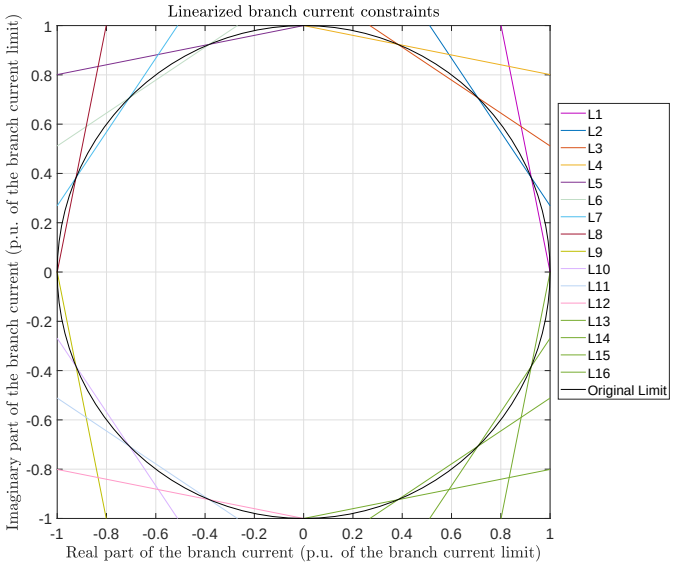

Figure 6.5: Linearized branch current constraint.

be expressed as a linear function of $\Delta \mathrm{P}^{\mathrm{Net}}_{its}$ and $\Delta \mathrm{Q}^{\mathrm{Net}}_{its}$ with constant coefficients $\mathbf{I}^{0,\mathrm{Real}}_{lt}$, $\mathbf{I}^{\mathrm{P,Real}}_{lit}$ and $\mathbf{I}^{\mathrm{Q,Real}}_{lit}$ (respectively $\mathbf{I}^{0,\mathrm{Imag}}_{lt}$, $\mathbf{I}^{\mathrm{P,Imag}}_{lit}$ and $\mathbf{I}^{\mathrm{Q,Imag}}_{lit}$):

$$I^{\mathrm{Real}}_{lts} = \mathbf{I}^{0,\mathrm{Real}}_{lt} + \sum_{i\in\mathbb{B}} \left(\mathbf{I}^{\mathrm{P,Real}}_{lit} \, \Delta P^{\mathrm{Net}}_{its} + \mathbf{I}^{\mathrm{Q,Real}}_{lit} \, \Delta Q^{\mathrm{Net}}_{its} \right) \qquad \forall l \in \mathbb{L}, \ \forall s \in \mathbb{S}, \tag{6.22}$$

$$I^{\mathrm{Imag}}_{lts} = \mathbf{I}^{0,\mathrm{Imag}}_{lt} + \sum_{i\in\mathbb{B}} \left(\mathbf{I}^{\mathrm{P,Imag}}_{lit} \, \Delta P^{\mathrm{Net}}_{its} + \mathbf{I}^{\mathrm{Q,Imag}}_{lit} \, \Delta Q^{\mathrm{Net}}_{its} \right) \qquad \forall l \in \mathbb{L}, \ \forall s \in \mathbb{S}. \tag{6.23}$$

6.6.2.3 Maximum & Minimum Voltage Magnitude Constraint of Nodes

The voltage magnitude of node i (i.e. V_{its}) can be expressed as a linear function of the nodal active/reactive power deviations (i.e. $\Delta \mathrm{P}^{\mathrm{Net}}_{its}$ and $\Delta \mathrm{Q}^{\mathrm{Net}}_{its}$) with constant coefficients $\mathbf{V}^{0}_{it}$, $\mathbf{V}^{\mathrm{P}}_{it}$ and $\mathbf{V}^{\mathrm{Q}}_{it}$:

$$V_{its} = \mathbf{V}^{0}_{it} + \sum_{j\in\mathbb{B}} \left(\mathbf{V}^{\mathrm{P}}_{ijt} \, \Delta P^{\mathrm{Net}}_{jts} + \mathbf{V}^{\mathrm{Q}}_{ijt} \, \Delta Q^{\mathrm{Net}}_{jts} \right), \tag{6.24}$$

Consequently, the nodal voltage magnitude limits can be linearly modeled as:

$$\mathrm{V}^{\mathrm{Min}}_{i} \le V_{its} \le \mathrm{V}^{\mathrm{Max}}_{i} \qquad \forall i \in \mathbb{B}, \forall t \in \mathbb{T}, \forall s \in \mathbb{S}, \tag{6.25}$$

where $\mathrm{V}^{\mathrm{Min}}_{i}$ and $\mathrm{V}^{\mathrm{Max}}_{i}$ are the minimum and maximum voltage magnitude limits of node i.

It is worth noting that the expressions (6.16)-(6.25) are applicable to both meshed and

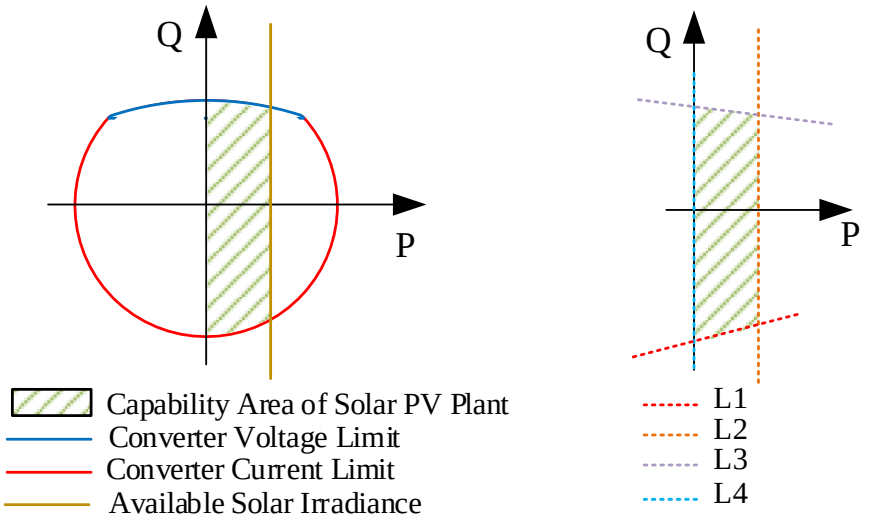

Figure 6.6: Capability curve of a solar PV plant.

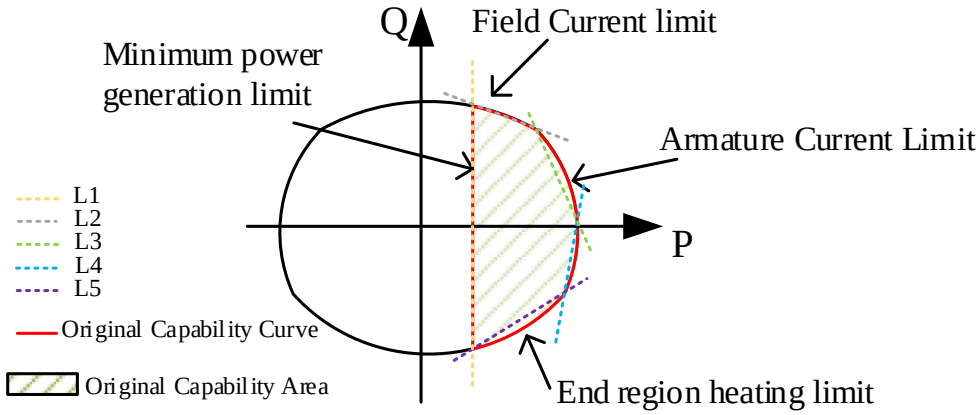

Figure 6.7: Capability curve of a dispatchable distributed generator (DDG).

radial grids by virtue of the linearized grid model. Their coefficients are functions of the grid admittance matrix, nodal active/reactive power injections for the base case operating point and the voltage magnitude at node 0' (slack node) [90]- [91].

6.6.3 Modeling the Capability Limits of DERs

The power capability limits of DERs are typically nonlinear. These nonlinear constraints can be linearized by using a pre-defined number of linear boundaries. For instance, Fig. 6.6 shows the capability curve of a solar PV plant from [137], and its linearized version. Similarly, Fig. 6.7 shows the capability curve of a DDG from [138], like a gas turbine.

Based on the linearized models of the capability limits of DDGs and SDGs, the operational constraints of SDG h and DDG k are as:

$$\mathbf{R}^{0}_{mhts} + \mathbf{R}^{\mathrm{P}}_{mhts}\,\Delta \mathrm{P}^{\mathrm{SDG,P}}_{hts} + \mathbf{R}^{\mathrm{Q}}_{mhts}\, f^{\mathrm{SDG,Q}}_{hts} \leq 0 \qquad \forall m \in \mathbb{C}_h, \forall h \in \mathbb{SDG},\ \forall s \in \mathbb{S}. \tag{6.26}$$

$$\mathbf{D}^{0}_{mkt} + \mathbf{D}^{\mathrm{P}}_{mk}\ f^{\mathrm{DDG,P}}_{kts} + \mathbf{D}^{\mathrm{Q}}_{mk}\, f^{\mathrm{DDG,Q}}_{kts} \leq 0 \qquad \forall m \in \mathbb{C}_k,\ \forall k \in \mathbb{DDG},\ \forall s \in \mathbb{S}. \tag{6.27}$$

6.7 On The Convexity of The FPC Area of ADN

Relying on the linearized model of the ADN's constraints presented in section 6.6.2, it can be formally proven that the FPC area is convex. To this end, the following theorems are introduced:

6.7.1 Theorems

Theorem 1: Assuming that the capability limits of all DERs of the ADN are convex areas[4] and that the linearized grid model (6.21)-(6.25) holds, the FPC area of the ADN for a given scenario is a convex area.

Theorem 2: The FPC area of the ADN obtained by considering all scenarios is convex in the $F^{\mathrm{P}}_{0't} - F^{\mathrm{Q}}_{0't}$ plane.

Contrariwise, for the given point $\left[f^{\mathrm{P}}_{0'ts}, f^{\mathrm{Q}}_{0'ts}\right]^{\mathrm{T}}$, the corresponding operating point $\boldsymbol{X}_{ts}$ can be calculated as:

$$\Delta P^{\mathrm{Net}}_{its} = \mathbf{P}'^{0}_{it} + \sum_{j \in \mathbb{B}} \left(\mathbf{P}'^{\mathrm{P}}_{it}\, f^{\mathrm{P}}_{0'ts} + \mathbf{P}'^{\mathrm{Q}}_{it}\, f^{\mathrm{P}}_{0'ts} \right) \qquad \forall s \in \mathbb{S}. \tag{6.28}$$

$$\Delta Q^{\mathrm{Net}}_{its} = \mathbf{Q}'^{0}_{it} + \sum_{j \in \mathbb{B}} \left(\mathbf{Q}'^{\mathrm{P}}_{it}\, f^{\mathrm{P}}_{0'ts} + \mathbf{Q}'^{\mathrm{Q}}_{it}\, f^{\mathrm{P}}_{0'ts} \right) \qquad \forall s \in \mathbb{S}. \tag{6.29}$$

Operating point $\boldsymbol{X}_{ts}$ is said feasible if it satisfies the capability limits of all DERs and the operational constraints of the ADN in (6.21) and (6.25).

6.7.2 Proof of Theorem 1

Let $\boldsymbol{X}_{ts} = \left[\ \Delta P^{\mathrm{Net}}_{1ts}, \ldots, \Delta P^{\mathrm{Net}}_{\mathrm{N_B}ts}, \Delta Q^{\mathrm{Net}}_{1ts}, \ldots, \Delta Q^{\mathrm{Net}}_{\mathrm{N_B}ts}\ \right]^{\mathrm{T}}$ denotes the vector of the operating point of the ADN collecting the deviations of the nodal active/reactive power injections from the base case operating point. Point $\left[f^{\mathrm{P}}_{0'ts}, f^{\mathrm{Q}}_{0'ts}\right]^{\mathrm{T}}$ in the $F^{\mathrm{P}}_{0't} - F^{\mathrm{Q}}_{0't}$ plane indicates the corresponding point to the operating point $\boldsymbol{X}_{ts}$, which is calculated using (6.18) and (6.19).

[4] Capability curves of DERs are typically convex, see for instance [137], [138], [139].

For a given scenario s, the goal here is to mathematically prove that if two points 1 (i.e. $\left[f_{0'ts}^{\mathrm{P}\ 1}, f_{0'ts}^{\mathrm{Q}\ 1}\right]^{\mathrm{T}}$) and 2 (i.e $\left[f_{0'ts}^{\mathrm{P}\ 2}, f_{0'ts}^{\mathrm{Q}\ 2}\right]^{\mathrm{T}}$) belong to the FPC area of scenario s, then all points located on the line connecting them to each other also belong to that FPC area. In other words:

$$if \quad \begin{bmatrix} f_{0'ts}^{\mathrm{P}\ 1} \\ f_{0'ts}^{\mathrm{Q}\ 1} \end{bmatrix} \in A_s^{\mathrm{FPC}} \quad \& \quad \begin{bmatrix} f_{0'ts}^{\mathrm{P}\ 2} \\ f_{0'ts}^{\mathrm{Q}\ 2} \end{bmatrix} \in A_s^{\mathrm{FPC}} \quad \Rightarrow \quad \begin{bmatrix} f_{0'ts}^{\mathrm{P}\ 3} \\ f_{0'ts}^{\mathrm{Q}\ 3} \end{bmatrix} \in A_s^{\mathrm{FPC}}, \tag{6.30}$$

where superscripts 1, 2 and 3 denote the index of points, A_s^{FPC} indicates the FPC area obtained by considering single scenario s and $\begin{bmatrix} f_{0'ts}^{\mathrm{P}\ 3} \\ f_{0'ts}^{\mathrm{Q}\ 3} \end{bmatrix}$ is a point located on the line connecting points 1 and 2 to each other:

$$\begin{bmatrix} f_{0'ts}^{\mathrm{P}\ 3} \\ f_{0'ts}^{\mathrm{Q}\ 3} \end{bmatrix} = (1-\alpha) \begin{bmatrix} f_{0'ts}^{\mathrm{P}\ 1} \\ f_{0'ts}^{\mathrm{Q}\ 1} \end{bmatrix} + \alpha \begin{bmatrix} f_{0'ts}^{\mathrm{P}\ 2} \\ f_{0'ts}^{\mathrm{Q}\ 2} \end{bmatrix}, \tag{6.31}$$

where α is a constant between 0 and 1.

Considering the fact that points 1 and 2 belong to the FPC area (as stated in (6.30)) and they are feasible, thus, it can be inferred that:

- Points $\boldsymbol{X}_{ts}{}^1$ and $\boldsymbol{X}_{ts}{}^2$ exist that satisfy (6.18) and (6.19) :

$$f_{0'ts}^{\mathrm{P}\ 1} = \mathbf{P}_t^0 + \sum_{i\in\mathbb{B}} \left(\mathbf{P}_{it}^{\mathrm{P}}\, \Delta P_{its}^{\mathrm{Net}\,1} + \mathbf{P}_{it}^{\mathrm{Q}}\, \Delta Q_{its}^{\mathrm{Net}\,1}\right), \tag{6.32}$$

$$f_{0'ts}^{\mathrm{Q}\ 1} = \mathbf{Q}_t^0 + \sum_{i\in\mathbb{B}} \left(\mathbf{Q}_{it}^{\mathrm{P}}\, \Delta P_{its}^{\mathrm{Net}\,1} + \mathbf{Q}_{it}^{\mathrm{Q}}\, \Delta Q_{its}^{\mathrm{Net}\,1}\right), \tag{6.33}$$

$$f_{0'ts}^{\mathrm{P}\ 2} = \mathbf{P}_t^0 + \sum_{i\in\mathbb{B}} \left(\mathbf{P}_{it}^{\mathrm{P}}\, \Delta P_{its}^{\mathrm{Net}\,2} + \mathbf{P}_{it}^{\mathrm{Q}}\, \Delta Q_{its}^{\mathrm{Net}\,2}\right), \tag{6.34}$$

$$f_{0'ts}^{\mathrm{Q}\ 2} = \mathbf{Q}_t^0 + \sum_{i\in\mathbb{B}} \left(\mathbf{Q}_{it}^{\mathrm{P}}\, \Delta P_{its}^{\mathrm{Net}\,2} + \mathbf{Q}_{it}^{\mathrm{Q}}\, \Delta Q_{its}^{\mathrm{Net}\,2}\right), \tag{6.35}$$

- Points $\boldsymbol{X}_{ts}{}^1$ and $\boldsymbol{X}_{ts}{}^2$ satisfy the capability limits of all DERs limits.
- Points $\boldsymbol{X}_{ts}{}^1$ and $\boldsymbol{X}_{ts}{}^2$ satisfy the ADN's nodal voltage constraints. Based on (6.24)-(6.25), it can be mathematically expressed for each node like j as:

$$\mathrm{V}_i^{\mathrm{Min}} \le \mathbf{V}_{it}^0 + \sum_{j\in\mathbb{B}} \left(\mathbf{V}_{ijt}^{\mathrm{P}}\ \Delta P_{jts}^{\mathrm{Net}\,1} + \mathbf{V}_{ijt}^{\mathrm{Q}}\ \Delta Q_{jts}^{\mathrm{Net}\,1}\right) \le \mathrm{V}_i^{\mathrm{Max}}, \tag{6.36}$$

$$\mathrm{V}_i^{\mathrm{Min}} \le \mathbf{V}_{it}^0 + \sum_{j\in\mathbb{B}} \left(\mathbf{V}_{ijt}^{\mathrm{P}}\ \Delta P_{jts}^{\mathrm{Net}\,2} + \mathbf{V}_{ijt}^{\mathrm{Q}}\ \Delta Q_{jts}^{\mathrm{Net}\,2}\right) \le \mathrm{V}_i^{\mathrm{Max}}, \tag{6.37}$$

- Points $\boldsymbol{X}_{ts}{}^1$ and $\boldsymbol{X}_{ts}{}^2$ satisfy the maximum current flow limits of all branches. Based on (6.21)-(6.23), it can be mathematically expressed for each branch like l

as:

$$\mathbf{A}_{nl}^{\text{Real}} I_{lts}^{\text{Real}^1} + \mathbf{A}_{nl}^{\text{Imag}} I_{lts}^{\text{Imag}^1} \leq \mathbf{A}_{nl}^{0} \qquad \forall n \in \mathbb{C}_l, \tag{6.38}$$

$$\mathbf{A}_{nl}^{\text{Real}} I_{lts}^{\text{Real}^2} + \mathbf{A}_{nl}^{\text{Imag}} I_{lts}^{\text{Imag}^2} \leq \mathbf{A}_{nl}^{0} \qquad \forall n \in \mathbb{C}_l, \tag{6.39}$$

Based on the above-mentioned notations and definitions along with the assumptions of the theorem, it is here intended to prove that point $\left[f_{0'ts}^{\text{P}\ 3}, f_{0'ts}^{\text{Q}\ 3}\right]^{\text{T}}$, defined in (6.31), belongs to the FPC area of scenario s. To this end, lets consider point $\boldsymbol{X}_{ts}{}^3$:

$$\boldsymbol{X}_{ts}{}^3 = (1-\alpha)\,\boldsymbol{X}_{ts}{}^1 + \alpha \boldsymbol{X}_{ts}{}^2., \tag{6.40}$$

The following proves that point $\boldsymbol{X}_{ts}{}^3$ satisfies all gird/DERs constraints and corresponds to point $\left[f_{0'ts}^{\text{P}\ 3}, f_{0'ts}^{\text{Q}\ 3}\right]^{\text{T}}$ in $F_{0't}^{\text{P}} - F_{0't}^{\text{Q}}$ plane.

Proof of $\boldsymbol{X}_{ts}{}^3$ satisfies the capability limits of DERs:
Both $\boldsymbol{X}_{ts}{}^1$ and $\boldsymbol{X}_{ts}{}^2$ satisfy the capability limits of all DERs. Since capability limits of DERs are assumed to be convex areas, thus any point like $\boldsymbol{X}_{ts}{}^3$ defined based on (6.40) satisfies these capability limits.

Proof of $\boldsymbol{X}_{ts}{}^3$ satisfies the nodal voltage constrainte of the ADN:
It is shown that for the given points $\boldsymbol{X}_{ts}{}^1$ and $\boldsymbol{X}_{ts}{}^2$ respectively satisfying (6.36) and (6.37), any point like $\boldsymbol{X}_{ts}{}^3$ defined based on (6.40) satisfies (6.25). To this end, first (6.36) and (6.37) are respectively multiplied by $(1-\alpha)$ and α. Then they are added to each other and composed with (6.40) yielding:

$$\text{V}_i^{\text{Min}} \leq \mathbf{V}_{it}^{0} + \sum_{j \in \mathbb{B}} \left(\mathbf{V}_{ijt}^{\text{P}}\ \Delta P_{jts}^{\text{Net}^3} + \mathbf{V}_{ijt}^{\text{Q}}\ \Delta Q_{jts}^{\text{Net}^3} \right) \leq \text{V}_i^{\text{Max}}, \tag{6.41}$$

Expression (6.41) demonstrates that $\boldsymbol{X}_{ts}{}^3$ satisfies the nodal voltage constraints of the ADN.

Proof of $\boldsymbol{X}_{ts}{}^3$ satisfies the maximum current flow limits of all branches:
Considering the given points $\boldsymbol{X}_{ts}{}^1$ and $\boldsymbol{X}_{ts}{}^2$ respectively satisfying (6.38) and (6.39), it is shown that any point like $\boldsymbol{X}_{ts}{}^3$ defined based on (6.40) satisfies (6.21). To this end, first (6.38) and (6.39) are respectively multiplied by $(1-\alpha)$ and α. Then, they are added to each and composed with (6.22), (6.23) and (6.40) yielding:

$$\mathbf{A}_{nl}^{\text{Real}} I_{lts}^{\text{Real}^3} + \mathbf{A}_{nl}^{\text{Imag}} I_{lts}^{\text{Imag}^3} \leq \mathbf{A}_{nl}^{0} \qquad \forall n \in \mathbb{C}_l, \tag{6.42}$$

Expression (6.42) demonstrates that $\boldsymbol{X}_{ts}{}^3$ satisfies the maximum current flow limits of all branches.

Proof of $\boldsymbol{X}_{ts}{}^3$ corresponds to point $\left[f_{0'ts}^{\text{P}\ 3}, f_{0'ts}^{\text{Q}\ 3}\right]^{\text{T}}$:

It is shown that for the given points ${\boldsymbol{X}_{ts}}^1$ and ${\boldsymbol{X}_{ts}}^2$ satisfying (6.32)-(6.35), any point like ${\boldsymbol{X}_{ts}}^3$ defined based on (6.40) satisfies (6.18) and (6.19). To this end, first (6.32) and (6.34) are respectively multiplied by $(1-\alpha)$ and α. Then they are added to each other and composed with (6.31) and (6.40) yielding:

$$ {f_{0'ts}^{\mathrm{P}}}^3 = \mathbf{P}_t^0 + \sum_{i\in\mathbb{B}} \left(\mathbf{P}_{it}^{\mathrm{P}} \, \Delta P_{its}^{\mathrm{Net}^3} + \mathbf{P}_{it}^{\mathrm{Q}} \, \Delta Q_{its}^{\mathrm{Net}^3} \right), \tag{6.43} $$

Second (6.33) and (6.35) are respectively multiplied by $(1-\alpha)$ and α. Then they are added to each other and composed with (6.31) and (6.40) yielding:

$$ {f_{0'ts}^{\mathrm{Q}}}^3 = \mathbf{Q}_t^0 + \sum_{i\in\mathbb{B}} \left(\mathbf{Q}_{it}^{\mathrm{P}} \, \Delta P_{its}^{\mathrm{Net}^3} + \mathbf{Q}_{it}^{\mathrm{Q}} \, \Delta Q_{its}^{\mathrm{Net}^3} \right), \tag{6.44} $$

Expressions (6.43) and (6.44) demonstrate that ${\boldsymbol{X}_{ts}}^3$, defined in (6.40), corresponds to $\left[{f_{0'ts}^{\mathrm{P}}}^3, {f_{0'ts}^{\mathrm{Q}}}^3 \right]^{\mathrm{T}}$ in $F_{0't}^{\mathrm{P}} - F_{0't}^{\mathrm{Q}}$ plane, defined in (6.31).

Based on the above-mentioned proofs, it is trivial that ${\boldsymbol{X}_{ts}}^3$ is a feasible points and consequently $\left[{f_{0'ts}^{\mathrm{P}}}^3, {f_{0'ts}^{\mathrm{Q}}}^3 \right]^{\mathrm{T}}$ belongs to the FPC area of the ADN.

6.7.3 Proof of Theorem 2

The method introduced in section 6.5 defines the boundary of the FPC area, in each direction θ (as shown in Fig. 6.3), as the minimum amount of power flexibility that ADN can provide over all scenarios. It can be mathematically expressed as:

$$ A_{\mathbb{S}}^{\mathrm{FPC}} = \bigcap_{s\in\mathbb{S}} A_s^{\mathrm{FPC}}, \tag{6.45} $$

where $A_{\mathbb{S}}^{\mathrm{FPC}}$ indicates the FPC area obtained by considering all scenarios belonging to $\mathbb{S}$, A_s^{FPC} indicates the FPC area obtained by considering single scenario s and operator $\cap$ calculates the intersection of all areas.

On the one hand, Theorem 1 proved that A_s^{FPC} is convex for each scenario s. On the other hand, the intersection of a number of convex areas returns a convex area [140]. Thus, it is trivial that $A_{\mathbb{S}}^{\mathrm{FPC}}$ is convex.

6.7.4 Principal Result

Based on Theorems 1 and 2, the main result of this section is now presented:

Considering the fact that the FPC area is convex, it can be concluded that linearly interpolating the points of the FPC curve, as carried out in step 3 of section 6.5, results in a conservative feasible approximation of the FPC curve.

6.8 Determining the Number of Scenarios

This section is intended to determine the number of scenarios belonging to $\mathbb{S}$, i.e. N_s, which should be taken into account in the scenario-based robust optimization problem (6.5)-(6.10), in order to guarantee that the achieved optimal solution (i.e. $F^{\mathrm{P}}_{0't}$ and $F^{\mathrm{Q}}_{0't}$) satisfies all the grid constraints considering all possible realizations of the uncertain parameters (i.e., loads $\Delta\mathrm{P}^{\mathrm{D}}_{its}$, $\Delta\mathrm{Q}^{\mathrm{D}}_{its}$ and stochastic generation $\Delta\mathrm{P}^{\mathrm{SDG}}_{its}$) with an expected probability larger or equal than $1-\varepsilon$ and with a confidence level of $1-\beta$.

Theorem 3: The above-mentioned target can be achieved provided that:

$$\mathrm{N}_s \geq \frac{2}{\varepsilon}\ln\frac{1}{\beta} + 2\left(2\mathrm{N}^{\mathrm{DDG}}+\mathrm{N}^{\mathrm{SDG}}\right) + \frac{2\left(2\mathrm{N}^{\mathrm{DDG}}+\mathrm{N}^{\mathrm{SDG}}\right)}{\varepsilon}\ln\frac{2}{\varepsilon} \tag{6.46}$$

where $\mathrm{N}^{\mathrm{DDG}}$ and $\mathrm{N}^{\mathrm{SDG}}$ are the number of DDGs and SDGs installed in the ADN, respectively.

Proof of Theorem 3: For the sake of brevity, let us consider an abstract representation of a linear robust optimization problem. To this end, $\mathscr{R}$ is used for the set of real numbers; N_v for the number of optimization variables; vector $\boldsymbol{x} \in \mathscr{R}^{\mathrm{N}_v}$ for the optimization variables; linear function $f(\boldsymbol{x}) \in \mathscr{R}$ for the optimization objective function; N_u for the number of uncertain parameters; vector $\mathbf{u} \in \mathscr{R}^{\mathrm{N}_u}$ for the uncertain parameters; vector $\mathbf{u}^{\max} \in \mathscr{R}^{\mathrm{N}_u}$ for the upper-limit of $\mathbf{u}$; vector $\mathbf{u}^{\min} \in \mathscr{R}^{\mathrm{N}_u}$ for the lower-limit of $\mathbf{u}$; N_c for the number of optimization constraints; linear vector-function $\mathscr{C}(\boldsymbol{x},\mathbf{u}) \in \mathscr{R}^{\mathrm{N}_c}$ for the optimization constraints. Now, a linear robust optimization problem can be mathematically stated as:

$$\min_{\boldsymbol{x}} \; f(\boldsymbol{x}) \tag{6.47}$$

subject to

$$\mathscr{C}(\boldsymbol{x},\mathbf{u}) \leq 0 \qquad \forall \mathbf{u}^{\min} \leq \mathbf{u} \leq \mathbf{u}^{\max}. \tag{6.48}$$

Due to the presence of $\mathbf{u}$ in (6.48), problem (6.47)-(6.48) encompasses an infinite number of constraints, thus, it is a semi-infinite optimization problem for which finding the solution is a formidable task [141], [142]. A computationally feasible technique to solve this robust optimization problem is to convert it to a scenario-based robust optimization problem. To this purpose, let first slightly relax its constraints and convert it to a chance-constrained optimization problem as:

$$\min_{\boldsymbol{x}} \; f(\boldsymbol{x}) \tag{6.49}$$

subject to

$$\text{Probability}\{\mathscr{C}(\boldsymbol{x},\mathbf{u}) > 0\} \leq \varepsilon \qquad \forall \mathbf{u}^{\min} \leq \mathbf{u} \leq \mathbf{u}^{\max}, \tag{6.50}$$

where $0 \leq \varepsilon \leq 1$ indicates the allowable probability of the constraints violation. In this problem, it is accepted that the optimal solution violates constraints with expected probability of less than ε for all possible realizations of $\mathbf{u}$. It is obvious that the optimal solution of the chance-constrained problem outperforms the optimal solution of its robust counterpart. However, it is notable that the chance-constrained problem (6.49)-(6.50) gets closer to its robust counterpart (6.47)-(6.48) for decreasing ε. This chance-constrained optimization problem again similar to its robust counterpart is intractable. In order to solve this problem, reference [141] devised the scenario-based robust optimization problem as:

$$\min_{\boldsymbol{x}} \; f(\boldsymbol{x}) \tag{6.51}$$

subject to

$$\mathscr{C}(\boldsymbol{x}, \mathbf{u}_s) \leq 0 \qquad\qquad \forall s \in \mathbb{S}, \tag{6.52}$$

where $\mathbf{u}_s$ is one realization of $\mathbf{u}$ and $\mathbf{u}^{\min} \leq \mathbf{u}_s \leq \mathbf{u}^{\max}$. The optimal solution of the scenario-based robust optimization problem must only satisfy the constraints for a limited number, N_s, of scenarios (i.e. realization of uncertainties). Reference [141], mathematically proved that the optimal solution of the scenario-based robust optimization problem (6.51)-(6.52) is also an optimal solution of the chance-constrained problem (6.49)-(6.50) with feasibility level $1-\varepsilon$ and confidence interval $1-\beta$, provided that:

$$\mathrm{N}_s \geq \frac{2}{\varepsilon}\ln\frac{1}{\beta} + 2\mathrm{N}_\mathrm{v} + \frac{2\mathrm{N}_\mathrm{v}}{\varepsilon}\ln\frac{2}{\varepsilon} \tag{6.53}$$

it illustrates that if the problem (6.51)-(6.52) is solved for the finite number N_s of scenarios, then, the achieved optimal solution satisfies all constraints for most of the other unseen scenarios. In other words, the explicit satisfaction of N_s scenarios automatically generalizes the satisfaction of other scenarios. Therefore, in order to solve the robust optimization problem (6.47)-(6.48) with feasibility level $1-\varepsilon$ and confidence interval $1-\beta$, it is sufficient to solve its scenario-based robust counterpart (6.51)-(6.52) while selecting N_s based on inequality (6.53).

In the scenario-based robust optimization problem (6.5)-(6.10), all optimization variables belonging to ψ can be linearly expressed based on $f_{kts}^{\mathrm{DDG,P}}$, $f_{kts}^{\mathrm{DDG,Q}}$ and $f_{hts}^{\mathrm{SDG,Q}}$. Accordingly, for this problem, N_v can be calculated as:

$$\mathrm{N}_v = 2\mathrm{N}^{\mathrm{DDG}} + \mathrm{N}^{\mathrm{SDG}}, \tag{6.54}$$

where $\mathrm{N}^{\mathrm{DDG}}$ and $\mathrm{N}^{\mathrm{SDG}}$ are the number of DDGs and SDGs installed in the ADN, respectively.

Table 6.1: Characteristics of Solar PV Generators.

Solar PV Stochastic Distributed Generators (SDGs)				
Connected to node	5	14	20	22
Nominal power (kVA)	300	350	350	300

Table 6.2: Characteristics of Wind Generators.

Wind Stochastic Distributed Generators (SDGs)			
Connected to node	11	16	26
Nominal power (kVA)	300	450	450

Table 6.3: Characteristics of Dispatchable Distributed Generators.

Dispatchable Distributed Generators				
Connected to node	3	9	17	31
Nominal power (kVA)	500	500	700	700
Minimum active power generation limit (kW)	10	10	20	20

6.9 Case Study

The modified IEEE 33-bus distribution test system [143], shown in Fig. 6.2, is utilized as the case study to derive the FPC area. The modification refers to the presence of SDGs, composed by solar PV and wind generators, and DDGs. The characteristics of solar/wind SDGs and DDGs are given in Table 6.1, Table 6.2 and Table 6.3, respectively. In line with the flexibility allocation procedure introduced in Section 6.3, it is considered that:

- The scheduling time horizon is 24 hours and refers to the next day;
- The next day consists of 24 time slots, each with duration of 1-hour;
- The FPC area of the ADN for each time slot of the next day is estimated one hour before the beginning of the next day.

The solar PV and load profiles (i.e. base case operating point), over 24 hours of study, are constructed based on real measurements from a monitored primary high-to-medium voltage substation in the south of Switzerland. Moreover, the wind profiles are extracted from [144]. All loads are assumed voltage-independent and with power factor equal to 0.95. Accordingly, the profiles of nodal active power consumption of loads for the base

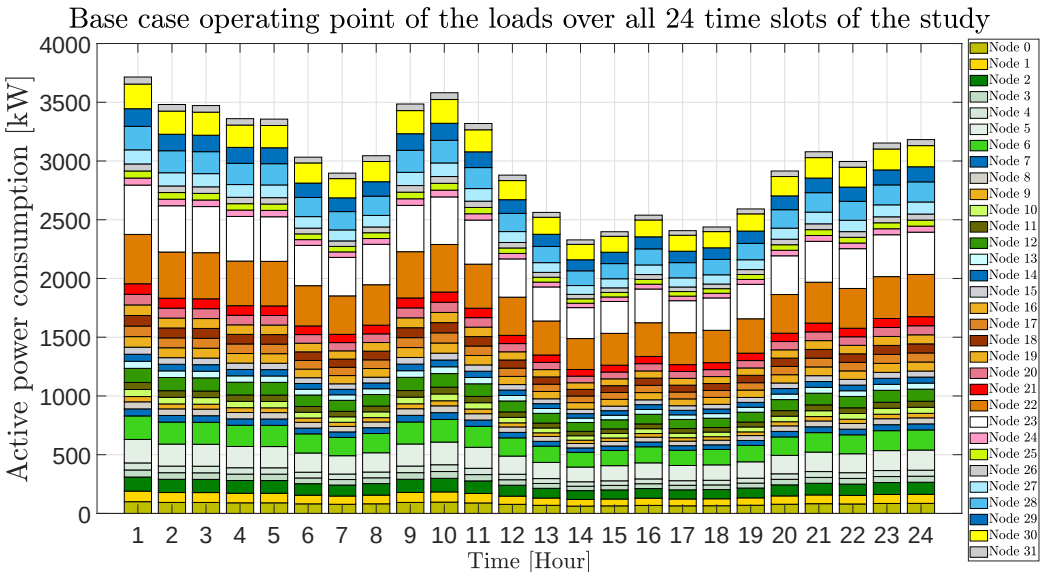

Figure 6.8: Base case operating point of the loads over all 24 time slots of the study.

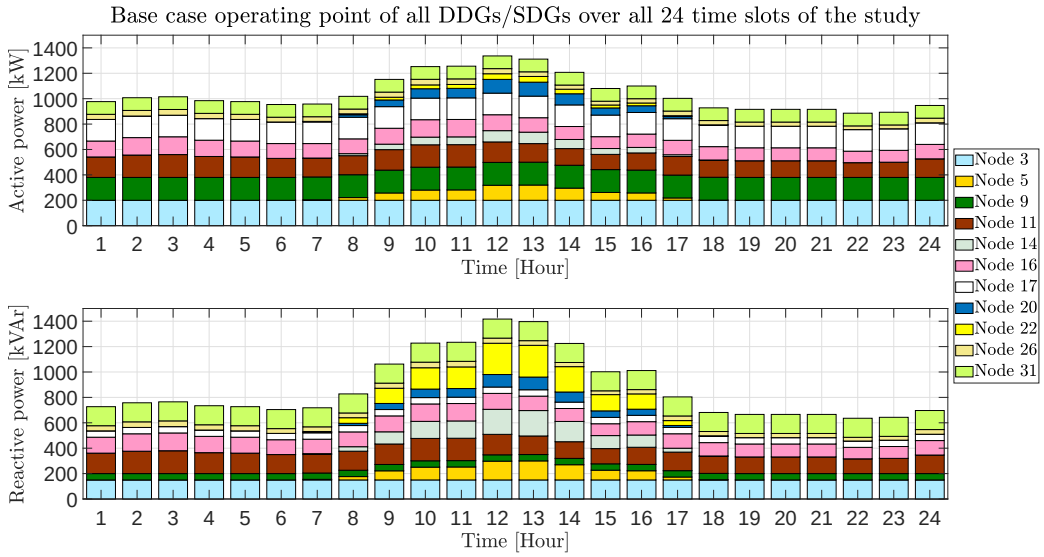

Figure 6.9: Base case operating point (active/reactive Power generation) of the DDGs & SDGs over all 24 time slots of the study.

case operating point over 24 hours of study are shown in Fig. 6.8. Injections of both SDGs and DDGs are also assumed voltage-independent. The profiles of active/reactive power generation of all distributed generators for the base case operating point (i.e. forecasted operating point) over 24 hours of study are shown in Fig. 6.9. Statutory minimum/maximum voltage limits are chosen as 0.95 pu and 1.05 pu.

It is assumed that the day-ahead forecast errors of the nodal active power consumption/generation are independent and identically distributed. The active power forecast

error of each load is sampled from a normal distribution with 0 mean and such that the standard deviation of the total load forecast error is 3% of the total load of the ADN, as in [42]. The deviation of active power generation of each SDG from its forecasted value is sampled from a normal distribution with 0 mean and such that the standard deviation of the whole system stochastic generation forecast error is 7% of the total system stochastic generation forecast, as in [19]. This approach is used to model the uncertainties. The number of scenarios, N_s, is determined based on the approach introduced in Section 6.8. To this end, the upper bound of the probability of constraint violation by the optimal solution at a random realization of the uncertainties, ε, is fixed equal to 4% with confidence level, $1-\beta$, equal to 99.99%. It should be noted that ε refers to the violation of any single constraint. Considering expression (6.53) along with $N^{DG} = 4$ and $N^{SG} = 7$, the number of scenarios should be 2904. Accordingly, N_s is slightly overestimated and defined equal to 3000.

6.10 Investigating the Performance of the Method

This sections aims to investigate the performance of the proposed method on the case study introduced in section 6.9. In this regard, the problem is modeled by using YALMIP-MATLAB [46] and solved with GUROBI [47] on a Windows based system with a 2.8 GHz Xeon CPU and 32 GB of RAM.

6.10.1 Impact of the Selected Granularity on the Estimated FPC Area

This section is intended to provide a wide perception about the impact of the selected granularity on:

- the precision of the estimated FPC area;
- the computation time of the method.

To this end, it estimates FPC area for several values of the granularity. Fig. 6.10 shows the surface the FPC area and computation time for the first time slot of the day as a function of the granularity. It shows that, by increasing the granularity, the precision of the estimated FPC area improves at the cost of a higher computation time. However, when granularity goes beyond 400 kVA, the precision of the estimated FPC area does not change considerably, while the computation time drastically increases. Therefore, in the following analysis, 400 kVA is retained as the value of granularity as it achieves a reasonable trade-off between degree of approximation and computational time. The estimated FPC areas for granularity values of 400 kVA and 100 kVA are shown in Fig. 6.11. As it can be seen, the two FPC areas are similar, thus denoting that, in this case, the lower granularity achieves a good degree of approximation.

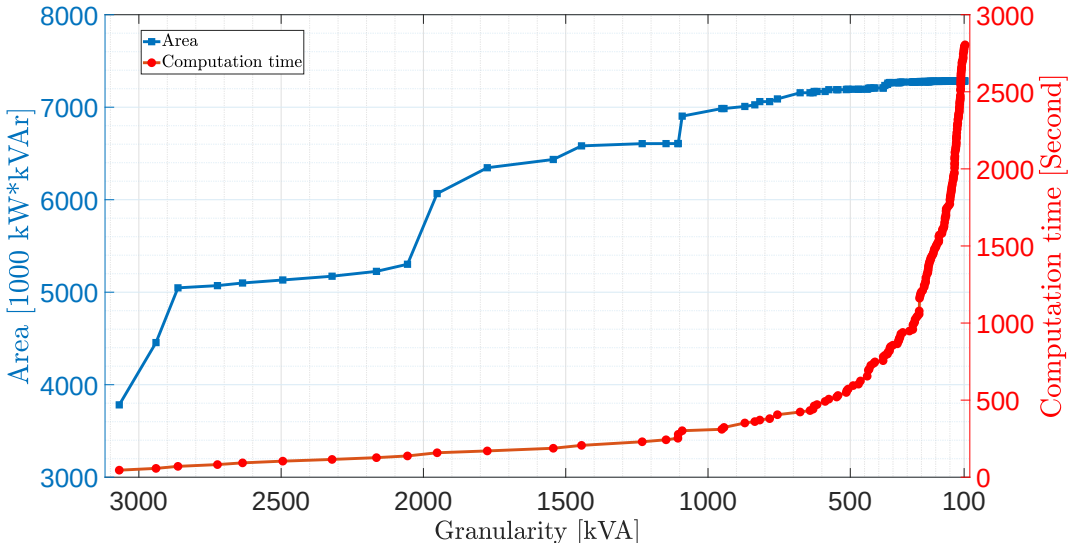

Figure 6.10: Impact of the defined granularity on the precision of the estimated FPC area and its computation time ($N_s = 3000$).

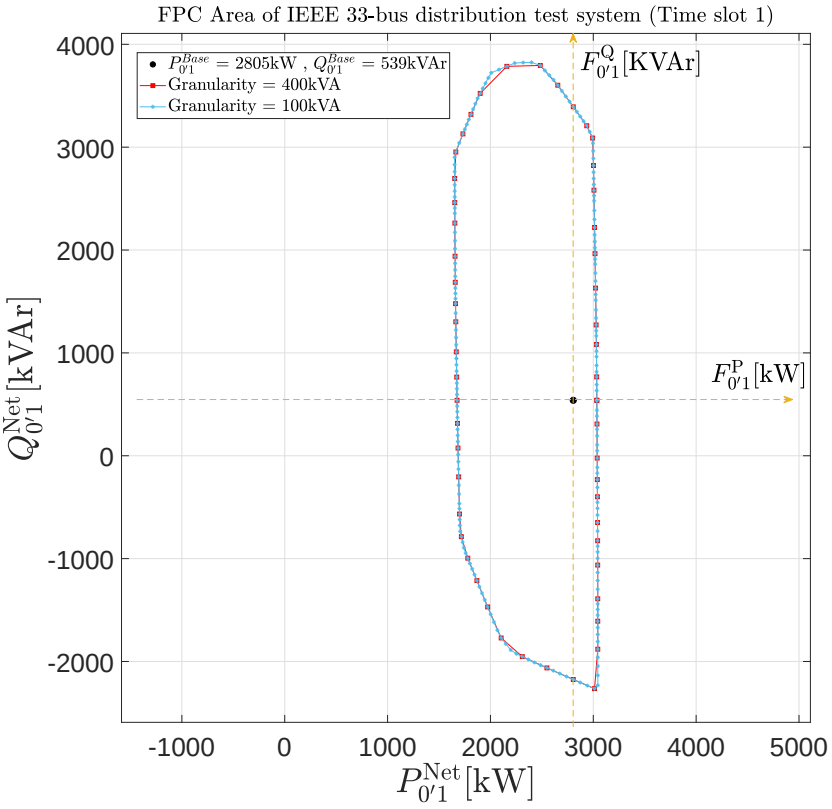

Figure 6.11: Estimated FPC area for the maximum granularity equal to 100 kVA and 400 kVA.

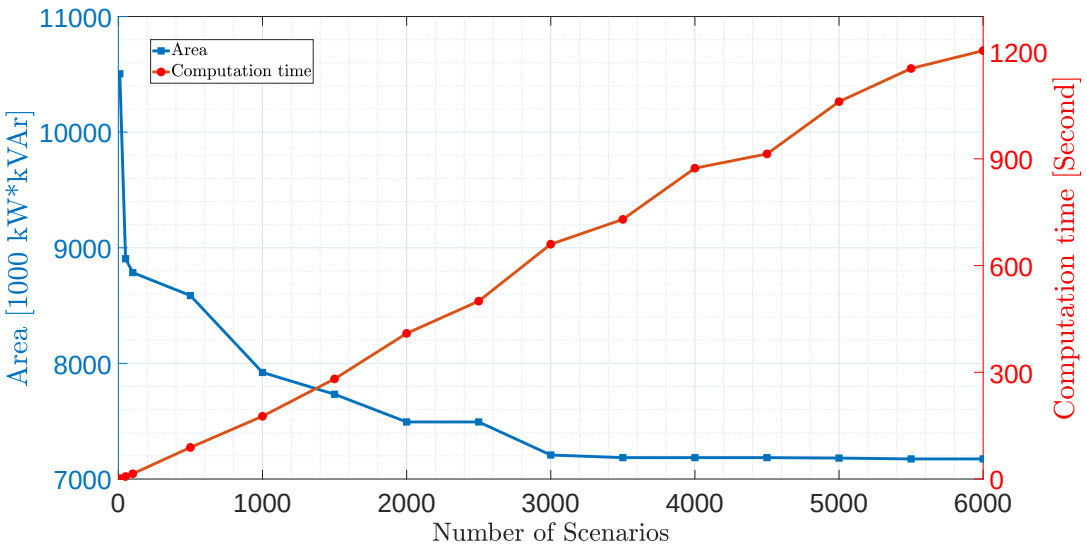

Figure 6.12: Impact of the number of selected scenarios on the precision of the estimated FPC area, and its computation time (granularity = 400 KVA).

6.10.2 Impact of the Number of Selected Scenarios on the Estimated FPC Area

The impact of the number of selected scenarios, N_s, on the precision of the estimated FPC area and on the computation time is investigated by choosing several values of N_s. Fig. 6.12 shows the surface of FPC area and computation time for the first time slot of the day as a function of N_s. It corroborates that:

- estimating the FPC area considering only a single scenario, i.e. neglecting uncertainties, leads to a FPC area which is significantly far from the one that considers uncertainties;
- by increasing N_s, the precision of the estimated FPC area improves at the cost of a higher computation time. However, when N_s goes beyond 3000, the precision of the estimated FPC area does not change significantly, whereas the computation time drastically increases.

6.10.3 Evolution over Time of the Estimated FPC Areas

The FPC areas of the ADN are estimated for all 24 time slots of study and are shown in Fig. 6.13. In this figure, the FPC areas are represented in $F^{P}_{0't}$-$F^{Q}_{0't}$ plane instead of $P^{Net}_{0't}$-$Q^{Net}_{0't}$ to better highlight the evolution of the FPC areas over the period of study. As it can be seen, the FPC areas of all time intervals have different shapes, denoting that integrating forecasting scenarios is critical to achieve an accurate representation of

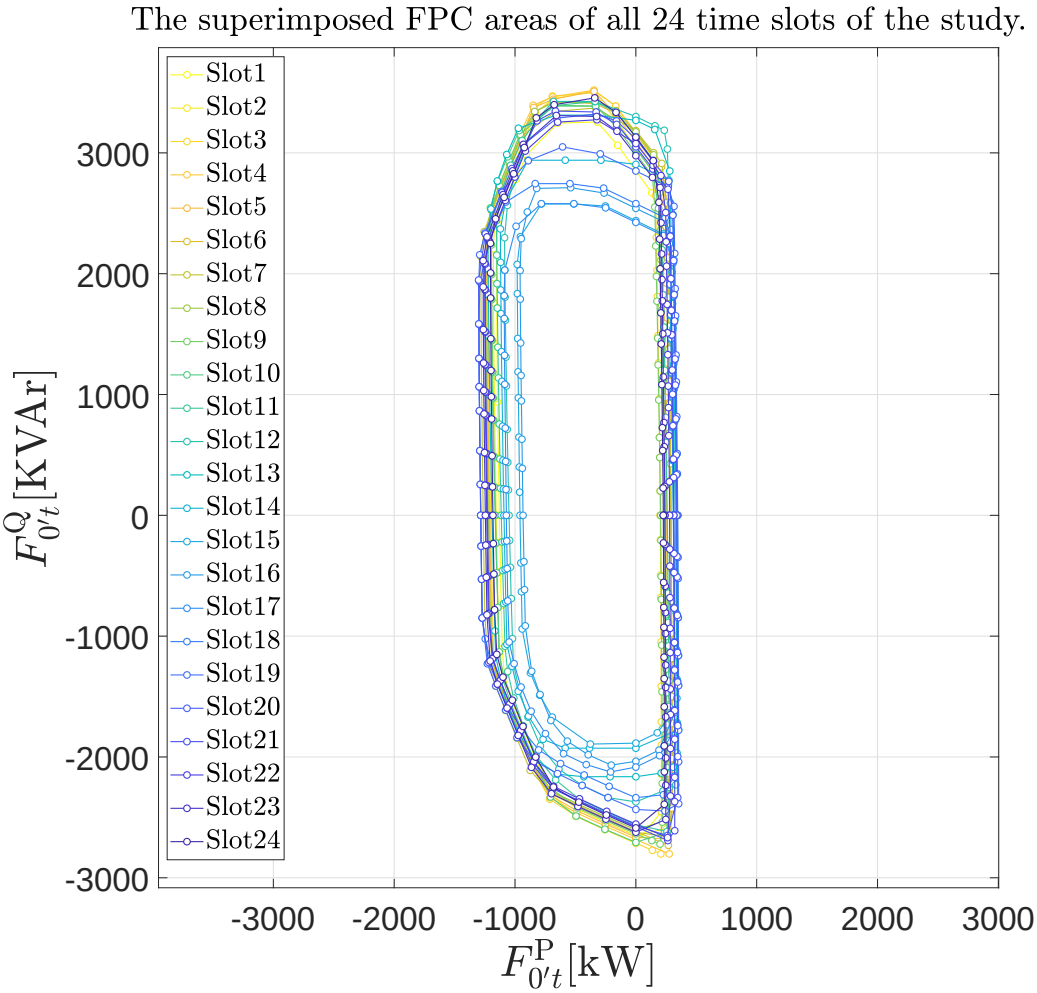

Figure 6.13: The superimposed FPC areas of all 24 time slots of the study.

the dynamic capacity of ADNs for power flexibility provision. As expected, the FPC areas shown in Fig. 6.13 are convex, therefore they can be embedded efficiently in existing convex optimization tools [145] used by operators for optimal allocation of power flexibility (reserve) without impacting on their tractability. The FPC area of each time slot is estimated in less than 500 seconds.

6.10.4 On the Feasibility of the Estimated FPC Area

The proposed method for estimating the FPC area models grid constraints using a linearized power flow model, thus, the estimated FPC area may overestimate the real one. In other words, some points belonging to the estimated FPC area may actually be infeasible operating points. In this respect, since the feasibility of all the estimated FPC area points cannot be explicitly investigated, only those suspected to be infeasible are investigated. The selected points belong to the estimated FPC curve. Actually,

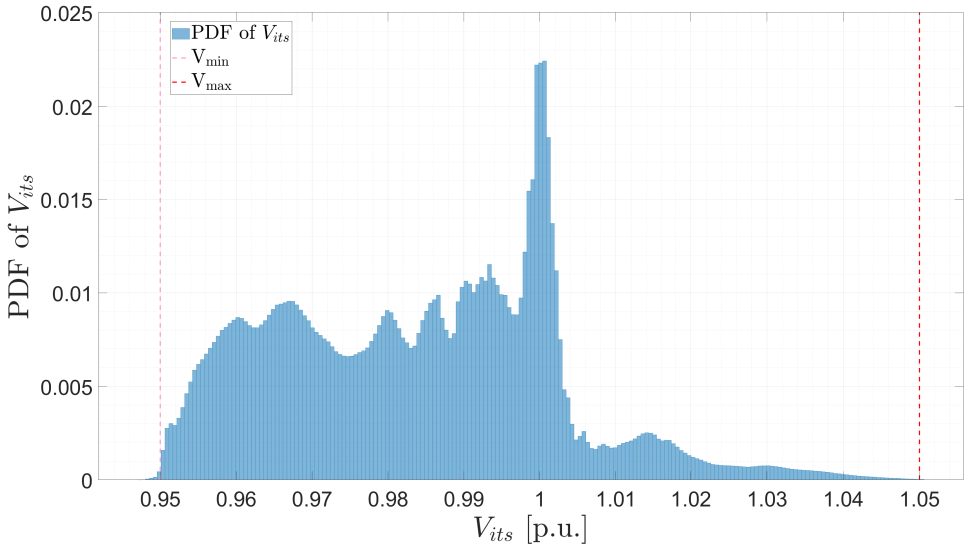

Figure 6.14: Probability density function of the voltage magnitudes of all buses (for the vertexes forming FPC curve) extracted from the AC power flow results.

we consider only the vertexes that permitted to build that curve. According to our modeling, for each of these vertexes, one or more grid/DERs constraints are activated meaning that vertex is supposed to be close to the infeasibility region. This is assumed to be a pertinent choice even if it could appear not sufficient to decide on the feasibility of all the estimated FPC area. A vertex of the FPC curve is considered feasible if the corresponding AC power flow result satisfies all grid constraints. Considering all 24 time slots and all vertexes of the FPC curves (as shown in Fig. 6.13), the probability density functions (PDFs) of the voltage magnitude of all nodes and current magnitude of all branches (extracted from the AC power flow results) can be built as shown in Fig. 6.14 and Fig. 6.15, respectively. Fig. 6.14 and Fig. 6.15 corroborate that a single voltage and current constraint were violated in less than 0.057% and 0.3% of the cases, respectively.

6.11 Conclusion

This chapter proposes a method to estimate the FPC area of an ADN for a desired time horizon while considering forecast errors, and operational constraints of the grid (i.e., nodal voltages and line currents, modeled with a linearized power flow model) and of DERs. The method consists in solving, for a certain search direction in the $F^{\mathrm{P}}_{0't}$-$F^{\mathrm{Q}}_{0't}$ plane, an optimization problem to estimate the maximum active and reactive power flexibility that the ADN can provide in that direction, allowing to establish a point of the FPC curve. The procedure is initially applied to the four main search directions (i.e., 0, 90, 180, and 270 degrees), and then repeated for angle sub-multiples until the distance between each consecutive couple of estimated points of the FPC curve is less

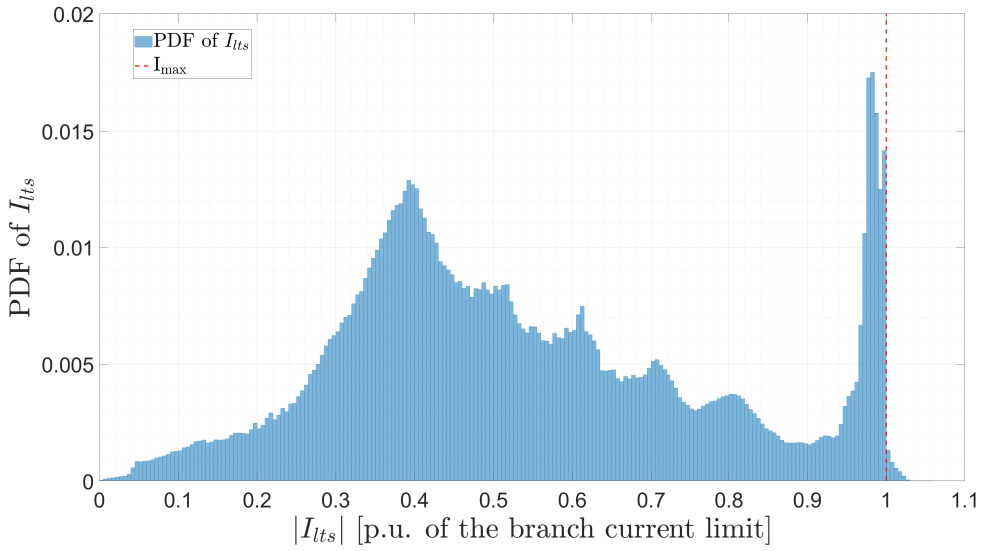

Figure 6.15: Probability density function of the current magnitude of all branches (for the vertexes forming FPC curve) extracted from the AC power flow results.

than a pre-defined granularity. The identified points are linearly interpolated and used to approximate the FPC area. It is proven that, assuming convex capabilities curves of DERs and a linearized power flow model, the estimated FPC area is feasible and convex. The optimization problem relies on a linearized grid model to represent grid constraints and forecasts scenarios to model uncertainties of loads and renewable generation. This tractable linear robust formulation achieves to estimate the FPC area efficiently while hedging against uncertainties and accounting for typical operational constraints of ADNs.

The modified IEEE 33-bus test system is used to illustrate the effectiveness and capability of the proposed method. A 24-hour time horizon with 24 time slots is chosen to estimate the FPC area. The results show that, for the considered case study, the method is able to precisely estimate the FPC area for the whole scheduling horizon in less than 600 seconds when selecting 400 kVA as the granularity level. Most notably, they show that the accuracy of the estimated FPC area, in the considered case study, does not improve when increasing the granularity to less than 400 kVA. As expected from the formulation, all estimated FPC areas are convex, thus they can be conveniently embedded in the upper-layer decision making problems without impacting tractability and convexity.

7 Coordinating Distributed Energy Resources and Utility-Scale Battery Energy Storage System for Power Flexibility Provision Under Uncertainty

> I'd put my money on the sun and solar energy. What a source of power! I hope we don't have to wait until oil and coal run out before we tackle that.
>
> — Thomas A. Edison

Relying on the power flexibility of distributed energy resources (DERs) located in an active distribution network (ADN), this ADN will be able to provide power flexibility to the upper-layer grid at their point of common coupling (PCC). In this context, this chapter presents a two-stage ADN management method to deliver, at the PCC, the power flexibility that the upper-layer grid operator would request minutes-ahead real-time operation.

The **first stage** is carried out minutes-ahead real-time operation. It updates the power set-points of DERs considering their offer curves as well as the uncertainties stem from the short-term forecast errors of demand and renewable generation profiles. The inter-temporal constraints and losses of the grid are accounted for by exploiting a linearized dynamic optimal power flow model, whereby the first stage is implemented as a linear scenario-based optimization problem.

The **second stage** is carried out during real-time operation. It relies on a linear optimization problem, thereby adjusting the power flexibility injection of a utility-scale battery energy storage system (ESS) to mitigate the imbalance at the PCC inherent in the above-mentioned uncertainties.

Finally, the performance of the proposed method is tested in the case of a real ADN located in the city of Aigle in southwest of Switzerland.

Keywords: Active distribution network (ADN), ADN management, distributed energy resources (DERs), energy storage system (ESS), power flexibility, real-time control, linear scenario-based optimization, uncertainty.

7.1 State of the Art

Grid operators deploy active & reactive power flexibility to securely steer the electric power system and supply the electricity demand of end-users. To put it simply, they leverage active & reactive power flexibility to counteract the impact of unforeseeable events and uncertainties, thereby, preserving the security of supply and respecting grid constraints.

*The **active/reactive power flexibility** can be defined as additional bi-directional active/reactive power a given resource can provide to the grid by regulating up or down its operating point, i.e. increasing or decreasing its active/reactive power consumption/generation* [17].

Continuous, economical and adequate provision of power flexibility is therefore of paramount importance and inadequate level of power flexibility might result in limited load shedding or widespread blackout.

The electric power system has been recently embracing more and more renewable energy sources (RESs) to satisfy the new environmental requirements and policies. This is giving rise to not only a surge in uncertainties stemming from forecast errors of renewable generation, but also a significant fall in the size of conventional dispatchable power plants. In other words, this transition is putting the electric power system in the situation where the size of power flexibility providers pales in comparison with the size of uncertainties. Consequently, the traditional mechanisms for power flexibility provision are no longer able to efficiently accomplish their tasks.

The proliferating number of distributed energy resources (DERs) located at active distribution networks (ADNs) [13] can be considered as an opportunity to deal with the power flexibility provision issue in the emerging architecture of the electric power system. More specifically, the potential active/reactive power flexibility of DERs can be exploited/aggregated to provide a variety of services like congestion management and frequency/voltage regulation not only to the ADN but also to the upper-layer grid [13, 17, 21, 25, 29]. In order to exchange such a flexibility between ADN and its upper-layer grid, tighter collaborations among different actors, including consumers, DER owners, transmission system operators (TSOs) and distribution system operators (DSOs), should be developed and implemented [25].

In this context, [19, 146] propose new approaches to deal with power flexibility pro-

vision at **transmission level**. The work in [146] proposes a multi-stage method for scheduling the power flexibility of various resources, including thermal units, hydro pumped-storage units and utility-scale batteries, to provide ancillary services to the transmission grid. Work in [19] takes into account the power flexibility of DERs located at distribution level and introduces a method to quantify the amount of power flexibility that the TSO requires from each DSO.

On the other hand, to deal with power flexibility provision issue at **distribution level** specifically, various DERs and ADN management schemes have been recently introduced in [147–153] to tap the potential flexibility of DERs. A real-time demand-response scheme is proposed in [147] to mitigate the voltage fluctuations in an ADN. In [148], a stochastic dynamic programming approach is developed to supply the local demand of an isolated nano grid by deploying the power flexibility of energy storage systems and dispatchable generators while considering the uncertainties of PV generation. An optimal power flow management technique is presented in [149] to provide congestion management service in an ADN. The work in [150] proposes a geometric approach to aggregate the power flexibility of thermostatically controlled loads for the purpose of frequency regulation. For day-ahead operation planning of ADNs, dynamic optimal power flow models are designed in [151] and [152] to maximize the exported power to the upper-layer grid while considering the inter-temporal constraints of energy storage systems and wind uncertainties. Work in [154] introduced a two-stage method to deal with active power uncertainties of demand and renewable energy resources at a distribution feeder. The first stage of the method dispatches (a day before the real-time grid operation) the operating point of the whole feeder at its PCC. Then, during the real-time grid operation, the second stage leverages a model predictive control strategy to control the active power injection of the battery with the purpose of minimizing deviation from the day-ahead defined set-point at the PCC of the feeder. [155] extended the work of [154] to account for grid's contrarians. An optimal inverter dispatch framework is presented in [153] that relies on the power flexibility of PVs' inverters to avoid overvoltage in ADNs while considering uncertainties of PV generation. The works in [17] and [29] introduces optimization-based methods to estimate the range of active and reactive power flexibility that an ADN can provide to the upper-layer grid at their point of common coupling (PCC) during each time slot of the next day.

7.2 Motivations

Although a variety of methods have been developed to unlock and take advantage of the power flexibility of DERs, the existing literature however lacks a framework to answer:

How much active/reactive power flexibility should each distributed energy resource

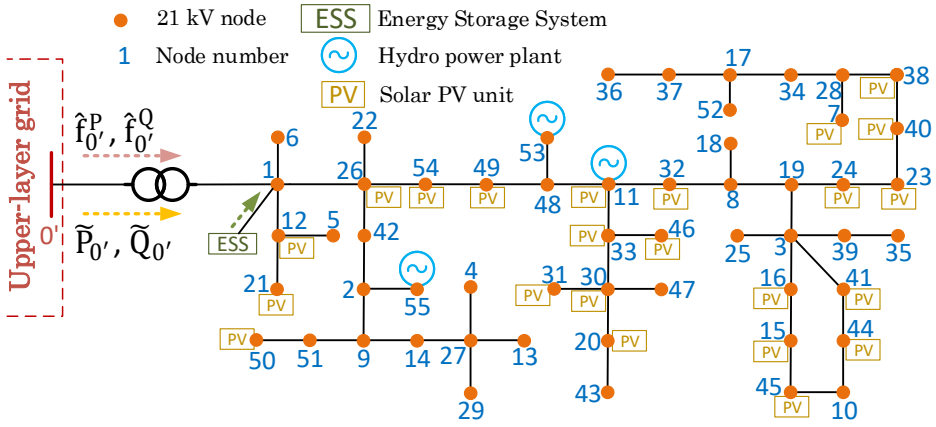

Figure 7.1: The single line diagram of an active distribution network located in Aigle (a city in southwest of Switzerland).

(DER) provide during the real-time grid operation in such a way that the ADN can provide, with minimum deviation, the minutes-ahead active/reactive power flexibility requested by the upper-layer grid at the PCC?

Based on the method [17] proposed in chapter 6, an ADN operator can offer to the upper-layer grid its FPC area (i.e. its capability for active/reactive power flexibility provision) for each time slot[1] of a specified time horizon [2]. Then, for each time slot of real time operation and a given flexibility request from the upper-layer grid, the ADN operator needs to determine then deploy the contribution[3] of each DER in order to fulfill at best that request. However, on the one hand, continuous deviations from this target are unavoidable during the time slot due to the uncertainties inherent in the demand and renewable generation. On the other hand, generally DERs do not have the capability to track automatically and continuously any quantity remotely located such as the power flexibility requested at the PCC. Therefore, to tackle these two challenges, this chapter assumes that the ADN is equipped with a battery energy storage system (ESS) connected at the root of the ADN's grid, as illustrated in Fig. 7.1. This ESS, endowed with appropriate communication and automatic control facilities, aims exclusively at absorbing as much as possible the above-mentioned deviations. Actually, the ESS does not compete with the DERs to provide flexibility to the upper-layer grid.

In view of the above, this chapter proposes a two-stage approach for providing power flexibility from an ADN to its upper layer grid. At each time slot, first the power set-points of the DERs are updated. Then, the ESS is continuously controlled to achieve the target while starting from a specific power set-point value helping to preserve its

[1] For example with 15-minute or 1-hour duration
[2] For example next day or next week
[3] Unique value for the whole time slot.

state of energy (SOE). The details of both stages are presented and illustrated in the next sections.

7.3 Problem Statement

The problem treated in this chapter can be set out focusing on a single time slot of T minutes duration as outlined in Fig. 7.2. This figure embraces three time periods:

- **Time slot**: It is a time period of T minutes duration. On the basis of the day-ahead energy market outcome, the scheduled operating point of the ADN is known and unique over each time slot (see details in Section 7.5). Moreover, the requested active/reactive power flexibility of the upper-layer grid operator is a unique value over each time slot.
- **Sub-slot**: Each time slot consists of a number of sub-slots with duration of τ_1 minutes. The first stage of the method models the trajectory of uncertainties, i.e. the forecast errors of demand and renewable generation, with time resolution of τ_1.
- **Time-interval**: Each sub-slot consists of a number of time-intervals with duration of τ_2 minutes. The second stage of the method is executed at the beginning of each time-interval.

On the basis of the day-ahead energy market outcome, the day-ahead scheduled active and reactive power flows at the PCC of the ADN, i.e. $\widetilde{P}_{0'}$ and $\widetilde{Q}_{0'}$, are known. They are of the time resolution of T minutes, i.e. a unique operating point for each time slot. Then, t_0 minutes prior to the beginning of each time slot, the upper-layer grid operator sends to the ADN operator its active/reactive power flexibility request, i.e. $\widehat{f}^{P}_{0'}$ and $\widehat{f}^{Q}_{0'}$. They are of the time resolution of T minutes, i.e. unique values for the whole time slot. These two terms form the targeted operating point at the ADN's PCC (over the coming time slot) as:

$$P^{\text{Target}}_{0'} = \widetilde{P}_{0'} + \widehat{f}^{P}_{0'}, \tag{7.1}$$

$$Q^{\text{Target}}_{0'} = \widetilde{Q}_{0'} + \widehat{f}^{Q}_{0'}, \tag{7.2}$$

This targeted operating point is followed thanks to the two-stage method introduced in this chapter:

1. **Stage 1:** it is entitled **updating the power set-points of DERs and ESS**. t_{ADN} minutes prior the beginning of each time slot, the first stage determines the new power set-points of the DERs considering their offer curves and accommodating at best the uncertainties stem from the short term forecast errors of demand and

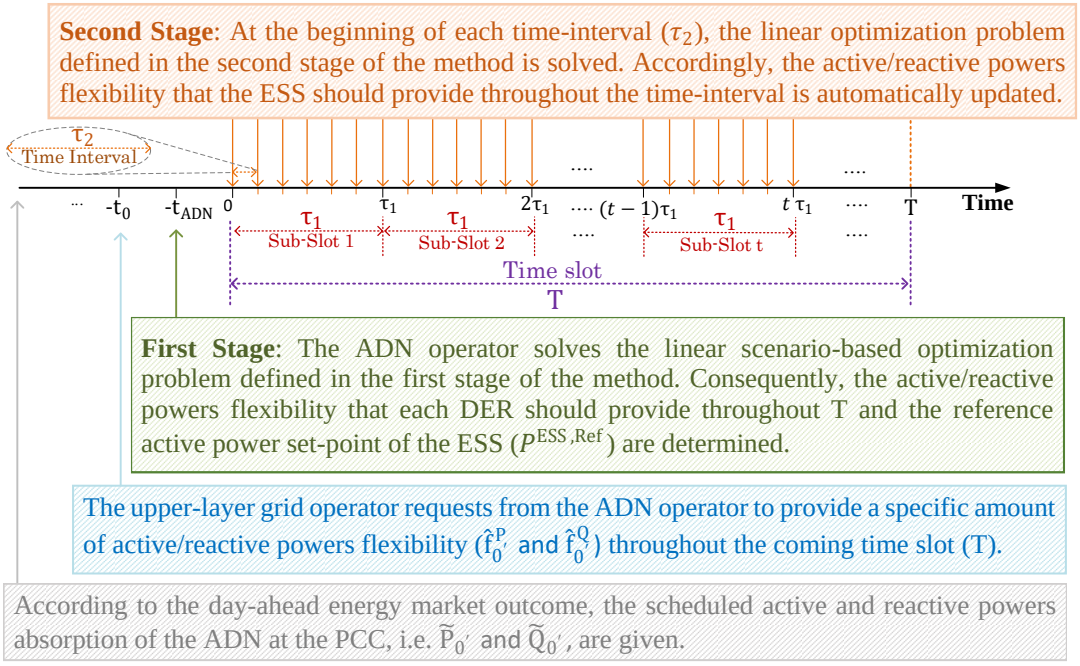

Figure 7.2: The timeline of the proposed method for a time slot.

renewable generation profiles during the time slot. Simultaneously, regarding these uncertainties, it determines a reference value [4] for the ESS power set-point. This reference value helps the ESS to achieve its task guaranteeing an appropriate SOE level during the whole time slot. The determination of all these power set-points is formulated as a linear scenario-based optimization problem where the constraints and the losses of the grid are accounted for thanks to a linearized dynamic power flow model.

2. **Stage 2:** it is entitled **EES real-time control**. Throughout the time slot, all DERs except the ESS follow their power set-points determined in the first stage. Then, to mitigate the deviations from the targeted operating point at PCC which result from the load and generation uncertainties (i.e. short-term forecast errors), this stage constructs a linear optimization problem considering the operational constraints of the ESS, whereby it adjusts the reference power set-point of the ESS determined in the first stage.

7.4 Contributions & Novelties

Original contributions of this chapter can be enumerated as:

[4] Unique value for the whole time slot.

1. It introduces a two-stage ADN management method to exploit/aggregate the power flexibility of DERs with the aim of providing an specific amount of active/reactive power flexibility to the upper-layer grid at the ADN's PCC. To the best knowledge of the author, it is the first-ever work addressing this concept.
2. It constructs linear models for the ESS's constraints, DERs'offer curves and objective function, whereby, it offers linear tractable algorithms for the first and second stages of the method.
3. Thanks to the presented linear models, it casts the first stage of the method as a scenario-based linear dynamic power flow model. In addition to the technical constraints of the grid, DERs and the ESS, this model takes into account the grid's power losses and temporal variations and uncertainties of demand/renewable generation throughout the time slot.
4. It develops a real-time control strategy for the ESS and mathematically formulates it as a linear optimization problem.
5. It is the first-ever method that divides the net power injection of the ESS into two terms to elaborately preserve the ESS's SOE as well as take advantage at most of the power flexibility of the ESS, as detailed in 7.5. The results, presented in section 7.8, highlight the advantage of this novel approach for managing the ESS's SOE.
6. It illustrates the performance of the proposed method on a real distribution network located in the city of Aigle in southwest of Switzerland.

7.5 First Stage: Updating the Power Set-Point of DERs and ESS

To preset the mathematical formulation of the first stage, let i and j be the indices for the nodes excluding the PCC node (i.e. $0'$); $\mathbb{B}$ the set of nodes excluding $0'$; t and t' the indices for the sub-slots (as depicted in Fig. 7.2); $\mathbb{T}$ the set of sub-slots belonging to time slot T; s the index for scenarios modeling the forecast errors of demand and renewable generation; $\mathbb{S}$ the set of selected credible scenarios; l the index for the branches; $\mathbb{L}$ the set of branches of the ADN; k the index for the dispatchable distributed generators (DDGs); $\mathbb{DDG}_i$ the set of DDGs connected to node i; $\mathbb{DDG}$ the set of DDGs located in the ADN; h the index for the renewable distributed generators (RDGs); $\mathbb{RDG}_i$ the set of RDGs connected to node i; $\mathbb{RDG}$ the set of RDGs located in the ADN; operator $|.|$ denotes the absolute values of its argument. Without loss of the problem's generality, it is here assumed that:

- Each DDG can take only a single power set-point over the whole time slot T;

- DDGs can provide active and reactive power flexibility, i.e. $f_k^{\mathrm{DDG,P}}$ and $f_k^{\mathrm{DDG,Q}}$, in addition to their scheduled[5] active/reactive power injections, i.e. $\widetilde{\mathrm{P}}_k^{\mathrm{DDG}}$ and $\widetilde{\mathrm{Q}}_k^{DDG}$;
- The trajectory of the forecasted[6] active power injection of the RDGs, i.e. $\widehat{\mathrm{P}}_{ht}^{\mathrm{RDG}}$, are considered with time resolution of τ_1;
- The scheduled[5] reactive power injection of RDGs, i.e. $\widetilde{\mathrm{Q}}_h^{\mathrm{RDG}}$, are assumed to be 0;
- RDGs are sources of active power uncertainties, i.e. $\Delta\mathrm{P}_{hts}^{\mathrm{RDG}}$. Thus, they might deviate from their forecasted[6] active power injection $\widehat{\mathrm{P}}_{ht}^{\mathrm{RDG}}$. However, they can provide reactive power flexibility, i.e. $f_h^{\mathrm{RDG,Q}}$ (unique value for the whole time slot);
- The trajectory of the forecasted[6] active/reactive power absorption of loads, i.e. $\widehat{\mathrm{P}}_{it}^{\mathrm{D}}$ and $\widehat{\mathrm{Q}}_{it}^{\mathrm{D}}$, are considered with time resolution of τ_1;
- Loads are sources of active/reactive power uncertainties, i.e. $\Delta\mathrm{P}_{its}^{\mathrm{D}}/\Delta\mathrm{Q}_{its}^{\mathrm{D}}$.Thus, they might deviate from their forecasted[6] active/reactive power absorption, i.e. $\widehat{\mathrm{P}}_{it}^{\mathrm{D}}/\widehat{\mathrm{Q}}_{it}^{\mathrm{D}}$;
- The forecast errors[6] of renewable generation and demand, i.e. $\Delta\mathrm{P}_{hts}^{\mathrm{RDG}}$, $\Delta\mathrm{P}_{its}^{\mathrm{D}}$ and $\Delta\mathrm{Q}_{its}^{\mathrm{D}}$ are modeled through a set of scenarios with time resolution of τ_1;
- The scheduled[5] active/reactive power injections of the ESS (connected at the root of the ADN as shown in Fig. 7.1) are 0;
- The rationale behind modeling the ESS in the first stage is to preserve its SOE, i.e. empower the ESS to provide successfully flexibility during the second stage. Since the ESS's SOE is directly affected only by its active power flexibility provision, the first stage assumes the reactive power flexibility provision of the ESS equal to zero. Therefore, the first stage determines only the net active power injection of the ESS, i.e. $\mathrm{P}_{ts}^{\mathrm{ESS,Net}}$, for each sub-slot t and scenario s. $\mathrm{P}_{ts}^{\mathrm{ESS,Net}}$ consists in the sum of two terms:

$$P_{ts}^{\mathrm{ESS,Net}} = P^{\mathrm{ESS,\ Ref}} + f_{ts}^{\mathrm{ESS,P}}, \tag{7.3}$$

  $P^{\mathrm{ESS,\ Ref}}$ indicates the reference power set-point of the ESS over the whole time slot. It is positive or negative active power that the ESS should exchange over the whole time slot to restore an adequate SOE. For each individual scenario s, $f_{ts}^{\mathrm{ESS,P}}$ indicates the final adjustment of the ESS's set-point over sub-slot t that is expected to be accomplished by the ADN operator during the second stage.

[5] which are known from the day-ahead energy market outcome.

[6] The forecast is carried out based on the most recent available data at t_0 with time resolution of τ_1.

7.5.1 Objective Function

The objective function is designed to satisfy as much as possible the targeted power flow at the PCC with minimum cost. It can be mathematically formulated as:

$$\min_{\xi} C^{\text{Imb}}_{0'} + C^{\text{ESS}} + \sum_{k\in\mathbb{DDG}} [C^{\text{DDG,P+}}_{k} + C^{\text{DDG,P-}}_{k}], \tag{7.4}$$

where ξ indicates the set of optimization variables as:

$$\begin{aligned}\xi = \{&f^{\text{DDG,P}}_{k}, f^{\text{DDG,Q}}_{k}, f^{\text{RDG,Q}}_{h}, P^{\text{ESS,Net}}_{ts}, P^{\text{ESS,Ref}}, f^{\text{ESS,P}}_{ts},\\ &P_{0'ts}, Q_{0'ts}, V_{its}, I^{\text{Real}}_{lts}, I^{\text{Imag}}_{lts}\},\end{aligned} \tag{7.5}$$

the undefined variables of (7.5) will be introduced in the rest of the section beside their corresponding constraints.

The objective function (7.4) includes three parts:

7.5.1.1 Penalizing the Imbalance of the ADN at the PCC

The active and reactive power imbalances of the ADN at the PCC are (for all t in $\mathbb{T}$ and s in $\mathbb{S}$):

$$P^{\text{Imb}}_{0'ts} = P_{0'ts} - \text{P}^{\text{Target}}_{0'}, \tag{7.6}$$

$$Q^{\text{Imb}}_{0'ts} = Q_{0'ts} - \text{Q}^{\text{Target}}_{0'}, \tag{7.7}$$

where $P_{0'ts}$ and $Q_{0'ts}$ are respectively active/reactive power flow at the PCC, as detailed in (7.32) and (7.33). The proposed method tries to follow the targeted power flow at the PCC with minimum deviations throughout the time slot. Thus, it assigns a virtual cost to the active/reactive power imbalances as:

$$C^{\text{Imb}}_{0'} = \pi^{\text{Imb,P}}_{0'} \sum_{s\in\mathbb{S}}\sum_{t\in\mathbb{T}} \left|P^{\text{Imb}}_{0'ts}\right| + \pi^{\text{Imb,Q}}_{0'} \sum_{s\in\mathbb{S}}\sum_{t\in\mathbb{T}} \left|Q^{\text{Imb}}_{0'ts}\right|, \tag{7.8}$$

where $\pi^{\text{Imb,P}}_{0'}$ and $\pi^{\text{Imb,Q}}_{0'}$ are virtual large weighting coefficients. Minimizing the nonlinear term (7.8), i.e. the first part of (7.4), has a linear equivalent counterpart as:

$$\min \pi^{\text{Imb,P}}_{0'} \sum_{s\in\mathbb{S}}\sum_{t\in\mathbb{T}} \gamma^{\text{Imb,P}}_{0'ts} + \pi^{\text{Imb,Q}}_{0'} \sum_{s\in\mathbb{S}}\sum_{t\in\mathbb{T}} \gamma^{\text{Imb,Q}}_{0'ts}, \tag{7.9}$$

subject to (for all t in $\mathbb{T}$ and s in $\mathbb{S}$):

$$-\gamma^{\text{Imb,P}}_{0'ts} \le P^{\text{Imb}}_{0'ts} \le \gamma^{\text{Imb,P}}_{0'ts}, \tag{7.10}$$

$$-\gamma^{\text{Imb,Q}}_{0'ts} \le Q^{\text{Imb}}_{0'ts} \le \gamma^{\text{Imb,Q}}_{0'ts}, \tag{7.11}$$

where $\gamma^{\text{Imb,P}}_{0'ts}$ and $\gamma^{\text{Imb,Q}}_{0'ts}$ are non-negative auxiliary variables.

7.5.1.2 Penalizing the Deployed Flexibility From the ESS

To keep at most the capability of the ESS for providing both upward and downward active power flexibility, the first stage aims to maintain the SOE close to the middle of its maximum and minimum allowed values by defining the targeted active power set-point of the ESS, i.e. $\text{P}^{\text{PESS,Target}}$, as:

$$\Delta\text{SOE}^{\text{ESS,Target}} = \text{SOE}^{\text{ESS}}_0 - \frac{\text{SOE}^{\text{ESS,Max}} + \text{SOE}^{\text{ESS,Min}}}{2}, \tag{7.12}$$

$$\text{P}^{\text{ESS,Target}} = \begin{cases} \frac{60}{\text{T}\eta^+}\ \Delta\text{SOE}^{\text{ESS,Target}} & \text{if } \Delta\text{SOE}^{\text{ESS,Target}} \leq 0 \\ \frac{60\eta^-}{\text{T}}\ \Delta\text{SOE}^{\text{ESS,Target}} & \text{if } \Delta\text{SOE}^{\text{ESS,Target}} \geq 0 \end{cases} \tag{7.13}$$

where $\text{SOE}^{\text{ESS}}_0$ is the initial[7] SOE, $\text{SOE}^{\text{ESS,Max}}$ and $\text{SOE}^{\text{ESS,Min}}$ are respectively maximum and minimum limit of the ESS's SOE. $\Delta\text{SOE}^{\text{ESS,Target}}$ is the difference between the initial SOE and the average of $\text{SOE}^{\text{ESS,Min}}$ and $\text{SOE}^{\text{ESS,Max}}$. η^+ and η^- are the charging and discharging efficiency of the ESS, respectively. Multiplier $\frac{1}{T/60}$ converts the duration of the time slot from minute to hour.

The first stage tries to minimize the required active power flexibility from the ESS during the second stage, i.e. $f^{\text{ESS,P}}_{ts}$, and to keep $\text{P}^{\text{ESS,Ref}}$ close to the targeted value $\text{P}^{\text{ESS,Target}}$. These two goals are achieved by defining the virtual cost:

$$C^{\text{ESS}} = \pi^{\text{ESS,P}} \sum_{s\in\mathbb{S}} \sum_{t\in\mathbb{T}} \left| f^{\text{ESS,P}}_{ts} \right| + \pi^{\text{ESS,SOE}} \left| P^{\text{ESS,Ref}} - \text{P}^{\text{ESS,Target}} \right| + \sum_{s\in\mathbb{S}} \sum_{t\in\mathbb{T}} \left| \gamma^{\text{ESS,Pnet}}_{ts} \right|, \tag{7.14}$$

where $\pi^{\text{ESS,P}}$ and $\pi^{\text{ESS,SOE}}$ are virtual weighting coefficients. The third term, i.e. $\gamma^{\text{ESS,Pnet}}_{ts}$, is an auxiliary variable defined to support the linear model of the evolution of the SOE over time, as detailed in (7.16), (7.19) and (7.44).

In order to prevent the power flexibility $f^{\text{ESS,P}}_{ts}$ to compete with the power flexibility from the DDGs as a contribution to the power flexibility request of the upper-layer grid operator, the weighting coefficient $\pi^{\text{ESS,P}}$ must be large in comparison with the DDG flexibility offer prices. In addition, the average of $f^{\text{ESS,P}}_{ts}$ over all scenarios is enforced to be zero, thereby:

$$\frac{1}{\text{N}_\text{s}} \sum_{s\in\mathbb{S}} f^{\text{ESS,P}}_{ts} = 0 \qquad \forall t \in \mathbb{T}, \tag{7.15}$$

[7] $\text{SOE}^{\text{ESS}}_0$ is ESS's SOE at the beginning of the time slot. $\text{SOE}^{\text{ESS}}_0$ is assumed equal to the ESS's SOE at t_{ADN}.

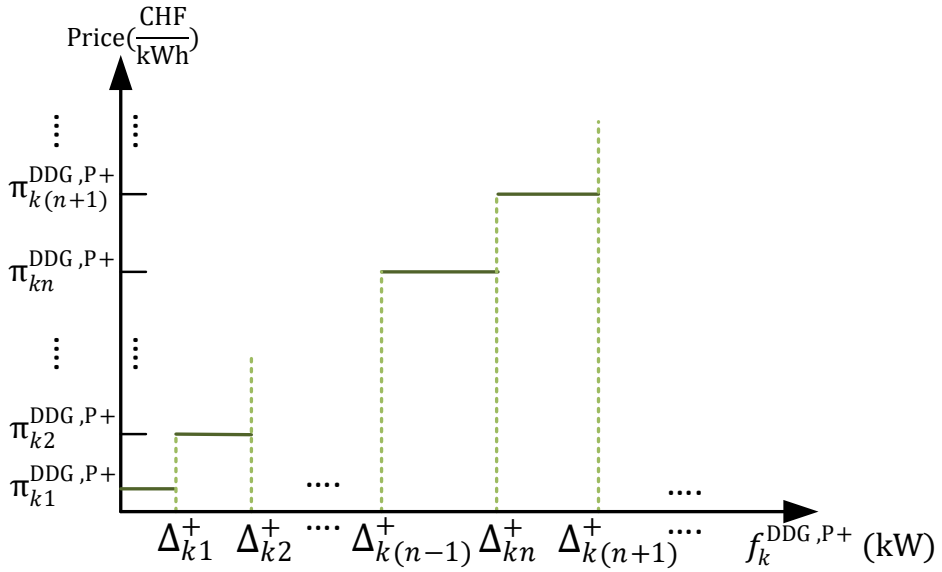

CHF, i.e. Confederation Helvetica Franc, is the currency of Switzerland.

Figure 7.3: Offer curve of DDG k for upward active power flexibility provision.

where N_s is the number of scenarios belonging to $\mathbb{S}$. This constraint helps to avoid a constant offset of $f^{\text{ESS,P}}_{ts}$ all along the whole time slot. It is notable that (7.3), (7.14) and (7.15) enforce the average of the ESS's net provided active power flexibility, i.e. $P^{\text{ESS,Net}}_{ts}$, over all scenarios to be a constant value equal to $P^{\text{ESS,Target}}$. Thus, its SOE is expected to remain close to the middle.

Minimizing the nonlinear term (7.14), i.e. the second part of (7.4), has a linear equivalent counterpart as:

$$\min \pi^{\text{ESS,P}} \sum_{s\in\mathbb{S}} \sum_{t\in\mathbb{T}} \gamma^{\text{ESS,P}}_{ts} + \pi^{\text{ESS,SOE}} \gamma^{\text{ESS,SOE}} + \sum_{s\in\mathbb{S}} \sum_{t\in\mathbb{T}} \gamma^{\text{ESS,Pnet}}_{ts}, \tag{7.16}$$

subject to (for all t in $\mathbb{T}$ and s in $\mathbb{S}$):

$$-\gamma^{\text{ESS,P}}_{ts} \le f^{\text{ESS,P}}_{ts} \le \gamma^{\text{ESS,P}}_{ts}, \tag{7.17}$$

$$-\gamma^{\text{ESS,SOE}} \le P^{\text{ESS,Ref}} - P^{\text{ESS,Target}} \le \gamma^{\text{ESS,SOE}}, \tag{7.18}$$

$$-\gamma^{\text{ESS,Pnet}}_{ts} \le P^{\text{ESS,Net}}_{ts} \le \gamma^{\text{ESS,Pnet}}_{ts}, \tag{7.19}$$

where $\gamma^{\text{ESS,P}}_{ts}$, $\gamma^{\text{ESS,SOE}}$ and $\gamma^{\text{ESS,Pnet}}_{ts}$ are non-negative auxiliary variables.

7.5.1.3 Cost of Flexibility Procurement from DERs

The provided active power flexibility of DDG k, i.e. $f_k^{\mathrm{DDG,P}}$, can be divided into two non-negative components called upward, i.e. $f_k^{\mathrm{DDG,P+}}$, and downward, i.e. $f_k^{\mathrm{DDG,P-}}$, as:

$$f_k^{\mathrm{DDG,P}} = f_k^{\mathrm{DDG,P+}} - f_k^{\mathrm{DDG,P-}} \qquad \forall k \in \mathbb{DDG}, \tag{7.20}$$

Each DDG offers its prices for the upward and downward active power flexibility provision to the ADN operator through two separate offer curves. For instance, the offer curve of DDG k for its upward active power flexibility is shown in Fig. 7.3 where n is the index for the offered blocks of DDG k; $\pi_{kn}^{\mathrm{DDG,P+}}$ is the price over the nth block; $\Delta_{k(n-1)}^{+}$ and Δ_{kn}^{+} are the beginning and the end of the nth block.

The area under the offer curve defines $C_k^{\mathrm{DDG,P+}}$ indicating the cost that the ADN operator pays to DDG k to procure $f_k^{\mathrm{DDG,P+}}$ for one hour. $C_k^{\mathrm{DDG,P+}}$ is a piece-wise linear function of $f_k^{\mathrm{DDG,P+}}$:

$$C_k^{\mathrm{DDG,P+}} = \pi_{\mathrm{kn}}^{\mathrm{DDG,P+}} f_k^{\mathrm{DDG,P+}} - \pi_{kn}^{\mathrm{DDG,P+}} \Delta_{k(n-1)}^{+} + \sum_{n'=1}^{n-1} \pi_{\mathrm{kn'}}^{\mathrm{DDG,P+}} \Delta_{kn'}^{+} \qquad \Delta_{k(n-1)}^{+} \le f_k^{\mathrm{DDG,P+}} \le \Delta_{kn}^{+}, \forall n. \tag{7.21}$$

where n' is the index for the offered blocks of DDG k. In the same way, $C_k^{\mathrm{DDG,P-}}$ can be calculated as:

$$C_k^{\mathrm{DDG,P-}} = \pi_{\mathrm{kn}}^{\mathrm{DDG,P-}} f_k^{\mathrm{DDG,P-}} - \pi_{kn}^{\mathrm{DDG,P-}} \Delta_{k(n-1)}^{-} + \sum_{n'=1}^{n-1} \pi_{\mathrm{kn'}}^{\mathrm{DDG,P-}} \Delta_{kn'}^{-} \qquad \Delta_{k(n-1)}^{-} \le f_k^{\mathrm{DDG,P-}} \le \Delta_{kn}^{-}, \forall n. \tag{7.22}$$

The third part of the objective function (7.4) aims at minimizing $C_k^{\mathrm{DDG,P+}}$ and $C_k^{\mathrm{DDG,P-}}$ which are positive increasing functions. Thus, the optimum solution entails that only one of the two variables $f_k^{DDG,P+}$ and $f_k^{\mathrm{DDG,P-}}$ can be nonzero. In other words, $f_k^{\mathrm{DDG,P+}}$ and $f_k^{\mathrm{DDG,P-}}$ are complementary variables and DDG k can provide either upward or downward active power flexibility (not both simultaneously).

The third part of (7.4), i.e. the sum of (7.21) and (7.22), is a piece-wise linear function. However, it has a linear equivalent as:

$$\min \sum_{k \in \mathbb{DDG}} \left[\gamma_k^{\mathrm{DDG,P+}} + \gamma_k^{\mathrm{DDG,P-}} \right], \tag{7.23}$$

$$\frac{\mathrm{T}}{60} C_k^{\mathrm{DDG,P+}} \le \gamma_k^{\mathrm{DDG,P+}}, \qquad \forall k \in \mathbb{DDG}, \tag{7.24}$$

$$\frac{\mathrm{T}}{60} C_k^{\mathrm{DDG,P-}} \le \gamma_k^{\mathrm{DDG,P-}}, \qquad \forall k \in \mathbb{DDG}, \tag{7.25}$$

where multiplier $\frac{\mathrm{T}}{60}$ converts the cost during an hour, i.e. $C_k^{\mathrm{DDG,P+}}$ and $C_k^{\mathrm{DDG,P-}}$, to the cost during T minutes of a time slot; $\gamma_k^{\mathrm{DDG,P+}}$ and $\gamma_k^{\mathrm{DDG,P-}}$ are non-negative auxiliary variables.

In regard to the reactive power flexibility, it is assumed that the ADN operator has long-term contracts with DERs and can procure their reactive power flexibility without any additional cost. Thus, the reactive power flexibility procurement from DDGs and RDGs causes no cost.

7.5.2 Modeling the Constraints of the Grid, DERs and ESS

This section constructs a scenario-based dynamic power flow model to model the technical constraints of the grid, DERs and the ESS. This model takes into account the grid's power losses and temporal variations and uncertainties of demand/renewable generation throughout the time slot. This model is extracted from the linearized power flow model presented in [90]. It expresses power flow at the PCC, voltage magnitudes of nodes and current phasors of all branches as linear functions of the nodal injections. As detailed in [90], the coefficients of the linear functions can be calculated in close form from the grid admittance matrix, the voltage magnitude at the PCC (slack node) and grid operating point.

The nodal active/reactive power injections at node i during sub-slot t and scenario s, i.e. P_{its} and Q_{its}, consists of two terms:

$$P_{its} = \widehat{\mathrm{P}}_{it} + \Delta P_{its} \tag{7.26}$$

$$Q_{its} = \widehat{\mathrm{Q}}_{it} + \Delta Q_{its}. \tag{7.27}$$

1. $\widehat{\mathrm{P}}_{it}/\widehat{\mathrm{Q}}_{it}$: It indicates the ***forecasted*** nodal active/reactive power injections, i.e., combination of the ***forecasted*** and/or ***scheduled*** values (for all nodes i in $\mathbb{B}$ and t in $\mathbb{T}$):

$$\widehat{\mathrm{P}}_{it} = -\widehat{\mathrm{P}}^{\mathrm{D}}_{it} + \sum_{k \in \mathbb{DDG}_i} \widetilde{\mathrm{P}}^{\mathrm{DDG}}_{k} + \sum_{h \in \mathrm{RDG}_i} \widehat{\mathrm{P}}^{\mathrm{RDG}}_{ht}, \tag{7.28}$$

$$\widehat{\mathrm{Q}}_{it} = -\widehat{\mathrm{Q}}^{\mathrm{D}}_{it} + \sum_{k \in \mathbb{DDG}_i} \widetilde{\mathrm{Q}}^{\mathrm{DDG}}_{k} + \sum_{h \in \mathbb{RDG}_i} \widetilde{\mathrm{Q}}^{\mathrm{RDG}}_{ht}, \tag{7.29}$$

2. $\Delta P_{its}/\Delta Q_{its}$: It indicates the nodal active/reactive power deviations from $\widehat{\mathrm{P}}_{it}/\widehat{\mathrm{Q}}_{it}$ (for all nodes i in $\mathbb{B}$, t in $\mathbb{T}$, and s in $\mathbb{S}$):

$$\Delta P_{its} = -\Delta P^{\mathrm{D}}_{its} + \sum_{k \in \mathbb{DDG}_i} f^{\mathrm{DDG,P}}_{k} + \sum_{h \in \mathbb{RDG}_i} \Delta \mathrm{P}^{\mathrm{RDG}}_{hts} + \mathrm{a}_{\mathrm{ESS}}\, P^{\mathrm{ESS,Net}}_{ts} \tag{7.30}$$

$$\Delta Q_{its} = -\Delta Q^{\mathrm{D}}_{its} + \sum_{k \in \mathbb{DDG}_i} f^{\mathrm{DDG,Q}}_{k} + \sum_{h \in \mathbb{RDG}_i} f^{\mathrm{RDG,Q}}_{h} \tag{7.31}$$

where $\mathrm{a}_{\mathrm{ESS}}$ is a constant parameter equal to 1 if $i = 1$ and 0 otherwise.

7.5.2.1 The Active/Reactive Power Flow at the PCC

The active (respectively reactive) power flow at the PCC[8], for all t in $\mathbb{T}$ and s in $\mathbb{S}$, can be expressed as a linear function with constant coefficients $\mathbf{P}^0_t$, $\mathbf{P}^{\mathrm{P}}_{it}$ and $\mathbf{P}^{\mathrm{Q}}_{it}$ ($\mathbf{Q}^0_t$, $\mathbf{Q}^{\mathrm{P}}_{it}$ and $\mathbf{Q}^{\mathrm{Q}}_{it}$) as:

$$P_{0't s} = \mathbf{P}^0_t + \sum_{i\in\mathbb{B}} \left(\mathbf{P}^{\mathrm{P}}_{it}\, \Delta \mathrm{P}_{its} + \mathbf{P}^{\mathrm{Q}}_{it}\, \Delta \mathrm{Q}_{its}\right), \tag{7.32}$$

$$Q_{0't s} = \mathbf{Q}^0_t + \sum_{i\in\mathbb{B}} \left(\mathbf{Q}^{\mathrm{P}}_{it}\, \Delta \mathrm{P}_{its} + \mathbf{Q}^{\mathrm{Q}}_{it}\, \Delta \mathrm{Q}_{its}\right), \tag{7.33}$$

7.5.2.2 Voltage Magnitude Constraint of the ADN nodes

The voltage magnitude of node i, for all t in $\mathbb{T}$ and s in $\mathbb{S}$, can be expressed as a linear function with constant coefficients $\mathbf{V}^0_{it}$, $\mathbf{V}^{\mathrm{P}}_{ijt}$ and $\mathbf{V}^{\mathrm{Q}}_{ijt}$:

$$V_{its} = \mathbf{V}^0_{it} + \sum_{j\in\mathbb{B}} \left(\mathbf{V}^{\mathrm{P}}_{ijt}\ \Delta P_{jts} + \mathbf{V}^{\mathrm{Q}}_{ijt}\ \Delta \mathrm{Q}_{jts}\right), \tag{7.34}$$

whereby the nodal voltage magnitude limits can be linearly expressed as:

$$\mathrm{V}^{\mathrm{Min}}_i \le V_{its} \le \mathrm{V}^{\mathrm{Max}}_i \qquad \forall i \in \mathbb{B}, \forall t \in \mathbb{T}, \forall s \in \mathbb{S}, \tag{7.35}$$

where $\mathrm{V}^{\mathrm{Min}}_i$ and $\mathrm{V}^{\mathrm{Max}}_i$ are the minimum and maximum voltage magnitude limit of node i.

7.5.2.3 Current Flow Constraint of the ADN branches

The real (respectively imaginary) part of the current phasor of branch l, for all t in $\mathbb{T}$ and s in $\mathbb{S}$, can be expressed as a linear function with constant coefficients $\mathbf{I}^{0,\mathrm{Real}}_{lt}$, $\mathbf{I}^{\mathrm{P,Real}}_{lit}$ and $\mathbf{I}^{\mathrm{Q,Real}}_{lit}$ (respectively $\mathbf{I}^{0,\mathrm{Imag}}_{lt}$, $\mathbf{I}^{\mathrm{P,Imag}}_{lit}$ and $\mathbf{I}^{\mathrm{Q,Imag}}_{lit}$):

$$I^{\mathrm{Real}}_{lts} = \mathbf{I}^{0,\mathrm{Real}}_{lt} + \sum_{i\in\mathbb{B}} \left(\mathbf{I}^{\mathrm{P,Real}}_{lit}\ \Delta P_{its} + \mathbf{I}^{\mathrm{Q,Real}}_{lit}\ \Delta Q_{its}\right), \tag{7.36}$$

$$I^{\mathrm{Imag}}_{lts} = \mathbf{I}^{0,\mathrm{Imag}}_{lt} + \sum_{i\in\mathbb{B}} \left(\mathbf{I}^{\mathrm{P,Imag}}_{lit}\ \Delta P_{its} + \mathbf{I}^{\mathrm{Q,Imag}}_{lit}\ \Delta Q_{its}\right). \tag{7.37}$$

Relying on (7.36) and (7.37), the ampacity constraint of branch l[9] can be expressed as:

$$I^{\mathrm{Real}^2}_{lts} + I^{\mathrm{Imag}^2}_{lts} \le \mathrm{I}^{\mathrm{Max}^2}_l \qquad \forall l \in \mathbb{L}, \forall t \in \mathbb{T},\ \forall s \in \mathbb{S} \tag{7.38}$$

[8] Positive active (respectively reactive) power flow means that the ADN absorbs active (respectively reactive) power from the upper-layer grid at its PCC.

[9] The maximum current flow limit of branch l is modeled for its both sending and receiving ends.

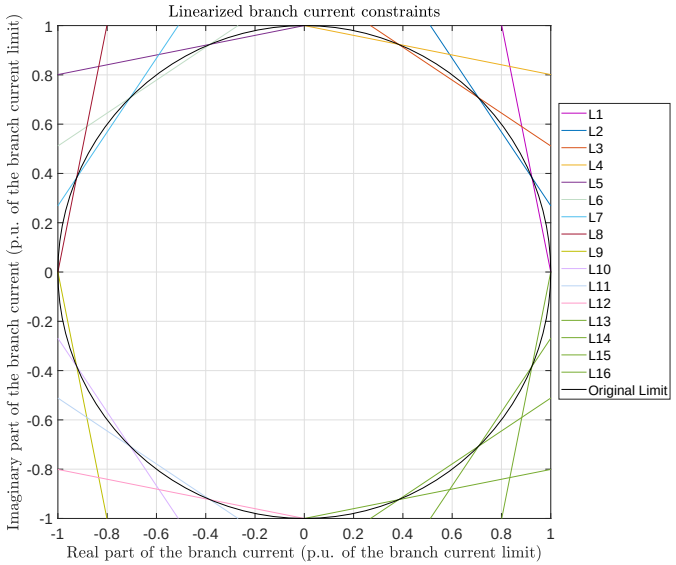

Figure 7.4: Linearized ampacity constraint of a branch.

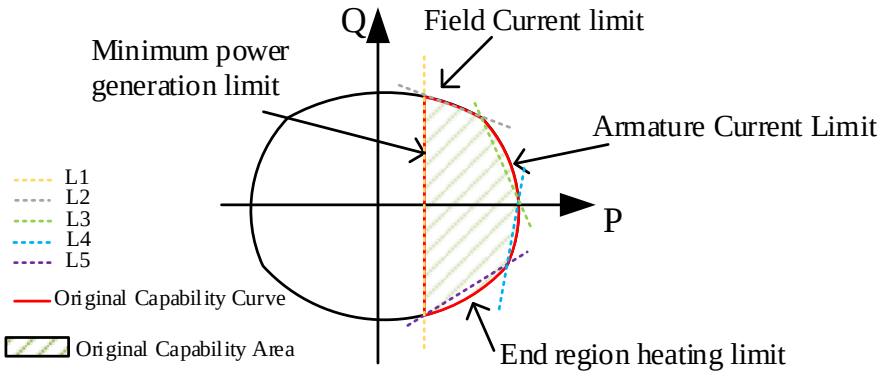

Figure 7.5: Capability area of a dispatchable generator.

where I_l^{Max} is the maximum current flow limit of branch l. As shown in Fig. 7.4, the nonlinear constraint (7.38) can be approximated as a set of linear constraints with constant coefficients $\mathbf{A}_{fl}^{\text{Real}}$, $\mathbf{A}_{fl}^{\text{Imag}}$ and $\mathbf{A}_{fl}^{0}$:

$$\mathbf{A}_{fl}^{\text{Real}} I_{lts}^{\text{Real}} + \mathbf{A}_{fl}^{\text{Imag}} I_{lts}^{\text{Imag}} \leq \mathbf{A}_{fl}^{0} \qquad \forall l \in \mathbb{L}, \forall f \in \mathbb{A}_l, \forall t \in \mathbb{T}, \ \forall s \in \mathbb{S}, \tag{7.39}$$

where $\mathbb{A}_l$ is the set of linear constraints modeling the nonlinear ampacity constraint of branch l and f is the index for those linear constraints belonging to $\mathbb{A}_l$.

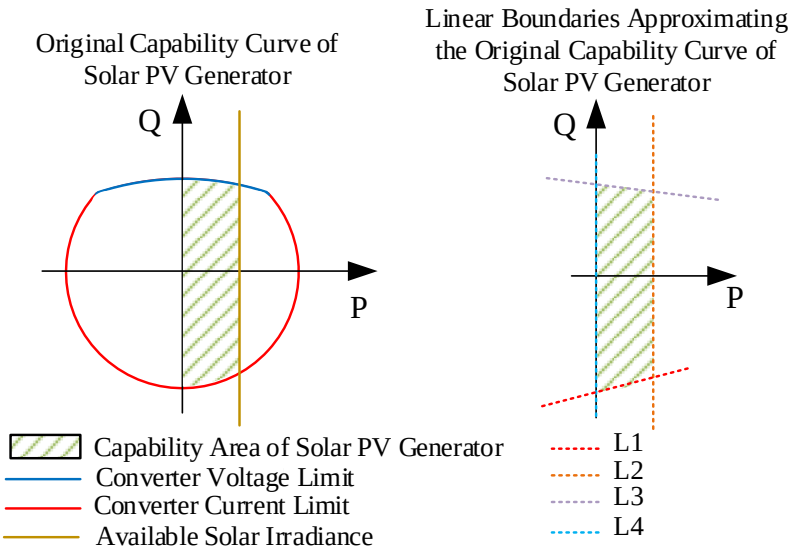

Figure 7.6: Capability area of a solar PV generator.

7.5.2.4 Modeling the Capability Area of DERs

To take advantage at most of the total available power flexibility of DERs, the proposed method considers the real nonlinear capability area of each DER and approximates it by using a set of linear boundaries, as exemplified in Fig. 7.5 and Fig. 7.6. In this way, the capability area of DDG k can be expressed as a set of linear constraints with constant coefficients $\mathbf{D}^{0}_{km}$, $\mathbf{D}^{\mathrm{P}}_{km}$ and $\mathbf{D}^{\mathrm{Q}}_{km}$ as:

$$\mathbf{D}^{0}_{km} + \mathbf{D}^{\mathrm{P}}_{km} f^{\mathrm{DDG,P}}_{k} + \mathbf{D}^{\mathrm{Q}}_{km} f^{\mathrm{DDG,Q}}_{k} \leq 0 \qquad \forall k \in \mathbb{DDG}, \forall m \in \mathbb{A}_{k}, \tag{7.40}$$

and the capability limits of RDG h can be expressed as a set of linear constraints with constant coefficients $\mathbf{R}^{0}_{hmts}$, $\mathbf{R}^{P}_{hmts}$ and $\mathbf{R}^{Q}_{hmts}$ as:

$$\mathbf{R}^{0}_{hmts} + \mathbf{R}^{\mathrm{P}}_{hmts} \Delta P^{\mathrm{RDG}}_{hts} + \mathbf{R}^{\mathrm{Q}}_{hmts} f^{\mathrm{RDG,Q}}_{h} \leq 0 \qquad \forall h \in \mathbb{RDG}, \forall m \in \mathbb{A}_{h}, \forall t \in \mathbb{T},\ \forall s \in \mathbb{S}, \tag{7.41}$$

where $\mathbb{A}_{k}$ and $\mathbb{A}_{h}$ are the sets of linear constraints modeling the nonlinear capability area of DDG k and RDG h, respectively. m is the index for the linear constraints belonging to $\mathbb{A}_{k}$ or $\mathbb{A}_{h}$.

7.5.2.5 Modeling the Constraints of the Battery ESS

The power and energy limits of the ESS can be expressed as:

$$-S^{\mathrm{ESS,Max}} \leq P^{\mathrm{ESS,Net}}_{ts} \leq S^{\mathrm{ESS,Max}} \qquad \forall t \in \mathbb{T},\ \forall s \in \mathbb{S}, \tag{7.42}$$

$$\mathrm{SOE}^{\mathrm{ESS,Min}} \leq SOE^{\mathrm{ESS}}_{ts} \leq \mathrm{SOE}^{\mathrm{ESS,Max}} \qquad \forall t \in \mathbb{T},\ \forall s \in \mathbb{S}, \tag{7.43}$$

where $S^{\text{ESS,Max}}$ is the ESS's rated power limit; SOE_{ts}^{ESS} is the ESS's SOE over sub-slot t and scenario s. The evolution of SOE_{ts}^{ESS} over time can be expressed as a linear function of $P_{ts}^{\text{ESS,Net}}$ and $\gamma_{ts}^{\text{ESS,Pnet}}$ (the auxiliary variable defined in (7.16) and (7.19) characterizing the absolute value of $P_{ts}^{\text{ESS,Net}}$) [140]:

$$\begin{aligned} SOE_{ts}^{\text{ESS}} \;=\; \text{SOE}_0^{\text{ESS}} \;+\; \frac{\tau_1}{3600}\sum_{t'=1}^{t}\eta^{+}\left[\frac{\gamma_{t's}^{\text{ESS,Pnet}} - P_{t's}^{\text{ESS,Net}}}{2}\right] - \\ -\;\frac{\tau_1}{3600}\sum_{t'=1}^{t}\frac{1}{\eta^{-}}\left[\frac{\gamma_{t's}^{\text{ESS,Pnet}} + P_{t's}^{\text{ESS,Net}}}{2}\right] \qquad \forall t\in\mathbb{T},\forall s\in\mathbb{S}. \end{aligned} \tag{7.44}$$

7.5.3 Linear Scenario-Based Optimization Problem Formulation

Thanks to the introduced equivalent linear optimization problems for all three terms of the objective function (7.4) and the presented framework for modeling the constraints of the grid, DERs and ESS, the frist stage of the method can be formulated as a linear scenario-based optimization problem:

$$\begin{aligned} \min_{\xi'}\; \pi_{0'}^{\text{Imb,P}}\sum_{s\in\mathbb{S}}\sum_{t\in\mathbb{T}}\gamma_{0'ts}^{\text{Imb,P}} \;+\; \pi_{0'}^{\text{Imb,Q}}\sum_{s\in\mathbb{S}}\sum_{t\in\mathbb{T}}\gamma_{0'ts}^{\text{Imb,Q}} \;+ \\ +\;\pi^{\text{ESS,P}}\sum_{s\in\mathbb{S}}\sum_{t\in\mathbb{T}}\gamma_{ts}^{\text{ESS,P}} \;+\; \pi^{\text{ESS,SOE}}\,\gamma^{\text{ESS,SOE}} + \\ +\;\sum_{s\in\mathbb{S}}\sum_{t\in\mathbb{T}}\gamma_{ts}^{\text{ESS,Pnet}} + \sum_{k\in\mathbb{DDG}}\left[\gamma_k^{\text{DDG,P+}} + \gamma_k^{\text{DDG,P-}}\right], \end{aligned} \tag{7.45}$$

subject to (7.3), (7.6), (7.7), (7.10), (7.11), (7.15), (7.17)-(7.19), (7.20)-(7.22), (7.24), (7.25), (7.30)-(7.37), (7.39), (7.40)-(7.44). ξ' indicates the set of optimization variables consisting of ξ, introduced in (7.5), and the auxiliary variables as:

$$\begin{aligned} \xi' = \xi \cup \{P_{0'ts}^{\text{Imb}},\, Q_{0'ts}^{\text{Imb}},\, f_k^{\text{DDG,P+}},\, f_k^{\text{DDG,P-}},\, \gamma_{0'ts}^{\text{Imb,P}},\, \gamma_{0'ts}^{\text{Imb,Q}}, \\ ,\gamma_{ts}^{\text{ESS,P}},\, \gamma^{\text{ESS, SOE}},\, \gamma_{ts}^{\text{ESS,Pnet}},\, \gamma_k^{\text{DDG,P+}},\, \gamma_k^{\text{DDG,P-}}\}, \end{aligned} \tag{7.46}$$

where operator $\cup$ calculates the union of two sets.

7.6 Second Stage: ESS Real-Time Control

The second stage of the method starts at the beginning of the time slot and lasts until the end of the time slot, as illustrated in Fig. 7.2. This stage is designated to mitigate the impact of the mismatch between the forecasted[10] consumption/generation of loads/RDGs and the realized ones on the active/reactive power imbalance at the PCC. Relying on a linear optimization problem, it controls the active/reactive power injections of the ESS to track the targeted active/reactive power flow at the PCC, i.e.

[10] The forecast carried out based on the most recent available data at t_0.

$P_{0'}^{\text{Target}}$ and $Q_{0'}^{\text{Target}}$, while respecting the operational constraints of the ESS. The outlines of the control strategy are:

1. The whole time slot is split into N_κ time-intervals with duration τ_2 and κ is the index for time-intervals.

2. The reference active power set-point of ESS during each time-interval κ can be retrieved from the value of $P^{\text{ESS, Ref}}$ determined at the first stage:

$$\widehat{\mathrm{P}}_\kappa^{\text{ESS,Ref}} = P^{\text{ESS, Ref}} \qquad \kappa = 1, ..., \mathrm{N}_\kappa, \tag{7.47}$$

3. The control strategy is executed at the beginning of each time-interval κ. The control action consists in determining and actuating the additional active and reactive power flexibility, with respect to the reference power set-point $\widehat{\mathrm{P}}_\kappa^{\text{ESS,Ref}}$, that the ESS should provide during the current time-interval κ, i.e. $f_\kappa^{\text{ESS,P}}$ and $f_\kappa^{\text{ESS,Q}}$. They are constant values over the whole time-interval κ.

4. At the beginning of the time-interval κ, the most recent realized active/reactive power flows at the PCC, i.e. $P_{0'(\kappa-1)}$ and $Q_{0'(\kappa-1)}$ are measured. Moreover, the actuated active/reactive power of the ESS, i.e. $\widehat{\mathrm{P}}_{(\kappa-1)}^{\text{ESS,Ref}} + \mathrm{f}_{(\kappa-1)}^{\text{ESS,P}}$ and $\mathrm{f}_{(\kappa-1)}^{\text{ESS,Q}}$, during the previous time-interval are known based on the outcome of the accomplished control over time-interval $\kappa - 1$. Therefore, the net realized active/reactive power absorption of the ADN excluding ESS, i.e. $\mathrm{P}_{(\kappa-1)}^{\text{ADN}}$ and $\mathrm{Q}_{(\kappa-1)}^{\text{ADN}}$ can be easily calculated as:

$$\mathrm{P}_{(\kappa-1)}^{\text{ADN}} = \mathrm{P}_{0'(\kappa-1)} + \widehat{\mathrm{P}}_{(\kappa-1)}^{\text{ESS,Ref}} + \mathrm{f}_{(\kappa-1)}^{\text{ESS,P}} \tag{7.48}$$

$$\mathrm{Q}_{(\kappa-1)}^{\text{ADN}} = \mathrm{Q}_{0'(\kappa-1)} + \mathrm{f}_{(\kappa-1)}^{\text{ESS,Q}}, \tag{7.49}$$

   whereby the net realized active/reactive power absorption of the ADN during the time-interval κ is predicted to be equal to the one realized in the former time-interval. Thus, the active/reactive power flow at PCC during the time-interval κ is predicted to be:

$$P_{0'\kappa} = \mathrm{P}_{(\kappa-1)}^{\text{ADN}} - \widehat{\mathrm{P}}_\kappa^{\text{ESS,Ref}} - f_\kappa^{\text{ESS,P}} \tag{7.50}$$

$$Q_{0'\kappa} = \mathrm{Q}_{(\kappa-1)}^{\text{ADN}} - f_\kappa^{\text{ESS,Q}}, \tag{7.51}$$

To mathematically formulate the control strategy, let us assume to be at the beginning of the time-interval κ. The control objective is to keep $P_{0'\kappa}$ and $Q_{0'\kappa}$ close to $\mathrm{P}_{0'}^{\text{Target}}$ and $\mathrm{Q}_{0'}^{\text{Target}}$, respectively. This control objective can be formulated as:

$$\min_{\psi_\kappa} \pi_{0'}^{\text{Imb,P}} \left| P_{0'\kappa} - \mathrm{P}_{0'}^{\text{Target}} \right| + \pi_{0'}^{\text{Imb,Q}} \left| Q_{0'\kappa} - \mathrm{Q}_{0'}^{\text{Target}} \right| + \gamma_\kappa^{\text{ESS,Pnet}}, \tag{7.52}$$

where $\pi_{0'}^{\text{Imb,P}}$ and $\pi_{0'}^{\text{Imb,Q}}$ are weighting coefficients; the third term, i.e. $\gamma_{\kappa}^{\text{ESS,Pnet}}$, is a non-negative auxiliary variable defined to linearly model the evolution of the SOE over time-interval κ, as detailed in (7.54), (7.57) and (7.61); ψ_{κ} indicates the set of control variables as:

$$\psi_{\kappa} = \{f_{\kappa}^{\text{ESS,P}}, f_{\kappa}^{\text{ESS,Q}}\}. \tag{7.53}$$

The nonlinear objective function (7.53) has an equivalent linear optimization problem as:

$$\min_{\psi_{\kappa}} \ \pi_{0'}^{\text{Imb,P}} \gamma_{\kappa}^{\text{Imb,P}} + \pi_{0'}^{\text{Imb,Q}} \gamma_{\kappa}^{\text{Imb,Q}} + \gamma_{\kappa}^{\text{ESS,Pnet}}, \tag{7.54}$$

subject to

$$-\gamma_{\kappa}^{\text{Imb,P}} \leq P_{0'\kappa} - \text{P}_{0'}^{\text{Target}} \leq \gamma_{\kappa}^{\text{Imb,P}} \tag{7.55}$$

$$-\gamma_{\kappa}^{\text{Imb,Q}} \leq Q_{0'\kappa} - \text{Q}_{0'}^{\text{Target}} \leq \gamma_{\kappa}^{\text{Imb,Q}} \tag{7.56}$$

$$-\gamma_{\kappa}^{\text{ESS,Pnet}} \leq \widehat{\text{P}}_{\kappa}^{\text{ESS,Ref}} + f_{\kappa}^{\text{ESS,P}} \leq \gamma_{\kappa}^{\text{ESS,Pnet}} \tag{7.57}$$

where $\gamma_{\kappa}^{\text{Imb,P}}$, $\gamma_{\kappa}^{\text{Imb,Q}}$ are non-negative auxiliary variables.

The power limit of the ESS can be expressed as:

$$(\widehat{\text{P}}_{\kappa}^{\text{ESS,Ref}} + f_{\kappa}^{\text{ESS,P}})^2 + {f_{\kappa}^{\text{ESS,Q}}}^2 \leq {\text{S}^{\text{ESS,Max}}}^2 \tag{7.58}$$

where $\text{S}^{\text{ESS,Max}}$ is the ESS's rated power limit. Similar to the approach adopted for linearizing constraint (7.38) and depicted in Fig. 7.4, the nonlinear constraint (7.58) can be expressed as a set of linear constraints with constant coefficients $\mathbf{E}_m^0$, $\mathbf{E}_m^{\text{P}}$ and $\mathbf{E}_m^{\text{Q}}$ as:

$$\mathbf{E}_m^0 + \mathbf{E}_m^P(\widehat{\text{P}}_{\kappa}^{\text{ESS,Ref}} + f_{\kappa}^{\text{ESS,P}}) + \mathbf{E}_m^{\text{Q}} f_{\kappa}^{\text{ESS,Q}} \leq 0 \qquad \forall m \in \mathbb{A}_e, \tag{7.59}$$

where $\mathbb{A}_e$ is the set of linear constraints modeling the nonlinear maximum power constraint of the ESS, m is the index for the linear constraints belonging to $\mathbb{A}_e$.

The energy limits of the ESS can be modeled as:

$$\text{SOE}^{\text{ESS,Min}} \leq SOE_{\kappa}^{\text{ESS}} \leq \text{SOE}^{\text{ESS,Max}} \tag{7.60}$$

The evolution of $SOE_{\kappa}^{\text{ESS}}$ over time-interval κ can be expressed as a linear function of $\widehat{\text{P}}_{\kappa}^{\text{ESS,Ref}}$, $f_{\kappa}^{\text{ESS,P}}$ and $\gamma_{\kappa}^{\text{ESS,Pnet}}$ (the auxiliary variable defined in (7.52), (7.54) and (7.57) characterizing the absolute value of $\widehat{\text{P}}_{\kappa}^{\text{ESS,Ref}} + f_{\kappa}^{\text{ESS,P}}$) [140]:

$$\begin{aligned} SOE_{\kappa}^{\text{ESS}} = \text{SOE}_{\kappa-1}^{\text{ESS}} &+ \frac{\tau_2}{3600}\eta^{+}\left[\frac{\gamma_{\kappa}^{\text{ESS,Pnet}} - \widehat{\text{P}}_{\kappa}^{\text{ESS,Ref}} - f_{\kappa}^{\text{ESS,P}}}{2}\right] \\ &- \frac{\tau_2}{3600}\frac{1}{\eta^{-}}\left[\frac{\gamma_{\kappa}^{\text{ESS,Pnet}} + \widehat{\text{P}}_{\kappa}^{\text{ESS,Ref}} + f_{\kappa}^{\text{ESS,P}}}{2}\right] \end{aligned} \tag{7.61}$$

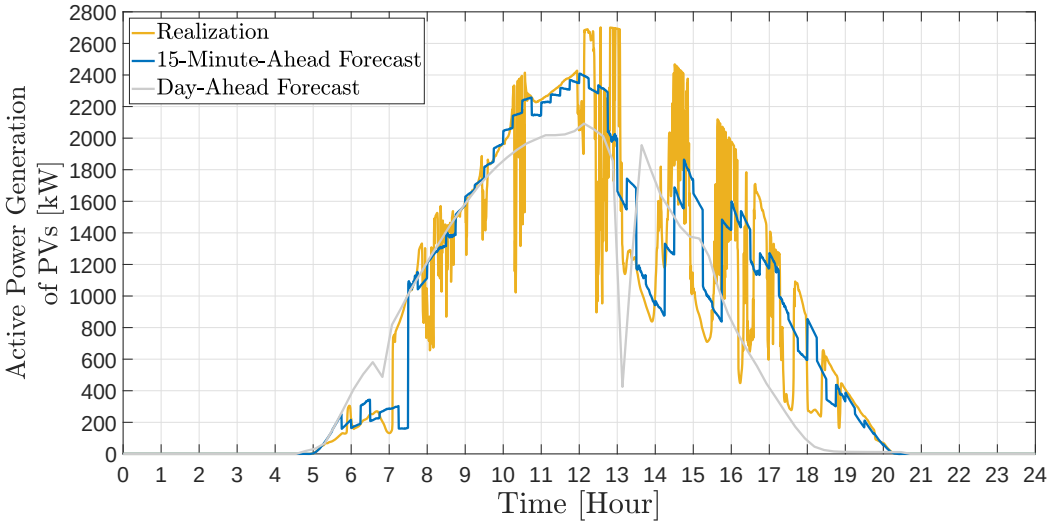

Figure 7.7: Realization vs day-ahead/15-minute ahead forecast of the net active power generation of PVs.

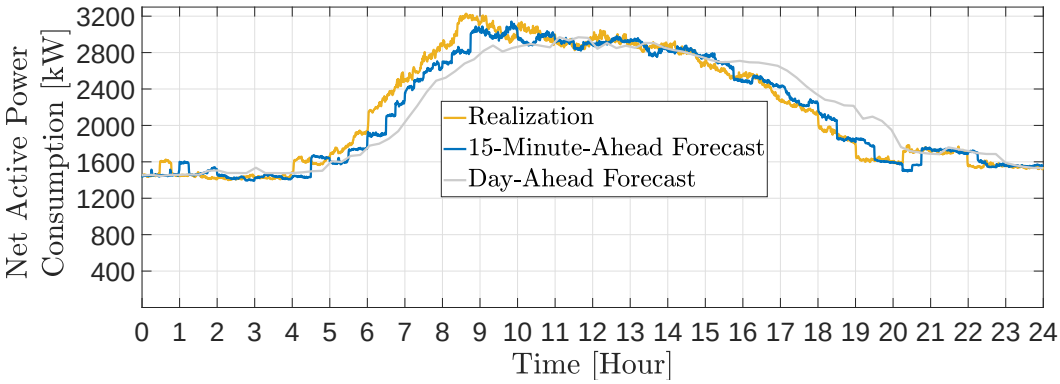

Figure 7.8: Realization vs day-ahead/15-minute ahead forecast of the net active power demand of loads.

The objective function (7.54) subject to (7.50), (7.51), (7.55)-(7.57), (7.59)-(7.61) forms a linear optimization problem whose the solution determines the final power set-point of the ESS over the time-interval κ.

7.7 Case Study

The performance of the method is validated considering the real distribution network shown in Fig. 7.1, which is located in the city of Aigle, in southwest of Switzerland. It includes 55 buses at 21 kV accommodating 2700 kWp installed solar PV units (RDGs), 2150 kW installed hydro-power units (DDGs) and a 1000 kVA/500 kWh utility-scale Lithium Titanate ESS with charging (discharging) efficiency of 94% (96%). In line with

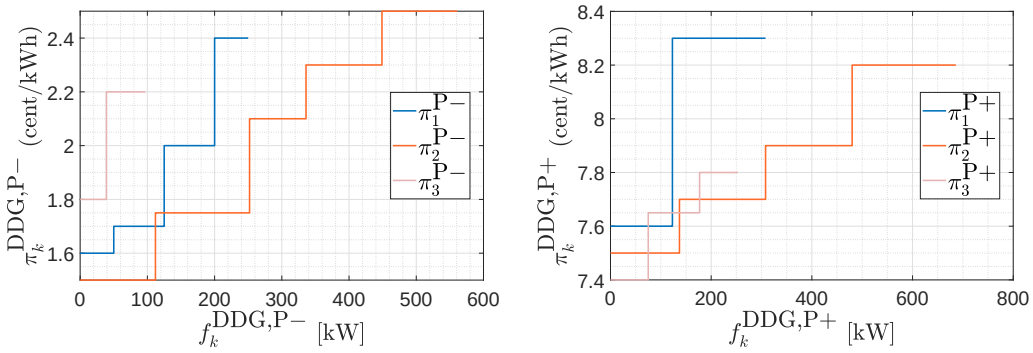

Figure 7.9: Offer curve of DDGs for active power flexibility provision.

the timeline of the problem detailed in Fig. 7.2, t_0, t_{ADN}, T, τ_1 and τ_2 are considered 15 minutes, 15 minutes, 15 minutes, 30 seconds, 1 second respectively. A particular day where the solar irradiance is very volatile is considered as 24 hours of study. Fig. 7.7 and Fig. 7.8 respectively show the net active power generation/consumption of PVs/loads throughout the day (realization vs forecasts). The k-nearest neighbors algorithm [156] is exploited to carry out the 15-minute ahead forecasts and to generate the 1000 scenarios required in the first stage of the method, i.e. $s \in \mathbb{S}$. The ESS's SOE at the beginning of the day is set to 250 kWh and the active/reactive power flexibility request of the upper-layer grid, $\widehat{f}_{0'}^{P}$ and $\widehat{f}_{0'}^{Q}$, are respectively set equal to -400 kW[11] and 0 kVAr throughout the day. Minimum and maximum of the nodal voltage magnitude limits are chosen as 0.95 p.u. and 1.05 p.u. The objective function's weighting coefficients $\pi_{0'}^{\mathrm{Imb,P}}$, $\pi_{0'}^{\mathrm{Imb,Q}}$, $\pi^{\mathrm{ESS,P}}$ and $\pi^{\mathrm{ESS,SOE}}$ are respectively assumed 100 cent/kW, 50 cent/kVAr, 30 cent/kW, 10 cent/kW, to prioritize different terms of the objective function for deploying the available local flexibility. The offer curves of DDGs are shown in Fig. 7.9, where indices 1, 2 and 3 refer to the DDGs connected to nodes 11, 53 and 55. Then, the problem is modeled by using YALMIP-MATLAB [46] and solved with GUROBI solver [47].

7.8 Investigating the Performance of the method

The performance of the method is investigated by applying it to the case study introduced in section 7.7 which corresponds to a particular day with extreme volatile solar irradiance. Fig. 7.10 shows the profiles of the targeted active power operating point, i.e. $P_{0'}^{\mathrm{Target}}$, (red curve) along with the realized active power flow at the PCC before (orange curve) and after (green curve) applying the method. For the sake of brevity, lets introduce ***difference*** as difference between the red and orange curves. ***difference***

[11] Negative active (respectively ractive) power flexibility means that the ADN absorbs less active (respectively reactive) power from the upper-layer grid at its PCC in comparison with the scheduled value, i.e. $\widetilde{P}_{0'}$ ($\widetilde{Q}_{0'}$).

is composed of the sum of two terms:

1. The requested power flexibility of the upper-layer grid.
2. The day-ahead forecast errors of demand and renewable generation.

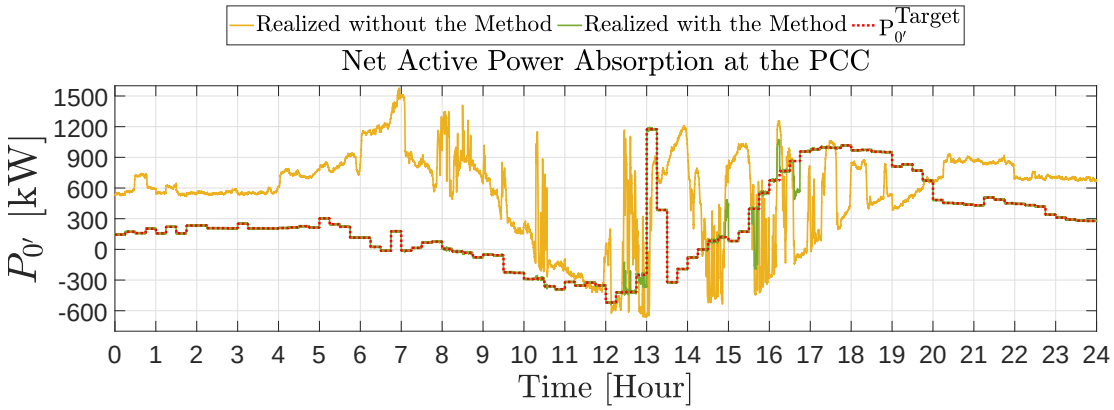

Figure 7.10: Realized active power flow at the PCC.

Due to the absence of solar irradiance, over periods (00:00 to 05:00) and (20:00 to 24:00) uncertainties result solely from the forecast error of demand leading to moderate day-ahead and 15-minute-ahead forecast errors with (average, maximum) of (60kW, 287kW) and (54kW, 224kW), respectively. Consequently, ***difference*** over these two periods embraces small volatility and mainly reflects the requested power flexibility at the PCC, thus, the ESS can accomplish its task, i.e. mitigating the impact of the 15-minute-ahead forecast errors on the imbalance at the PCC, by taking up a marginal activity as shown in Fig. 7.10. As result of this marginal activity, the ESS's SOE remains near to the middle, i.e. 250 kWh as shown in Fig. 7.11, whereby the reference active power set-point of the ESS ($P^{\text{ESS, Ref}}$) is set equal to zero over most of these two periods as shown in Fig. 7.12. Furthermore, the power flexibility of DERs is mainly procured to cover the requested power flexibility of the upper-layer grid, as shown in Fig. 7.13.

In contrast, over period (05:00 to 20:00) the uncertainties, in addition to the moderate forecast error of demand, contain extremely volatile forecast error of PVs leading to day-ahead and 15-minute-ahead forecast errors with (average, maximum) of (544kW, 2238kW) and (292kW, 1435kW), respectively. Consequently, ***difference*** over this period features an extreme volatility and the ESS plays a crucial role to mitigate the impact of the 15-minute-ahead forecast error on the imbalance at the PCC while restoring its SOE to the middle, as shown in Fig. 7.11 and Fig. 7.12.

Fig. 7.12 explicitly represents all terms defined in the first and second stages of the method to appropriately operate the ESS. $\text{P}^{\text{ESS,Target}}$ is a constant parameter (over each time slot) defined in the first stage and is responsible for restoring the ESS's SOE to the middle. As it can be seen in Fig. 7.12, the first stage sets $P^{\text{ESS, Ref}}$ equal to $\text{P}^{\text{ESS,Target}}$

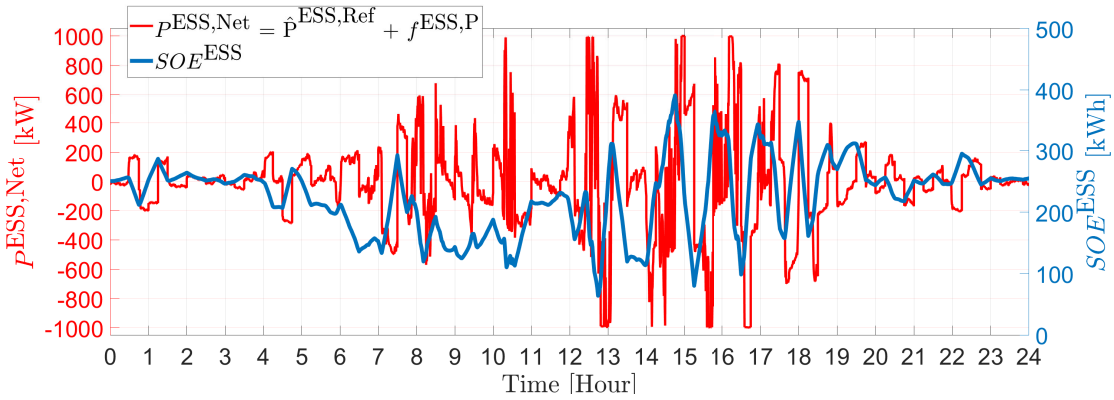

Figure 7.11: Evolution of the ESS's SOE/net power injection throughout the day.

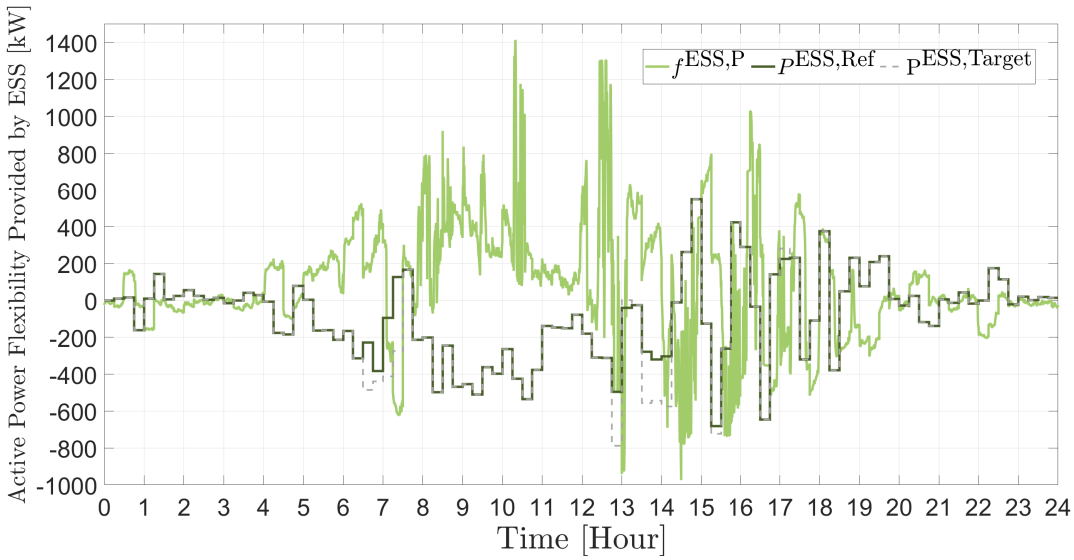

Figure 7.12: The ESS's reference power set-point (1^{st} Stage) and the ESS's targeted active power set-point (1^{st} Stage) along with the final adjustment of active power set-point of the ESS during the 2^{nd} stage.

over all time slots except for the time slots where there is a lack of local active power flexibility. In other words, the total available flexibility of DDGs cannot satisfy the flexibility demand:

$$\sum_{k \in \mathbb{DDG}} f_k^{DDG,P} < -P^{ESS,Target} - \hat{f}_{0'}^{P} \tag{7.62}$$

It should be noted that:

- positive value of $f_k^{DDG,P}$ means that DDG k injects active power flexibility to the grid.

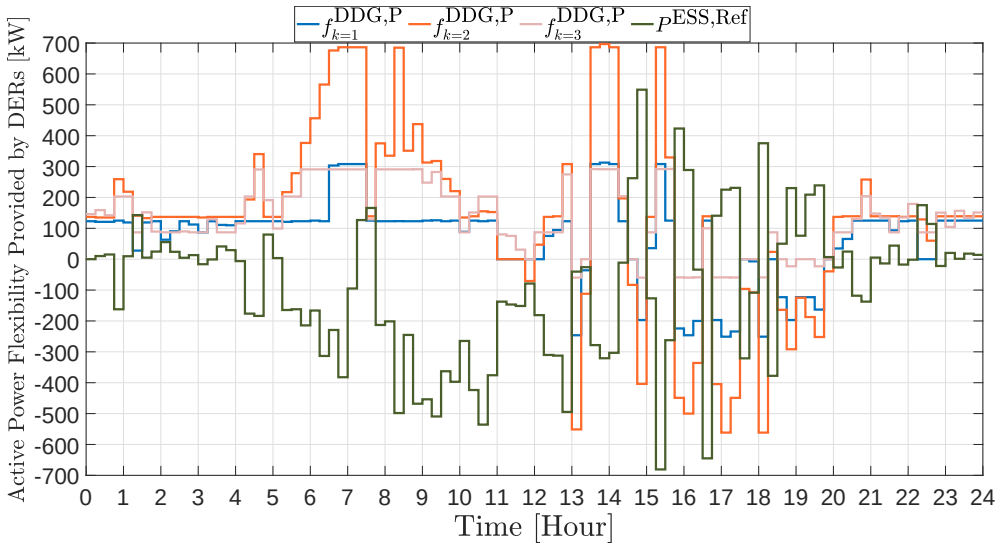

Figure 7.13: Provided active power flexibility of the DDGs along with the determined reference active power set-point of the ESS.

- positive value of $P^{ESS,Target}$ means the targeted active power set-point of the ESS is intended to make the ESS inject active power to the grid.
- positive value of $\widehat{f}^{P}_{0'}$ means that the ADN absorbs more active power from the upper-layer grid at its PCC in comparison with the scheduled value, i.e. $\widetilde{P}_{0'}$.

In addition to $P^{ESS,\ Ref}$ and $P^{ESS,Target}$, Fig. 7.12 illustrates the final adjustment of the active power set-point of the ESS during the second stage, i.e. $f^{ESS,P}$. It is worth mentioning that $P^{ESS,\ Ref}$ and $P^{ESS,Target}$ are of the time resolution of T = 15min, thereby having a unique value over each time slot T = 15min. However, $f^{ESS,P}$ is of the time resolution of τ_2 = 1Sec, thereby having a unique value over each time-interval τ_2 = 1Sec. The sum of $P^{ESS,\ Ref}$ and $f^{ESS,P}$ forms the ESS's net active power injection, i.e. $P^{ESS,Net}$, which directly affects the ESS's SOE, i.e. SOE^{ESS}. Fig. 7.11 simultaneously illustrates the amount of $P^{ESS,Net}$ and SOE^{ESS} throughout the day.

Fig. 7.13 illustrates how the active power flexibility of DERs (i.e. $\sum_{k\in\mathbb{DDG}} f_k^{DDG,P}$) are procured for the purpose of 1-satisfying the requested active power flexibility of the upper-layer grid (i.e. $\widehat{f}^{P}_{0'}$) as well as 2-helping the ESS to restore its SOE to the middle (i.e. $P^{ESS,\ Ref}$).

Fig. 7.14 illustrates the realized reactive power flow at the PCC. Thanks to the active/reactive power flexibility provided by all DERs (shown in Fig. 7.13 and Fig. 7.15), the method succeeds to track the targeted active/reactive power flow at the PCC ($P^{Target}_{0'}$, $Q^{Target}_{0'}$) with average accuracy of (98.14%, 99.99%) throughout 24 hours of study.

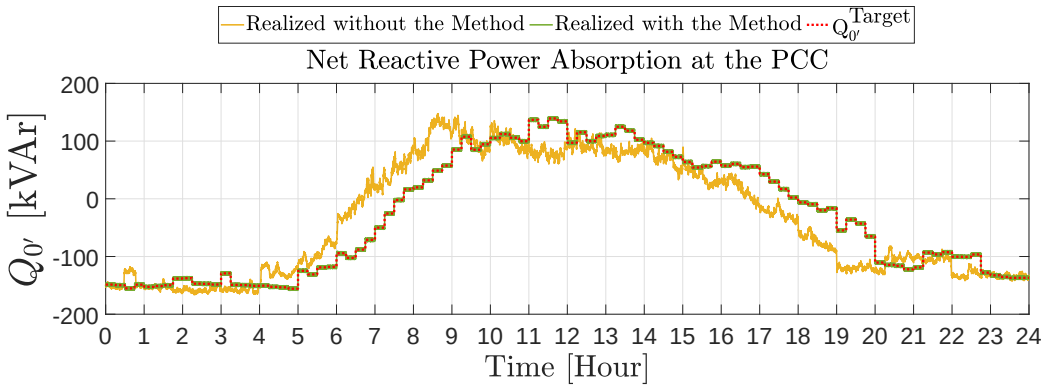

Figure 7.14: Realized reactive power flow at the PCC.

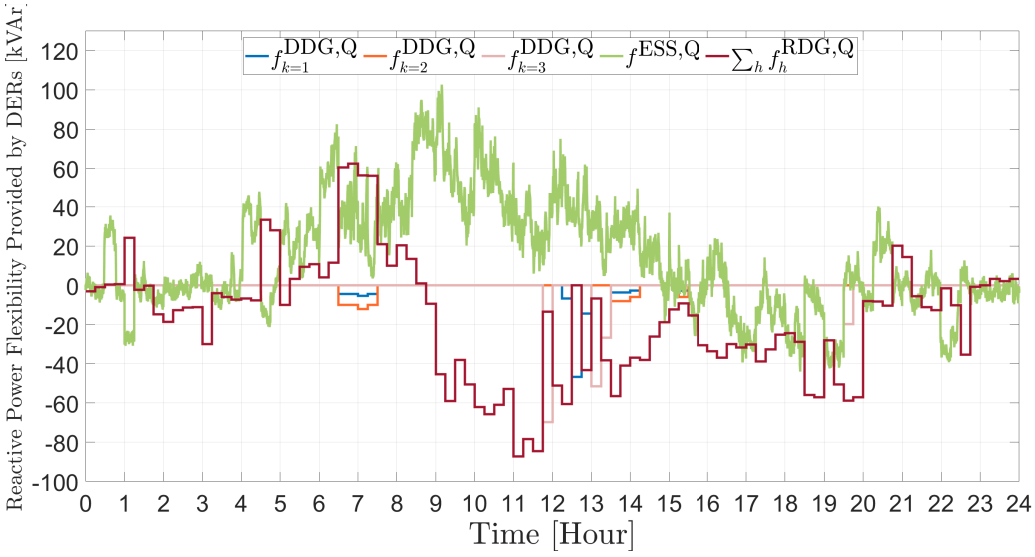

Figure 7.15: Provided reactive power flexibility of the DDGs and ESS.

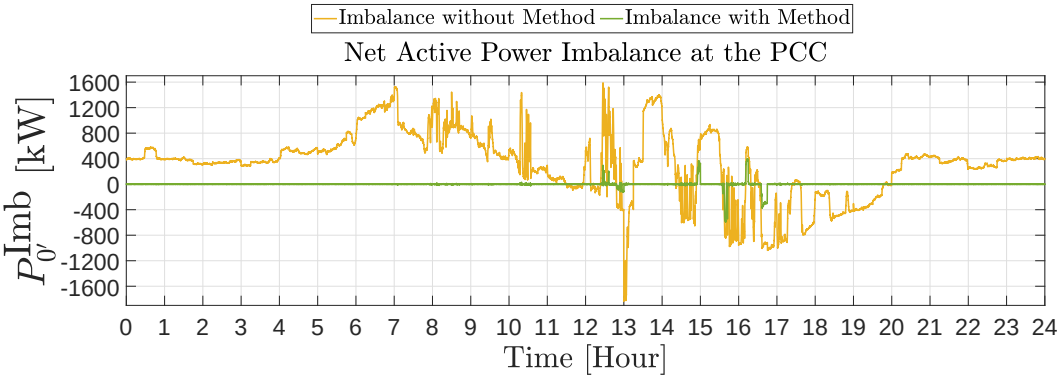

Figure 7.16: Realized active power imbalance at the PCC.

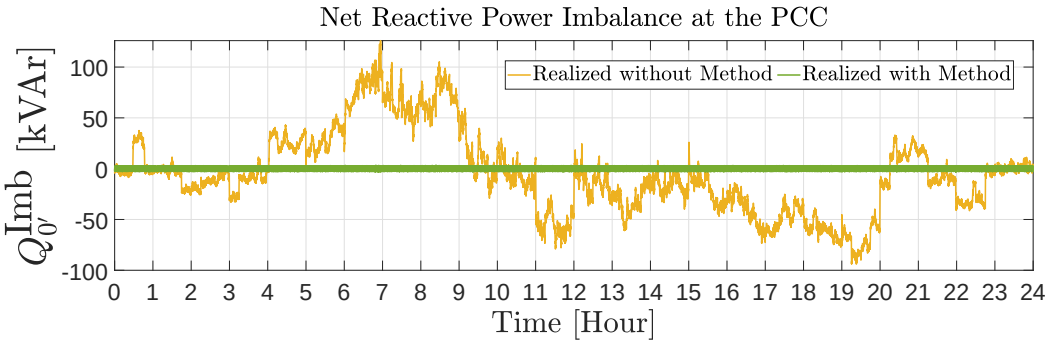

Figure 7.17: Realized reactive power imbalance at the PCC.

7.8.1 Statistical Analysis of the Active/Reactive Power Imbalance at the PCC

Fig. 7.16 and Fig. 7.17 respectively illustrate the profiles of the active and reactive power imbalance at the PCC, i.e $P^{\text{Imb}}_{0'}$ and $Q^{\text{Imb}}_{0'}$, before (orange curve) and after (green curve) applying the method. The active (respectively reactive) power imbalance at the PCC can be easily computed by subtracting the targeted active (respectively reactive) power flow at the PCC from the realized active (respectively reactive) power flow at the PCC, as mathematically stated in 7.7 (respectively 7.8).

Fig. 7.16 reveals that the active power imbalance at the PCC is almost negligible for the most part of the day. To provide precise details about the active power imbalance at the PCC, Fig. 7.18 shows the probability distribution function (PDF) as well as cumulative density function (CDF) of the active power imbalance at the PCC. The former is represented via blue bars while the latter is represented via a red curve. They reveal that the active power imbalance at the PCC is less than 10 kW over 96.64% of the day, i.e. 23 hours and 12 minutes. Furthermore, the PDF and consequently CDF of $P^{\text{Imb}}_{0'}$ are symmetrical. It empirically bears testimony to the fact that the method tracks the targeted active power set-point at the PCC with slight and unbiased error.

Fig. 7.17 reveals that the reactive power imbalance at the PCC is virtually zero throughout the day. To statistically prove it, PDF (blue bars) and CDF (red curve) of the reactive power imbalance at the PCC is represented in Fig. 7.19. It concretely discloses that the reactive power imbalance at the PCC is less than 5 kVAr over the whole day. Most notably, the PDF and consequently CDF of $Q^{\text{Imb}}_{0'}$ are symmetrical. It empirically proves that the method tracks the targeted reactive power set-point at the PCC with slight and unbiased error.

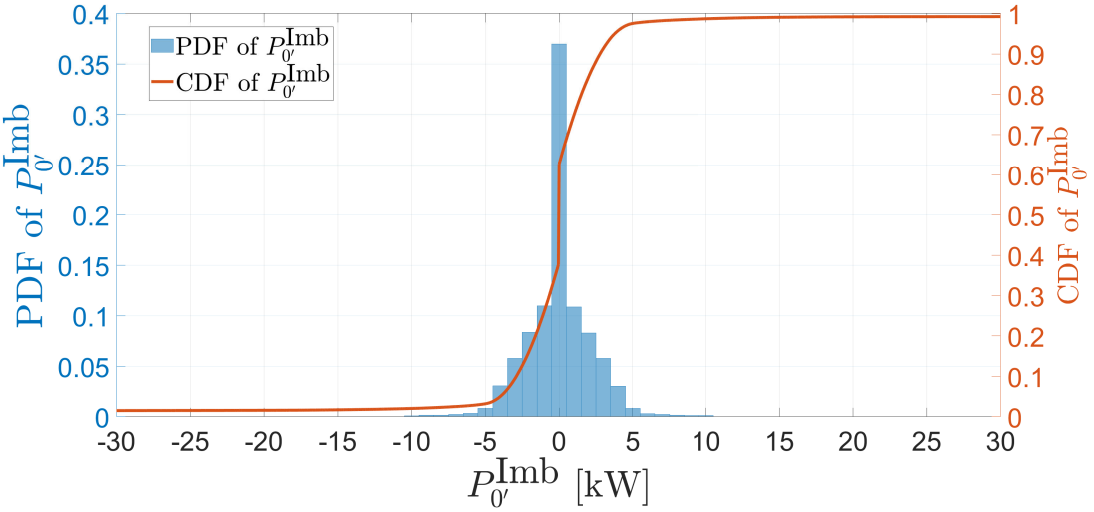

Figure 7.18: Probability/Cumulative density function of the active power imbalance at the PCC.

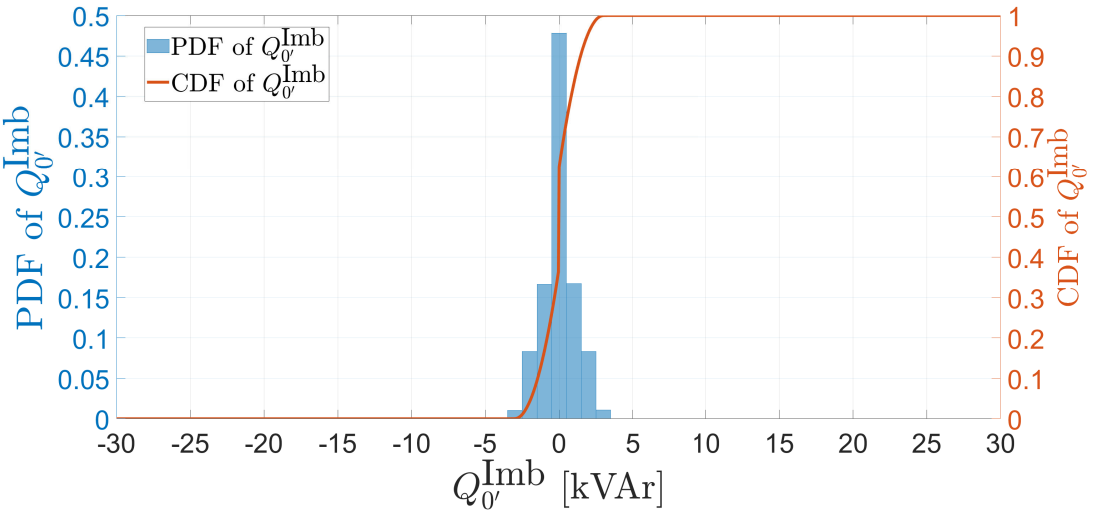

Figure 7.19: Probability/Cumulative density functions of the reactive power imbalance at the PCC.

7.8.2 Investigating the Computation Burden of the Method

It is worth mentioning that the computation time of the first stage (for each time slot) and the second stage (for each time-interval) of the method are 8.79 sec and 3.1 msec, respectively. This privileged feature of the method is achieved thanks to the linear tractable formulations presented for both stages of the method. The tractability and agility of the method make it an applicable solution even for larger real-world distribution networks.

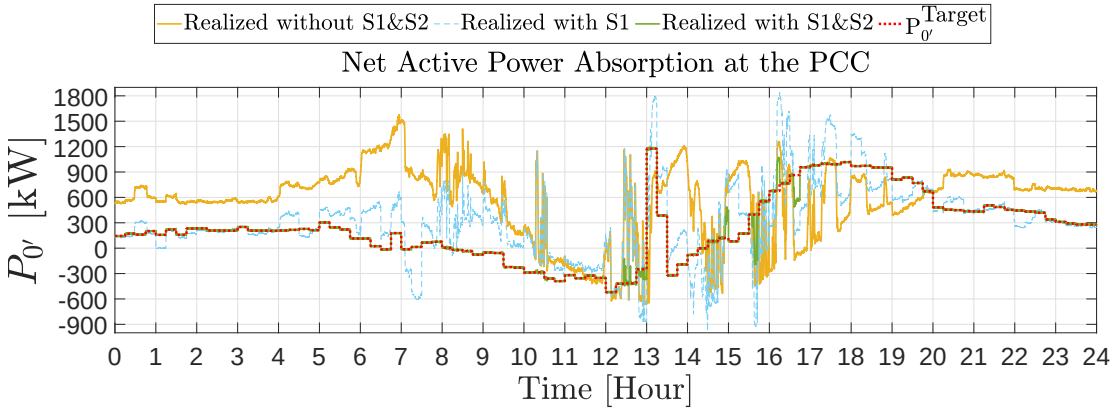

Figure 7.20: Realized active power flow at the PCC after applying first and second stages.

7.8.3 Investigating the Performance of Each Stage Individually

This section unfolds Fig. 7.10 and Fig. 7.14 to set out the role and performance of each stage individually, as shown in Fig. 7.20 and Fig. 7.21[12]. These two figures embrace 4 profiles:

1. **Red curve:** Profile of the targeted active/reactive power flow at the PCC, i.e. $P_{0'}^{Target}/Q_{0'}^{Target}$.
2. **Orange curve:** Profile of the realized active/reactive power flow at the PCC before applying the first and second stages.
3. **Blue curve:** Profile of the realized active/reactive power flow at the PCC after applying the first stage.
4. **Green curve:** Profile of the realized active/reactive power flow at the PCC after applying the first and second stages.

For the sake of brevity, lets introduce ***difference without S1&S2*** as difference between the red and orange curves. ***difference without S1&S2*** is formed of the sum of two terms:

1. The requested power flexibility of the upper-layer grid.
2. The day-ahead forecast errors of demand and renewable generation.

First Stage:
The first stage of the method is executed at $t_0 = -15$min where the exact consumption/ generation of loads/renewable generation are not known. The first stage, therefore, has

[12] In Fig. 7.20 and Fig. 7.21, S1 and S2 stand for the first and second stages, respectively.

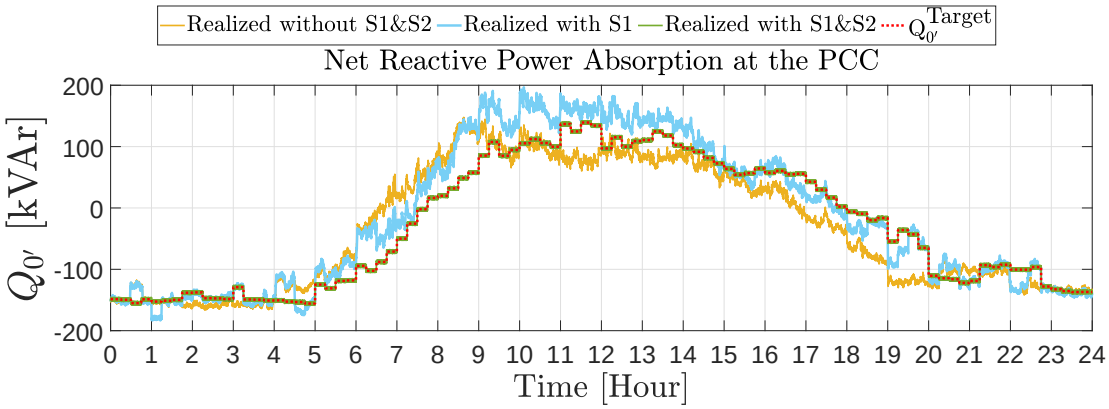

Figure 7.21: Realized reactive power flow at the PCC after applying first and second stages.

to rely on the most recent available data, i.e. the forecasts carried out at $t_0 = -15$min. As a consequence, the first stage perceives the day-ahead forecast errors of demand and renewable generation as difference between the day-ahead and 15-minute-ahead forecasts. Given this fact, the first stage updates the set-points of DERs to fully cancel out ***difference without S1&S2*** as well as restore the ESS's SOE. Throughout the time slot, the DERs follow their updated set-point, as a consequence ***difference without S1&S2*** shrinks to ***difference with S1*** which corresponds to the difference between the red and blue curves. As a general rule, the accuracy of the 15-minute-ahead forecasts are higher than those of the day-ahead forecasts, therefore, it is expected that ***difference with S1*** stays largely smaller than ***difference without S1&S2***, as it can be seen in Fig. 7.20 and Fig. 7.21.

Second Stage:
The second stage of the method is carried out during the real-time operation (at the beginning of each time-interval) where the actual consumption/generation of the loads/renewable generation are realized and the DERs follow their set-points determined in the first stage (15 minutes prior to the beginning of the time slot). This stage adjusts the active/reactive power flexibility injections of the ESS to mitigate the deviations from the targeted operating point ($P_{0'}^{Target}/Q_{0'}^{Target}$). To put it simply, the second stage tries to cancel out the impact of 15-minute-ahead forecast errors on the imbalance at the PCC.

7.8.4 Investigating the Capability Area of DERs in P-Q Plane

The method, presented in this chapter, considers the real nonlinear capability area of each DER and approximates it by using a set of linear boundaries. In this way, it tries to take advantage at most of the total available power flexibility of DERs. In this context, Fig. 7.22 and Fig. 7.23 simultaneously illustrate the net active and reactive

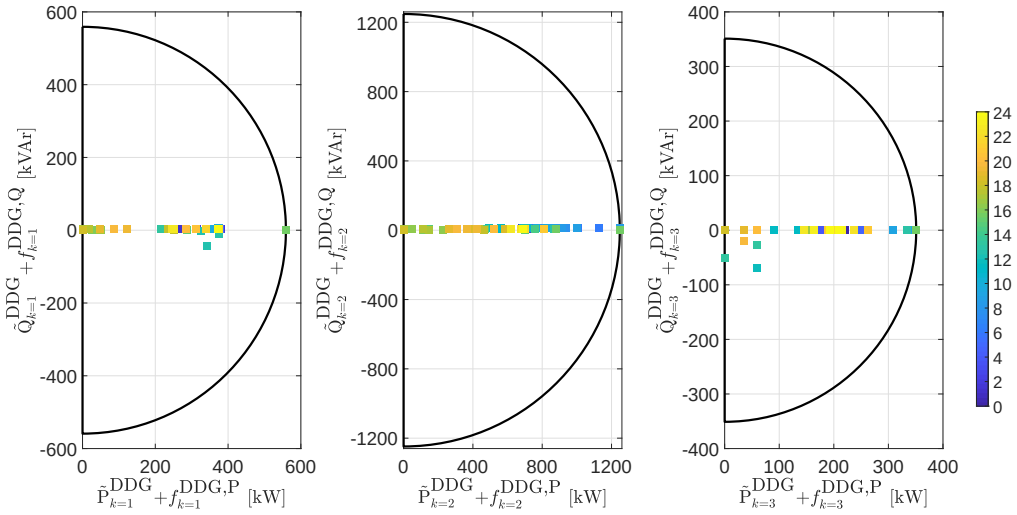

Figure 7.22: Operating points of DDGs in P-Q plane over 24 hours of study.

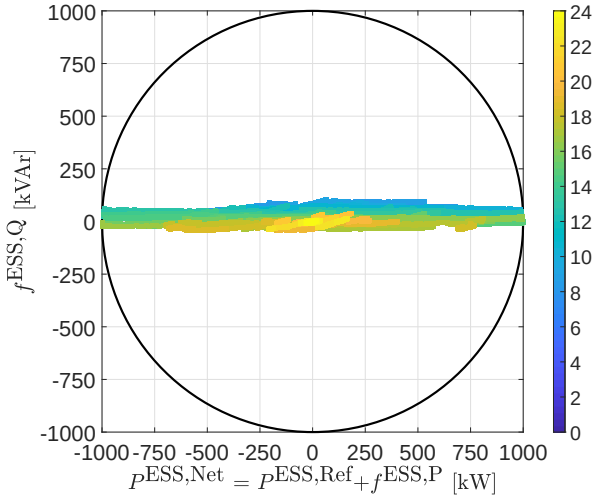

Figure 7.23: Operating points of the EES in P-Q plane over 24 hours of study.

power injections (scheduled power set-point plus provided power flexibility) of the DERs in P-Q plane over 24 hour of study. As it can be seen, throughout the day all DERs' constraints are respected.

7.8.5 Highlighting the Paramount Importance of the ESS Modeling

One of original contributions of the chapter is related to the ESS modeling. Therefore, this section is intended to concretely highlight the privileged features of the ESS's linear model presented in this chapter. To this end, lets draw a comparison between two cases:

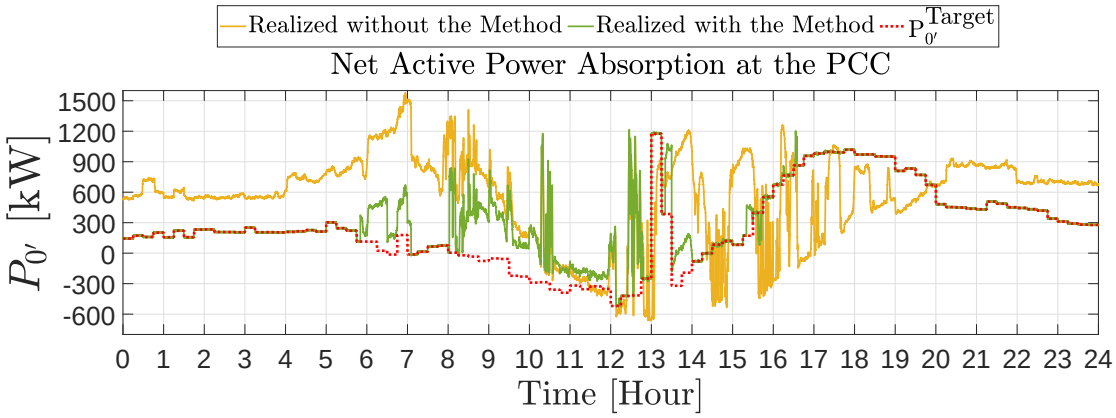

Figure 7.24: Realized active power flow at the PCC (Case 2: $P^{\text{ESS, Ref}} = 0$)

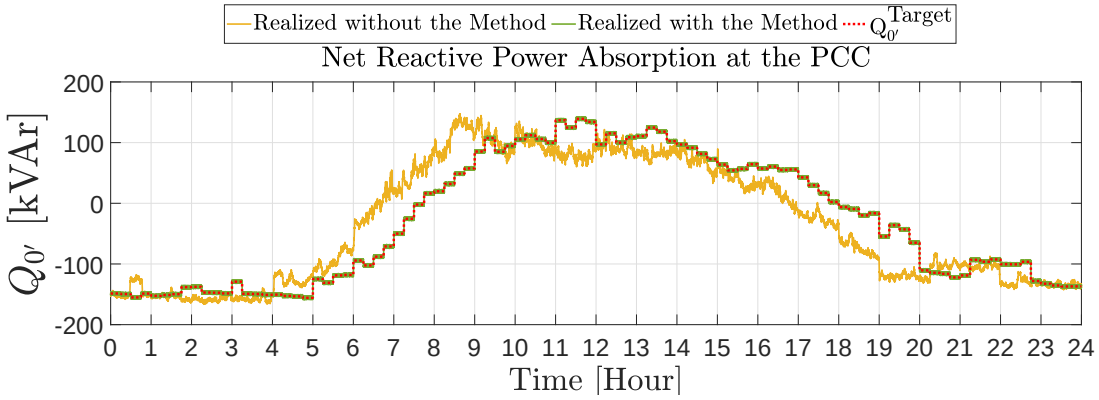

Figure 7.25: Realized reactive power flow at the PCC (Case 2: $P^{\text{ESS, Ref}} = 0$).

1. **Case 1**: It corresponds to the method presented in the chapter where **term $P^{\text{ESS, Ref}}$ is embedded in the first stage to manage the ESS's SOE**. The achieved results for this case are shown in Fig. 7.10 - Fig. 7.23. Fig. 7.10 and Fig. 7.14 particularly indicate that, in spite of the large and volatile uncertainties, the ESS succeeded to track the target, i.e. ($P_{0'}^{Target}$, $Q_{0'}^{Target}$), with average accuracy of (98.14%, 99.99%) throughout 24 hours of study. This quality of result is achieved thanks to the appropriate decision made in the first stage, i.e. $P^{\text{ESS, Ref}}$ which is exclusively designated to manage the ESS's SOE. However, in total, during 41 minutes and 53 seconds (cumulated time) of the day, the ESS cannot thoroughly track $P_{0'}^{Target}$ due to the fact that the 15-minute-ahead forecast error of PVs is larger than the rated power limit of the ESS, i.e. 1000 kW. In this respect, Fig. 7.11 shows the ESS reaching its maximum rated power limit in multiple times, but it never reaches its energy limits thanks to $P^{\text{ESS, Ref}}$.

2. **Case 2**: It corresponds to the method presented in the chapter except that **term $P^{\text{ESS, Ref}}$ is not embedded in the first stage, i.e.** $P^{\text{ESS, Ref}} = 0$. The achieved results for this case are shown in Fig. 7.24, Fig. 7.25. They show that the ESS tracks the

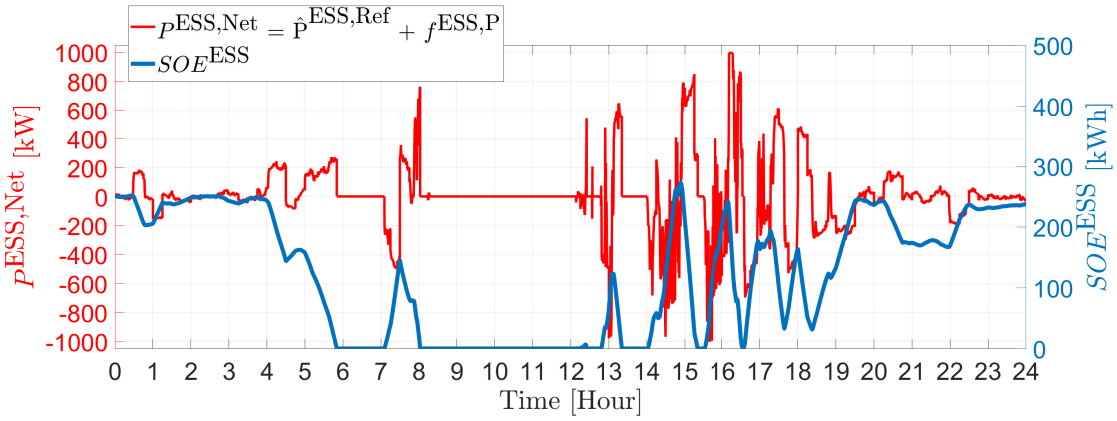

Figure 7.26: Evolution of the ESS's SOE/net power injection throughout the day (Case 2: $P^{\text{ESS, Ref}} = 0$).

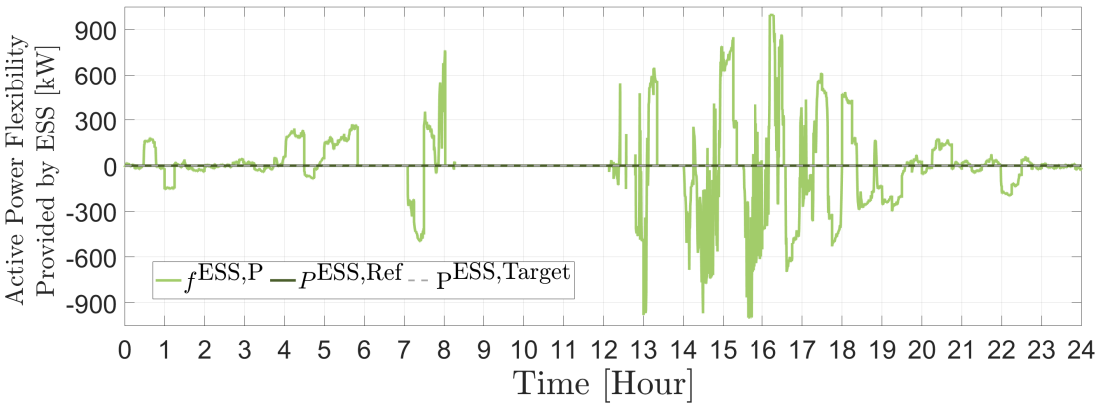

Figure 7.27: The ESS's reference power set-point (1^{st} Stage) and the ESS's targeted active power set-point (1^{st} Stage) along with the final adjustment of active power set-point of the ESS during the 2^{nd} stage (Case 2: $P^{\text{ESS, Ref}} = 0$).

target, i.e. $(P_{0'}^{\text{Target}}, Q_{0'}^{\text{Target}})$, with average accuracy of $(73.92\%, 0.9981\%)$ throughout 24 hours of study. In contrast to Case 1, Case 2 fails to precisely track the targeted active power set-point due to the fact that the ESS reaches its energy limit in total, during 6 hours and 40 minutes and 16 seconds (cumulated time) of the day. In this regard, Fig. 7.26 and Fig. 7.27 are presented to clarify the state of the ESS throughout the day. As it can be seen, for the most part of period (05:00 to 20:00) where the uncertainties are very volatile, and consequently, the ESS's power flexibility is needed more than other periods, the ESS runs out of energy, thereby, is largely useless. Moreover, Fig. 7.28 and Fig. 7.29 are also presented here to provide a deep knowledge about the performance of the method for Case 2 where term $P^{\text{ESS, Ref}}$ is not embedded in the first stage.

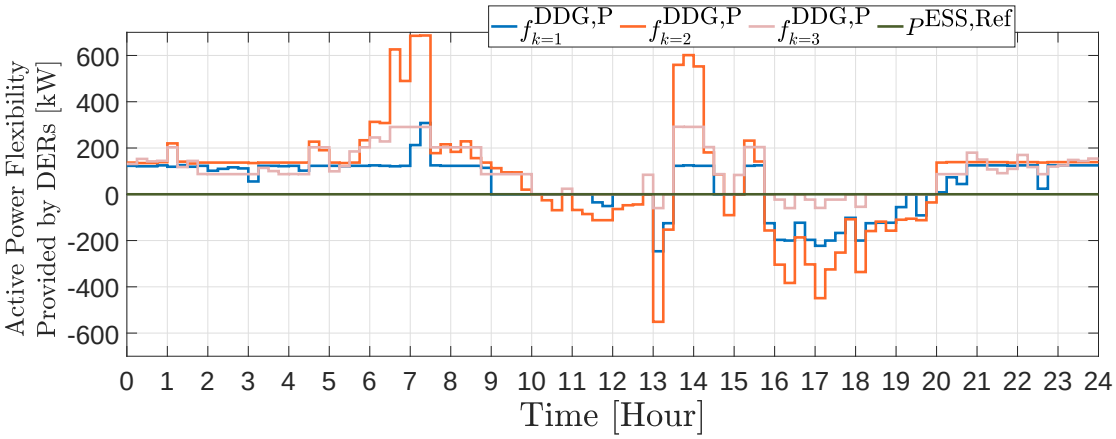

Figure 7.28: Provided active power flexibility of the DDGs along with the determined reference active power set-point of the ESS (Case 2: $P^{\mathrm{ESS,\ Ref}} = 0$).

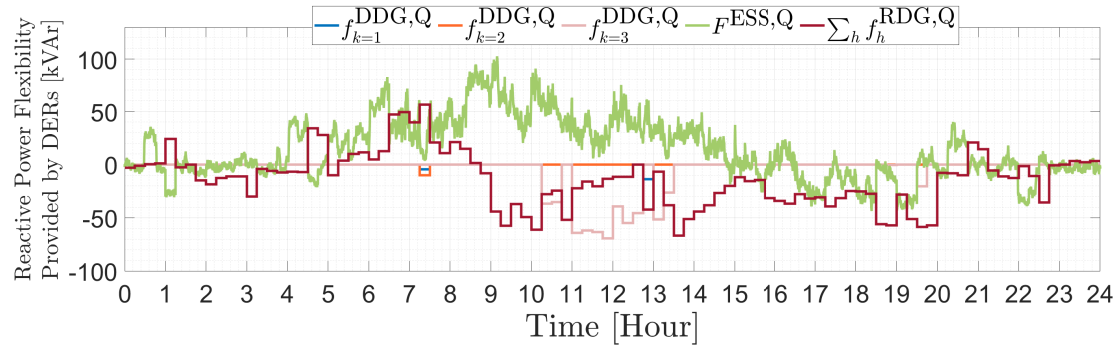

Figure 7.29: Provided reactive power flexibility of the DDGs and ESS (Case 2: $P^{\mathrm{ESS,\ Ref}} = 0$).

7.9 Conclusion

To help unlocking the potential power flexibility available in ADNs, this chapter proposes a two-stage DERs/ESS coordination and control method to provide power flexibility at the ADN's PCC. Based on the active/reactive power flexibility request of the upper-layer grid operator, it firstly relies on a linear scenario-based optimization problem to determine the optimal amount of the power flexibility that each DER should provide. To this end, it considers offer curve of DERs, uncertainties of demand and renewable generation as well as operational constraints of the grid and DERs/ESS. Then, during the real-time operation, it exploits a linear optimization formulation to control the active/reactive power injection of a utility-scale ESS to precisely track the requested power flexibility at the ADN's PCC while counteracting the impact of the day-ahead forecast errors. A real distribution network located in the city of Aigle in southwest of Switzerland is used to validate the performance of the proposed method. The results show that the method is able to precisely satisfy the flexibility request of

the upper-layer grid operator at the PCC, while successfully managing the ESS's SOE.

8 Conclusion

> Thomas Edison dreamed of a lamp that could be operated by electricity, began where he stood to put his dream into action, and despite more than ten thousand failures, he stood by that dream until he made it a physical reality. Practical dreamers do not quit.
>
> — Napoleon Hill

8.1 Summary

The thesis sets itself the target of developing new frameworks to deal with power flexibility provision issue in the modern electric power systems where the size of ancillary services providers pales in comparison with the size of uncertainties. In this respect, the thesis constructed four frameworks to address four main questions whose treatments, to the best knowledge of the author, are missing in the literature:

1. **Chapter 2**: To deal with solely active power flexibility issue, what is the optimal size of active power flexibility that a transmission system operator (TSO) must book from power flexibility providers (including aggregated flexibility of distribution networks) over a specified time horizon (next day or week)?
2. **Chapter 4**: To deal with both active and reactive power flexibility issues, what is the optimal size of active and reactive power flexibility that a TSO must book from power flexibility providers (including aggregated flexibility of distribution networks) over a specified time horizon (next day or week)?
3. **Chapter 6**: How much are the maximum active/reactive power flexibility an active distribution network (ADN) can provide upon request at its point of common coupling (PCC) to the upper-layer grid?
4. **Chapter 7**: How much active/reactive power flexibility should each distributed

energy resource (DER) provide during the real-time grid operation in such a way that the ADN can provide, with minimum deviation, the minutes-ahead active/reactive power flexibility requested by the upper-layer grid at the PCC?

8.2 Contributions

The first contribution of the thesis was constructing (in chapters 2 and 4) risk-aware linear decision making tools for TSOs to tackle the above-mentioned questions 1 and 2. Moreover, two TSO-DSO coordination frameworks were designed to empower TSO and DSO exchange power flexibility without revealing their confidential grids data. Another unique contribution of the thesis was constructing the case study model of the Swiss transmission network (used for planing and operational studies) on the basis of the data provided by Swissgrid. The thesis evaluated the efficiency of the tools developed in chapters 2 and 4 by applying them to the Swiss transmission network. The achieved results corroborated that the Swiss TSO requires the power flexibility of flexible distribution networks to be able to securely steer their grids with high share of stochastic generation.

As a cornerstone for chapter 4, chapter 3 established a linearized power flow model for transmission networks. This linearized power flow model explicitly characterizes all grid constraints as linear functions of the nodal injections while considering shunt susceptance of branches as well as active/reactive power losses of the transmission grid. Moreover, it offered linear functions to express active/reactive power injections of slack bus as well as reactive power injections of PV buses as linear functions of the active/reactive power injections of the other buses.

The thesis (in chapter 5) provided a comprehensive survey on the the existing power flow models and consequently opted the best power flow model for managing the power flexibility of DERs installed in ADNs as detailed in 5.2. Indeed, chapter 5 consolidated the frameworks designed in chapter 6 and chapter 7.

Another prominent contribution of the thesis was developing (in chapter 6) a framework to tackle the above-mentioned question 3. The developed framework robustly predicts the flexibility provision capability (FPC) area of an ADN considering grid's constraints, grid's losses and uncertainties associated with forecast errors. Most notably, it was mathematically proven that, assuming convex capabilities curves of DERs and a linearized power flow model, the predicted FPC area is feasible and convex.

Another valuable contribution of the thesis (in chapter 7) was introducing a two-stage DERs & energy storage system (ESS) coordination and control method to treat the above-mentioned question 4. This method consists of the first-ever technique that divides the net power injection of the ESS into two terms to elaborately preserve the

ESS's state of energy (SOE) as well as take advantage at most of the power flexibility of the ESS. The presented results highlight the advantage of this novel technique for managing the ESS's SOE.

The last but not least contribution of the thesis that might stay hidden is that the thesis opted real-world transmission/distribution networks (the transmission network of Switzerland and a distribution network located in the city of Aigle in southwest of Switzerland) as case studies. To construct these case studies, the thesis processed/-analyzed massive raw data associated with transmission/distribution grid's topology, profile of renewable generation, profile of demand, power flexibility market of Switzerland.

All developed frameworks help realizing a two-fold goal:

- Unlocking the potential active and reactive power flexibility of DERs located in distribution networks.
- Improving and facilitating coordination between the TSO and distribution system operators (DSOs) to exchange bi-directional active/reactive power flexibility.

In sum, the main contribution of the thesis can be summarized as:

This thesis is envisaged to modernize the traditional top-to-down (from transmission system to distribution systems) power flexibility provision mechanism to a bi-directional power flexibility provision structure between TSO and DSOs.

8.3 Future Works

A great deal of work have still remained to revolutionize collaborations between TSO and DSO, thereby empowering them to exchange bi-direction power flexibility[1]. In general, TSO-DSO collaboration can be revolutionized if all different layers of the problem (shown in Fig. 8.1) are treated:

1. **Power System Layer:** This layer is intended to address technical issues associated to the electric power system. These technical issues can be summarized in 4 questions presented in section 8.1. All 4 questions were treated in this thesis. However, it is suggested to extend the framework developed in chapter 6 to be able to account for ESSs as well. Moreover, this thesis strongly advises to extend research on stochastic generation prediction approaches to improve their precision. The main reason behind this advice is that poor predictions cause that

[1] It is worth highlighting that many large projects such as SmartNet, FlexPlan, OneNet have been lunched to address this problem.

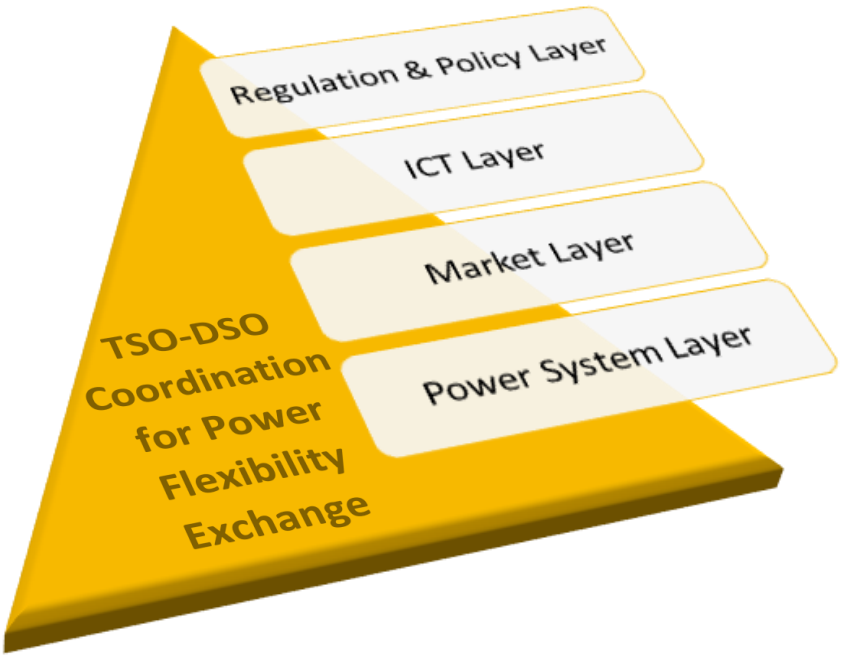

Figure 8.1: Different layers of the TSO-DSO coordination problem for exchanging bi-directional power flexibility.

the grid operators make wrong decisions and schedule their grid inappropriately (i.e. the schedule operating point and the realized operating point during the real-time grid operation are too far from each other). Consequently, grid operators will require more power flexibility during the real-time grid operation to counteract the impact of their inappropriate scheduling.

2. **Market Layer:** This layer sets out to introduce novel energy and power flexibility market structures to enable all DERs, DSOs, aggregators and TSO collaboration with each other to unlock potential power flexibility of DERs. The main obstacles in the way of designing such a power flexibility market are that 1-DREs belong to different owners, 2-different entities like TSO, DSO and DERs are not willing to share their data with each other. Therefore, the designed market must allow all entities to coordinate their power flexibility demand/capability with each other without revealing their confidential data. Moreover, the designed market must decrease the temporal granularity of the power flexibility market (for example from 24 hours to 1 hour) to allow all DERs to participate in the power flexibility market and accordingly unlock their potential power flexibility. It is suggested that benefits of decreasing the temporal granularity of the power flexibility market are quantified by leveraging the frameworks introduced in this thesis. On the other hand, it is suggested to design bedding strategies for ESSs with the purpose of facilitating the integration of ESSs in the power flexibility market.

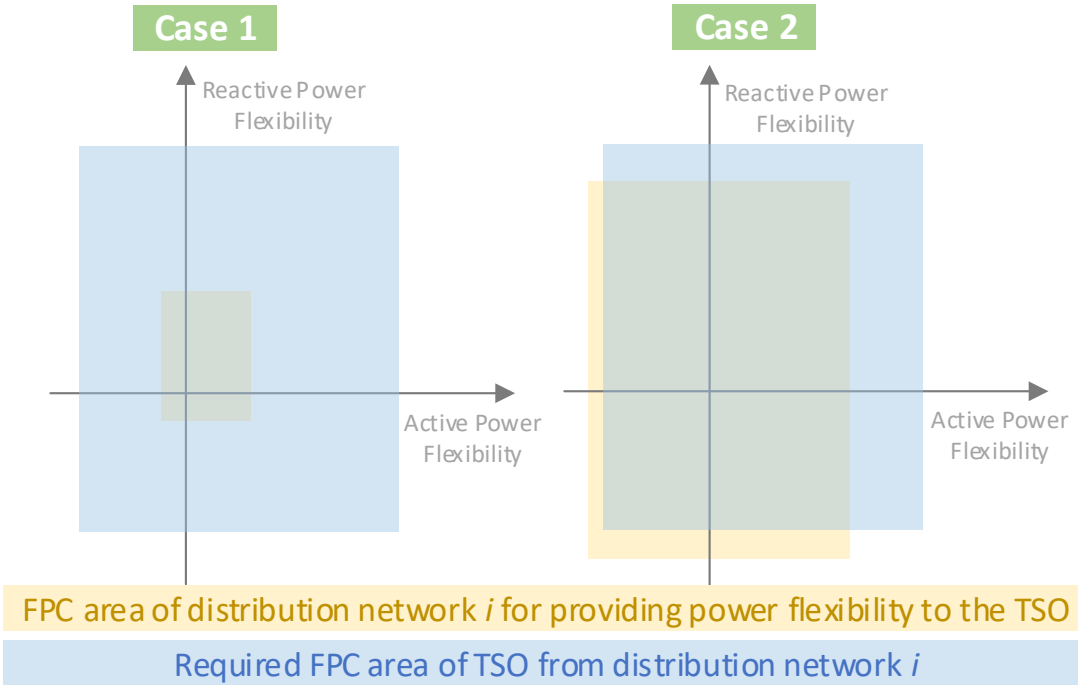

Figure 8.2: Gap between the TSO's required FPC area and the FPC area of a distribution network.

3. **Information & Communications Technology (ICT) Layer:** This layer aims to design the data communication networks that are required to implement the frameworks developed in the power system layer as well as power flexibility markets designed in the market layer. These data communication networks must prepare a secure and reliable communication between different entities. Moreover, the international energy agency (IEA) has recently reported that significant cyber-attack incidents in electric power systems are surging from 2 incidents in 2016 to 10 incidents in 2019 [157]. This fact has also been highlighted in the Global Risk Report 2020 of World Economic Forum [158] where cyber-attacks have been accounted as one of the top ten global risks in terms of impact and likelihood. Therefore, it is suggested to perform deep research on designing data communication networks for electric power system that are robust against cyber-attacks. Moreover, it is strongly suggested to develop novel methods to detect false data injection and accordingly preserve the cyber-security of the electric power system against false data.

4. **Regulation & Policy Layer:** This layer is intended to define regulations governing the power system layer, market layer and ICT layer. More importantly, this layer offers policies to promote DERs' power flexibility provision and accordingly TSO-DSO collaboration for exchanging bi-directional power flexibility. In order to establish promoting policies, grid operators need to have concrete insight about

the technical aspects of their grid. In this respect, the TSO can leverage the framework developed in chapter 4 and quantifies its required FPC area from each flexible distribution network considering multiple representative days. On the other hand, each DSO can leverage the framework constructed in chapter 6 and quantifies its capability for power flexibility provision (represented as a FPC area) considering multiple representative days. Then, TSO and each individual DSO can share their FPC areas with each other, thereby, determining the gap between TSO's power flexibility demand and capability of that distribution network for providing power flexibility to the TSO. As shown in Fig. 8.2, the discovered gap might be large like case 1 or might be small like case 2. Grid operators and policy makers can use the discovered gap as an indicator to wisely establish promoting policies such as providing incentives to help all entities to evolve towards the ultimate plan, i.e. bi-directional power flexibility exchange between TSO and DSO. For example, case 2 represents the situations where almost no incentive is required whereas case 1 represents situations where establishing promoting policies such as providing incentives are necessaries. Last but not least, the magnitude of gap can be used to prioritize provision of incentives between different distribution networks (the larger gap, the higher priority).

A The Swiss Power Flexibility Market

> I never did anything by accident, nor did any of my inventions come by accident; they came by work.
>
> — Thomas A. Edison

This appendix is intended to briefly introduce the power flexibility market of Switzerland. Moreover, this appendix analyzes the data associated to the power flexibility market of Switzerland over the year 2019, whereby, it provides a deep insight into a real-world power flexibility market. Above all, it extracts the prices of secondary and tertiary active power flexibility (booked by Swissgrid over 2019) which are used in chapter 2 and chapter 4 to develop offer curves. Moreover, it extracts the prices of deployed upward and downward active power flexibility (i.e. upward/downward imbalance prices) which are used in chapter 2 and chapter 4.

Transmission system operator (TSO) of Switzerland, i.e. Swissgrid, is responsible for reliable and secure operation of the Swiss transmission gird. In this regard, Swissgrid continuously monitors its grid and coordinates its operating point with downstream distribution networks and neighboring TSOs. To tackle this important task, the TSO needs ancillary services. Ancillary services (power flexibility or reserve) can be defined as the services that empower the TSO to securely steer its grid [1].

The Swiss electric power system follows sequential market structure where energy and flexibility markets are separately organized. Moreover, Swissgrid (the Swiss TSO) is responsible for procurement of ancillary services [1] including:

- Frequency control (primary, secondary, tertiary control);
- Voltage support;
- Compensation of active power losses;
- Black start and island operation capability;
- System coordination (including congestion management service);
- Balance group management;
- Operational measurement.

It is worth highlighting that different terms are used to refer to frequency control such as: 1-frequency control services, 2-active power flexibility, 3-active power reserve and 4-reserve. The detailed description of all types of ancillary services can be found in [1]. However, the following elaborates on 3 different types of frequency control (i.e. active power flexibility).

The electric power networks can keep working if and only if the generation and consumption of electricity are in equilibrium. More specifically, the frequency of the network must be preserved close to 50 Hertz as stable as possible. As illustrated in Fig. A.1, if the balance between generation and consumption is breached, transmission system operators within the ENTSO-E[1] apply a three-stage procedure to swiftly recover the balance and eliminate grid's frequency deviation. First, primary frequency control[2] is automatically/promptly provided thanks to automatic frequency controllers. Thus, this type of service might be activated for any imbalance between generation and consumption occurring in the synchronized grid of ENTSO-E (causing frequency deviation) . If the frequency deviation lasts for more than 30 seconds, the secondary frequency control [3] is activated to replace the primary frequency control. The secondary frequency control is completely activated in 5 minutes, moreover, this service is solely activated inside the affected control area (place close to the occurred imbalance). Finally, if the frequency deviation lasts for more than 5 minutes, then the tertiary frequency control [4] is manually activated to replace the secondary frequency control.

[1] European Network of Transmission System Operators for Electricity

[2] primary frequency control might be called as 1-primary control, 2-primary reserve, 3-primary active power flexibility or 4-frequency containment reserve (FCR).

[3] secondary frequency control might be called as 1-secondary control, 2-secondary reserve, 3-spinning reserve, 4-secondary active power flexibility or 5-frequency restoration reserve (FRR).

[4] tertiary frequency control might be called as 1-tertiary control, 2-tertiary reserve, 3-non-spinning reserve, 4-tertiary active power flexibility or 5-replacement reserve.

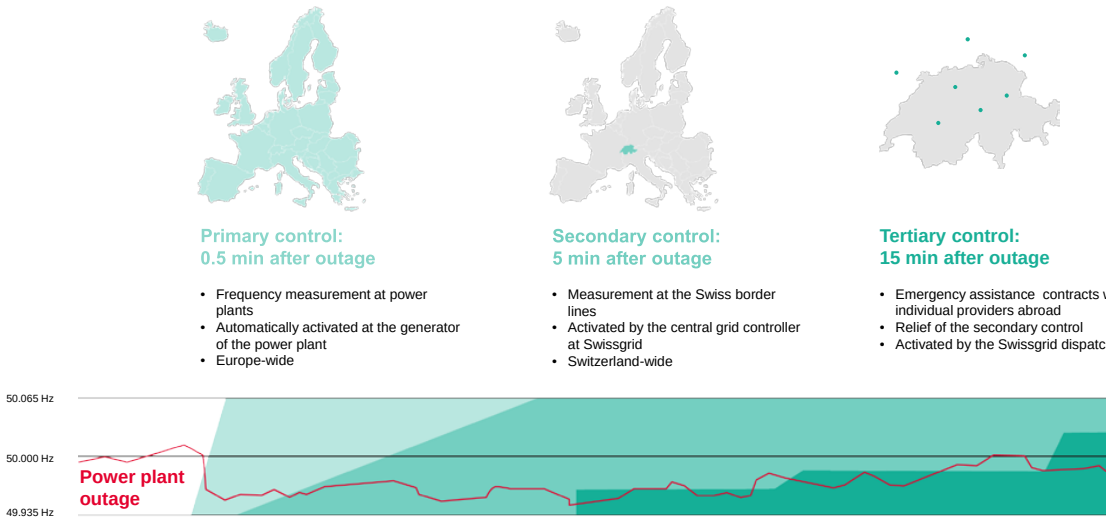

Figure A.1: Primary, secondary and tertiary frequency control services in ENTSO-E [1].

A.1 Analyzing The Swiss Power Flexibility Market over the Year 2019

Imbalance between active power generation and consumption might occur due to unexpected contingencies or forecast errors of stochastic generation and consumption. In such cases, Swissgrid deploys either upward or downward active power flexibility (i.e. balance energy) to fix the grid's frequency as close as possible to 50 Hertz. The prices associated with the deployed upward and downward active power flexibility are regularly published on the website of Swissgrid [45]. On the other hand, prior to the real-time grid operation, Swissgrid prepares itself to deal with imbalance. More specifically, Swissgrid books primary, secondary, and tertiary active power flexibility in week-ahead or day-ahead markets. Consequently, if an unforeseen imbalance occurs, the TSO deploys the booked power flexibility and restores the balance. Swissgrid Company regularly publishes the volumes as well as prices of the booked primary, secondary, and tertiary active power flexibility on its website [44]. The following dives into the data pertained to the year 2019 [44, 45], whereby, it extracts important features and information of the Swiss power flexibility market over the year 2019.

A.1.1 Deployed Upward and Downward Active Power Flexibility

Fig. A.2 and Fig. A.3 respectively illustrate probability/cumulative density functions of the price of the deployed upward and downward active power flexibility (i.e. $\pi'^{\mathrm{P+}}$ and $\pi'^{\mathrm{P-}}$) over 2019.

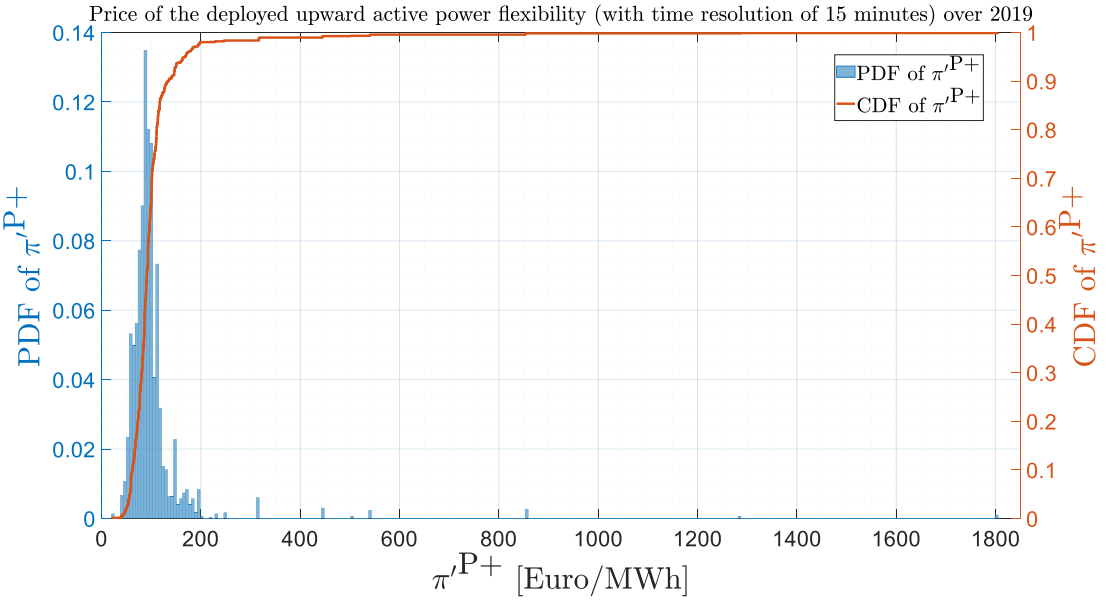

Figure A.2: Probability/Cumulative density function of the price of the deployed upward active power flexibility (π'^{P+}) over the year 2019.

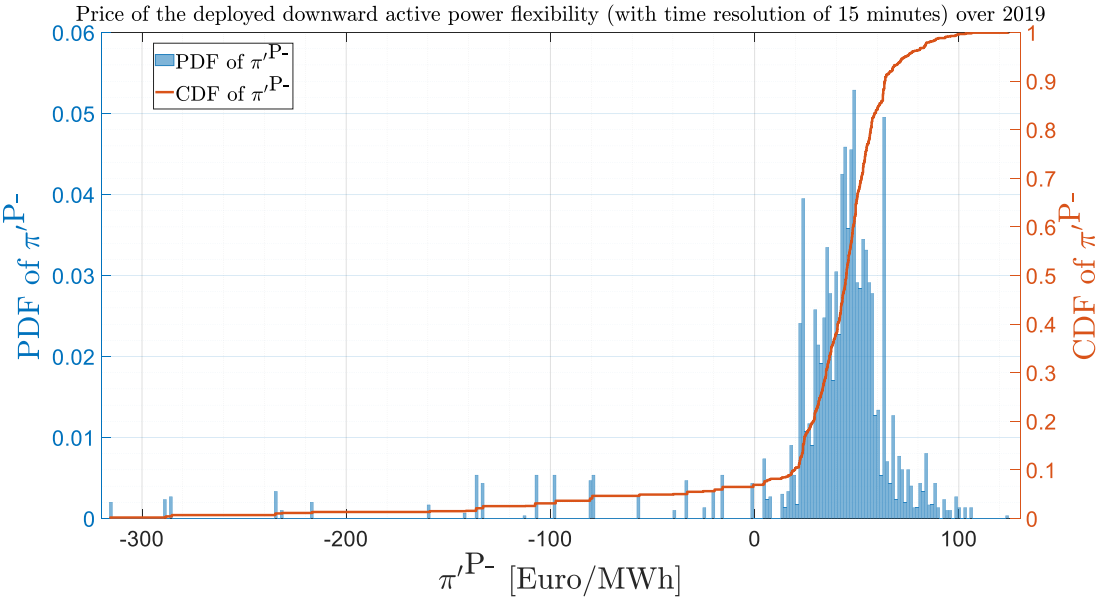

Figure A.3: Probability/Cumulative density function of the price of the deployed downward active power flexibility (π'^{P-}) over the year 2019.

Fig. A.4 illustrates the average price of the deployed upward/downward active power flexibility (i.e. π'^{P+}/π'^{P-}) over each month of 2019.

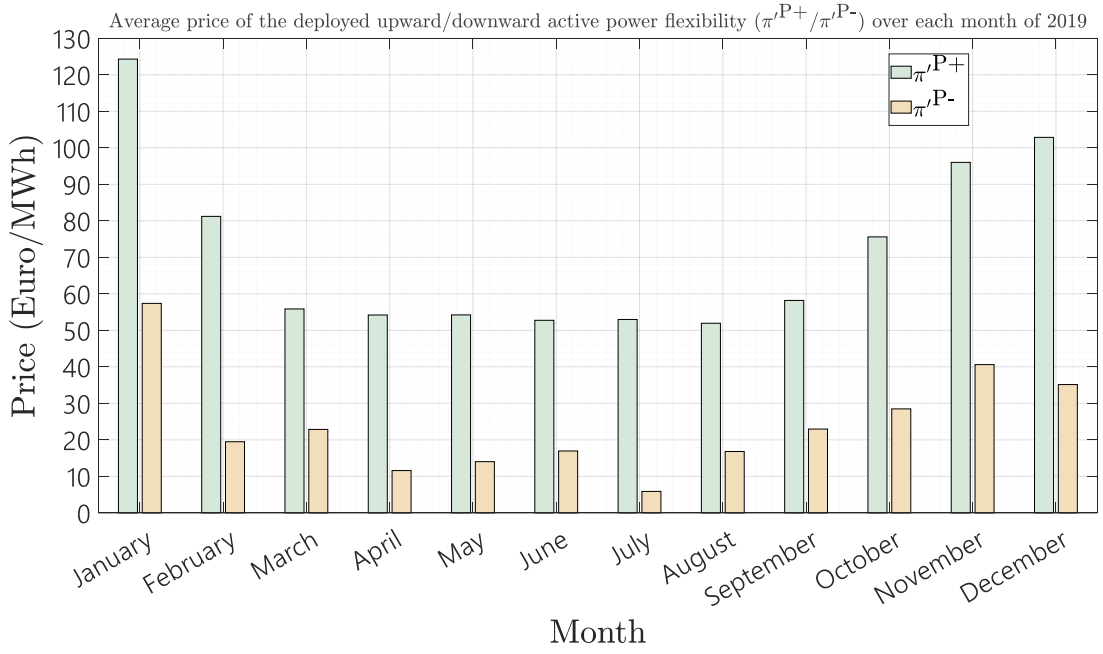

Figure A.4: Average price of the deployed upward/downward active power flexibility (π'^{P+}/π'^{P-}) over each month of 2019.

A.1.2 Booked Primary Active Power Flexibility

Fig. A.5 shows probability and cumulative density functions of the price of the booked primary active power flexibility ($\pi^{P,Primary}$) over the year 2019. It should be highlighted that primary active power flexibility is a symmetrical product, i.e. both upward and downward flexibility are traded together. Moreover, primary active power flexibility is organized/booked in the weekly market. Fig. A.6 shows the average price of the booked primary active power flexibility ($\pi^{P,Primary}$) over each month of 2019.

On the basis of ENTSO-E requirements, Swissgrid must constantly keep (i.e. book) around 70 MW primary active power flexibility.

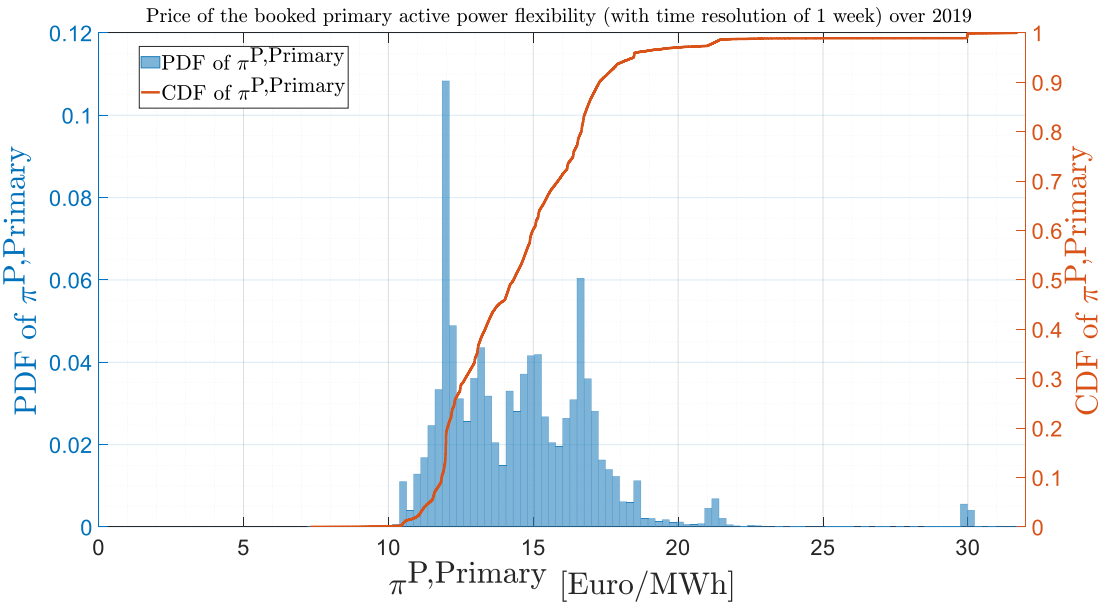

Figure A.5: Probability/Cumulative density function of the price of the booked primary active power flexibility ($\pi^{P,Primary}$) over the year 2019.

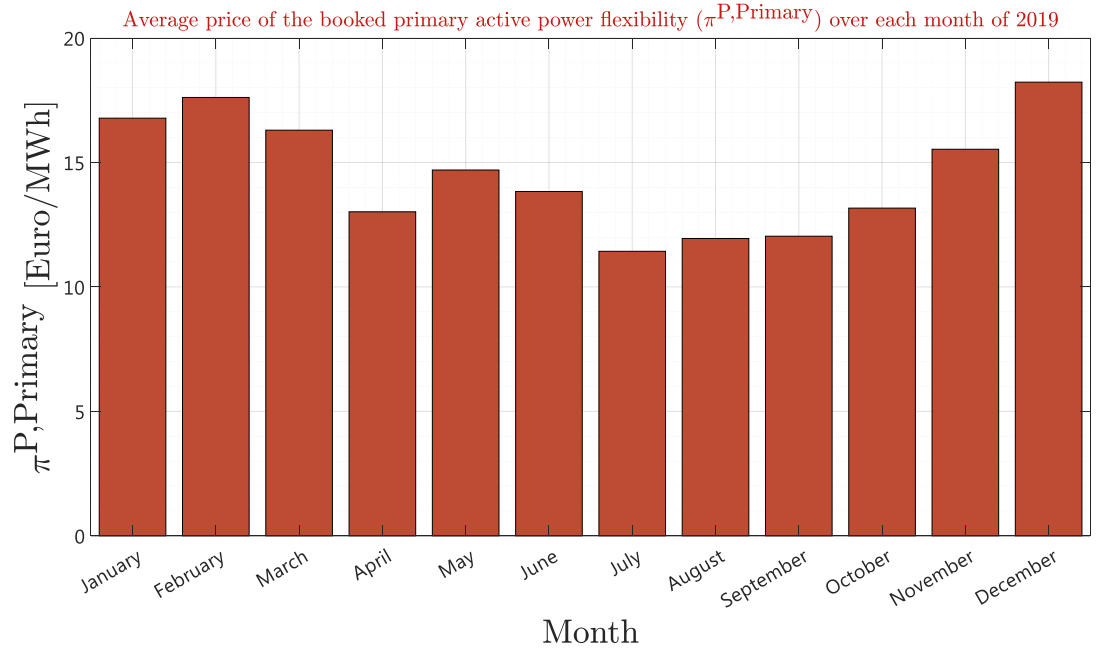

Figure A.6: Average price of the booked primary active power flexibility ($\pi^{P,Primary}$) over each month of 2019.

A.1.3 Booked Secondary Active Power Flexibility

Fig. A.7 and Fig. A.8 respectively represent probability/cumulative density functions of the price and volume of the booked secondary active power flexibility (i.e. $\pi^{\text{P,secondary}}$ and $F^{\text{P,Secondary}}$) over the year 2019. It should be highlighted that secondary active power flexibility is a symmetrical product. Moreover, secondary active power flexibility is organized/booked in the weekly market.

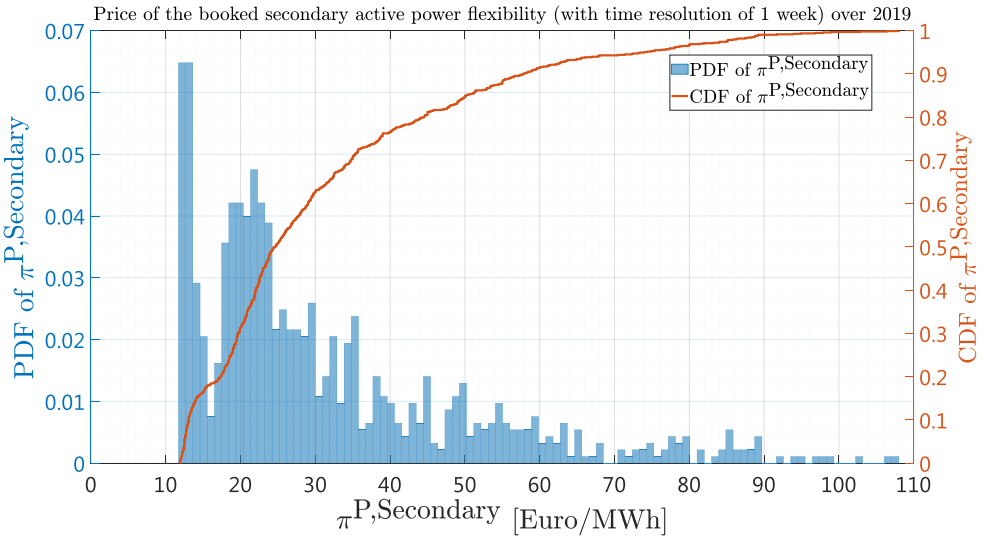

Figure A.7: Probability/Cumulative density function of the price of the booked secondary active power flexibility ($\pi^{\text{P,secondary}}$) over the year 2019.

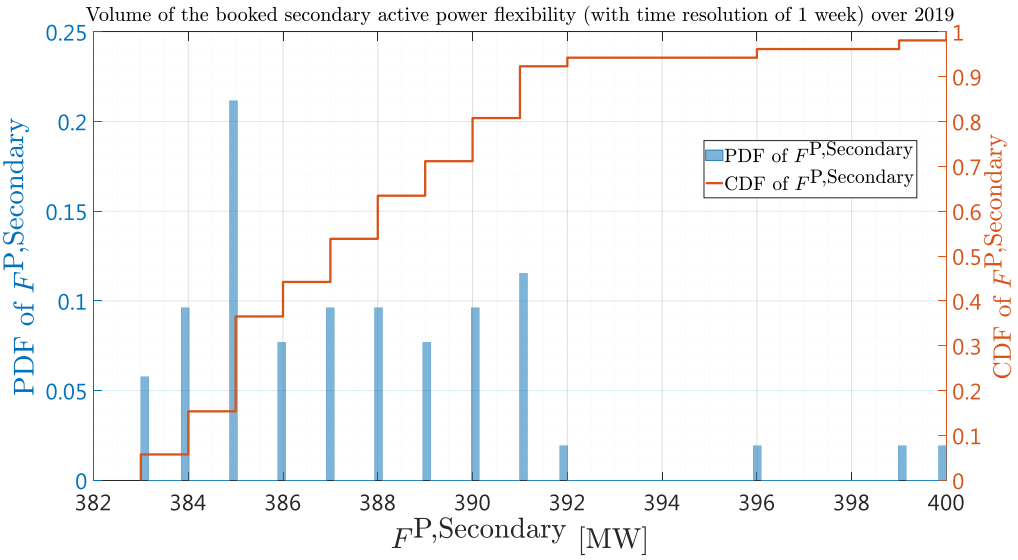

Figure A.8: Probability/Cumulative density function of the volume of the booked secondary active power flexibility ($F^{\text{P,Secondary}}$) over the year 2019.

Fig. A.9 and Fig. A.10 respectively represent the average price and average volume of the booked secondary active power flexibility ($\pi^{\text{P,Secondary}}$) over each month of 2019.

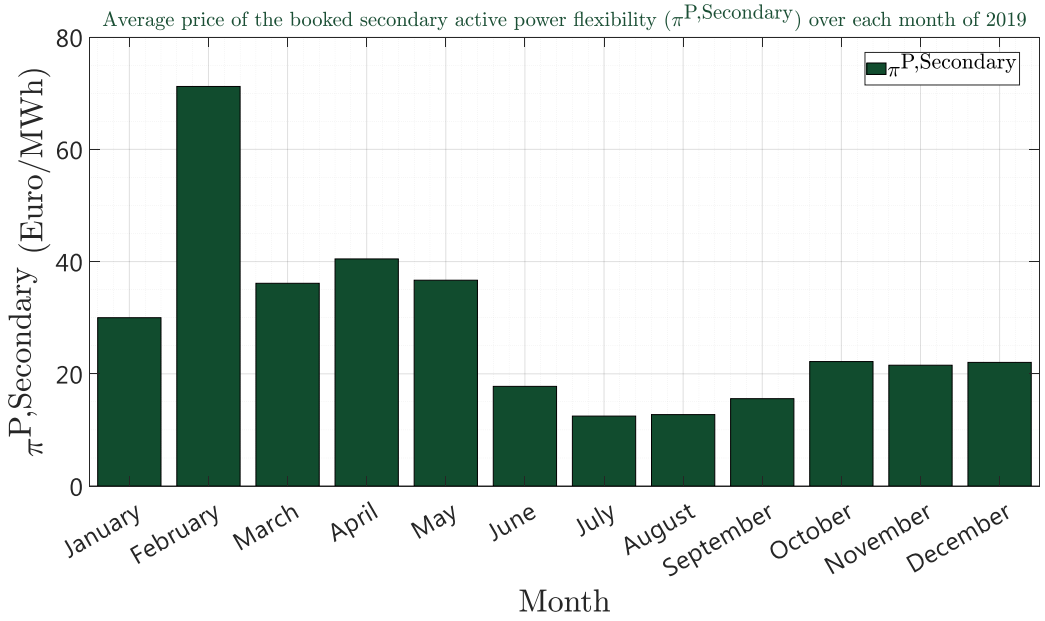

Figure A.9: Average price of the booked secondary active power flexibility ($\pi^{\text{P,Secondary}}$) over each month of 2019.

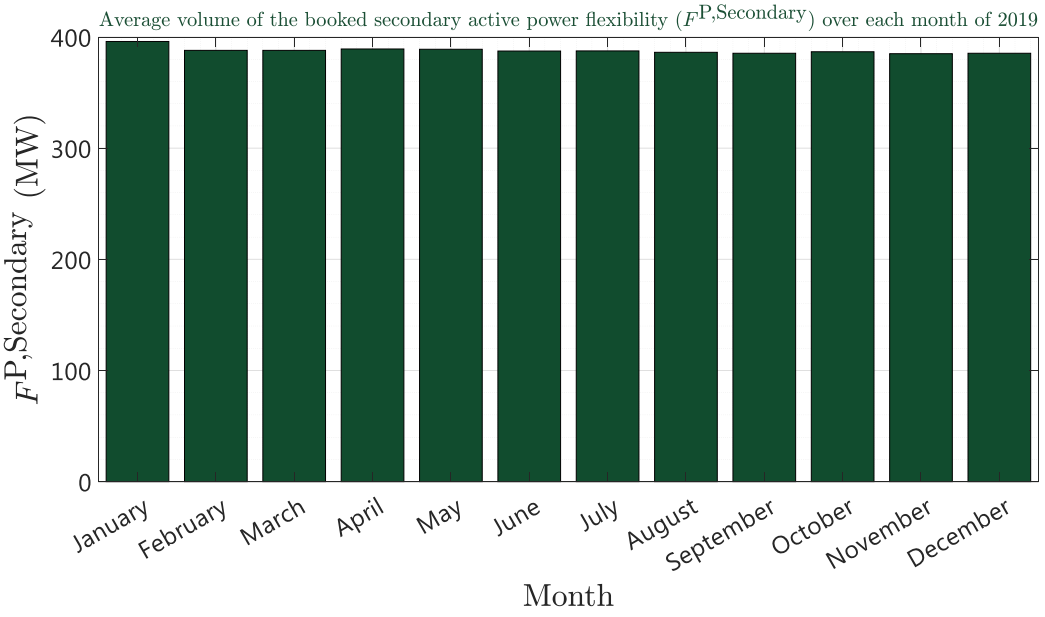

Figure A.10: Average volume of the booked secondary active power flexibility ($\pi^{\text{P,Secondary}}$) over each month of 2019.

A.1.4 Booked Tertiary Active Power Flexibility

It should be highlighted that tertiary active power flexibility is an unsymmetrical product, thus, upward and downward tertiary active power flexibility can be traded separately. Moreover, there are two markets for tertiary active power flexibility, i.e. weekly or daily markets.

A.1.4.1 Weekly Tertiary Market

Fig. A.11 and Fig. A.12 respectively represent probability/cumulative density functions of the price and volume of the upward tertiary active power flexibility (i.e. $\pi^{\text{P+,Tertiary}}_{\text{weekly}}$ and $F^{\text{P+,Tertiary}}_{\text{weekly}}$) booked from the weekly tertiary market over the year 2019.

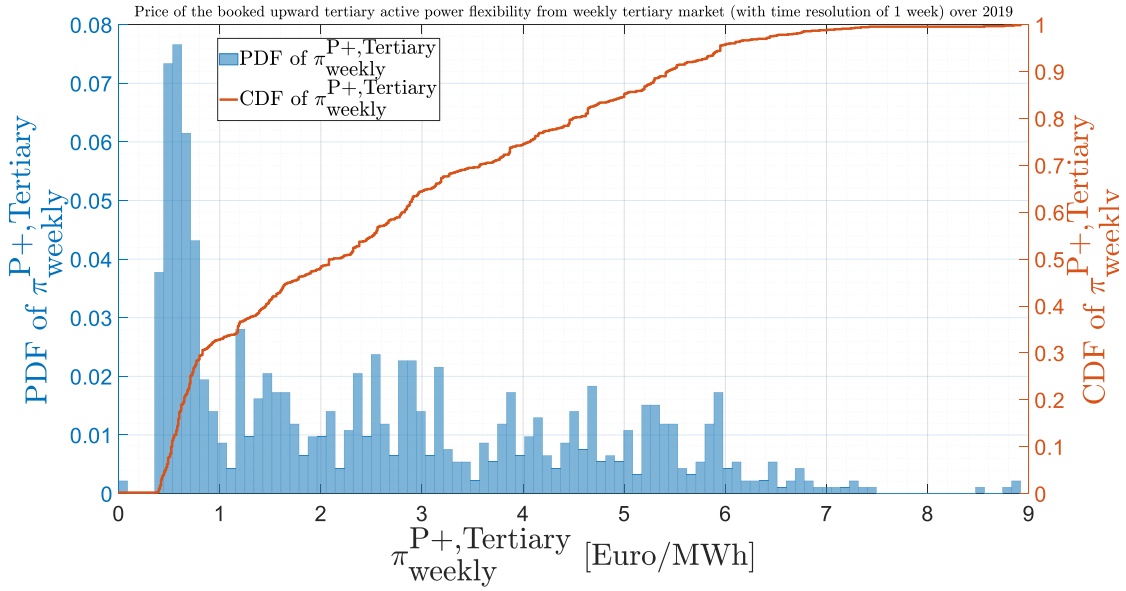

Figure A.11: Probability/Cumulative density function of the price of the upward tertiary active power flexibility ($\pi^{\text{P+,Tertiary}}_{\text{weekly}}$) booked from the weekly tertiary market over the year 2019.

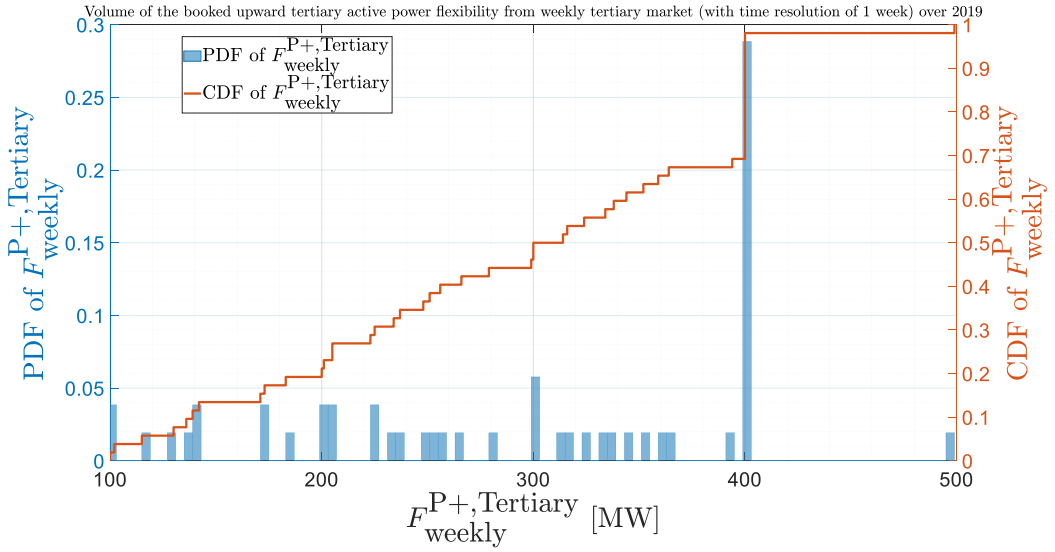

Figure A.12: Probability/Cumulative density function of the volume of the upward tertiary active power flexibility ($F^{P+,Tertiary}_{weekly}$) booked from the weekly tertiary market over the year 2019.

Fig. A.13 and Fig. A.14 respectively represent probability/cumulative density functions of the price and volume of the downward tertiary active power flexibility (i.e. $\pi^{P-,Tertiary}_{weekly}$ and $F^{P-,Tertiary}_{weekly}$) booked from the weekly tertiary market over the year2019.

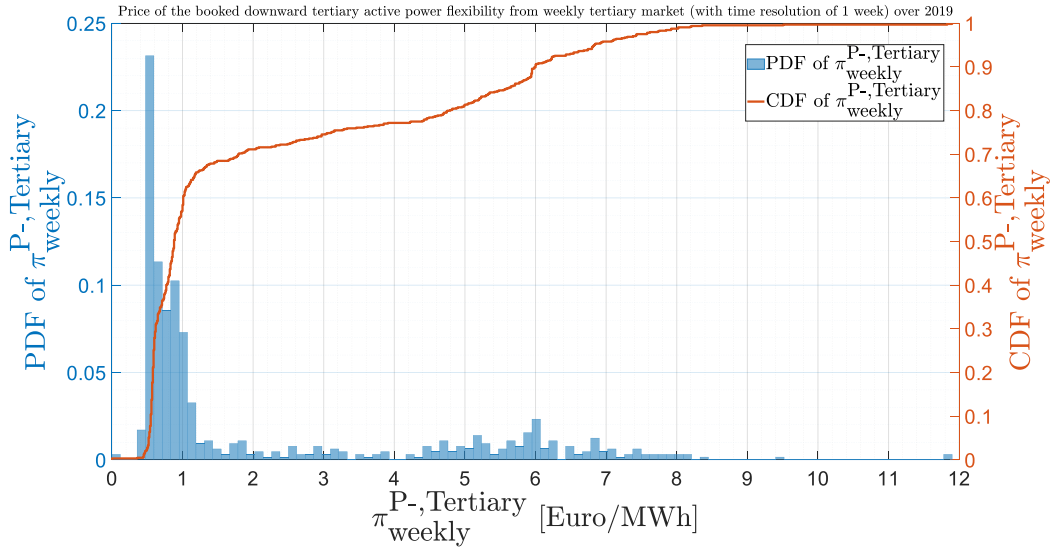

Figure A.13: Probability/Cumulative density function of the price of the downward tertiary active power flexibility ($\pi^{P-,Tertiary}_{weekly}$) booked from the weekly tertiary market over the year 2019.

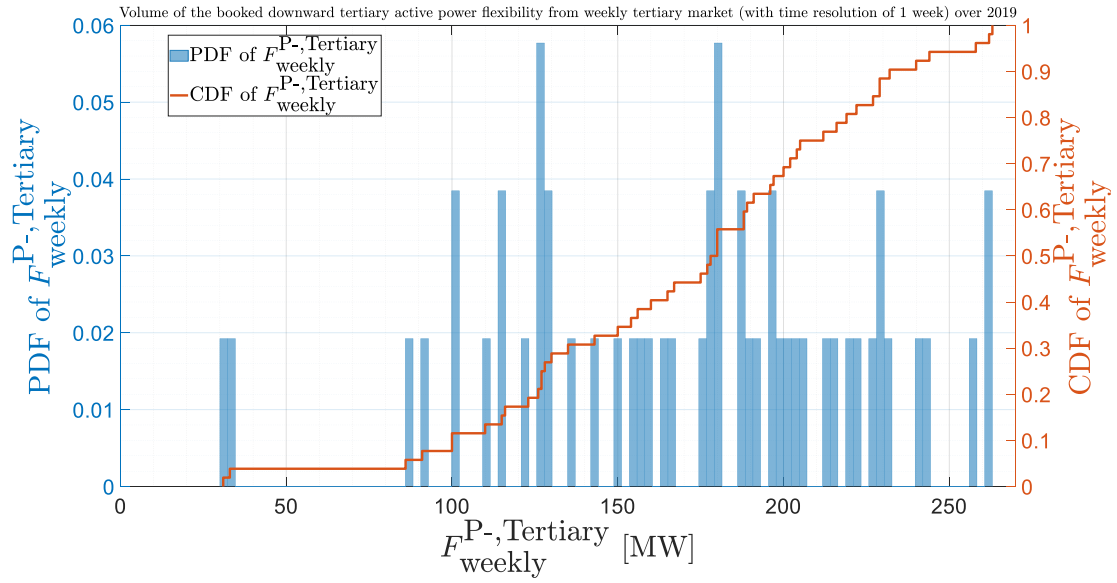

Figure A.14: Probability/Cumulative density function of the volume of the downward tertiary active power flexibility ($F^{\text{P-,Tertiary}}_{\text{weekly}}$) booked from the weekly tertiary market over the year 2019.

A.1.4.2 Daily Tertiary Market

Fig. A.15 and Fig. A.16 respectively represent probability/cumulative density functions of the price and volume of the upward tertiary active power flexibility (i.e. $\pi^{\text{P+,Tertiary}}_{\text{daily}}$ and $F^{\text{P+,Tertiary}}_{\text{daily}}$) booked from the daily tertiary market over the year 2019.

Figure A.15: Probability/Cumulative density function of the price of the upward tertiary active power flexibility ($\pi^{\text{P+,Tertiary}}_{\text{daily}}$) booked from the daily tertiary market over the year 2019.

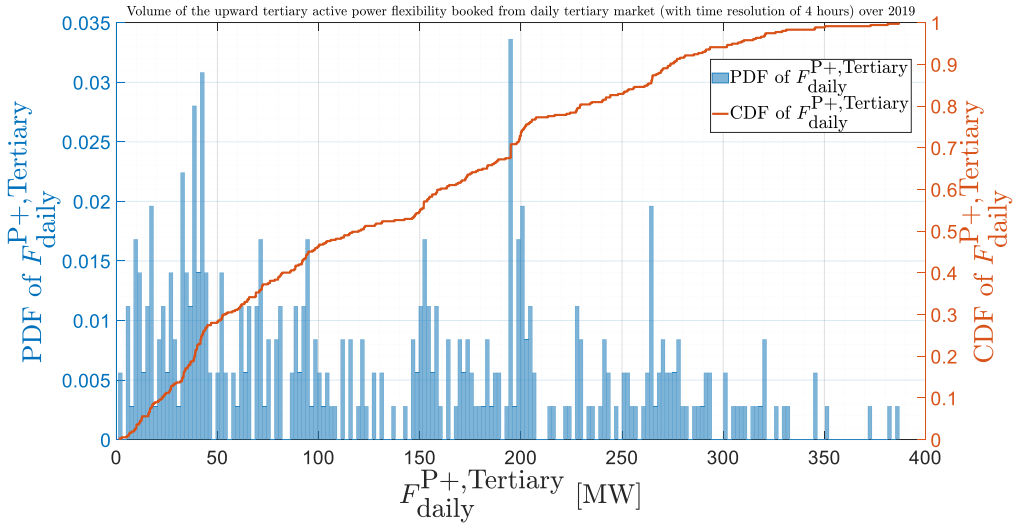

Figure A.16: Probability/Cumulative density function of the volume of the upward tertiary active power flexibility ($F^{\text{P+,Tertiary}}_{\text{daily}}$) booked from the daily tertiary market over the year 2019.

Fig. A.17 and Fig. A.18 respectively represent probability/cumulative density functions of the price and volume of the downward tertiary active power flexibility (i.e. $\pi^{\text{P-,Tertiary}}_{\text{daily}}$ and $F^{\text{P-,Tertiary}}_{\text{daily}}$) booked from the daily tertiary market over the year 2019.

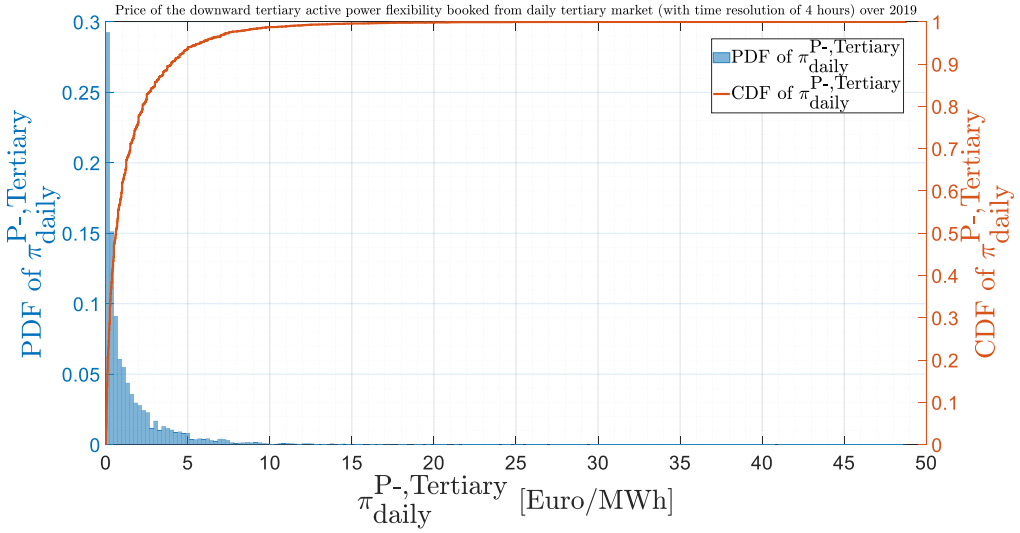

Figure A.17: Probability/Cumulative density function of the price of the downward tertiary active power flexibility ($\pi^{\text{P-,Tertiary}}_{\text{daily}}$) booked from the daily tertiary market over the year 2019.

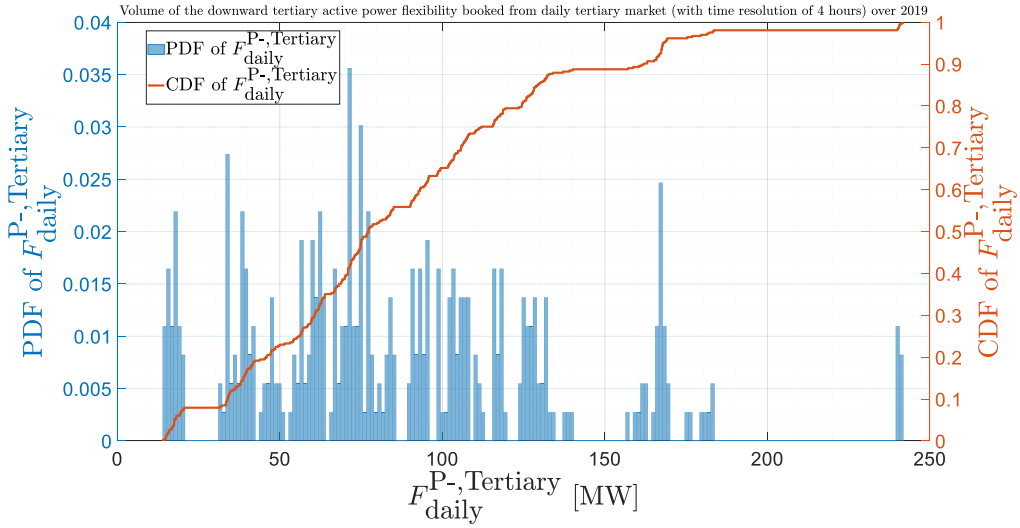

Figure A.18: Probability/Cumulative density function of the volume of the downward tertiary active power flexibility ($F^{\text{P-,Tertiary}}_{\text{daily}}$) booked from the daily tertiary market over the year 2019.

Fig. A.19 represents the average prices of the upward tertiary active power flexibility booked from daily ($\pi^{\text{P+,Tertiary}}_{\text{daily}}$) and weekly ($\pi^{\text{P+,Tertiary}}_{\text{weekly}}$) tertiary markets over each month of 2019. Moreover, $\pi^{\text{P+,Tertiary}}_{\text{Total}}$ represents the weighted average of $\pi^{\text{P+,Tertiary}}_{\text{daily}}$ and $\pi^{\text{P+,Tertiary}}_{\text{weekly}}$.

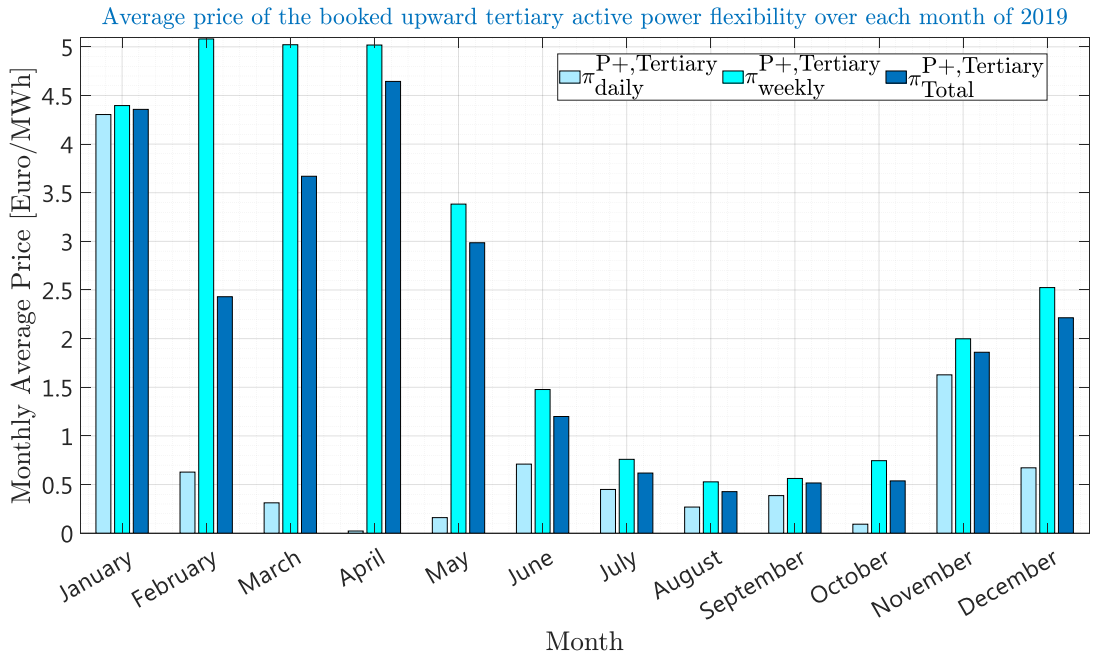

Figure A.19: Average price of the booked upward tertiary active power flexibility over each month of 2019.

Fig. A.20 represents the average volumes of the upward tertiary active power flexibility booked from daily ($F^{\text{P+,Tertiary}}_{\text{daily}}$) and weekly ($F^{\text{P+,Tertiary}}_{\text{weekly}}$) tertiary markets over each month of 2019. Moreover, $F^{\text{P+,Tertiary}}_{\text{Total}}$ represents the sum of $F^{\text{P+,Tertiary}}_{\text{daily}}$ and $F^{\text{P+,Tertiary}}_{\text{weekly}}$.

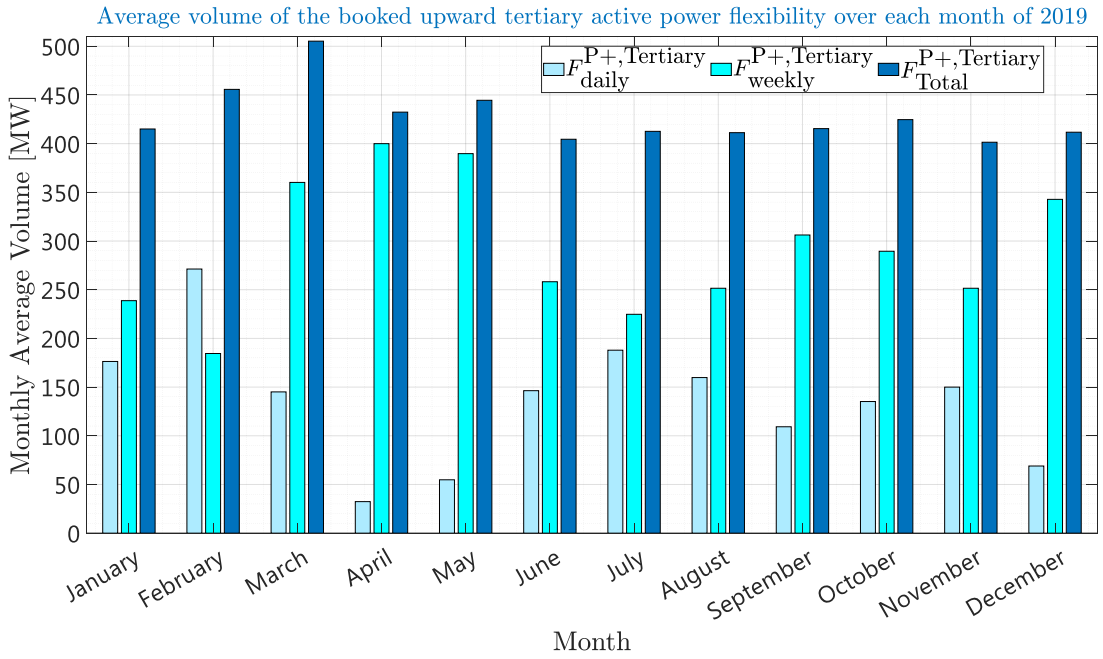

Figure A.20: Average volume of the booked upward tertiary active power flexibility over each month of 2019.

Fig. A.21 represents the average prices of the downard tertiary active power flexibility booked from daily ($\pi^{\text{P-,Tertiary}}_{\text{daily}}$) and weekly ($\pi^{\text{P-,Tertiary}}_{\text{weekly}}$) tertiary markets over each month of 2019. Moreover, $\pi^{\text{P-,Tertiary}}_{\text{Total}}$ represents the weighted average of $\pi^{\text{P-,Tertiary}}_{\text{daily}}$ and $\pi^{\text{P-,Tertiary}}_{\text{weekly}}$.

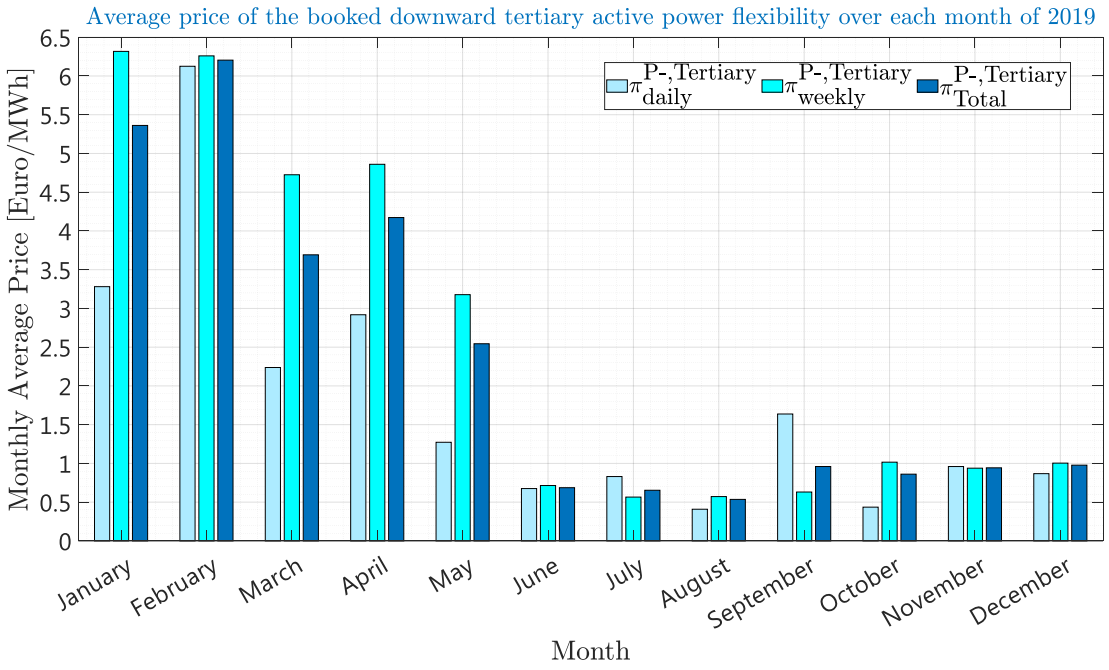

Figure A.21: Average price of the booked downward tertiary active power flexibility over each month of 2019.

Fig. A.22 represents the average volumes of the downward tertiary active power flexibility booked from daily ($F^{\text{P-,Tertiary}}_{\text{daily}}$) and weekly ($F^{\text{P-,Tertiary}}_{\text{weekly}}$) tertiary markets over each month of 2019. Moreover, $F^{\text{P-,Tertiary}}_{\text{Total}}$ represents the sum of $F^{\text{P-,Tertiary}}_{\text{daily}}$ and $F^{\text{P-,Tertiary}}_{\text{weekly}}$.

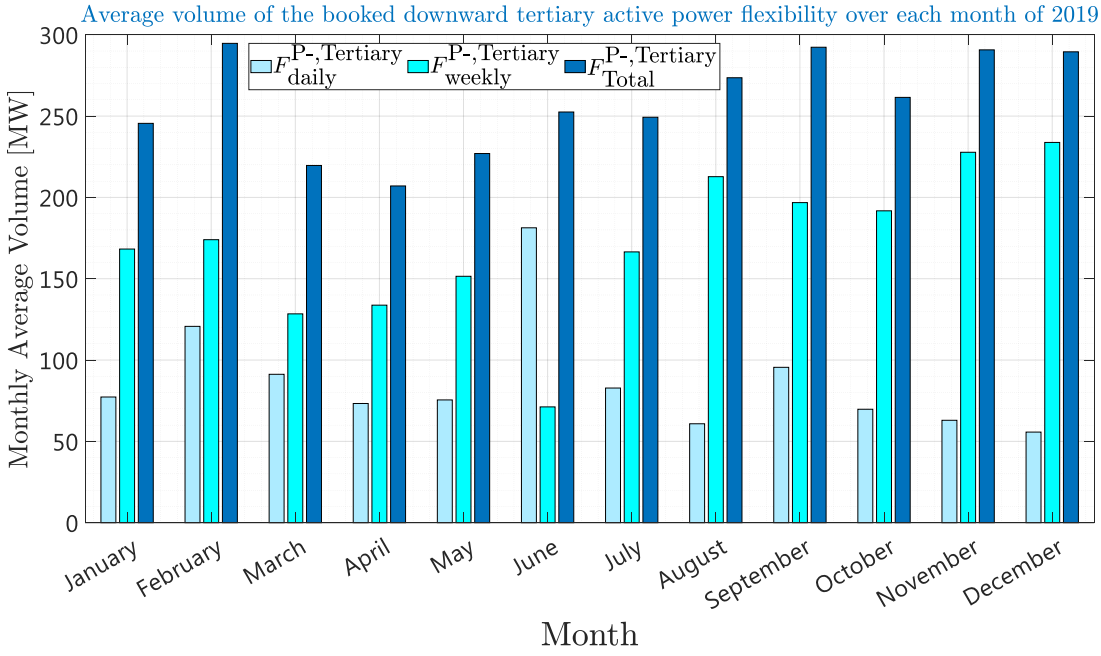

Figure A.22: Average volume of the booked downward tertiary active power flexibility over each month of 2019.

B Sequential Monte Carlo Simulation for Contingency Modeling

> I never did anything by accident, nor did any of my inventions come by accident; they came by work.
>
> — Thomas A. Edison

A widely accepted approach for generating scenarios modeling transmission grid's contingencies (i.e. power plant outages and transmission line/transformer outages) is Sequential Monte Carlo (SMC) simulation [159], [160]. In order to generate NS scenarios modeling transmission grid's contingencies over NT hours (for example 24 hours of the next day), SMC simulation is carried out over NT*NS hours where each NT-hour corresponds to a single scenario as shown in Fig. B.1. The transmission grid contingencies, including power plant outages and transmission line/transformer outages, are modeled as binary parameters. More specifically, the state of power plants and transmission lines/transformers are modeled as independent two-states 0, 1 Markov chains where 1 stands for availability and 0 stands for unavailability. Then, the following procedure is adopted to model the state of each component over NT*NS hours:

1. The initial state of component c is assumed available (i.e. 1).
2. A sample of time to failure (t') is drawn from the exponential distribution with average of MTTF_c. MTTF_c indicates the mean time to failure of component c;
3. The state of component c is set equal to 1 for t= 1, 2,..., t'.

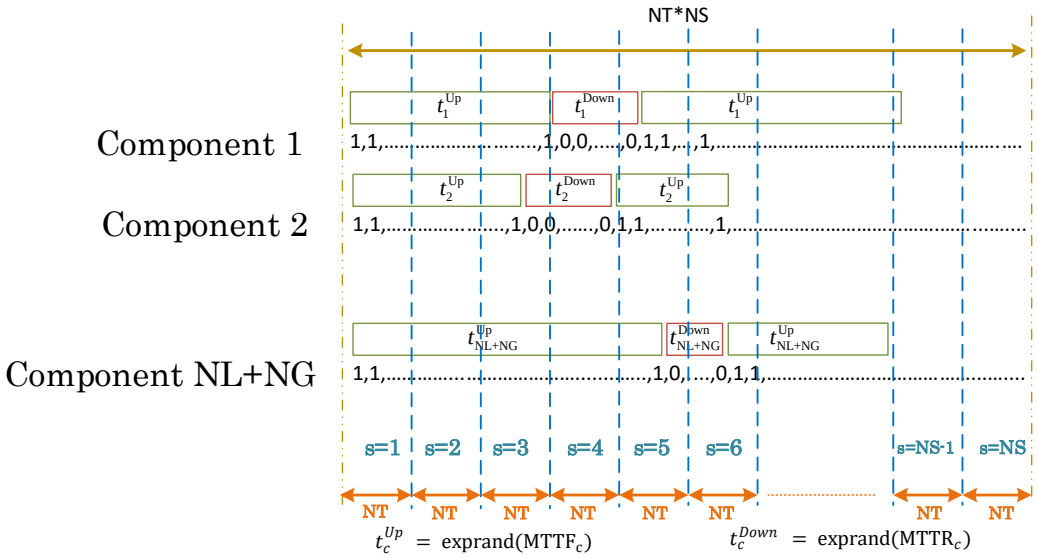

Figure B.1: Generated scenarios modeling transmission grid's contingencies.

4. A sample of time to repair (t'') is drawn from the exponential distribution with average of MTTR$_c$. MTTR$_c$ indicates the mean time to repair of component c;
5. The state of component c is set equal to 0 for t = t'+1, t'+2,..., t'+t''.
6. Steps 2 to 5 are followed to generate a series of 1 and 0 with length of NT*NS modeling the state of component c.

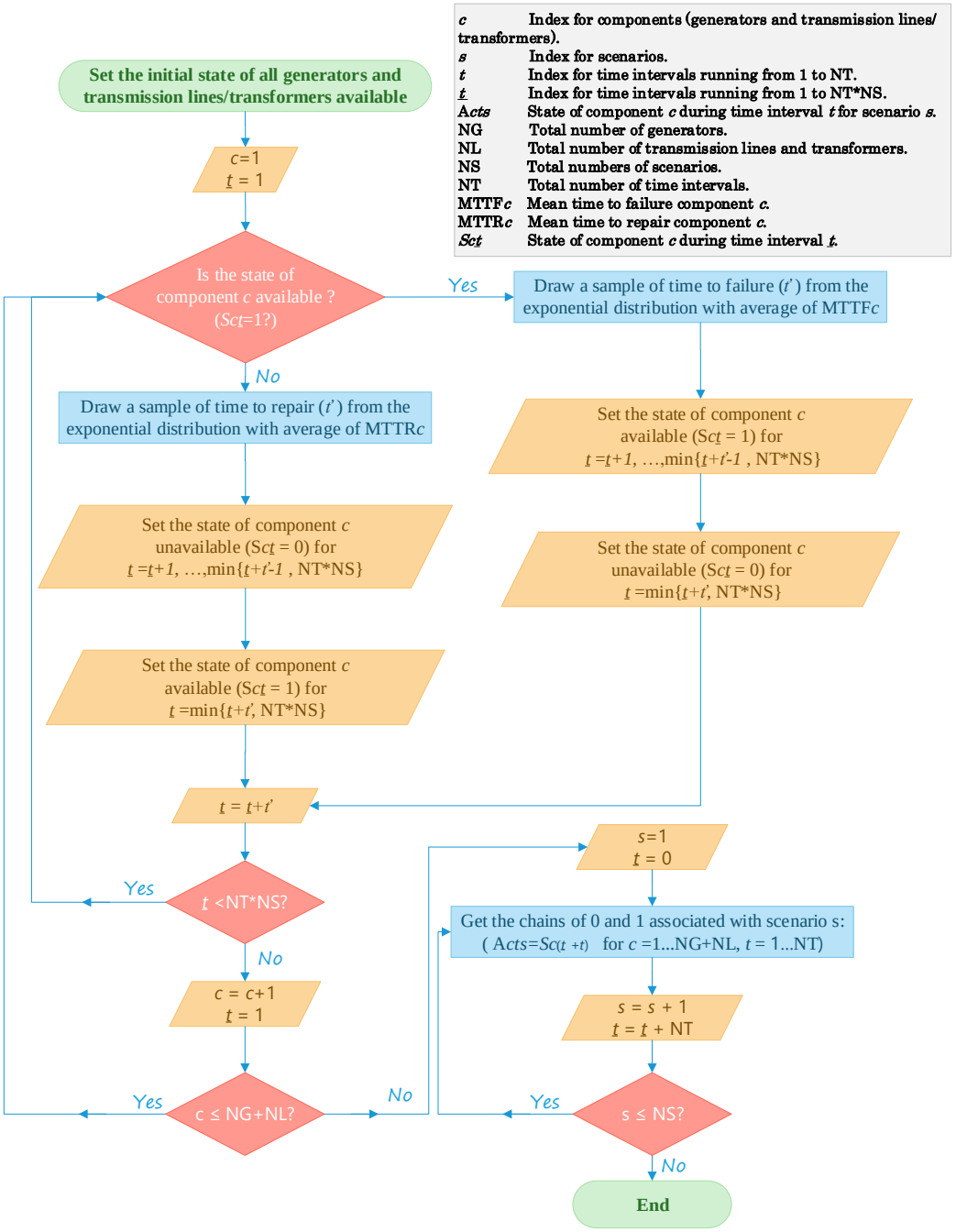

Figure B.2: Flowchart of component's state simulation based on Sequential Monte Carlo simulation approach.

Bibliography

[1] C. Hodel, "Overview of ancillary services," tech. rep., Swissgrid Ltd, 2019.

[2] "World Energy Transitions Outlook: 1.5°C Pathway," tech. rep., International Renewable Energy Agency, 2021. [Online]. Available: https://www.irena.org/publications/2021/Jun/World-Energy-Transitions-Outlook.

[3] P. Pradhan, L. Costa, D. Rybski, W. Lucht, and J. P. Kropp, "A Systematic Study of Sustainable Development Goal (SDG) Interactions," *Earth's Future*, vol. 5, no. 11, pp. 1169–1179, 2017.

[4] "Transforming our world: The 2030 agenda for sustainable development," tech. rep., United Nations (UN), 2015.

[5] "Electricity Market Report," tech. rep., International Energy Agency (IEA), July 2021. [Online]. Available: https://www.iea.org/reports/electricity-market-report-july-2021.

[6] "Renewable Power Generation Costs 2020," tech. rep., International Renewable Energy Agency, 2020. [Online]. Available: https://www.irena.org/publications/2021/Jun/Renewable-Power-Costs-in-2020.

[7] "Power system organisational structures for the renewable energy era," tech. rep., International Renewable Energy Agency, 2020. [Online]. Available:https://www.irena.org/publications/2020/Jan/IRENA-Power-system-structures.

[8] J. E. Novacheck, G. L. Brinkman, and G. S. Porro, "Operational Analysis of the Eastern Interconnection at Very High Renewable Penetrations," Tech. Rep. NREL/TP–6A20-71465, 1476255, Sept. 2018. [Online]. Available: http://www.osti.gov/servlets/purl/1476255/.

[9] "New Energy Outlook 2021," tech. rep., Bloomberg New Energy Finance, July 2021.

[10] "Net Zero by 2050 - A Roadmap for the Global Energy Sector," tech. rep., International Energy Agency (IEA), July 202. [online]: https://www.iea.org/reports/net-zero-by-2050.

[11] T. Mai, M. M. Hand, S. F. Baldwin, R. H. Wiser, G. L. Brinkman, P. Denholm, D. J. Arent, G. Porro, D. Sandor, D. J. Hostick, M. Milligan, E. A. DeMeo, and M. Bazilian, "Renewable Electricity Futures for the United States," *IEEE Transactions on Sustainable Energy*, vol. 5, pp. 372–378, Apr. 2014.

[12] D. McCollum, L. G. Echeverri, K. Riahi, and S. Parkinson, "SDG 7 ensure access to affordable, reliable, sustainable and modern energy for all," tech. rep., United Nations (UN).

[13] L. Mehigan, J. P. Deane, B. P. O. Gallachóir, and V. Bertsch, "A review of the role of distributed generation (DG) in future electricity systems," *Energy*, vol. 163, pp. 822–836, Nov. 2018.

[14] H. Gerard, E. Rivero, and D. Six, "Basic schemes for TSO-DSO coordination and ancillary services provision," tech. rep., SmartNet, 2016.

[15] G. Migliavacca, M. Rossi, H. Gerard, M. Džamarija, S. Horsmanheimo, C. Madina, I. Kockar, G. Leclecq, M. Marroquin, and H. Svendsen, "TSO-DSO coordination and market architectures for an integrated ancillary services acquisition : the view of the SmartNet project," in *CIGRE*, (France), Aug. 2018.

[16] G. Migliavacca, M. Rossi, D. Siface, M. Marzoli, H. Ergun, R. Rodríguez-Sánchez, M. Hanot, G. Leclerq, N. Amaro, A. Egorov, J. Gabrielski, B. Matthes, and A. Morch, "The Innovative FlexPlan Grid-Planning Methodology: How Storage and Flexible Resources Could Help in De-Bottlenecking the European System," *Energies*, vol. 14, p. 1194, Feb. 2021.

[17] M. Kalantar-Neyestanaki, F. Sossan, M. Bozorg, and R. Cherkaoui, "Characterizing the Reserve Provision Capability Area of Active Distribution Networks: A Linear Robust Optimization Method," *IEEE Transactions on Smart Grid*, vol. 11, pp. 2464–2475, May 2020.

[18] M. Kalantar-Neyestanaki and R. Cherkaoui, "Coordinating Distributed Energy Resources and Utility-Scale Battery Energy Storage System for Power Flexibility Provision Under Uncertainty," *IEEE Transactions on Sustainable Energy*, vol. 12, pp. 1853–1863, Oct. 2021.

[19] M. Kalantar-Neyestanaki, M. Bozorg, F. Sossan, and R. Cherkaoui, "Allocation of Frequency Control Reserve from Aggregated Resources of Active Distribution Systems," in *2018 Power Systems Computation Conference (PSCC)*, pp. 1–8, June 2018.

[20] M. Kalantar-Neyestanaki, M. Bozorg, F. Sossan, and R. Cherkaoui, "Allocation of Active Power Reserve from Active Distribution Networks Using a Cost-Benefit Approach: Application to Swissgrid Network," in *2019 IEEE Milan PowerTech*, pp. 1–6, June 2019.

[21] N. M. Haegel, R. Margolis, T. Buonassisi, D. Feldman, A. Froitzheim, R. Garabedian, M. Green, S. Glunz, H.-M. Henning, B. Holder, I. Kaizuka, B. Kroposki, K. Matsubara, S. Niki, K. Sakurai, R. A. Schindler, W. Tumas, E. R. Weber, G. Wilson, M. Woodhouse, and S. Kurtz, "Terawatt-scale photovoltaics: Trajectories and challenges," *Science*, vol. 356, pp. 141–143, Apr. 2017.

[22] "Climate Change and Renewable Energy: National Policies and the role of communities, cities and regions," p. 60.

[23] *Renewable energy sources and climate change mitigation: special report of the Intergovernmental Panel on Climate Change*, vol. 49. New York: Cambridge University Press, July 2012.

[24] P. Díaz Redondo and O. van Vliet, "Modelling the Energy Future of Switzerland after the Phase Out of Nuclear Power Plants," *Energy Procedia*, vol. 76, pp. 49–58, Aug. 2015.

[25] G. Migliavacca, ed., *TSO-DSO Interactions and Ancillary Services in Electricity Transmission and Distribution Networks: Modeling, Analysis and Case-Studies*. Springer International Publishing, 2020.

[26] "IEC White Paper: Grid integration of large-capacity Renewable Energy sources and use of large-capacity Electrical Energy Storage," 2012.

[27] "Integrating intermittent renewables sources into the EU electricity system by 2020."

[28] E. Panos, T. Kober, and A. Wokaun, "Long term evaluation of electric storage technologies vs alternative flexibility options for the Swiss energy system," *Applied Energy*, vol. 252, p. 113470, Oct. 2019.

[29] F. Capitanescu, "TSO–DSO interaction: Active distribution network power chart for TSO ancillary services provision," *Electric Power Systems Research*, vol. 163, pp. 226–230, Oct. 2018.

[30] K. Van den Bergh and E. Delarue, "Energy and reserve markets: interdependency in electricity systems with a high share of renewables," *Electric Power Systems Research*, vol. 189, p. 106537, Dec. 2020.

[31] P. González, J. Villar, C. A. Díaz, and F. A. Campos, "Joint energy and reserve markets: Current implementations and modeling trends," *Electric Power Systems Research*, vol. 109, pp. 101–111, Apr. 2014.

[32] R. Domínguez, G. Oggioni, and Y. Smeers, "Reserve procurement and flexibility services in power systems with high renewable capacity: Effects of integration on different market designs," *International Journal of Electrical Power & Energy Systems*, vol. 113, pp. 1014–1034, Dec. 2019.

[33] D. S. Kirschen, "Power system security," *Power Engineering Journal*, vol. 16, pp. 241–248, Oct. 2002.

[34] C. Maurer, S. Krahl, and H. Weber, "Dimensioning of secondary and tertiary control reserve by probabilistic methods," *European Transactions on Electrical Power*, vol. 19, no. 4, pp. 544–552, 2009.

[35] R. Doherty and M. O'Malley, "A new approach to quantify reserve demand in systems with significant installed wind capacity," *IEEE Transactions on Power Systems*, vol. 20, pp. 587–595, May 2005.

[36] F. Bouffard, F. Galiana, and A. Conejo, "Market-clearing with stochastic security-part II: case studies," *IEEE Transactions on Power Systems*, vol. 20, pp. 1827–1835, Nov. 2005.

[37] A. Ahmadi Khatir, R. Cherkaoui, and O. Alizadeh Mousavi, "Preventive and corrective security market model," in *17th Power Systems Computation Conf*, (Stockholm), 2011.

[38] F. Aminifar, M. Fotuhi-Firuzabad, and M. Shahidehpour, "Unit Commitment With Probabilistic Spinning Reserve and Interruptible Load Considerations," *IEEE Transactions on Power Systems*, vol. 24, pp. 388–397, Feb. 2009.

[39] M. Shahidehpour, H. Yamin, and Z. Li, *Market Operations in Electric Power Systems*. New York, USA: John Wiley & Sons, Inc., Apr. 2002.

[40] J. Lin and F. H. Magnago, *ELECTRICITY MARKETS: Theories and Applications*. John Wiley & Sons, 2017.

[41] A. E. Boardman, D. H. Greenberg, A. R. Vining, and D. L. Weimer, *Cost-Benefit Analysis: Concepts and Practice*. Cambridge University Press, Dec. 2017.

[42] M. Bozorg, F. Sossan, J.-Y. Le Boudec, and M. Paolone, "Influencing the bulk power system reserve by dispatching power distribution networks using local energy storage," *Electric Power Systems Research*, vol. 163, pp. 270–279, Oct. 2018.

[43] "Energy statistic Switzerland," tech. rep., Swissgrid Ltd, Aarau, 2021. https://www.swissgrid.ch/en/home/customers/topics/energy-data-ch.html.

[44] Swissgrid, "Tender for control power," tech. rep., Swissgrid Ltd, Aarau, 2021. https://www.swissgrid.ch/en/home/customers/topics/ancillary-services/tenders.html.

[45] "Balance energy in the Swissgrid control area," tech. rep., Swissgrid Ltd, 2021. https://www.swissgrid.ch/en/home/customers/topics/bgm/balance-energy.html.

[46] J. Lofberg, "YALMIP : a toolbox for modeling and optimization in MATLAB," in *2004 IEEE International Conference on Robotics and Automation*, pp. 284–289, Sept. 2004.

[47] "Gurobi Optimizer Reference Manual," 2020.

[48] "3rd ENTSO-E Guideline for Cost Benefit Analysis of Grid Development Projects," tech. rep., ENTSO-E, 2020.

[49] A. J. Wood, F. W. Bruce, and B. S. Gerald, *Power Generation, Operation and Control*. United States of America: Wiley, 3 ed., 2013.

[50] W. F. Tinney and C. E. Hart, "Power Flow Solution by Newton's Method," *IEEE Transactions on Power Apparatus and Systems*, vol. PAS-86, pp. 1449–1460, Nov. 1967.

[51] B. Stott, "Review of load-flow calculation methods," *Proceedings of the IEEE*, vol. 62, pp. 916–929, July 1974.

[52] Y. Qi, D. Shi, and D. Tylavsky, "Impact of assumptions on DC power flow model accuracy," in *2012 North American Power Symposium (NAPS)*, pp. 1–6, Sept. 2012.

[53] B. Stott, J. Jardim, and O. Alsac, "DC Power Flow Revisited," *IEEE Transactions on Power Systems*, vol. 24, pp. 1290–1300, Aug. 2009. Conference Name: IEEE Transactions on Power Systems.

[54] Z. Yang, H. Zhong, Q. Xia, and C. Kang, "Solving OPF using linear approximations: fundamental analysis and numerical demonstration," *IET Generation, Transmission & Distribution*, vol. 11, no. 17, pp. 4115–4125, 2017.

[55] R. Kaye and F. Wu, "Analysis of linearized decoupled power flow approximations for steady-state security assessment," *IEEE Transactions on Circuits and Systems*, vol. 31, pp. 623–636, July 1984.

[56] J. W. Simpson-Porco, "Lossy DC Power Flow," *IEEE Transactions on Power Systems*, vol. 33, pp. 2477–2485, May 2018.

[57] P. Yan and A. Sekar, "Study of linear models in steady state load flow analysis of power systems," in *2002 IEEE Power Engineering Society Winter Meeting. Conference Proceedings (Cat. No.02CH37309)*, vol. 1, pp. 666–671 vol.1, Jan. 2002.

[58] R. Baldick, "Variation of distribution factors with loading," *IEEE Transactions on Power Systems*, vol. 18, pp. 1316–1323, Nov. 2003. Conference Name: IEEE Transactions on Power Systems.

[59] C. Coffrin and P. Van Hentenryck, "A Linear-Programming Approximation of AC Power Flows," *arXiv:1206.3614 [cs, math]*, Aug. 2013. arXiv: 1206.3614.

[60] H. Zhang, G. T. Heydt, V. Vittal, and J. Quintero, "An Improved Network Model for Transmission Expansion Planning Considering Reactive Power and Network Losses," *IEEE Transactions on Power Systems*, vol. 28, pp. 3471–3479, Aug. 2013. Conference Name: IEEE Transactions on Power Systems.

[61] H. Zhang, V. Vittal, G. T. Heydt, and J. Quintero, "A relaxed AC optimal power flow model based on a Taylor series," in *2013 IEEE Innovative Smart Grid Technologies-Asia (ISGT Asia)*, pp. 1–5, Nov. 2013. ISSN: 2378-8542.

[62] S. M. Fatemi, S. Abedi, G. B. Gharehpetian, S. H. Hosseinian, and M. Abedi, "Introducing a Novel DC Power Flow Method With Reactive Power Considerations," *IEEE Transactions on Power Systems*, vol. 30, pp. 3012–3023, Nov. 2015.

[63] Z. Yang, K. Xie, J. Yu, H. Zhong, N. Zhang, and Q. Xia, "A General Formulation of Linear Power Flow Models: Basic Theory and Error Analysis," *IEEE Transactions on Power Systems*, vol. 34, pp. 1315–1324, Mar. 2019.

[64] S. V. Dhople, S. S. Guggilam, and Y. C. Chen, "Linear approximations to AC power flow in rectangular coordinates," in *2015 53rd Annual Allerton Conference on Communication, Control, and Computing (Allerton)*, pp. 211–217, Sept. 2015.

[65] Z. Li, J. Yu, and Q. H. Wu, "Approximate Linear Power Flow Using Logarithmic Transform of Voltage Magnitudes With Reactive Power and Transmission Loss Consideration," *IEEE Transactions on Power Systems*, vol. 33, pp. 4593–4603, July 2018.

[66] H. Kile, K. Uhlen, L. Warland, and G. Kjølle, "A comparison of AC and DC power flow models for contingency and reliability analysis," in *2014 Power Systems Computation Conference*, pp. 1–7, Aug. 2014.

[67] T. Overbye, X. Cheng, and Y. Sun, "A comparison of the AC and DC power flow models for LMP calculations," in *37th Annual Hawaii International Conference on System Sciences, 2004. Proceedings of the*, pp. 9 pp.–, Jan. 2004.

[68] H. Cetinay, S. Soltan, F. A. Kuipers, G. Zussman, and P. Van Mieghem, "Comparing the Effects of Failures in Power Grids Under the AC and DC Power Flow Models," *IEEE Transactions on Network Science and Engineering*, vol. 5, pp. 301–312, Oct. 2018.

[69] K. Dvijotham and D. K. Molzahn, "Error bounds on the DC power flow approximation: A convex relaxation approach," in *2016 IEEE 55th Conference on Decision and Control (CDC)*, pp. 2411–2418, Dec. 2016.

[70] K. Purchala, L. Meeus, D. Van Dommelen, and R. Belmans, "Usefulness of DC power flow for active power flow analysis," in *IEEE Power Engineering Society General Meeting, 2005*, pp. 454–459 Vol. 1, June 2005. ISSN: 1932-5517.

[71] K. Baker, "Solutions of DC OPF are Never AC Feasible," in *Proceedings of the Twelfth ACM International Conference on Future Energy Systems*, (Virtual Event Italy), pp. 264–268, ACM, June 2021.

[72] J. Rissman, C. Bataille, E. Masanet, N. Aden, W. R. Morrow, N. Zhou, N. Elliott, R. Dell, N. Heeren, B. Huckestein, J. Cresko, S. A. Miller, J. Roy, P. Fennell, B. Cremmins, T. Koch Blank, D. Hone, E. D. Williams, S. de la Rue du Can, B. Sisson, M. Williams, J. Katzenberger, D. Burtraw, G. Sethi, H. Ping, D. Danielson, H. Lu, T. Lorber, J. Dinkel, and J. Helseth, "Technologies and policies to decarbonize global industry: Review and assessment of mitigation drivers through 2070," *Applied Energy*, vol. 266, p. 114848, May 2020.

[73] G. C. Kryonidis, C. S. Demoulias, and G. K. Papagiannis, "A new voltage control scheme for active medium-voltage (MV) networks," *Electric Power Systems Research*, vol. 169, pp. 53–64, Apr. 2019.

[74] G. Fusco and M. Russo, "A Decentralized Approach for Voltage Control by Multiple Distributed Energy Resources," *IEEE Transactions on Smart Grid*, pp. 1–1, 2021.

[75] J. Höckner, S. Voswinkel, and C. Weber, "Market distortions in flexibility markets caused by renewable subsidies – The case for side payments," *Energy Policy*, vol. 137, p. 111135, Feb. 2020.

[76] "Black System South Australia 28 September 2016," tech. rep., Australian Energy Market Operator, Sept. 2016.

[77] "1200 MW Fault Induced Solar Photovoltaic Resource Interruption Disturbance Report," tech. rep., North American Electric Reliability Corporation, 2017.

[78] S. Goutte and P. Vassilopoulos, "The value of flexibility in power markets," *Energy Policy*, vol. 125, pp. 347–357, Feb. 2019.

[79] E. Luo, P. Cong, H. Lu, and Y. Li, "Two-Stage Hierarchical Congestion Management Method for Active Distribution Networks With Multi-Type Distributed Energy Resources," *IEEE Access*, vol. 8, pp. 120309–120320, 2020.

[80] S. Acharya, M. S. E. Moursi, and A. Al-Hinai, "Coordinated Frequency Control Strategy for an Islanded Microgrid With Demand Side Management Capability," *IEEE Transactions on Energy Conversion*, vol. 33, pp. 639–651, June 2018.

[81] A. Kulmala, S. Repo, and P. Järventausta, "Coordinated Voltage Control in Distribution Networks Including Several Distributed Energy Resources," *IEEE Transactions on Smart Grid*, vol. 5, pp. 2010–2020, July 2014.

[82] M. Zerva and M. Geidl, "Contribution of active distribution grids to the coordinated voltage control of the swiss transmission system," in *2014 Power Systems Computation Conference*, pp. 1–8, Aug. 2014.

[83] G. Valverde, D. Shchetinin, and G. Hug-Glanzmann, "Coordination of Distributed Reactive Power Sources for Voltage Support of Transmission Networks," *IEEE Transactions on Sustainable Energy*, vol. 10, pp. 1544–1553, July 2019.

[84] D. B. Arnold, M. D. Sankur, M. Negrete-Pincetic, and D. S. Callaway, "Model-Free Optimal Coordination of Distributed Energy Resources for Provisioning Transmission-Level Services," *IEEE Transactions on Power Systems*, vol. 33, pp. 817–828, Jan. 2018.

[85] S. Karagiannopoulos, C. Mylonas, P. Aristidou, and G. Hug, "Active Distribution Grids Providing Voltage Support: The Swiss Case," *IEEE Transactions on Smart Grid*, pp. 1–1, 2020.

[86] A. Abessi, V. Vahidinasab, and M. S. Ghazizadeh, "Centralized Support Distributed Voltage Control by Using End-Users as Reactive Power Support," *IEEE Transactions on Smart Grid*, vol. 7, pp. 178–188, Jan. 2016.

[87] F. Capitanescu, "OPF integrating distribution systems flexibility for TSO real-time active power balance management," in *Mediterranean Conference on Power Generation, Transmission, Distribution and Energy Conversion (MEDPOWER 2018)*, pp. 1–5, Nov. 2018.

[88] H. P. Williams, *Model Building in Mathematical Programming*. England: John Wiley & Sons, 2013.

[89] "Tariffs and remunreation rates for the Swiss transmission grid," tech. rep., Swissgrid Ltd, Aarau, 2021. https://www.swissgrid.ch/en/home/customers/topics/tariffs.html.

[90] A. Bernstein and E. Dall'Anese, "Linear power-flow models in multiphase distribution networks," in *2017 IEEE PES Innovative Smart Grid Technologies Conference Europe (ISGT-Europe)*, pp. 1–6, Sept. 2017.

[91] A. Bernstein, C. Wang, E. Dall'Anese, J. L. Boudec, and C. Zhao, "Load Flow in Multiphase Distribution Networks: Existence, Uniqueness, Non-Singularity and Linear Models," *IEEE Transactions on Power Systems*, vol. 33, pp. 5832–5843, Nov. 2018.

[92] Carpentier, J, "Contribution a l'etude du dispatching economique.," *Bulletin de la Societe Francaise des Electriciens 3.1*, pp. 431–447, 1962.

[93] M. Huneault and F. Galiana, "A survey of the optimal power flow literature," *IEEE Transactions on Power Systems*, vol. 6, pp. 762–770, May 1991.

[94] J. Momoh, R. Adapa, and M. El-Hawary, "A review of selected optimal power flow literature to 1993. I. Nonlinear and quadratic programming approaches," *IEEE Transactions on Power Systems*, vol. 14, pp. 96–104, Feb. 1999.

[95] J. Momoh, M. El-Hawary, and R. Adapa, "A review of selected optimal power flow literature to 1993. II. Newton, linear programming and interior point methods," *IEEE Transactions on Power Systems*, vol. 14, pp. 105–111, Feb. 1999.

[96] S. Frank, I. Steponavice, and S. Rebennack, "Optimal power flow: a bibliographic survey I: Formulations and deterministic methods," *Energy Systems*, vol. 3, pp. 221–258, Sept. 2012.

[97] S. Frank, I. Steponavice, and S. Rebennack, "Optimal power flow: a bibliographic survey II: Non-deterministic and hybrid methods," *Energy Systems*, vol. 3, pp. 259–289, Sept. 2012.

[98] D. K. Molzahn and Hiskens, Ian A., *A Survey of Relaxations and Approximations of the Power Flow Equations*. IEEE, 2019.

[99] E. P. de Carvalho, A. dos Santos, and T. F. Ma, "Reduced gradient method combined with augmented Lagrangian and barrier for the optimal power flow problem," *Applied Mathematics and Computation*, vol. 200, pp. 529–536, July 2008.

[100] Y. Y. Hong, "Enhanced Newton optimal power flow approach: experiences in taiwan power system," *IET Generation, Transmission and Distribution*, vol. 139, pp. 205–210, May 1992.

[101] G. L. Torres and V. H. Quintana, "An interior-point method for nonlinear optimal power flow using voltage rectangular coordinates," *IEEE Transactions on Power Systems*, vol. 13, pp. 1211–1218, Nov. 1998.

[102] W. Yan, J. Yu, D. Yu, and K. Bhattarai, "A new optimal reactive power flow model in rectangular form and its solution by predictor corrector primal dual interior point method," *IEEE Transactions on Power Systems*, vol. 21, pp. 61–67, Feb. 2006.

[103] A. A. Sousa, G. L. Torres, and C. A. Cañizares, "Robust Optimal Power Flow Solution Using Trust Region and Interior-Point Methods," *IEEE Transactions on Power Systems*, vol. 26, pp. 487–499, May 2011.

[104] M. S. Kumari and S. Maheswarapu, "Enhanced Genetic Algorithm based computation technique for multi-objective Optimal Power Flow solution," *International Journal of Electrical Power & Energy Systems*, vol. 32, pp. 736–742, July 2010.

[105] M. R. AlRashidi and M. E. El-Hawary, "Hybrid Particle Swarm Optimization Approach for Solving the Discrete OPF Problem Considering the Valve Loading Effects," *IEEE Transactions on Power Systems*, vol. 22, pp. 2030–2038, Nov. 2007.

[106] B. Das and P. K. Verma, "Artificial neural network-based optimal capacitor switching in a distribution system," *Electric Power Systems Research*, vol. 60, pp. 55–62, Dec. 2001.

[107] M. A. Abido, "Optimal Power Flow Using Tabu Search Algorithm," *Electric Power Components and Systems*, vol. 30, pp. 469–483, May 2002.

[108] S. H. Low, "Convex Relaxation of Optimal Power Flow—Part I: Formulations and Equivalence," *IEEE Transactions on Control of Network Systems*, vol. 1, pp. 15–27, Mar. 2014.

[109] S. H. Low, "Convex Relaxation of Optimal Power Flow—Part II: Exactness," *IEEE Transactions on Control of Network Systems*, vol. 1, pp. 177–189, June 2014.

[110] X. Bai, H. Wei, K. Fujisawa, and Y. Wang, "Semidefinite programming for optimal power flow problems," *International Journal of Electrical Power & Energy Systems*, vol. 30, pp. 383–392, July 2008.

[111] X. Bai and H. Wei, "Semi-definite programming-based method for security-constrained unit commitment with operational and optimal power flow constraints," *IET Generation, Transmission & Distribution*, vol. 3, pp. 182–197, Feb. 2009.

[112] J. Lavaei and S. H. Low, "Zero Duality Gap in Optimal Power Flow Problem," *IEEE Transactions on Power Systems*, vol. 27, pp. 92–107, Feb. 2012.

[113] B. C. Lesieutre, D. K. Molzahn, A. R. Borden, and C. L. DeMarco, "Examining the limits of the application of semidefinite programming to power flow problems," in *Annual Conference on Communication, Control, and Computing*, (Allerton), pp. 1492–1499, Sept. 2011.

[114] M. Baran and F. Wu, "Optimal capacitor placement on radial distribution systems," *IEEE Transactions on Power Delivery*, vol. 4, pp. 725–734, Jan. 1989.

[115] M. Baran and F. Wu, "Optimal sizing of capacitors placed on a radial distribution system," *IEEE Transactions on Power Delivery*, vol. 4, pp. 735–743, Jan. 1989.

[116] R. Jabr, "Radial distribution load flow using conic programming," *IEEE Transactions on Power Systems*, vol. 21, pp. 1458–1459, Aug. 2006.

[117] J. A. Taylor, *Conic optimization of electric power systems.* Thesis, Massachusetts Institute of Technology, 2011.

[118] J. A. Taylor and F. S. Hover, "Convex Models of Distribution System Reconfiguration," *IEEE Transactions on Power Systems*, vol. 27, pp. 1407–1413, Aug. 2012.

[119] M. Farivar and S. H. Low, "Branch Flow Model: Relaxations and Convexification—Part I," *IEEE Transactions on Power Systems*, vol. 28, pp. 2554–2564, Aug. 2013.

[120] M. Farivar and S. H. Low, "Branch Flow Model: Relaxations and Convexification—Part II," *IEEE Transactions on Power Systems*, vol. 28, pp. 2565–2572, Aug. 2013.

[121] L. Gan, N. Li, U. Topcu, and S. H. Low, "Exact Convex Relaxation of Optimal Power Flow in Radial Networks," *IEEE Transactions on Automatic Control*, vol. 60, pp. 72–87, Jan. 2015. Conference Name: IEEE Transactions on Automatic Control.

[122] K. Christakou, D.-C. Tomozei, J.-Y. Le Boudec, and M. Paolone, "AC OPF in radial distribution networks – Part II: An augmented Lagrangian-based OPF algorithm, distributable via primal decomposition," *Electric Power Systems Research*, vol. 150, pp. 24–35, Sept. 2017.

[123] K. Christakou, D.-C. Tomozei, J.-Y. Le Boudec, and M. Paolone, "AC OPF in radial distribution networks – Part I: On the limits of the branch flow convexification and the alternating direction method of multipliers," *Electric Power Systems Research*, vol. 143, pp. 438–450, Feb. 2017.

[124] M. Nick, R. Cherkaoui, J.-Y. L. Boudec, and M. Paolone, "An Exact Convex Formulation of the Optimal Power Flow in Radial Distribution Networks Including Transverse Components," *IEEE Transactions on Automatic Control*, vol. 63, pp. 682–697, Mar. 2018.

[125] A. Castillo, P. Lipka, J.-P. Watson, S. S. Oren, and R. P. O'Neill, "A successive linear programming approach to solving the iv-acopf," *IEEE Transactions on Power Systems*, vol. 31, pp. 2752–2763, July 2016.

[126] Q. Zhou and J. W. Bialek, "SIMPLIFIED CALCULATION OF VOLTAGE AND LOSS SENSITIVITY FACTORS IN DISTRIBUTION NETWORKS," p. 6, 2008.

[127] S. Bolognani and F. Dörfler, "Fast power system analysis via implicit linearization of the power flow manifold," in *2015 53rd Annual Allerton Conference on Communication, Control, and Computing (Allerton)*, pp. 402–409, Sept. 2015.

[128] S. Bolognani and S. Zampieri, "On the Existence and Linear Approximation of the Power Flow Solution in Power Distribution Networks," *IEEE Transactions on Power Systems*, vol. 31, pp. 163–172, Jan. 2016.

[129] Y. G. Rebours, D. S. Kirschen, M. Trotignon, and S. Rossignol, "A Survey of Frequency and Voltage Control Ancillary Services—Part I: Technical Features," *IEEE Transactions on Power Systems*, vol. 22, pp. 350–357, Feb. 2007.

[130] Y. G. Rebours, D. S. Kirschen, M. Trotignon, and S. Rossignol, "A Survey of Frequency and Voltage Control Ancillary Services—Part II: Economic Features," *IEEE Transactions on Power Systems*, vol. 22, pp. 358–366, Feb. 2007.

[131] M. Heleno, R. Soares, J. Sumaili, R. J. Bessa, L. Seca, and M. A. Matos, "Estimation of the flexibility range in the transmission-distribution boundary," in *2015 IEEE Eindhoven PowerTech*, pp. 1–6, June 2015.

[132] J. Silva, J. Sumaili, R. J. Bessa, L. Seca, M. A. Matos, V. Miranda, M. Caujolle, B. Goncer, and M. Sebastian-Viana, "Estimating the Active and Reactive Power Flexibility Area at the TSO-DSO Interface," *IEEE Transactions on Power Systems*, vol. 33, pp. 4741–4750, Sept. 2018.

[133] J. Silva, J. Sumaili, R. J. Bessa, L. Seca, M. Matos, and V. Miranda, "The challenges of estimating the impact of distributed energy resources flexibility on the TSO/DSO boundary node operating points," *Computers & Operations Research*, vol. 96, pp. 294–304, Aug. 2018.

[134] H. Gerard, E. I. Rivero Puente, and D. Six, "Coordination between transmission and distribution system operators in the electricity sector: A conceptual framework," *Utilities Policy*, vol. 50, pp. 40–48, Feb. 2018.

[135] F. P. Andrén, T. I. Strasser, J. L. Baut, M. Rossi, G. Viganò, G. D. Croce, S. Horsmanheimo, A. G. Azar, and A. Ibañez, "Validating Coordination Schemes between Transmission and Distribution System Operators using a Laboratory-Based Approach," in *2019 IEEE Milan PowerTech*, pp. 1–6, June 2019.

[136] M. Rossi, G. Viganò, G. Migliavacca, Y. Vardanyan, R. Ebrahimy, G. Leclercq, P. Sels, and M. Pavesi, "Testing TSO-DSO Interaction Schemes for the Participation of Distribution Energy Resources in the Balancing Market: the SmartNet Simulator," AIM, June 2019.

[137] A. Cabrera-Tobar, E. Bullich-Massagué, M. Aragüés-Peñalba, and O. Gomis-Bellmunt, "Capability curve analysis of photovoltaic generation systems," *Solar Energy*, vol. 140, pp. 255–264, Dec. 2016.

[138] P. Kundur and N. J. Balu, *Power System Stability And Control*. New York, NY, USA: McGraw-Hill.

[139] S. Engelhardt, I. Erlich, C. Feltes, J. Kretschmann, and F. Shewarega, "Reactive Power Capability of Wind Turbines Based on Doubly Fed Induction Generators," *IEEE Transactions on Energy Conversion*, vol. 26, pp. 364–372, Mar. 2011.

[140] S. P. Boyd and L. Vandenberghe, *Convex optimization*. Cambridge, UK ; New York: Cambridge University Press, 2004.

[141] M. C. Campi and S. Garatti, "The Exact Feasibility of Randomized Solutions of Uncertain Convex Programs," *SIAM Journal on Optimization*, vol. 19, pp. 1211–1230, Jan. 2008.

[142] G. C. Calafiore and M. C. Campi, "The scenario approach to robust control design," *IEEE Transactions on Automatic Control*, vol. 51, pp. 742–753, May 2006.

[143] M. E. Baran and F. F. Wu, "Network reconfiguration in distribution systems for loss reduction and load balancing," *IEEE Transactions on Power Delivery*, vol. 4, pp. 1401–1407, Apr. 1989.

[144] "HOMER - Hybrid Renewable and Distributed Generation System Design Software."

[145] L. Bam and W. Jewell, "Review: power system analysis software tools," in *IEEE Power Engineering Society General Meeting, 2005*, pp. 139–144 Vol. 1, June 2005. ISSN: 1932-5517.

[146] S. Xia, Z. Ding, T. Du, D. Zhang, M. Shahidehpour, and T. Ding, "Multitime Scale Coordinated Scheduling for the Combined System of Wind Power, Photovoltaic, Thermal Generator, Hydro Pumped Storage, and Batteries," *IEEE Transactions on Industry Applications*, vol. 56, pp. 2227–2237, May 2020.

[147] K. Christakou, D.-C. Tomozei, J.-Y. Le Boudec, and M. Paolone, "GECN: Primary Voltage Control for Active Distribution Networks via Real-Time Demand-Response," *IEEE Transactions on Smart Grid*, vol. 5, pp. 622–631, Mar. 2014.

[148] A. Salazar, A. Berzoy, W. Song, and J. M. Velni, "Energy Management of Islanded Nanogrids Through Nonlinear Optimization Using Stochastic Dynamic Programming," *IEEE Transactions on Industry Applications*, vol. 56, pp. 2129–2137, May 2020.

[149] M. J. Dolan, E. M. Davidson, I. Kockar, G. W. Ault, and S. D. J. McArthur, "Distribution Power Flow Management Utilizing an Online Optimal Power Flow Technique," *IEEE Transactions on Power Systems*, vol. 27, pp. 790–799, May 2012.

[150] L. Zhao, W. Zhang, H. Hao, and K. Kalsi, "A Geometric Approach to Aggregate Flexibility Modeling of Thermostatically Controlled Loads," *IEEE Transactions on Power Systems*, vol. 32, pp. 4721–4731, Nov. 2017.

[151] S. Gill, I. Kockar, and G. W. Ault, "Dynamic Optimal Power Flow for Active Distribution Networks," *IEEE Transactions on Power Systems*, vol. 29, pp. 121–131, Jan. 2014.

[152] A. Saint-Pierre and P. Mancarella, "Active Distribution System Management: A Dual-Horizon Scheduling Framework for DSO/TSO Interface Under Uncertainty," *IEEE Transactions on Smart Grid*, vol. 8, pp. 2186–2197, Sept. 2017.

[153] T. Ding, C. Li, Y. Yang, J. Jiang, Z. Bie, and F. Blaabjerg, "A Two-Stage Robust Optimization for Centralized-Optimal Dispatch of Photovoltaic Inverters in Active Distribution Networks," *IEEE Transactions on Sustainable Energy*, vol. 8, pp. 744–754, Apr. 2017.

[154] F. Sossan, E. Namor, R. Cherkaoui, and M. Paolone, "Achieving the Dispatchability of Distribution Feeders Through Prosumers Data Driven Forecasting and Model Predictive Control of Electrochemical Storage," *IEEE Transactions on Sustainable Energy*, vol. 7, pp. 1762–1777, Oct. 2016.

[155] R. K. Gupta, F. Sossan, and M. Paolone, "Grid-aware Distributed Model Predictive Control of Heterogeneous Resources in a Distribution Network: Theory and Experimental Validation," *IEEE Transactions on Energy Conversion*, pp. 1–1, 2020.

[156] Y. Chu and C. F. M. Coimbra, "Short-term probabilistic forecasts for Direct Normal Irradiance," *Renewable Energy*, vol. 101, pp. 526–536, Feb. 2017.

[157] "Power systems in transition: Challenges and opportunities ahead for electricity security," tech. rep., International Energy Agency, Nov. 2020. [Online]. Available: https://www.iea.org/reports/power-systems-in-transition.

[158] "Global Risk Report 2020," tech. rep., World Economic Forum, 2020. [Online]. Available: https://www.weforum.org/reports/the-global-risks-report-2020.

[159] R. Billinton, *Reliability Evaluation of Power Systems*. New York: Springer US, 1st edition ed., 1984.

[160] W. Li, *Risk Assessment of Power Systems*. United States of America: John Wiley & Sons, 2014.

MOHSEN KALANTAR NEYESTANAKI

Avenue du Tumple 7 ⋄ 1020 Renens, Vaud, Switzerland
+41 (0)78 640 48 26 ⋄ mohsen.kalantar.n@gmail.com

KEY COMPETENCIES

- Convex/Heuristic Optimization, Decision Making under Uncertainty, Stochastic/Robust Optimization, Model Predictive Control (MPC).
- Data Mining, Bad-Data Detection, State Estimation, Reliability Modeling & Assessment.
- Machine Learning-Based Prediction and Application of Data Science & Machine Learning in Power Systems.
- Transmission System Operator (TSO) & Distribution System Operator (DSO) Coordination.
- Optimal Planning, Operation and Control of Transmission/Distribution Networks.
- Optimal Planning, Operation and Control of Distributed Energy Resources & Energy Storage Systems.
- Wide-Area Monitoring, Protection and Control (WAMPAC) Systems and Phasor Measurement Units (PMUs).

EDUCATION

EPFL – École Polytechnique Fédérale de Lausanne February 2017 - Present
PhD in Electrical Engineering, Power Systems Group *Lausanne, Switzerland*

- Thesis title: " Advanced Frameworks to Aggregate and Unlock the Power Flexibility of Distributed Energy Resources Located in Active Distribution Networks"
(Supervisor: Prof. Rachid Cherkaoui)

SUT – Sharif University of Technology September 2011 - September 2013
M.Sc. in Electrical Engineering, Power Systems, ***GPA:19.01/20*** *Tehran, Iran*

- Thesis title: "Adaptive Backup Protection of Transmission Grids Utilizing Real-time Measurements of Phasor Measurement Units (PMUs)" (Supervisor: Prof. Ali-Mohammad Ranjbar)

SUT – Sharif University of Technology September 2006 - September 2011
B.Sc. in Electrical Engineering, Power, ***GPA:18.32/20*** *Tehran, Iran*

- Thesis title: 'Applications of Frequency Disturbance Recorders (FDRs) and Frequency Monitoring Network (FNET) for Power Systems" (Supervisor: Prof. Mahmud Fotuhi-Firuzabad)

SUT – Sharif University of Technology September 2006 - September 2011
B.Sc. in Physics (Double major program with Electrical Engineering), ***GPA:18.32/20*** *Tehran, Iran*

- Thesis title: 'Measuring the Gravitational Constant G Based on Various Methods"
(Supervisor: Prof. Azam Iraji Zad)

SCIENTIFIC PUBLICATIONS

Journal Papers

1. **M. Kalantar-Neyestanaki**, A. M. Ranjbar, "An Adaptive PMU-Based Wide Area Backup Protection Scheme for Power Transmission Lines," IEEE Transactions on Smart Grid, vol. 6, no. 3, pp. 1550–1559, May 2015.
2. **M. Kalantar-Neyestanaki**, F. Sossan, M. Bozorg, R. Cherkaoui, "Characterizing the Reserve Provision Capability Area of Active Distribution Networks: A Linear Robust Optimization Method," IEEE Transactions on Smart Grid, vol. 11, no. 3, pp. 2464–2475, November 2019.

3. **M. Kalantar-Neyestanaki**, R. Cherkaoui, "Coordinating Distributed Energy Resources and Utility-Scale Battery Energy Storage System for Power Flexibility Provision Under Uncertainty," IEEE Transactions on Sustainable Energy, 2021.

4. O. Galland, **M. Kalantar-Neyestanaki**, L. Eggenschwiler, P. Favre-Perrod, R. Cherkaoui, "Maintenir l'équilibre, à l'avenir aussi," bulletin.ch, April 2020 (In French).

Journal Papers Under Revision

5. **M. Kalantar-Neyestanaki**, R. Cherkaoui, "Risk-Aware Active Power Flexibility Allocation from TSO-DSO Interconnections: The Switzerland's Transmission Network," Under review at IEEE Systems Journal.

6. **M. Kalantar-Neyestanaki**, R. Cherkaoui, "Grid-Cognizant TSO and DSO Coordination Framework for Active and Reactive Power Flexibility Exchange: The Swiss Case Study," Under review at IEEE Transactions on Power Systems.

Conference Papers

7. A. Salehi Dobakhshari, **M. Kalantar-Neyestanaki** , A. M. Ranjbar, "Transmission Grid Fault Diagnosis by Wide Area Measurement System," International Power System Conference (PSC), pp 1-6, Tehran, Iran, November 12^{th}-14^{th}, 2012.

8. **M. Kalantar-Neyestanaki**, M. Bozorg, F. Sossan, R. Cherkaoui, "Allocation of Frequency Control Reserve from Aggregated Resources of Active Distribution Systems," Power System Computational Conference (PSCC), pp. 1-8, Dublin, Irland, June 11^{th}-15^{th}, 2018.

9. **M. Kalantar-Neyestanaki**, M. Bozorg, F. Sossan, R. Cherkaoui, "Allocation of Active Power Reserve from Active Distribution Networks Using a Cost-Benefit Approach: Application to Swissgrid Network," IEEE PowerTech, pp. 1-6, Milan, Italy, June 23^{rd}-27^{th}, 2019.

10. S. Bjarghov, **M. Kalantar-Neyestanaki**, R. Cherkaoui, H. Farahmand, "Battery Degradation-Aware Local Flexibility Market for Congestion Management," IEEE PowerTech, pp. 1-6, Madrid, Spain, June 28^{th}-July 2^{nd}, 2021.

AWARDS

- **Semi-finalist** in the National **Physics Olympiad** of Iran, April 2004.
- Distinguished as an **Exceptional Student** at Sharif University of Technology and received admission into the **double major program in Electrical Engineering and Physics** (Sep. 2009).
- **Ranked 1^{st}** among B.Sc. students, Power Systems Group, Electrical Engineering Department, Sharif University of Technology (entrance year: 2006)
- **Ranked 3^{rd}** among B.Sc. students, Physics Department, Sharif University of Technology (entrance year: 2006).
- Straight Admission (exempt from entrance exam) for M.Sc. program, Electrical Engineering Department, Sharif University of Technology (Sep. 2011).
- **Ranked** 1^{st} among M.Sc. students, power systems group, Electrical Engineering Department, Sharif University of Technology (entrance year: 2011).
- Member of the "Iranian National Elite Foundation".

PROFESSIONAL EXPERIENCE

IGMC – The Transmission System Operator of Iran January 2015 - December 2016
R&D Engineer *Tehran, Iran*

- Developing a grid-parameter-independent method to predict (detect) out-of-step condition of synchronous generators on the basis of the data gathered by wide area measurement system (WAMS).
- Applying the above-mentioned method to the transmission network of Iran operated by IGMC.
- Upgrading the wide area situational awareness dashboard of IGMC WAMS control center by constructing a graphical user interface to visualize real-time nodal phase angles of the nationwide transmission network of IGMC on geographical map.
- Evaluating the efficiency of the situational awareness system of IGMC WAMS control center.
- Evaluating the efficiency of the wide area monitoring, protection and control (WAMPAC) system of IGMC WAMS control center.

SUT – Sharif University of Technology September 2013 - January 2015
Senior Researcher *Tehran, Iran*

- Developing a transmission grid fault diagnosis method to detect the faulted line as well as fault location using a limited number of synchronized phasor measurements.
- Constructing an adaptive PMU-based wide area backup protection scheme for transmission grids.

INVOLVEMENT IN RESEARCH PROJECTS

PASREN Project **EPFL – École Polytechnique Fédérale de Lausanne**
*Joint Project between EPFL & **Swissgrid*** *February 2017 - October 2021*

- Constructing the case study model of the swiss transmission network (used for planing and operational studies) on the basis of the data provided by swissgrid.
- Developing a risk-aware active power flexibility allocation tool (formulated as a two-stage linear stochastic optimization problem) for swissgrid and applying it to Swissgrid's network.
- Introducing a grid&uncertainty-cognizant approach (formulated as a set of linear scenario-based robust optimization problems) to quantify the capability of active distribution networks for power flexibility provision to the TSO and applying it to the grid of Agile.
- Modernizing the traditional top-to-down (from transmission system to distribution systems) power flexibility provision mechanism to a bi-directional power flexibility provision structure between TSO and DSOs.

REel-DEMO **EPFL – École Polytechnique Fédérale de Lausanne**
*Joint Project Between EPFL & **Romande Energie*** *November 2018 - December 2020*

- Constructing a two-stage method, i.e. short-term scheduling (formulated as a linear stochastic optimization problem) and real-time control (formulated as a linear optimization-based control strategy), to empower distribution system operators (DSOs) to optimally procure the power flexibility of distributed energy resource located in their grid.
- Developing a machine learning-based approach to predict the active power generation of PV units and active power consumption of loads in the grid of Aigle.
- Developing a machine learning-based approach to generate scenarios for modeling the prediction errors of load consumption and PV generation considering the inter-temporal correlation of prediction errors.

PMU4WAP **SUT – Sharif University of Technology**
*Joint Project Between SUT & **IGMC (the TSO of Iran)*** *September 2012 - January 2015*

- Constructing the model of phasor measurement unit (PMU) in Matlab.
- Introducing the first-ever concept of backup protection zone consisting a set of transmission lines and buses with the purpose of implementing the wide area backup protection of transmission network.
- Developing a method to locate phasor measurement units in the transmission grid with the aim of implementing a wide area backup protection scheme.

- Developing a transmission grid fault diagnosis method to detect the faulted line as well as fault location using a limited number of synchronized phasor measurements.
- Constructing an adaptive PMU-based wide area backup protection scheme for transmission grids.

PRESENTATIONS AT CONFERENCES & SEMINARS

Oral Presentations

1. M. Kalantar-Neyestanaki, R. Cherkaoui, "A Comprehensive Survey of Ancillary Services Provision from Regional Energy Newrorks," Presented at the Swissgrid-EPFL Steering Committee Meeting, Swissgrid Ltd, Regional Office Bern, Bern, Switzerland, June 13th, 2017.
2. M. Kalantar-Neyestanaki, R. Cherkaoui, "Modeling the Aggregated Power Flexibility of Regional Energy Networks from TSO's Perspective," Presented at the Swissgrid-EPFL Steering Committee Meeting, Swissgrid Ltd, Regional Office Bern, Bern, Switzerland, November 21st, 2017.
3. M. Kalantar-Neyestanaki, R. Cherkaoui, "Constructing the Case Study Model of the Swiss Transmission Network (Used for Planing and Operational Studies) on the Basis of the Data Provided by Swissgrid," Presented at the Swissgrid-EPFL Steering Committee Meeting, Swissgrid Ltd, Regional Office Bern, Bern, Switzerland, May 16th, 2018.
4. M. Kalantar-Neyestanaki, R. Cherkaoui, "Provision of Ancillary Services from Regional Energy Networks: Characterizing the Reserve Provision Capability Area of Active Distribution Networks," Presented at the SCCER-FURIES Annual Conference 2018, Swiss Tech Convention Center-EPFL, Lausanne, Switzerland, October 22nd, 2018.
5. M. Kalantar-Neyestanaki, R. Cherkaoui, "Characterizing the Active/Reactive Power Flexibility Provision Capability (FPC) Area of Active Distribution Networks (ADNs)," Presented at the Swissgrid-EPFL Steering Committee Meeting, Swissgrid Ltd, Aarau (Headquarters), Switzerland, November 16th, 2018.
6. M. Kalantar-Neyestanaki, R. Cherkaoui, "Unlocking the Power Flexibility of Distributed Energy Resources Installed in Distribution Networks," Presented at the Romande Energie-EPFL Meeting, EPFL, Lausanne, Switzerland, November 25th, 2018.
7. M. Kalantar-Neyestanaki, R. Cherkaoui, "Advantages of Ancillary Services Provision from Distribution Networks," Presented at the DESL-PV lab Common Workshop, CSEM, Neuchˆatel, Switzerland, January 22nd, 2019.
8. M. Kalantar-Neyestanaki, R. Cherkaoui, "Modeling and Analysis of Distribution Networks for Power Flexibility Provision," Presented at the REel Demo Coordination Meeting, EPFL, Lausanne, Switzerland, March 12th, 2019.
9. M. Kalantar-Neyestanaki, R. Cherkaoui, "Risk-Aware Allocation of Active Power Flexibility from Active Distribution Networks Using a Cost-Benefit Approach: Application to the Swissgrid Network," Presented at the Swissgrid-EPFL Steering Committee Meeting, Swissgrid Ltd, Aarau (Headquarters), Aarua, Switzerland, May 29th, 2019.
10. M. Kalantar-Neyestanaki, R. Cherkaoui, "Provision of Ancillary Services From Regional Energy Networks," Presented at the FEN-EPFL Meeting, Research Center for Energy Networks (FEN), ETHZ, Zurich, Switzerland, August 28th, 2019.
11. M. Kalantar-Neyestanaki, R. Cherkaoui, "Characterizing the Reserve Provision Capability Area of Active Distribution Networks: A Linear Robust Optimization Method," Presented at the Joint Workshop DTU-EPFL, EPFL, Lausanne, Switzerland, September 2nd, 2019.

12. M. Kalantar-Neyestanaki, R. Cherkaoui, "Flexibility Provision from ADNs to Transmission System: A Comprehensive Approach," Presented at SCCER-FURIES Annual Conference 2019, Aarau, Switzerland, October 21st, 2019.

13. M. Kalantar-Neyestanaki, R. Cherkaoui, "Short-Term Scheduling of Active Distribution Networks for Flexibility Provision at the TSO-DSO Connection Point," Presented at the Swissgrid-EPFL Steering Committee Meeting, EPFL, Lausanne, Switzerland, December 11th, 2019.

14. M. Kalantar-Neyestanaki, R. Cherkaoui, "Uncertainty-Aware Coordinating Distributed Energy Resources for Active/Reactive Powers Flexibility Provision," Presented at the REeL Demo Coordination Meeting, EPFL, Lausanne, Switzerland, February 3rd, 2020.

15. M. Kalantar-Neyestanaki, R. Cherkaoui, "Optimal Scheduling and Control of Active Distribution Networks for Power Flexibility Provision at TSO-DSO Interface," Presented at the Swissgrid-EPFL Steering Committee Meeting (Online Zoom Meeting), May 28th, 2020.

16. M. Kalantar-Neyestanaki, R. Cherkaoui, "Grid-Cognizant Allocation of Active & Reactive Power Reserve from TSO-DSO Interconnections: Application to the Transmission Network of Switzerland," Presented at the Final Swissgrid-EPFL Steering Committee Meeting (Online Zoom Meeting), December 3rd, 2020.

Poster Presentations

17. M. Kalantar-Neyestanaki, R. Cherkaoui, "Allocation of Frequency Control Reserve from Aggregated Resources of Regional Energy Networks," Presented at SCCER-FURIES Annual Conference 2017, Swiss Tech Convention Center-EPFL, Lausanne, Switzerland, November 2nd, 2017.

18. M. Kalantar-Neyestanaki, R. Cherkaoui, "Provision of Ancillary Services from Regional Energy Networks: Characterizing the Reserve Provision Capability Area of Active Distribution Networks," Presented at the SCCER-FURIES Annual Conference 2018, Swiss Tech Convention Center-EPFL, Lausanne, Switzerland, October 22nd, 2018.

19. M. Kalantar-Neyestanaki, R. Cherkaoui, "Allocation of Frequency Control Reserve from Aggregated Resources of Regional Energy Networks," Presented at EPFL's 2nd Summer School on Energy, Champéry, Switzerland, June 10th-14th, 2019.

20. M. Kalantar-Neyestanaki, M. Bozorg, F. Sossan, R. Cherkaoui, "Allocation of Active Power Reserve from Active Distribution Networks Using a Cost-Benefit Approach: Application to Swissgrid Network," IEEE PowerTech, pp. 1-6, Milan, Italy, June 23rd-27th, 2019.

21. M. Kalantar-Neyestanaki, R. Cherkaoui, "Flexibility Provision from ADNs to Transmission System: A Comprehensive Approach," Presented at SCCER-FURIES Annual Conference 2019, Aarau, Switzerland, October 21st, 2019.

SUPERVISED STUDENTS

- Killian, D. G., "Evaluating the Performance of Local Quantile Regression (LQR), Local Gaussian Model (LGM) and Nadaraya–Watson Estimator for Predicting Wind Power Production", *M.Sc. Semester Project*.
- Rebecca Luther, M., "Optimal Power Flow in ewz Distribution Grid with High Penetration of Electrical Vehicles Utilizing Power Flexibility of Distributed Energy Resources (DERs)", *M.Sc. Thesis*.
- Savard, B., "Developing a Methodology to Generate Scenarios for Modeling the Short-Term Prediction Error of Wind Power Production Considering the Inter-Temporal Correlation of Prediction Errors", *B.Sc. Semester Project*, *Exchange B.Sc. Student from Laval University (Quebec, Canada)*.

- Bjarghov, S., "Constructing a Battery Degradation-Aware Local Flexibility Market for Congestion Management at Distribution Grids", *Visiting PhD Student from NTNU.*

TECHNICAL COURSES

NEPLAN Intensive Training Course — **Neplan AG**
Küsnacht, Switzerland — *March 18^{th}-20^{th}, 2019*

LabView Core I — **Staff Training Service, EPFL**
Lausanne, Switzerland — *September 2^{nd}-4^{th}, 2019*

LabView Core II — **Staff Training Service, EPFL**
Lausanne, Switzerland — *September 5^{th}-6^{th}, 2019*

Python Fundamentals — **Staff Training Service, EPFL**
Lausanne, Switzerland — *January 27^{th}-29^{th}, 2020*

Python for Data Science — **Staff Training Service, EPFL**
Lausanne, Switzerland — *March 4^{th}-5^{th}, 2020*

LabView Core III — **Staff Training Service, EPFL**
Lausanne, Switzerland — *September 14^{th}-16^{th}, 2020*

LabView DAQ (Data Acquisition) — **Staff Training Service, EPFL**
Lausanne, Switzerland — *September 9^{th}-17^{th}, 2020*

Python Advanced — **Staff Training Service, EPFL**
Lausanne, Switzerland — *December 8^{th}-10^{th}, 2020*

TEACHING EXPERIENCE

Teaching Assistant in Electrical Engineering Department, EPFL:

- M.Sc. Course "**Power Systems Dynamics**" 2017-present.
- M.Sc. Course "**Power System Restructuring and Deregulation**" 2017-present.
- PhD Course "**Transient and Dynamic Analysis of Electric Power Systems**" 2018-present.

Teaching Assistant in Electrical Engineering Department, Sharif university of technology:

- M.Sc. Course "**Advanced Power Systems Operation**" 2014-2015.
- B.Sc. Course "**Principles of Electrical Engineering**" 2014.
- B.Sc. Course "**Power System Protection**" 2013.
- B.Sc. Course "**Power System Analysis I**" 2012-2013.
- B.Sc. Course "**Electrical Energy Conversion I**" 2011-2012.

PEER REVIEWS

- IEEE Transactions on Power Systems, since 2014
- IEEE Transactions on Smart Grid, since 2014
- IEEE Transactions on Sustainable Energy, since 2017
- Elsevier Electrical Power and Energy Systems Journal, since 2015
- Elsevier Sustainable Energy, Grids and Networks Journal, since 2018
- Power Systems Computation Conference (PSCC), 2018 and 2020
- IEEE PowerTech, 2019 and 2021
- IEEE International Conference on Smart Energy Systems and Technologies, 2019

LANGUAGE SKILLS

English Full professional proficiency.
Persian Mother tongue.

TECHNICAL SKILLS

- Assembly Programming Language, C/C++, Matlab, Python.
- Bash Shell Scripting for High-Performance Computing (HPC).
- LabVIEW, GAMS, Yalmip, Simulink, SimpowerSystems, DIgSILENT, PSCAD/EMTDC, AutoCAD, NS2, NS3, OPNET.
- Pyomo, SciPy, Pandas, Sikit-learn, Keras.
- Convex Optimization, Linear Optimization, Stochastic Optimization, Robust Optimization, Bad-data detection, State Estimation.
- Latex and Microsoft Office.